Synthesis and Reactivity of Late Transition Metal Pincer Complexes: Progress toward Alkane Functionalization

Karena A. Smoll

A dissertation

submitted in partial fulfillment of the

requirements for the degree of

Doctor of Philosophy

University of Washington

2018

Reading Committee:

Karen I. Goldberg, Chair

D. Michael Heinekey

Julie Kovacs

Program Authorized to Offer Degree:

Department of Chemistry

University of Washington

Abstract

Synthesis and Reactivity of Late Transition Metal Pincer Complexes:
Progress toward Alkane Functionlization

Karena A. Smoll

Chair of the Supervisory Committee:
Prof. Karen I. Goldberg
Department of Chemistry

Commercially viable methods to directly and selectively functionalize hydrocarbon C-H bonds would have a significant impact in the chemical and fuel industries. Two desirable transformations are the partial oxidation of alkanes to alcohols and the conversion of alkanes to alkenes via alkane dehydrogenation. For such functionalizations to be useful on large scale, the most ideal oxidant is molecular oxygen because it is abundant, cheap, and benign. Late transition metal complexes are promising candidates for accomplishing these transformations due to their ability to activate C-H bonds and selectively react with O_2. As an introduction, chapter 1 surveys the literature for methane activation and functionalization and alkane dehydrogenation demonstrating what has been previously accomplished for these transformations and what improvements can be made.

Chapter 2 focuses on the partial oxidation of alkanes to alcohols and explores how O_2 reacts with late metal-carbon bonds. These findings could be applied to the design of new catalytic routes that combine C-H activation and functionalization using O_2 as the oxidant. To this end, the reactions of $^{t\text{Bu}}$PNP, $^{t\text{Bu}}$PCP, and $^{i\text{Pr}}$PCP Pd^{II}-Me complexes with O_2 are described and compared with the reported O_2 reactivity of related Pd^{II}-Me complexes. [($^{t\text{Bu}}$PNP)PdMe]Cl was found to react with O_2 upon photolysis, resulting in oxidation of the pincer ligand backbone to produce a ($^{t\text{Bu}}$PNO)PdCl complex. In contrast, photolysis of ($^{t\text{Bu}}$PCP)PdMe with O_2 resulted in oxidation of the Pd-Me moiety to form ($^{t\text{Bu}}$PCP)PdOCO_2H. Additionally, photolysis of ($^{i\text{Pr}}$PCP)PdMe with O_2 resulted in multiple products, suggesting that this complex is too active under photolytic conditions. Isotopic labeling, radical initiators, and solvent studies were employed to gain insight into the mechanisms of these unusual reactions of late metal alkyls with molecular oxygen.

Chapters 3 and 4 discuss work towards accessing novel Ir^{III} complexes for use in aerobic alkane dehydrogenation. Efforts have focused on the 1,3-bis(2'-pyridylimino)isoindoline (BPI-H) ligand framework. This ligand is ideal because it has been shown to be stable at high temperatures under oxidizing conditions and is easily modified to allow for variation of the electronic and steric effects. Chapter 3 discusses the synthesis and characterization of a series of both novel and known ^{R}BPI-H ligands. The percent volume buried has been calculated and compared for each ligand to determine how sterics affects the binding pocket or metalation of these ligand variations. ^{OMe}BPI-H, has the highest steric profile with a % volume buried of 71.9.

Chapter 4 describes efforts to metalate these ligands with iridium and rhodium and explores the reactivities of these complexes. Novel Ir^{III} complexes (BPI)IrEt(OAc) and (^{xylyl}BPI)IrEt(OAc) have been synthesized and fully characterized. The protonation, β-H

elimination, and C-H activation reactivity for (BPI)IrEt(OAc) in the context of alkane dehydrogenation was investigated. β-H elimination of (BPI)IrEt(OAc) was found to be reversible, with the equilibrium favoring the Ir-Et. In addition, (BPI)IrEt(OAc) was found to activate C_6D_6 to form (BPI)Ir(CD_2CD_3)(OAc) and (BPI)Ir(C_6D_5)(OAc) via H-D exchange at 70 °C. With $NaBAr^F_{24}$ present in the reaction of (BPI)IrEt(OAc) with C_6D_6, a dinuclear Ir complex [(BPI)Ir(CD_2CD_3)]$_2$(μ-OAc)]BAr^F_{24} is formed. This difference in reactivity is attributed to the presence of $NaBAr^F_{24}$ allowing a dinuclear complex to initially form in solution before C-H activation occurs. This differs in reactivity compared to the monomer with no $NaBAr^F_{24}$ present. The β-H elimination and C-H activation reactivity of (^{xylyl}BPI)IrEt(OAc) was also explored and preliminary results are discussed. β-H elimination of (^{xylyl}BPI)IrEt(OAc) was found to be more facile than (BPI)IrEt(OAc) to produce a stable Ir-H species. Additionally, the C-H activation reactivity of (^{xylyl}BPI)IrEt(OAc) mirrored that of (BPI)IrEt(OAc). (^{xylyl}BPI)IrEt(OAc) was found to activate C_6D_6 to form (^{xylyl}BPI)Ir(CD_2CD_3)(OAc) via H-D exchange at 70 °C. No Ir-C_6D_5 product was formed in this reaction likely due to the increased steric profile of ^{xylyl}BPI ligand. With $NaBAr^F_{24}$ present, a dinuclear Ir complex [(^{xylyl}BPI)Ir(CD_2CD_3)]$_2$(μ-OAc)]BAr^F_{24} is formed.

TABLE OF CONTENTS

List of Figures

List of Schemes

List of Tables

Acknowledgements

I want to start off by thanking everyone who has helped, inspired, and encouraged me to get to where I am today. My time in graduate school has went by so fast and I have had some really great experiences that I will always cherish.

I want to thank Mrs. Rodriguez at Fontana High School for first getting me interested in chemistry. I will never forget the fun times I had in your classes and the friendship we have built over the years.

To my graduate research advisor, Karen Goldberg, thank you so much for everything you have done for me during my time in graduate school. I would not be where I am today without your mentorship, guidance, and support. When I first came to the University of Washington your presentation on what the Goldberg lab did solidified the fact that I wanted to work with you. You were so enthusiastic and really highlighted the importance research has on the world and that excitement transferred to me. You have been a great mentor both professionally and personally and have helped me grow so much as a scientist. Your willingness to always talk about anything and your compassion and understanding really comes through and has created a sense of family and friendship in lab, something I think is so very important when attending graduate school. Thank you a million times.

To my family, my mom Catheryn, dad Eric, sister Raelina, and brother Eric, thank you for all your love and support. You have always encouraged me to follow my dreams no matter where that takes me. Raelina you bubbliness helps balance me when I am having a bad day and I am so proud of how far you have come! Eric you are extremely smart and have always appreciated the help and advice you give. To all my grandparents, Jesse, Geraldine, Dolores, Budford, and Clara, I miss you all and always have you in my heart. To Travis' family, Bob, Lisa, Bari, David, Michelle, John and Liesel, you are all amazing and have supported both Travis and I during our journey through graduate school and I thank you for that.

I have met so many amazing people in Seattle and could not have imagined how important you all would become in my life! To the Goldberg lab-Kelly Kim, Zuzana Culakova, Hannah Zeitler, Alex Phearman, Sophie Rubashkin, Amy Chu, Braden Zahora, Byongjoo Bark, Zoha Syed, Natalie Hillerson, Ash Wright, Magnus Johnson, Tim Brewster thank you for all your help and friendship. To dinner club, Sophia Cherry, Mike Cherry, Louise Guard, Tyler Stevens, Wilson Bailey, Cecily Ferguson, Ben Leipzig, Kim Quigley, and Jonathan Goldberg you are all the most amazing beautiful people and I am glad to have become so close to all of you. Wilson your cheeriness, friendliness, and mentorship really made graduate school 1000x better and I could not thank you enough. Andrew Chanez, we have been through college and now post college together. You have been and continue to be a great friend and I will always cherish that. To my hometown best friends, Noemi Loera, Vanessa Murrieta, and German Guerrero you guys are crazy and I love it! No matter where we are in life we remain close and I thank you for being there for me whenever.

Finally to my love, Travis Lekich, I am so grateful to have met you when starting graduate school. It has been the best years of my life with you by my side and I would not have it any other way. You have been there for the ups and downs and I could not have done it without you. You are my rock and have supported me in everything I do and I truly appreciate you. I love you so much and can't wait to see what the future holds for us.

Chapter 1

Introduction

1.1 Partial oxidation of hydrocarbons: An overview

Hydrocarbons from petroleum and natural gas supply over 90% of the carbon feedstock used in the chemical industry.[1] However, converting these materials to more valuable chemicals currently requires multiple steps and large energy inputs. Therefore, commercially viable methods to directly and selectively functionalize hydrocarbon C-H bonds would have a dramatic impact on the production of fuels and chemicals. In particular, the direct oxidation of methane and alkane feedstocks has been considered a "holy grail" in this field.[2] Methane, the main component of natural gas, is an important C1 feedstock; methane is used for methanol synthesis and in the Fischer-Tropsch process for higher alkanes.[3]

Methanol is currently produced industrially via a two-step energy intensive process that converts methane to syngas at high temperatures (800-950 °C) and subsequently uses the syngas to make methanol at high pressures. In this process, all the C-H bonds of methane are broken in the first step only to be reformed in the second and the overall process is significantly endothermic.[3] A direct conversion of methane to methanol under mild conditions would provide

benefits to the fuel and chemical industries by providing a more efficient route to methanol. However, selective functionalization of hydrocarbon C-H bonds has proven to be challenging. Since the products contain weaker C-H bonds compared to the starting materials, over-functionalization is a major issue. Additionally, for direct alkane functionalization to be useful on large scale, an inexpensive and environmentally benign oxidant is necessary. Oxygen, the oxidant of choice in most commercial commodity-scale organic oxidations, meets these requirements, but a viable process for C-H activation and functionalization using oxygen has yet to be realized. Progress in this field has been slow due to limited understanding of how oxygen reacts with organometallic complexes capable of activating strong C-H bonds.

1.2 Catalytic partial oxidation of methane

The need to develop direct selective C-H activation and functionalization methods has inspired the exploration of homogeneous transition metal complexes for this transformation. Late transition metal complexes can activate small traditionally inert molecules selectively, which make them ideal to pursue as catalysts for C-H alkane functionalization.[4] The first example of catalytic methane oxidation by a late transition metal catalyst was accomplished by Shilov and coworkers in 1972.[5] They found that a Pt^{II} complex served as a competent catalyst for the conversion of methane to methanol or methyl chloride in the presence of a Pt^{IV} salt as a stoichiometric oxidant (Scheme 1.1). Although this system suffered disadvantages such as low conversions, catalyst instability, and the use of an expensive stoichiometric oxidant, these findings sparked many further investigations into electrophilic activation of C-H bonds with late transition-metal complexes.

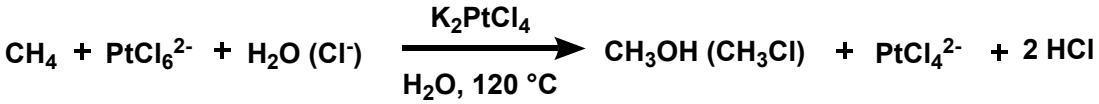

Scheme 1.1. Shilov methane to methanol system

Periana and coworkers reported the second example of catalytic methane functionalization in 1998.[6] Often referred to as the ‘Catalytica system’, this protocol uses a (bpym)$Pt^{II}Cl_2$ (bpym = bipyrimidine) catalyst precursor in neat H_2SO_4 at 220 °C to produce methyl bisulfate as the sole product (Scheme 1.2). A 90% methane conversion was reported with 80% selectively for methyl bisulfate resulting in an overall yield of 72%. This is, to date, the most active catalytic system for methane functionalization in terms of selectivity, conversion, and yield.[3] The success of this system was attributed to the lack of reactivity of the product vs. methane and the stability of the catalyst due to strong bpym ligand coordination. Unfortunately, the industrial utility of this system is severely limited due to catalyst inhibition by water (a by-product of the reaction) and challenges in separation of the oxidized product from H_2SO_4.

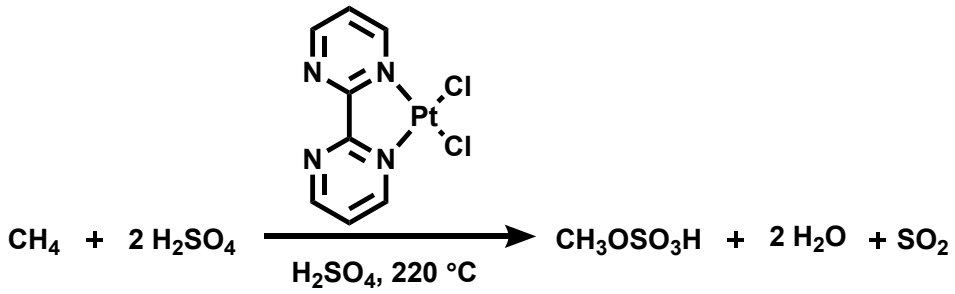

Scheme 1.2. Periana catalytica system

Another example of catalytic methane functionalization was reported by Strassner and coworkers in 2002.[7] They found that N-heterocyclic carbene (NHC) Pd^{II} complexes could catalyze the conversion of methane to trifluoroacetic acid methyl ester in trifluoroacetic acid and

$K_2S_2O_8$ at 80 °C (Scheme 1.3). Notably, this system demonstrated that NHC ligands could provide catalyst stability, even at high temperatures in the presence of strong oxidants. These hallmark examples of methane functionalization showcase the ability of platinum and palladium complexes to effect selective electrophilic activation of methane via C-H activation. In addition to selectively activating C-H bonds,[8] it has been demonstrated that palladium and platinum complexes can undergo productive reactions with O_2. This selective oxygen reactivity would be a critical advantage for a commercially viable process.[9] As such, palladium and platinum are promising candidates for the development of catalysts that can activate and functionalize C-H bonds using O_2 as the oxidant.

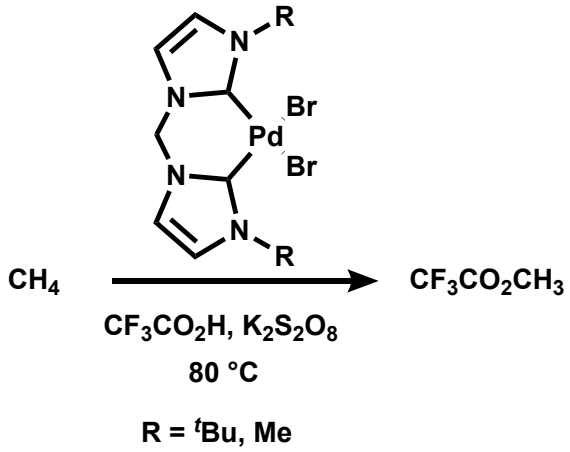

Scheme 1.3. Strassner (NHC)Pd system

1.3 Functionalization of alkanes to alkenes: An overview

Alkenes are another valuable feedstock used in many organic transformations and are important building blocks for a variety of commodity chemicals, including plastics, detergents, fuels, and alcohols.[10] One method from which alkenes are currently produced is thermal cracking of alkanes. Thermal cracking requires high temperatures (800-880 °C) resulting in a mixture of alkenes.[1] Overall, this process is both inefficient and expensive. Therefore, the development of

mild methods for the direct selective conversion of abundant hydrocarbon sources to alkenes would advance the chemical industry significantly. One such transformation is alkane dehydrogenation, the direct conversion of alkanes to alkenes with formal loss of H_2. Current alkane dehydrogenation methodologies can be categorized as either transfer or acceptorless reactions.[11]

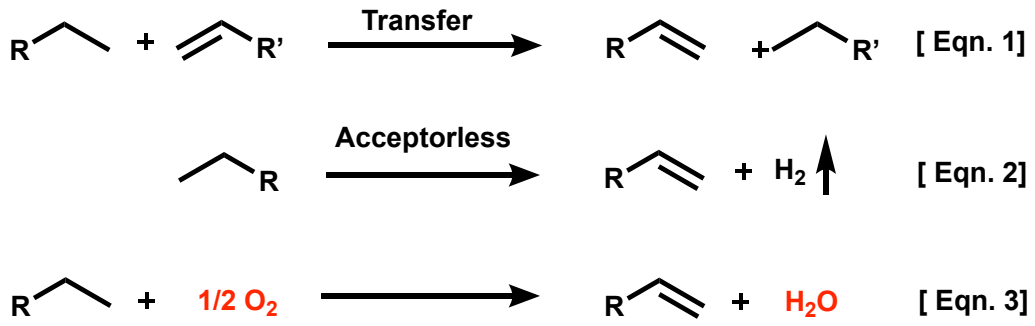

Scheme 1.4. Types of alkane dehydrogenation

Transfer dehydrogenation requires a sacrificial olefin as a hydrogen acceptor to make the dehydrogenation thermodynamically favorable (Scheme 1.4, Eqn. 1).[11-12] The first example of stoichiometric alkane dehydrogenation was reported by Crabtree and coworkers in 1979 using $[(H)_2Ir(acetone)_2(PPh_3)_2][BF_4]$ to convert cyclopentane and cyclooctane (COA) to cyclopentadiene and cyclooctadiene, respectively.[13] A hydrogen acceptor, *tert*-butylethylene (TBE), was used as the sacrificial olefin required to drive the endothermic loss of H_2. Soon after this discovery, catalytic transfer alkane dehydrogenation was reported by Felkin[14-16] and Crabtree,[17-19] with bis(trialkylphosphine)Ir complexes emerging as the most successful catalysts. However, the turnover numbers (TON) of these systems were limited by catalyst decomposition at the high temperatures needed.

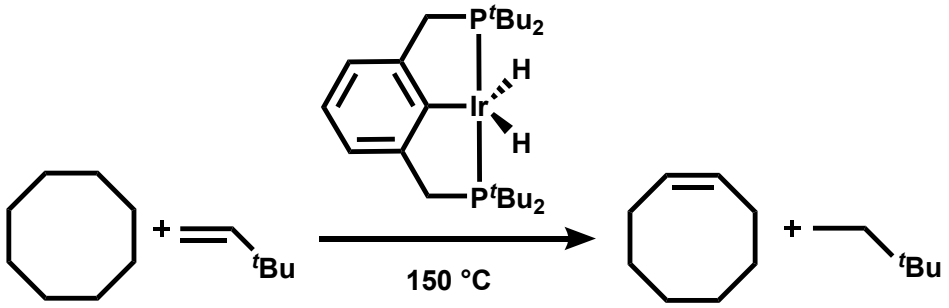

Scheme 1.5. Transfer dehydrogenation with ($^{t\text{Bu}}$PCP)IrH$_2$

To address these issues, researchers began to experiment with pincer ligands to afford more stability to the metal center.[11] The first report of alkane dehydrogenation catalyzed by pincer-ligated metal complexes was by Jensen, Kaska, and coworkers.[12a] They found that ($^{t\text{Bu}}$PCP)IrH$_2$ ($^{t\text{Bu}}$PCP = 2,6-bis[(di-*tert*-butylphosphino)methyl]phenyl) catalyzed the transfer dehydrogenation of COA in the presence of TBE resulting in 82 turnovers/hour at 150 °C (Scheme 1.5). In contrast to previous systems, ($^{t\text{Bu}}$PCP)IrH$_2$ displayed excellent thermal stability at 200 °C. Soon after, Goldman and coworkers found that the ^{i}Pr analog, ($^{i\text{Pr}}$PCP)IrH$_2$, catalyzed the transfer dehydrogenation of linear alkane n-octane to octenes at 150 °C with good regioselectively toward the α-olefin.[20] This regioselectively was hypothesized to be due to the less bulky ^{i}Pr groups.[20] Goldman and coworkers also undertook kinetic studies to determine the mechanism of transfer dehydrogenation by these (PCP)Ir complexes revealing that TBE hydrogenation was rate-determining.[21] Brookhart and coworkers later discovered that ($^{t\text{Bu}}$POCOP)Ir ($^{t\text{Bu}}$POCOP = κ^3-C$_6$H$_3$-2,6-(OP^{t}Bu$_2$)$_2$) catalysts afforded even higher TONs and turnover frequencies (TOFs) for COA/TBE transfer dehydrogenation.[22] After 40 hours at 200 °C, the ($^{t\text{Bu}}$POCOP)Ir catalyst had achieved 1580 TONs, a significant improvement over the 227 TONs observed with the ($^{t\text{Bu}}$PCP)Ir analog.[22] The rhodium complex ($^{t\text{Bu}}$PCP)RhH$_2$ was also found to catalyze COA

dehydrogenation at 150 °C, but decomposition occurred at 200 °C, suggesting that the iridium complex is stable at higher temperatures.[12b]

In contrast to transfer dehydrogenation, acceptorless dehydrogenation does not use a hydrogen acceptor and instead is performed at reflux temperatures to expel hydrogen and shift the equilibrium towards product (Scheme 1.4, Eqn. 2).[11,23] Crabtree and coworkers reported the first example of the acceptorless dehydrogenation of COA using $Ir(H)_2(TFA)(PCy_3)_2$ at 150 °C.[24] However, like early examples of transfer dehydrogenation, this system suffered from catalyst decomposition. Similarly, pincer-ligated complexes showed greater catalyst stability. Goldman and coworkers found that ($^{t\text{Bu}}$PCP)IrH_2 catalyzed the acceptorless dehydrogenation of COA and cyclodecane to COE and cyclodecene, respectively, without decomposition.[23] Additionally, 2 years later, Goldman found that the less sterically bulky analog ($^{i\text{Pr}}$PCP)IrH_4 ($^{i\text{Pr}}$PCP = 2,6-bis[(di-*iso*-propylphosphino)methyl]phenyl) dehydrogenated cyclodecane with 1000 TONs and was the first reported example of acceptorless dehydrogenation of linear alkanes (Scheme 1.6).[25]

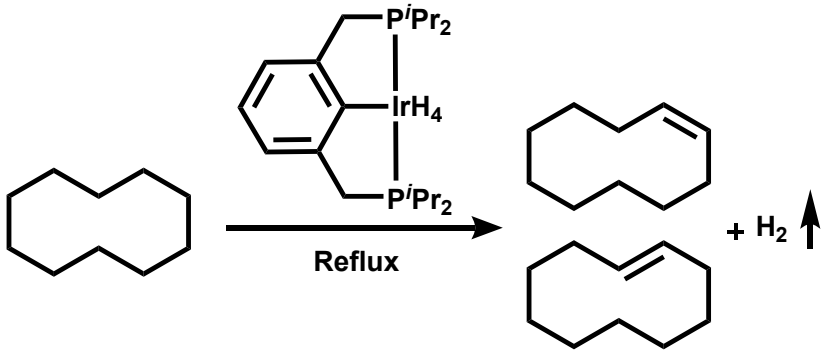

Scheme 1.6. Acceptorless dehydrogenation with ($^{i\text{Pr}}$PCP)IrH_2

The reported examples are some of the most successful for catalytic alkane dehydrogenation and yet these methods are not ready for commercial application. Beyond the TONs that are

relatively low for a commercial process, both transfer and acceptorless dehydrogenation have underlying issues that are challenging for large-scale production. For instance, for every olefin produced through transfer dehydrogenation, one olefin is consumed, making this process atom inefficient. In acceptorless dehydrogenation, reflux temperatures (≥ 200 °C) must be used to overcome the high enthalpic barrier due to H_2 release from the system.

Given these limitations, the use of oxygen as the hydrogen acceptor for alkane dehydrogenation is an attractive alternative (Scheme 1.4, Eqn. 3). Using O_2 could have dramatic advantages in terms of cost, efficiency, and environmental impact. In addition, water would be the only byproduct in the reaction. Although the use of oxygen would be advantageous, there are challenges to overcome, most notably selectivity and over-oxidation of substrate.

1.4 Dissertation Summary

The following chapters describe contributions to the general understanding of transition metal catalyzed C-H activation and functionalization and reactivity of organometallic complexes with O_2. The findings from these studies establish a foundation from which future efforts toward the aerobic oxidation of alkanes to alcohols and alkenes can be conducted. This work focuses on late transition metal complexes of groups 9 and 10 (Rh, Ir, Pd, and Pt), describing partial oxidation of alkanes to alcohols (Chapter 2) and alkane dehydrogenation (Chapters 3 and 4). Chapter 2 examines the reactivity of O_2 with M-C bonds. Specfically, the reactions of $^{t\text{Bu}}$PNP ($^{t\text{Bu}}$PNP = 2,6-bis-(di-*tert*-butylphosphinomethyl)-pyridine), $^{t\text{Bu}}$PCP, and $^{i\text{Pr}}$PCP Pd^{II}-Me complexes with O_2 are described and compared with the reported O_2 reactivity of related Pd^{II}-Me complexes. Isotopic labeling, radical initiators, and solvent studies were used to gain insight into the mechanisms of these reactions.

Chapters 3 and 4 discuss progress towards synthesizing novel Ir^{III} complexes for use in aerobic alkane dehydrogenation. The focus has been on the 1,3-bis(2'-pyridylimino)isoindoline (^{R}BPI-H) ligand framework due to its excellent thermal stability under oxidizing conditions and its facile preparation and amenability to modification for probing electronic and steric effects. Chapter 3 discloses the synthesis and characterization of a series of both novel and known ^{R}BPI-H ligands. Chapter 4 describes the metalations and attempted metalations of these ^{R}BPI-H ligand variations with iridium and rhodium. Novel Ir^{III} complexes, (BPI)IrEt(OAc) (BPI = 1,3-bis[2-(4-methylpyridyl)imino]isoindoline) and (^{xylyl}BPI)IrEt(OAc) (^{xylyl}BPI = 1,3-bis[2-(5-(3,5-xylyl)pyridyl)imino]isoindoline) have been synthesized and characterized. The protonation, β-H elimination, and C-H activation reactivity of (BPI)IrEt(OAc) has been explored and is discussed in detail.

1.5 Notes and References to Chapter 1

1. Weissermel, K.; Arpe, H. *Industrial Organic Chemistry, 4th ed.*; Wiley-VCH: Weinheim, 2003.
2. a) Arndtsen, B.A.; Bergman, R.G. ; Mobley, T.A.; Peterson, T.H. *Acc. Chem. Res.*, **1995**, *28*, 154-162. b) Goldberg, K.I.; Goldman, A.S. *Acc. Chem. Res.* **2017**, *50*, 620-626.
3. Caballero, A.; Perez, P.J. *Chem. Soc. Rev.* **2013**, *42*, 8809-8820.
4. Labinger, J.A.; Bercaw, J.E. *Nature* **2002**, *417*, 507-514.
5. a) Gol' dshleger, N.F.; Es' Kova, V.V.; Shilov, A.E.; Shteinman, A.A. *Zh. Fiz. Khim.* **1972**, *46*, 1353. b) Gol' dshleger, N.F.; Shteinman, A.A.; Shilov, A.E.; Es' Kova, V.V. *Russ. J. Phys. Chem.* **1972**, *46*, 785.
6. Periana, R.A.; Taube, D.J.; Gamble, S.; Taube, H.; Saton, T.; Fujii, H. *Science* **1998**, *280*, 560-564.
7. Muehlhofer, M.; Strassner, T.; Herrmann, W.A. *Angew. Chem. Int. Ed.* **2002**, *41*, 1745-1747.
8. a) Lersch, M.; Tilset, M. *Chem. Rev.* **2005**, *105*, 2471-2526. b) Neufeldt, S.R.; Sanford, M.S. *Acc. Chem. Res.* **2012**, *45*, 936-946.
9. Scheuermann, M.L.; Goldberg, K.I. *Chem.- Eur. J.* **2014**, *20*, 14556-14568.
10. a) Cossee, P. *Journal of Catalysis* **1964**, *3*, 80-88. b) Behr, A. In *Ullmann's Encyclopedia of Industrial Chemistry,* 5th Ed.; Elvers, B.; Hawkins, S.; Russey, W.; Eds.; VCH Verlagsgellschaft: Weinheim, **1989**, *A13*, 240-251. c) Brown, W.H.; Foote, C.S.; Iverson, B.L.; Anslyn, E.V. Reactions of Alkenes. Organic Chemistry, 5e; Brooks/Cole Cengage learning: Belmont, CA, 2009; 204-255.
11. Choi, J.; MacArthur, A.H.R.; Brookhart, M.; Goldman, A.S. *Chem. Rev.* **2011**, *111*, 1761-1779.
12. a) Gupta, M.; Hagen, C.; Flesher, R.J.; Kaska, W.C.; Jensen, C.M. *Chem. Commun.* **1996**, *0*, 2083-2084. b) Gupta, M.; Hagen, C.; Kaska, W.C.; Cramer, R.E.; Jensen, C.M. *J. Am. Chem. Soc.* **1997**, *119*, 840-841.
13. Crabtree, R.H.; Mihelcic, J.M.; Quirk, J.M. *J. Am. Chem. Soc.* **1979**, *101*, 7738- 7740.
14. Baudry, D.; Ephritikhine, M.; Felkin, H.; Holmes-Smith, R. *J. Chem. Soc., Chem. Commun.* **1983**, 788-789.
15. Felkin, H.; Fillebeen-Khan, T.; Gault, Y.; Holmes-Smith, R.; Zakrzewski, J. *Tetrahedron Lett.* **1984**, *25*, 1279-1282.
16. Felkin, H.; Fillebeen-Khan, T.; Holmes-Smith, R.; Lin, Y. *Tetrahedron Lett.* **1985**, *26*, 1999-2000.
17. Burk, M.J.; Crabtree, R.H.; Parnell, C.P.; Uriarte, R.J. *Organometallics* **1984**, *3,* 816-817.
18. Burk, M.J.; Crabtree, R.H.; McGrath, D.V. *J. Chem. Soc., Chem. Commun.* **1985**, 1829-1830.
19. Burk, M.J.; Crabtree, R.H. *J. Am. Chem. Soc.* **1987**, *109*, 8025-8032.
20. Liu, F.; Pak, E.B.; Singh, B.; Jensen, C.M.; Goldman, A.S. *J. Am. Chem. Soc.* **1999**, *121*, 4086-4087.
21. Renkema, K.B.; Kissin, Y.V.; Goldman, A.S. *J. Am. Chem. Soc.* **2003**, *125*, 7770-7771.
22. Gottker-Schnetmann, I.; White, P.; Brookhart, M. *J. Am. Chem. Soc.* **2004**, *126*, 1804-1811.
23. Xu, W.; Rosini, G.P.; Gupta, M.; Jensen, C.M.; Kaska, W.C.; Krogh-Jespersen, K.; Goldman, A.S. *Chem. Commun.* **1997**, 2273-2274.

24. Aoki, T.; Crabtree, R.H. *Organometallics* **1993**, *12*, 294-298.
25. Liu, F.; Goldman, A.S. *Chem. Commun.* **1999**, 655-656.

Chapter 2*

Reactivity of PNP and PCP Pd^{II}-Me Complexes with Molecular Oxygen

2.1 Introduction

As summarized in Chapter 1, complexes of platinum and palladium hold great interest for use as catalysts in the partial oxidation of hydrocarbons because of their ability to selectively activate inert C-H bonds[1] and to undergo productive reactions with O_2.[2] One potential pathway to accomplish the partial oxidation of alkanes to alcohols with O_2 is shown in Scheme 2.1. The cycle involves C-H activation at a low-valent metal center, followed by O_2 insertion into the M-alkyl bond, and finally release of the oxidized product.[3] Despite the advantages of oxygen as an oxidant for this transformation, there are only a handful of observations of O_2 insertion into Pd- and Pt-alkyl bonds that have been documented.[4-6] Therefore, mechanistic understanding and knowledge of the requirements for O_2 activation by M-alkyl complexes remain scarce. This limited knowledge hinders our ability to predict reaction outcomes and to develop viable catalytic systems for selective alkane oxidation. We seek to extend the handful of examples of

* The majority of the data presented in this chapter has been previously published: Reprinted with permission from Smoll, K.A.; Kaminsky, W.; Goldberg, K.I. *Organometallics* **2017**, *36*, 1213-1216. Copyright 2018 American Chemical Society.

oxygen insertion into Pd^{II}-C bonds that have been reported to a wider group of ligand environments. Furthermore, we seek insight into the parameters required for O_2 activation and the mechanisms of these O_2 activation reactions through the examination of steric and electronic effects on the metal complexes.

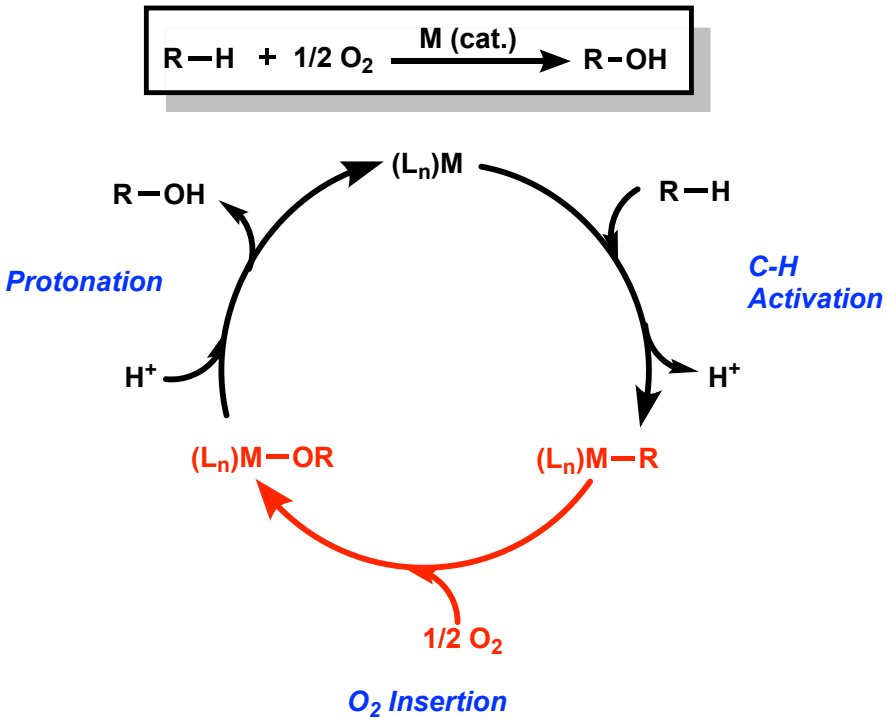

Scheme 2.1. Proposed cycle for the partial oxidation of alkanes

The first direct observation of O_2 insertion into the Pd-Me bond of (bpy)$PdMe_2$ (bpy = 2,2-bipyridine) to produce (bpy)PdMe(OOMe) was reported in 2009.[4] Extensive mechanistic studies were undertaken and the reaction was found to proceed via a radical chain mechanism, which was supported by the reproducibility of the reaction outcome when performed in the presence of the radical initiator azobisisobutyronitrile (AIBN). It was proposed that the mechanism proceeds (via the propagation step) by attack at the Pd^{II} center by a MeOO• radical to generate a five-coordinate Pd^{III} intermediate, followed by loss of Me• radical to generate the PdOOMe product. The chain continues as released Me• reacts with O_2 to generate the chain

carrier MeOO• (Scheme 2.2). A similar mechanism was proposed for the reaction of O_2 with a related Pt^{II}-Me complex.[4,5]

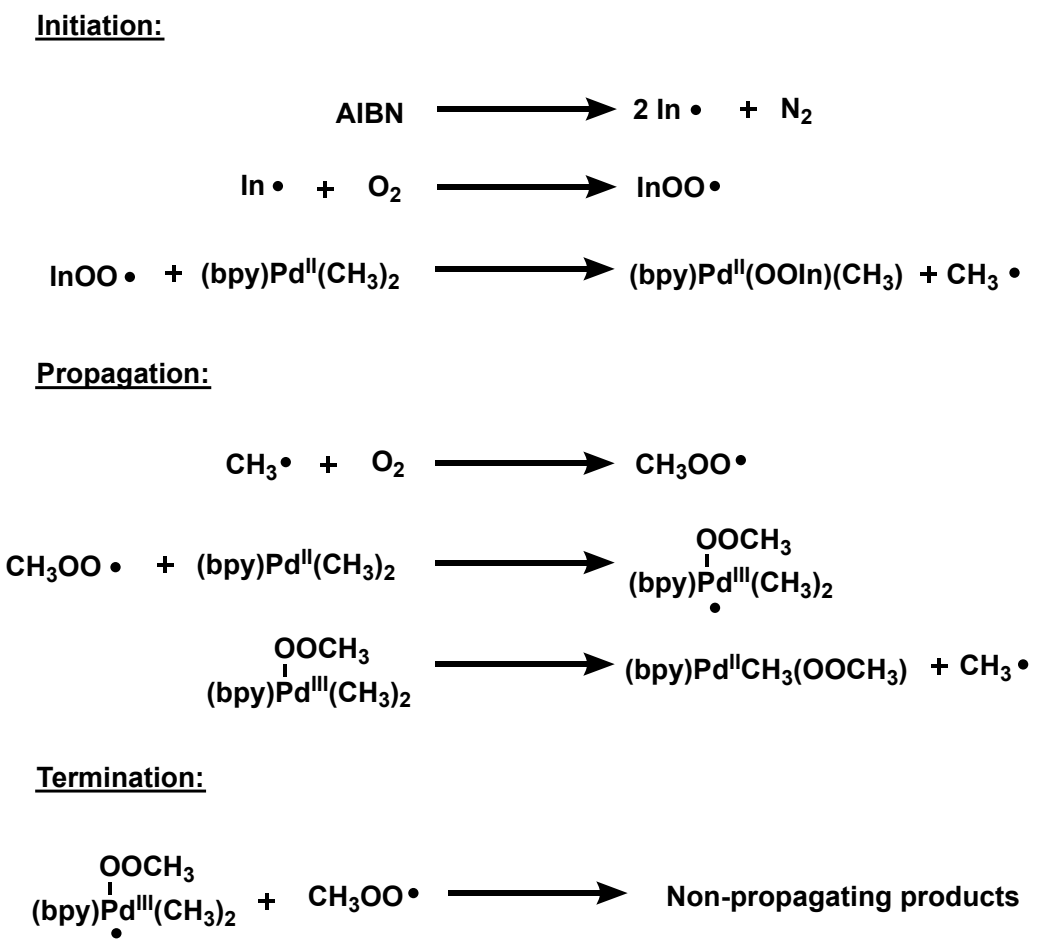

Scheme 2.2. Proposed radical chain mechanism from reaction of (bpy)$PdMe_2$ + O_2

Several substituted terpyridine M^{II}-Me (M= Pt, Pd) complexes have also been reported to react with O_2 to form M^{II}-OOMe complexes.[6] These reactions are promoted by UV light and are also proposed to proceed via a radical mechanism. In the proposed mechanism, exposure to light generates five-coordinate dinuclear triplet state intermediates that arise from weak M•••M interactions. These activated dinuclear species undergo reaction with O_2 to form superoxo and peroxo intermediates that further react to eventually form mononuclear M-OOMe products. Of

note, productive reactions were only observed when the ligand contained steric bulk close to the M-C bond.[6] Even more recently, Maseras and coworkers performed computational studies on the terpyridine systems and proposed a completely different mechanism that does not include dimer formation.[7] Instead, they propose that the terpyridine complexes, after excitation with light, immediately react with O_2 to form superoxo and peroxo species that eventually form the Pt-OOMe product. The proposed pathway differs depending on the substituents on the terpyridine ligand.[7]

To further understanding of the reactions of M-C bonds and O_2, we have examined the chemistry of pincer PNP and PCP Pd^{II}-Me complexes with O_2 ($^{t\text{Bu}}$PNP = 2,6-bis-(di-*tert*-butylphosphinomethyl)-pyridine, $^{t\text{Bu}}$PCP = 2,6-bis[(di-*tert*-butylphosphino)methyl]phenyl, and $^{i\text{Pr}}$PCP = 2,6-bis[(di-iso-propylphosphino)methyl]phenyl, Figure 2.1). The PNP and PCP pincer ligand sets have some common electronic features to the complexes that proceed via the radical chain substitution mechanism but are also tridentate and reasonably bulky, similar to the compounds which follow the photoactivated binuclear pathway. The novel reactivity observed, and described below, provides further insight into the factors needed for oxygen insertion reactions into Pd-Me bonds and will inform the future design of aerobic oxidation systems.

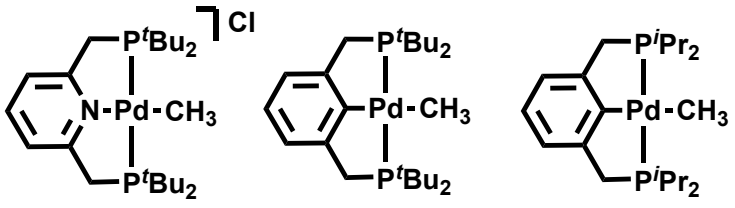

1 **6** **9**

Figure 2.1. Complexes explored for reactivity with O_2

2.2 Reactivity of [($^{t\text{Bu}}$PNP)PdMe]Cl (1) with molecular oxygen

To complement and expand on the O_2 insertion chemistry observed with (bpy)$PdMe_2$[4] and [(^{R}terpy)PdMe]SbF_6,[6] the reactivity of [($^{t\text{Bu}}$PNP)PdMe]Cl (**1**) with O_2 was explored. The 16 e^- d^8 metal pincer complex contains an open coordination site along the z-axis and therefore has the potential to expand its valency to five-coordinate similar to both the bpy and terpy systems. Additionally, complex **1** is cationic and has bulky *tert*-butyl groups on the phosphine arms of the PNP ligand (adjacent to the Pd-Me bond) making it comparable to [(^{R}terpy)PdMe]SbF_6. Notably, however, the steric bulk in the ^{R}terpy system is in the same plane as the Pd-Me bond and for the PNP system, it is above and below the square plane (Figure 2.1).

No changes were observed by ^{1}H or ^{31}P NMR spectroscopy when a solution of **1** in CD_3CN was exposed to 5 atm O_2 at temperatures ranging from 25 °C to 60 °C. Heating a CD_3CN solution of **1** with 5 atm O_2 to 65 °C in the presence of radical initiator AIBN resulted primarily in the expected decomposition of AIBN to N_2 and 2-cyano-2-propyl radicals (In•).[8,9] Only slight decomposition of **1** was observed under these conditions: 77% of **1** remained after 6 days of heating, with 18% converted to [($^{t\text{Bu}}$PNP)PdCl]X (**2**, X = $^-$OH or ^{t}Bu$_2$PO$^-$). Formation of **2** was confirmed by spiking the mixture with an independently prepared sample of [($^{t\text{Bu}}$PNP)PdCl]Cl.[10,11] In contrast to the efficient reaction of (bpy)$PdMe_2$ with O_2 in the presence of AIBN, which proceeded to completion at 50 °C within 18 hours, to form the insertion product (bpy)PdMe(OOMe),[4] **1** was essentially unreactive under similar conditions.

Since UV light had previously been used to promote reaction of [(^{R}terpy)PdMe]SbF_6 with O_2,[6] a CD_3CN solution of **1** and 5 atm O_2 was exposed to UV light (TLC lamp, 254 nm) for 25 hours (Scheme 2.3A). Two palladium-containing products were identified by ^{1}H and ^{31}P NMR spectroscopy. The major product (66.0 ppm, ^{31}P NMR) in 37% yield has C_{2v} symmetry based on

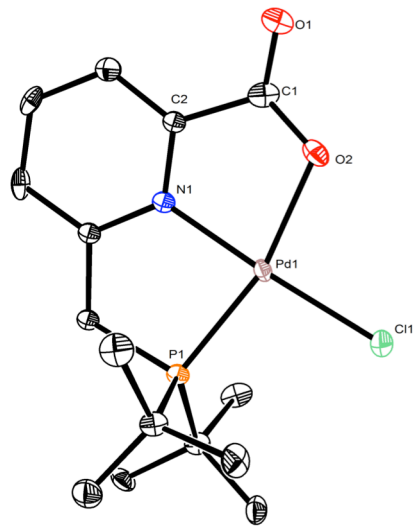

Figure 2.2: ORTEP[46] drawing of 3 with thermal ellipsoids at 50% probability. Hydrogen atoms excluded for clarity.

the associated ^{1}H NMR signals: virtual triplets (vt) at 1.44 and 3.86 ppm were observed for the ^{t}Bu and methylene protons on the ligand, respectively. This product was identified as [($^{t\text{Bu}}$PNP)PdCl]X (**2**, X = $^{-}$OH or $^{t}Bu_2PO^{-}$). The second product (96.7 ppm, ^{31}P NMR) in 30% yield with C_s symmetry was determined to be ($^{t\text{Bu}}$PNO)PdCl (**3**). Methanol (3.28 ppm, 3H, ^{1}H NMR) and $^{t}Bu_2PH(O)$ (66.2 ppm, ^{31}P NMR), both identified through spiking of the reaction mixture, were also observed in 20% and 13% yield, respectively.[12] Complex **3** was characterized by NMR spectroscopy (^{1}H, ^{31}P, ^{13}C) and X-ray crystallography. Its solid-state molecular structure shows a slightly distorted square planar geometry with bond angles of 176.8(3) and 164.4(3) Å for N(1)-Pd(1)-Cl(1) and P(1)-Pd(1)-O(2), respectively (Figure 2.2). The C(1)-O(1) and C(1)-O(2) bond lengths are 1.21(2) and 1.27(2) Å, consistent with more double-bond character for the former.

To investigate how **3** might be formed by reaction with O_2 under UV irradiation, a CD_3CN solution of **1** was irradiated with UV light under N_2 atmosphere for 5 hours. Two products were identified from this reaction: complex **2** and ($^{t\text{Bu}}$PNP*)PdCl (**4**, * denotes deprotonated methylene arm) in 37% and 56% yield, respectively (Scheme 2.3B). The production of **4** was accompanied by methane formation (0.20 ppm, ^{1}H NMR spectrum). Deprotonation of the methylene side arm in PNP metal complexes has been well studied by Milstein and coworkers.[10] However, since the transformation of **1** to **4** requires light and not base, a reasonable mechanism involves Pd-Me bond homolysis from **1** to generate Pd^{I}• and

Me• radicals.[13] Supporting this proposal, when a CD_3CN solution of **1** with 2,2,6,6-tetramethyl-1-piperidinyloxy (TEMPO) was exposed to UV light, TEMPO-Me, the expected product of Me• and TEMPO, was confirmed by ^1H NMR spectroscopy and GC-MS.[14] In the absence of TEMPO, it is proposed that the Me• then abstracts a H• from the PNP methylene arm to generate methane. De-aromatization of the pyridyl ring then produces a Pd^{II} center to which the Cl^- counter-ion coordinates to produce **4**.

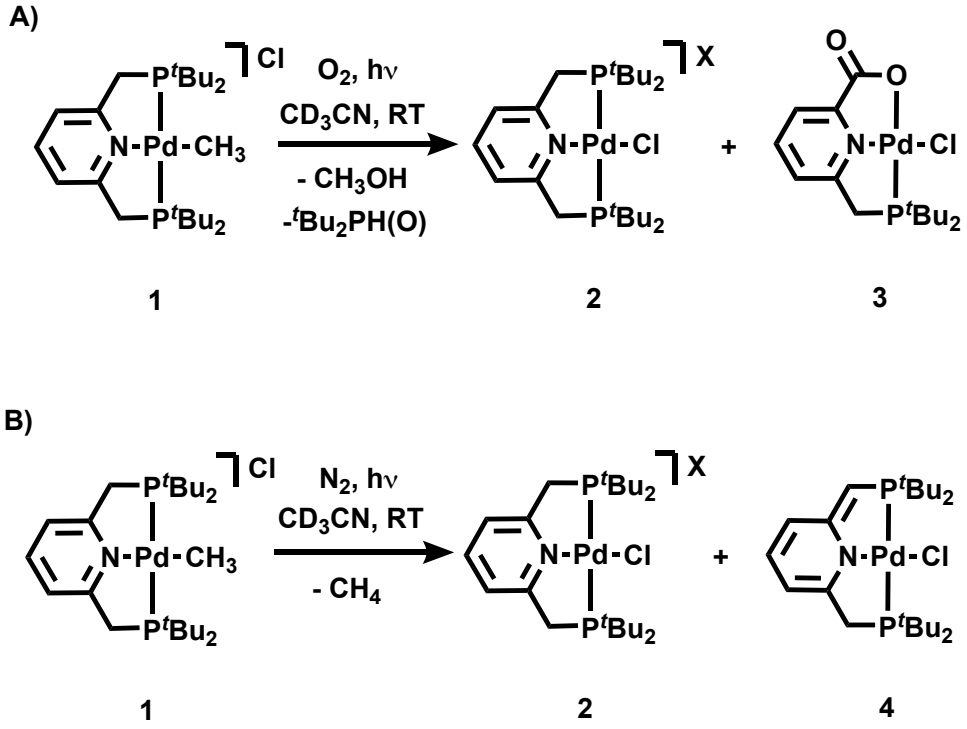

Scheme 2.3. A) Reaction of 1 with 5 atm O_2 in the path of UV light. B) Reaction of 1 under N_2 atmosphere in the path of UV light

The formation of **4** with irradiation under N_2 suggests that the photolytic reaction under O_2 to produce **3** may proceed through the initial formation of the de-aromatized complex **4**. Interestingly, evidence of methane formation was not observed in the O_2 reaction (Scheme 2.3A). Instead, methanol was identified as a product. It is well precedented that Me• radicals combine with O_2 to form MeOO• radicals.[15-17] There is also considerable literature precedence

for the formation of MeO• from MeOO• via two different pathways (Scheme 2.4).[17,18] Hanst *et al.* proposed that MeOO• can disproportionate to form MeO• and O_2 (Scheme 2.4, Eqn. 1). Bell *et al.* proposed that MeOO• and Me• radicals react to form MeO• (Scheme 2.4, Eqn. 2). However, under our reaction conditions (5 atm O_2) it is likely that most of the Me• radicals will react with O_2 to form MeOO•, therefore making the Hanst pathway (Scheme 2.4, Eqn. 1) more likely. It is proposed then that the reaction of **1** in the presence of O_2 in UV light produces Me•, by homolytic Pd-Me cleavage, and that Me• reacts with O_2 to form MeOO•, and then MeO• radical. Abstraction of H• from the PNP arm by a MeO• radical then leads to methanol and complex **4**, with coordination of the Cl^- counter-ion.

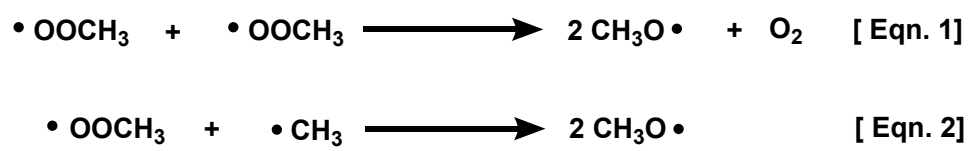

Scheme 2.4. Two possible pathways to form MeO radicals

To establish the viability of **4** as an intermediate in the formation of **3**, a C_6D_6 solution of independently prepared **4** was pressurized with 5 atm O_2. Complex **3** precipitated out of solution, and the corresponding phosphine oxide, $^tBu_2PH(O)$, was produced in 48% yield (determined via integration against an internal standard, Scheme 2.5). Performing this reaction in CD_3CN resulted in formation of **2**, **3**, and $^tBu_2PH(O)$, respectively (Scheme 2.5). Complex **2** could form in this reaction via re-protonation of the PNP arm of **4** by the *in situ* formed $^tBu_2PH(O)$. This reactivity was confirmed by introducing an independently prepared sample of $^tBu_2PH(O)$ to a CD_3CN solution of **4**, resulting in quantitative conversion to **2**. Complex **2** was not formed from **4** and O_2 in C_6D_6 solvent. This difference is attributed to the solubility of **4** in CD_3CN versus

C_6D_6. Complex **4** is soluble in C_6D_6, whereas it is slightly soluble in CD_3CN. As the oxidation in CD_3CN proceeds, product $^tBu_2PH(O)$ is therefore available to react with complex **4** as more **4** dissolves in the CD_3CN.

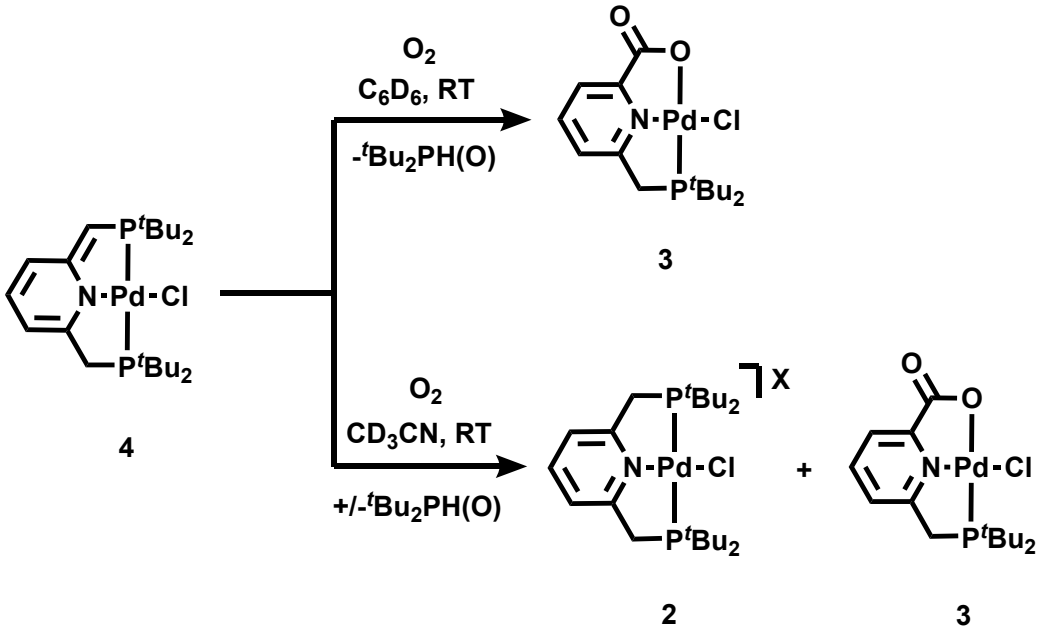

Scheme 2.5. Reactivity of 4 with O_2 in C_6D_6 and CD_3CN

In the observed reactivity of **1**, the chloride counter-ion binds to the metal center to produce stable Pd-Cl species. We hypothesized that a non-coordinating counter-ion may allow coordination of MeOO• or MeO• being formed in the reaction with O_2 and prevent oxidation of the pincer arm. Therefore, a CD_3CN solution of [($^{t\text{Bu}}$PNP)PdMe]SbF_6 (**5**) was pressurized with 5 atm O_2 and placed in the path of UV light (TLC, 254 nm). ^1H and ^{31}P NMR spectroscopy showed the disappearance of signals associated with **5** and the appearance of multiple unknown products. Methanol was also formed in the reaction (3.29 ppm, 3H, ^1H NMR). This result suggests that a H• is still being abstracted from the ligand arm to form methanol. However, unlike with **1**, there is no coordinating counter-ion to bind to the metal center to form stable

products resulting in multiple species. This also differs from Britovsek's work where he found [(^{R}terpy)PdMe]SbF_6 resulted in the insertion product.[6] The difference is likely due to the reactivity at the PNP ligand arm.

O_2 reactivity involving the backbone of a chelating ligand has been previously observed.[19] For example, Pt^{IV}-Me complexes bearing bidentate ligands added O_2 across the metal and ligand backbone when the ligand could generate a Lewis basic site through electronic resonance. When this basic site was not present, O_2 was not activated.[19c] In the PNP* system, resonance places a localized anionic charge on the methylene carbon with a re-aromatized pyridyl group. Additionally, related oxidative degradation of pyridylamine ligands at the carbon methylene group was observed for a variety of Fe complexes.[20] The overall transformation sequence for the reaction of O_2 with **1** is shown in Scheme 2.6.

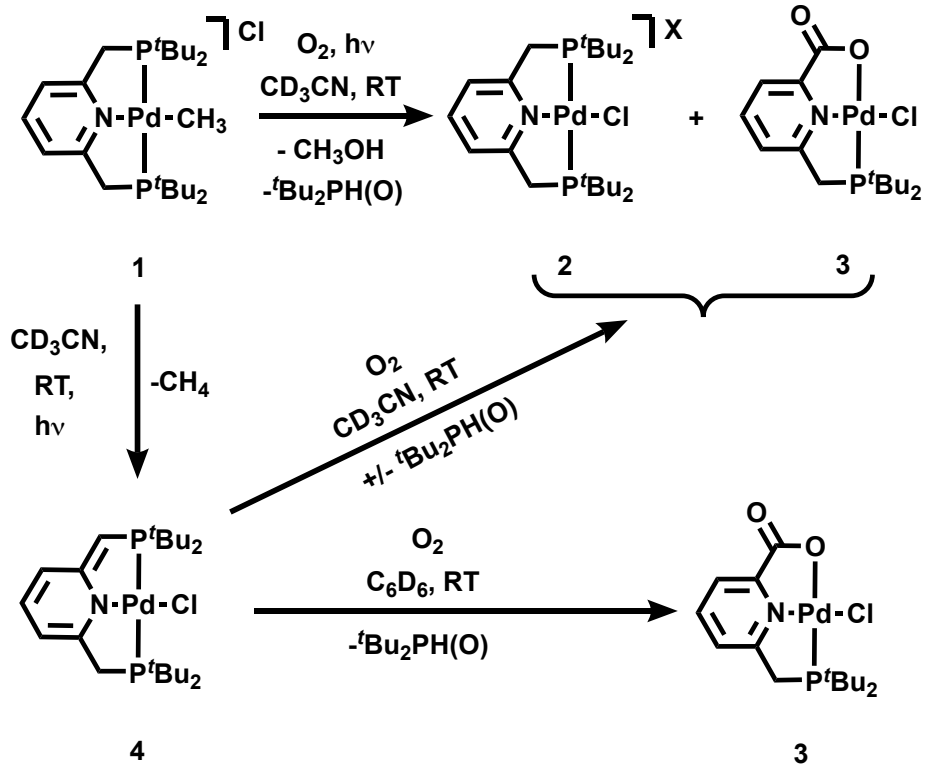

Scheme 2.6. Overall reaction of 1 with O_2 in the path of UV light

2.3 Reactivity of ($^{t\text{Bu}}$PCP)PdMe (6) with molecular oxygen

Seeking to inhibit involvement of the pincer backbone in the O_2 activation, we investigated the chemistry of the PCP ligated complex, ($^{t\text{Bu}}$PCP)PdMe (**6**), with O_2. The $^{t\text{Bu}}$PCP ligand motif has been shown to be stable towards O_2 as the corresponding ($^{t\text{Bu}}$PCP)PdH reacts with O_2 to generate a stable Pd-OOH complex.[21] Furthermore, complex **6** is neutral and has a strong *trans* donor opposite the Pd-Me bond, which is expected to weaken the Pd-Me bond and make it more labile. Notably, Grice *et al.* found that O_2 inserts exclusively into the Pt-Me bond of (PN)$PtMe_2$ (PN = 2-((di-tert-butylphosphino)methyl)pyridine) *trans* to the phosphine moiety, the stronger *trans* donor relative to nitrogen.[5]

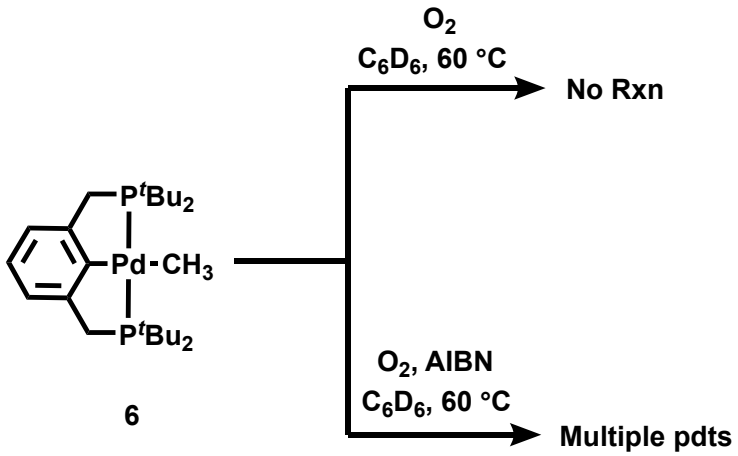

Scheme 2.7. Reactivity of 6 with O_2 at 60 °C

Heating a C_6D_6 solution of **6** with 5 atm O_2 to 60 °C resulted in no reaction after 3 days. However, heating a C_6D_6 solution of **6** with 5 atm O_2 in the presence of AIBN resulted in consumption of **6** within 24 hours (Scheme 2.7). Unfortunately, the reaction proceeded to form multiple products as determined by ^{1}H and ^{31}P NMR spectroscopy.[22] A singlet at 1.55 ppm, confirmed to be acetone, was observed in the ^{1}H NMR spectrum. Previously, Wenzel reported the reaction between (^{Ph}PP)Pt(CF_3)H (^{Ph}PP = *cis*-1,2 bis(diphenylphosphino)ethylene) and O_2 in

the presence of AIBN resulted in acetone.[9] A decomposition pathway was proposed wherein the 2-cyano-2-propyl radicals produced from AIBN reacted with O_2 to form peroxyl radicals that were converted to acetone following coordination of the metal (Scheme 2.8).[9] The formation of acetone in our reaction may occur via a similar decomposition pathway.

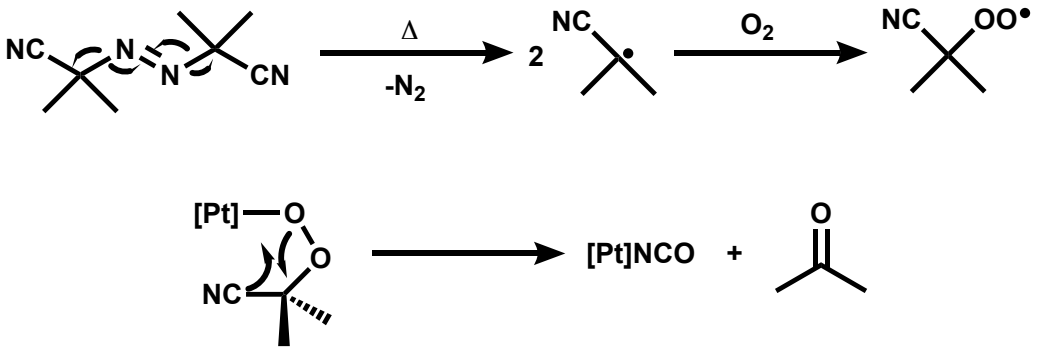

Scheme 2.8. Wenzel's decomposition pathway forming acetone

The complexity of the reaction of **6** with O_2 in the presence of AIBN led us to investigate the use of UV light as the reaction initiator. Irradiation of a C_6D_6 solution of **6** with UV light under 5 atm O_2 produced ($^{t\text{Bu}}$PCP)PdOCO_2H (**7**, 40-75% yield) and methanol (14% yield) after ca. 3 days of continuous irradiation (Scheme 2.9).[23] Sunlight as the light source was also found to initiate the reaction to produce **7**.[24] Complex **7** has been previously synthesized by the reaction of **6** with CO_2 in the presence of water.[25] The solid-state metrics and NMR spectroscopic features of **7** produced in the O_2 reaction of **6** are consistent with the previous report of this compound (Figure 2.3). However, the results reported herein represent an unprecedented method for its formation.

The formation of **7** from photolysis of **6** and O_2 was unexpected. To determine if the methyl group on **6** was the source of the central carbonate carbon, a C_6D_6 solution of ($^{t\text{Bu}}$PCP)Pd($^{13}CH_3$) **(6-^{13}C)** was pressurized with 5 atm O_2 and irradiated with UV light (254 nm) for ca. 5 days. The ^{1}H and ^{31}P NMR spectra indicated that **7** was formed in 45% yield. Notably, the ^{13}C NMR spectrum featured multiple isotopically labeled peaks at 161 ppm, 125 ppm, and 50 ppm corresponding to the central carbonate carbon of **7**,[25] CO_2,[26] and methanol,[26] respectively. An unidentified signal at 53 ppm was also present.[27] A doublet at 3.25 ppm ($^1J_{CH}$= 139 Hz) was observed in the ^{1}H NMR consistent with the methyl protons of $^{13}CH_3OH$.[28] Formation of $^{13}CH_3OH$ was also confirmed by GC-MS. These results suggest that the methyl group of **6** is being oxidized stepwise to methanol, carbon dioxide, and ultimately carbonate.

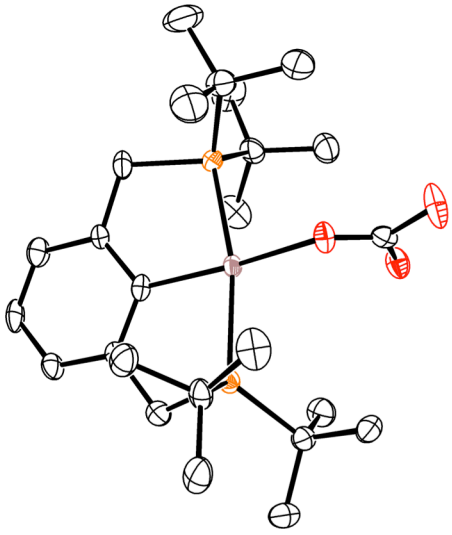

Figure 2.3: ORTEP[46] drawing of 7 with thermal ellipsoids at 50% probability. Hydrogen atoms excluded for clarity.

The formation of methanol suggested the possibility of ($^{t\text{Bu}}$PCP)PdOMe (**8**) as a potential intermediate in the formation of **7**. To investigate this possibility, a C_6D_6 solution of **8** with 5 atm O_2 was placed in the path of UV light (254 nm) for ca. 5 days. Complex **7** and methanol were formed in 58% and 32% yields, respectively. This result suggests that **8** could be an intermediate in the oxidation of the methyl group to carbonate, though it is not seen in the reactions performed. The overall reaction of **6** with O_2 in UV light is shown in Scheme 2.9.

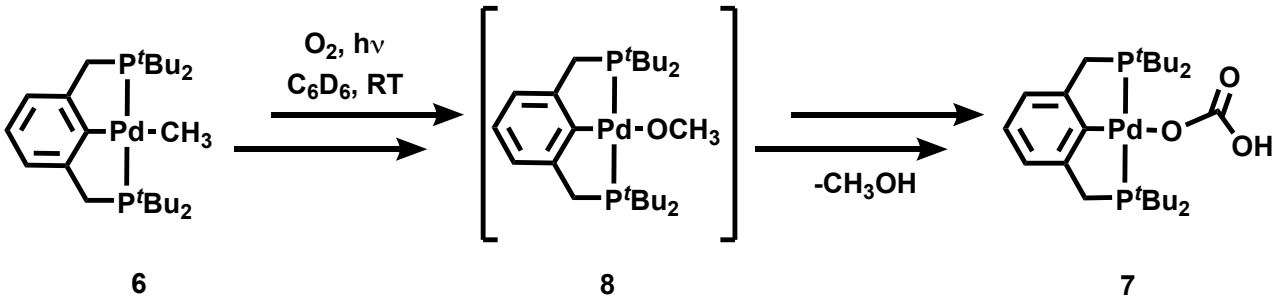

6 **8** **7**

Scheme 2.9. Overall reaction of 6 with O_2 in the path of UV light

The first step in reaction of **6** with O_2 under UV light is proposed to be homolysis of the Pd-Me bond to form Pd^{I}• and Me• radicals. To verify this, a C_6D_6 solution of **6** and TEMPO was placed in the path of UV light to produce TEMPO-Me (confirmed by ^{1}H NMR spectroscopy and GC-MS).[29] This behavior is again consistent with initial homolytic Pd-Me cleavage promoted by light, similar to the reactivity proposed for **1**. In the presence of O_2, the Me• radicals combine with O_2 to form MeOO•, which can continue on to form MeO• (Scheme 2.4, Eqn.1).[15-17] However, the PCP system differs from the PNP system because MeO• radicals do not abstract a H• from the pincer ligand backbone arm to form methanol. Instead, there is literature precedence for methanol production from MeO• with concomitant formation of formaldehyde (Scheme 2.10).[17,18,30] This step could account for the generation of methanol in addition to setting up the formation of CO_2 and carbonate by further oxidation of formaldehyde.[17] Of note, formaldehyde and other carboxylate derivatives (such as formate or formic acid) were not observed in the ^{1}H NMR spectrum of the reaction with O_2. However, a C_6D_6 solution of **6** with added formaldehyde was pressurized with 5 atm O_2 and placed in the path of UV light for ca. 7 days resulting in **7** and MeOH in 74% and 61% yield, respectively. This reaction produced the same amount of the carbonate complex **7** as reactions without added formaldehyde, but much more methanol (61% vs. 14%). This suggests that oxidation of

formaldehyde must occur to produce **7**, because the methyl group of **6** is mostly being converted to MeOH. Thus, organic radical oxidations could account for the formation of methanol and the eventual oxidation of the methyl group to produce the carbonate.[31]

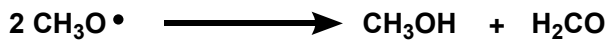

Scheme 2.10. Formation of methanol and formaldehyde from MeO radicals

2.4 Reactivity of ($^{i\text{Pr}}$PCP)PdMe (9) with molecular oxygen

Seeking to explore the influence of ligand sterics on the system, we next explored the reactivity of ($^{i\text{Pr}}$PCP)PdMe (**9**) with O_2. The sterically smaller ^{i}Pr groups around the metal center of **9** compared to the ^{t}Bu groups could determine if sterics inhibit the O_2 reactivity of **1** and **6** in the presence of AIBN. For **1** and **6**, the bulky ^{t}Bu groups on the phosphine could hinder O_2 reactivity by blocking axial coordination to the metal center as previously seen for H_2O coordination in a related (POCOP)Ir system (POCOP = C_6H_4-1,3-[OPR_2]$_2$).[32] Heating a C_6D_6 solution of **9** with 5 atm O_2 to 60 °C in the presence of AIBN resulted in complete disappearance of **9** and appearance of two new products with ^{31}P NMR signals at 62.5 and 63.7 ppm.[33] Unfortunately, a singlet at 1.55 ppm corresponding to acetone was present in the ^{1}H NMR spectrum, suggesting a decomposition pathway is occurring as was observed with **6** (Scheme 2.8).[9] However, unlike **6**, only two products were formed from **9** and O_2 allowing further exploration into the identity of these products. One possible product accompanying the formation of acetone from the decomposition pathway (Scheme 2.8) is the isocyanate complex, ($^{i\text{Pr}}$PCP)PdNCO (**10**). An IR spectrum of the reaction solution revealed the presence of a broad signal at 2210 cm^{-1}, which corresponds to an isocyanate stretch. Independent synthesis of **10** confirmed the presence of this product (63.7 ppm in the ^{31}P NMR spectrum). The second product

at 62.5 ppm is likely ($^{i\text{Pr}}$PCP)PdCN (**11**), which accompanied the formation of the isocyanate complex in the decomposition pathway proposed by Wenzel.[9,34] The overall reactivity of **9** with O_2 in the presence of AIBN is shown in Scheme 2.11.

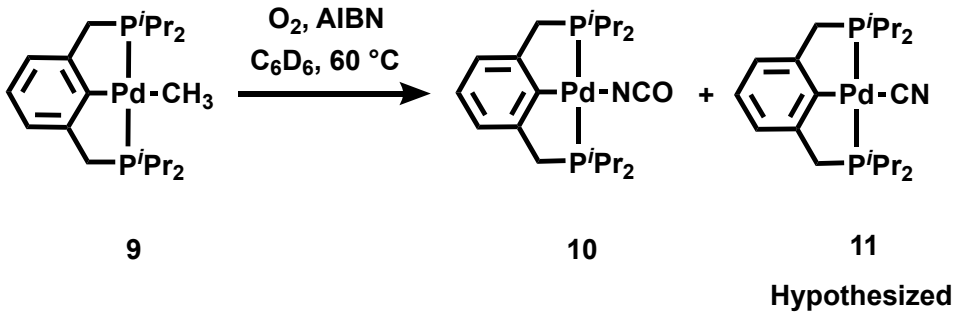

Scheme 2.11. Overall reaction of 9 with O_2 and AIBN at 60 °C

Wenzel performed his studies with both AIBN and 2,2'-azobis(2,4-dimethylvaleronitirile (Vazo 52) and found that both proceeded through the same decomposition pathway, forming the by-products acetone and 4-methyl-2-pentanone, respectively.[9] To demonstrate that a similar decomposition pathway is occurring in our system, a C_6D_6 solution of **9** with O_2 in the presence of Vazo 52 was heated to 60 °C for 24 hours. ^{1}H and ^{31}P NMR spectroscopy confirmed the formation of **10** and 4-methyl-2-pentanone. Thus, even with ^{i}Pr groups in place of ^{t}Bu groups, insertion products of O_2 into the Pd-Me bond are not observed with AIBN as the initiator. It is possible that ^{i}Pr groups may still be too bulky and inhibit MeOO• binding to the axial coordination site as observed with **1** and **6**.

Efforts to employ ambient light as the initiator resulted in no change to a C_6D_6 solution of **9** with O_2 after 6 days. However, a C_6D_6 solution of **9** with 5 atm O_2 in the path of UV light (TLC lamp, 254 nm) led to multiple products by ^{1}H and ^{31}P NMR spectroscopy. Methane was also present in this reaction (0.16 ppm in ^{1}H NMR). Irradiation of a C_6D_6 solution of **9** with UV

light without O_2 present also resulted in multiple products by ^1H and ^{31}P NMR spectroscopy. However, the products observed when O_2 was present differ from those when O_2 was absent. These results differ from our observations with **6** and suggest that the smaller steric profile of ^{i}Pr groups on the ligand make the complex more reactive under UV light and/or the β C-H bond of the ^{i}Pr group is involved in a decomposition reaction.[35]

2.5 Summary

The reactions of [($^{t\text{Bu}}$PNP)PdMe]Cl (**1**), ($^{t\text{Bu}}$PCP)PdMe (**6**), and ($^{i\text{Pr}}$PCP)PdMe (**9**) with O_2 led to entirely different results than previously reported reactions of Pd-Me complexes with O_2. There is strong evidence that photolysis for complexes **1** and **6** leads to Pd-Me bond homolysis. This is followed by reaction of Me• with O_2 to produce MeOO• and then further reaction of the organic radicals can produce MeO• species. With **1**, the MeO• radicals can abstract a H• from the PNP backbone to produce ($^{t\text{Bu}}$PNP*)PdCl (**4**). With a resonance-allowed localized anionic charge on a carbon in the ligand backbone, O_2 selectively oxidizes that position to produce ($^{t\text{Bu}}$PNO)PdCl (**3**). In contrast, with **6**, the generated MeO• radicals go on to MeOH and carbonyl derivatives that further oxidize to CO_2, ultimately forming the bicarbonate complex ($^{t\text{Bu}}$PCP)PdOCO$_2$H (**7**).

In contrast to previous reports of O_2 insertion into the Pd-Me bond, both the $^{t\text{Bu}}$PNP and $^{t\text{Bu}}$PCP PdMe systems react under UV irradiation by Pd-Me bond homolysis. The Me• radicals react with O_2 to form MeOO• but despite formation of MeOO•, we do not observe an associative substitution radical chain as was found for the aerobic oxidation of (bpy)PdMe$_2$.[4] It is conceivable that the bulky *tert*-butyl groups block approach of MeOO• to the Pd center. The formation of Me• radicals also stands in contrast to the results seen when the (^{R}terpy)PdMe cationic systems were photolyzed in the presence of O_2.[6] The bulk above and below the square

plane in the $^{t\text{Bu}}$PNP and $^{t\text{Bu}}$PCP PdMe systems may inhibit either dinuclear aggregation or O_2 coordination as was hypothesized in the terpy system.

Additionally, reducing the steric profile (as in ($^{i\text{Pr}}$PCP)PdMe (**9**)) resulted in enhanced reactivity under UV light, but AIBN still proved to be an ineffective initiator due to the undesired decomposition pathway leading to acetone, ($^{i\text{Pr}}$PCP)PdNCO (**10**), and ($^{i\text{Pr}}$PCP)PdCN (**11**).[9] This outcome suggests that ^{i}Pr groups may still be too bulky for O_2 coordination in the axial position. Work in this area can be continued by examining even less sterically encumbered ligands such as $^{\text{Me}}$PCP to further probe the reactivity of Pd-Me complexes with O_2. In addition, another graduate student is currently exploring other pincer ligands with reduced sterics such as 1,3-bis(2'-pyridylimino)isoindoline (BPI-H) (Chapter 3). Pd and Pt-Me complexes with this ligand have been found to react with O_2 and form the insertion products, Pd-OOMe and Pt-OOMe. Kinetic studies were undertaken and the reaction was found to proceed via the same radical chain mechanism found with (bpy)$PdMe_2$.[4,36] This work will help elucidate the requirements for O_2 activation, a critical step toward developing catalysts for aerobic oxidation of hydrocarbons.

2.6 Experimental

2.6.1 General Experimental:

Unless otherwise noted, all experiments and manipulations were performed under air-free conditions (standard high vacuum or Schlenk techniques under argon or nitrogen atmosphere, or in a nitrogen-filled glovebox). All glassware was oven dried or flame-dried prior to use. Both quartz and borosilicate J. Young NMR tubes were used for the photolysis reactions. The UV light sources were either a Hg/Xe arc lamp or a TLC multiband UV lamp. Reactions done in J. Young NMR tubes were degassed with 3 freeze, pump, thaw cycles before O_2 pressurization.

Oxygen gas was introduced to reactions in J. Young NMR tubes on a high-pressure gas manifold.[37] Toluene, dichloromethane, diethyl ether, and pentane were dried by passage through activated alumina and molecular sieves columns under a stream of argon. C_6D_6 was dried over Na^0/benzophenone or molecular sieves. Toluene-d_8 and THF-d_8 were dried over Na^0/benzophenone and vacuum-transferred prior to use. CD_3CN and CD_2Cl_2 were dried over CaH_2 and vacuum-transferred prior to use or over molecular sieves. ($^{t\text{Bu}}$PCP)PdMe (**6**),[38] ($^{t\text{Bu}}$PCP)PdOMe (**8**),[39] (TMEDA)$PdCl_2$,[40] (TMEDA)$PdMe_2$,[40] (TMEDA)PdMeCl,[40] (TMEDA)Pd($^{13}CH_3$)$_2$,[40] [($^{t\text{Bu}}$PNP)PdCl]Cl,[10] ($^{t\text{Bu}}$PNP*)PdCl (**4**),[10] ($^{t\text{Bu}}$PCP)PdOCO_2H (**7**),[41] ($^{t\text{Bu}}$PCP)PdOH,[42] ($^{i\text{Pr}}$PCP)PdCl,[43] ($^{i\text{Pr}}$PCP)PdMe (**9**),[44] ($^{i\text{Pr}}$PCP)PdOTf,[43,45] ($^{i\text{Pr}}$PCP)PdNCO (**10**),[45] were all synthesized according to literature procedures. All other reagents were used as received from commercial suppliers. NMR spectra were collected on Bruker AV300, AV301, DRX499, AV500, and AV700 spectrometers using 5mm medium-walled NMR tubes fitted with a J. Young Teflon valve. ^{1}H and ^{13}C{^{1}H} NMR spectra were referenced to residual protonated solvent signals. ^{31}P{^{1}H} NMR shifts were referenced to an 85% H_3PO_4 external standard. X-ray data was collected at -173 or -183 °C on a Bruker APEX II single crystal X-ray diffractometer using Mo-radiation.

2.6.2 Safety note on the handling of pressurized NMR tubes:

Caution should be exercised when handling pressurized J. Young NMR tubes and they should be transferred using secondary containment.

2.6.3 Synthesis and Characterization of Complexes:

[($^{t\text{Bu}}$PNP)PdMe]Cl (1): [($^{t\text{Bu}}$PNP)PdMe]Cl was synthesized via an adapted literature procedure.[10] A 25 mL round bottom flask fitted with a septum was charged with (TMEDA)PdMeCl (0.100 g, 0.367 mmol), $^{t\text{Bu}}$PNP (0.164 g, 0.414 mmol), and dichloromethane

(10 mL) in a nitrogen-filled glove box, resulting in a light yellow solution. The reaction mixture was then removed from the glove box and heated at 40 °C for 2 hours. The volatiles were removed under reduced pressure. The resulting yellow solid was washed with pentane (3 x 6 mL) to remove free TMEDA and dried under vacuum. Yield: 0.123 g (61%). The product was recrystallized by layering a saturated dichloromethane solution of **1** with pentane, resulting in white crystals. The crystals were washed with pentane and dried under vacuum.

$^{31}P\{^{1}H\}$ NMR (121 MHz, CD_2Cl_2): 55.19 (s). ^{1}H NMR (300 MHz, CD_2Cl_2): 0.84 (t, 3H, $^{3}J_{PH}$ = 5.18 Hz, Pd-CH_3), 1.36 (vt, 36H, $J \approx$ 7.30 Hz, C(CH_3)$_3$)), 3.79 (vt, 4H, $J \approx$ 3.81 Hz, CH_2-P), 7.67 (d, 2H, $^{3}J_{HH}$ = 7.86 Hz, PNP-aryl *H*), 7.92 (t, 1H, $^{3}J_{HH}$ = 8.06 Hz, PNP-aryl *H*).

[($^{t\mathrm{Bu}}$PNP)PdMe]SbF$_6$ (5): [($^{t\mathrm{Bu}}$PNP)PdMe]SbF$_6$ was synthesized via an adapted literature procedure.[10] A J. Young NMR tube was charged with [($^{t\mathrm{Bu}}$PNP)PdMe]Cl (10.5 mg, 0.019 mmol), $AgSbF_6$ (6.7 mg, 0.019 mmol), and dichloromethane-d_2 (0.4 mL) in a nitrogen-filled glove box with the light off. A white solid precipitated from the solution immediately. The reaction was stirred at room temperature in the dark for 30 minutes, after which the reaction was filtered into a new J. Young NMR tube, resulting in a yellow solution. The volatiles were removed under reduced pressure. The resulting yellow solid was dried overnight. Yield: 14.3 mg (100%).

$^{31}P\{^{1}H\}$ NMR (121 MHz, CD_2Cl_2): 55.02 (s). ^{1}H NMR (300 MHz, CD_2Cl_2): 0.86 (t, 3H, $^{3}J_{PH}$ = 5.4 Hz, Pd-CH_3), 1.35 (vt, 36H, $J \approx$ 7.2 Hz, C(CH_3)$_3$)), 3.66 (vt, 4H, $J \approx$ 3.7 Hz, CH_2-P), 7.48 (d, 2H, $^{3}J_{HH}$ = 7.8 Hz, PNP-aryl *H*), 7.85 (t, 1H, $^{3}J_{HH}$ = 7.9 Hz, PNP-aryl *H*).

^{t}Bu$_2$PH(O): A 10 mL Schlenk flask fitted with a septum was charged with (^{t}Bu)$_2$PCl (0.5 mL, 3 mmol) and dichloromethane in a nitrogen-filled glovebox. The reaction was removed from the

glovebox and cooled in an ice bath. Nitrogen-sparged H_2O (0.05 mL, 3 mmol) was slowly added to the cooled reaction solution via syringe while vigorously stirring. The reaction was allowed to warm to room temperature and stirred overnight. The solvent was removed under vacuum, resulting in a colorless oil. Yield: 0.4 g (100%).

$^{31}P\{^{1}H\}$ NMR (202 MHz, CD_3CN): 74.1 (broad s). ^{1}H NMR (500 MHz, CD_3CN): 1.30 (d, 18H, $^{3}J_{PH}$ = 16 Hz, C(C*H*$_3$)$_3$), 6.18 (d, 1H, $^{1}J_{PH}$ = 455Hz, P-*H*).[42]

(^{tBu}PNO)PdCl (3): A J.Young NMR tube was loaded with (^{tBu}PNP*)PdCl (**4**, 15.7 mg, 0.0293 mmol) and C_6D_6 (0.4 mL). The solution was degassed on the high vacuum line (by three freeze, pump, thaw cycles). The J. Young NMR tube was pressurized with 5 atm O_2 and stirred at room temperature under ambient light until reaction completion as indicated by NMR spectroscopy. The Pt product precipitated directly from the reaction solution. After the reaction reached completion (as observed via ^{1}H and ^{31}P NMR spectroscopy), the NMR tube was degassed on the high vacuum line (by three freeze, pump, thaw cycles). The solution was decanted off from the yellow precipitate. The solid was washed with benzene (0.4 mL x 4) and dried under vacuum. Yield = 5.9 mg (48%)

$^{31}P\{^{1}H\}$ NMR (121 MHz, CD_2Cl_2): 93.4 (s). ^{1}H NMR (300 MHz, CD_2Cl_2): 1.50 (d, 18H, $^{3}J_{PH}$ = 15.7 Hz, C(C*H*$_3$)$_3$), 3.51 (d, 2H, $^{2}J_{PH}$ = 10 Hz, C*H*$_2$-P), 7.62 (d, 1H, $^{3}J_{HH}$ = 7.7 Hz, PNP aryl-*H*), 7.94 (d, 1H, $^{3}J_{HH}$ = 7.6 Hz, PNP aryl-*H*), 8.04 (t, 1H, $^{3}J_{HH}$ = 7.8 Hz, PNP aryl-*H*). $^{13}C\{^{1}H\}$ NMR (126 MHz, CD_2Cl_2): 28.8 (d, $^{2}J_{PC}$ = 3.2 Hz, C(*C*H$_3$)$_3$), 35.1 (d, $^{1}J_{PC}$ = 25.6 Hz, *C*(CH$_3$)$_3$), 37.3 (d, $^{3}J_{PC}$ = 18.8 Hz, *C*H$_2$-P), 125.0 (d, $^{2}J_{PC}$= 11.5 Hz, *C*-aryl), 126.0 (s, *C*-aryl), 141.0 (s, *C*-aryl), 160.4 (s, *C*(O)$_2$).

$^{13}CH_3Li$: A 25 mL Schlenk flask fitted with a septum was charged with 1.7 cm Li wire in an

argon-filled glove box. The reaction was placed under an argon atmosphere on a Schlenk line and argon-sparged ether (5 mL) was added to the reaction flask. $^{13}CH_3I$ (0.4 mL, 6 mmol) was added dropwise to the reaction flask under an argon funnel. The reaction immediately turned to a yellow solution with a white precipitate. A few minutes later, the solution turned colorless with a white precipitate as the Li wire reacted. The reaction was stirred at room temperature for 1 hour. The solution was transferred into a 50 mL Schlenk flask under argon. The reaction flask was rinsed with argon-sparged ether (5 mL) and combined with the other ether solution. The solution was then filtered though a pipette with glass wool tightly packed. The solvent was removed under reduced pressure to yield a white powder. The product was dissolved in THF (10 mL) and titrated with 1-pyrene acetic acid to find the concentration of $^{13}CH_3Li$ as 0.28 M in THF.

^{1}H NMR (300 MHz, THF-d_8): 2.05 (d, 3H, J_{CH}= 98Hz). $^{13}C\{^1H\}$ NMR (75.47 MHz, THF-d_8): -15.10 (s).

(^{tBu}PCP)Pd($^{13}CH_3$) (6-^{13}C): Synthesis of (^{tBu}PCP)Pd($^{13}CH_3$) was based on a modified literature procedure for (^{tBu}PCP)PdMe.[38] A 10 mL Kontes valve flask was charged with (TMEDA)Pd($^{13}CH_3$)$_2$ (25.2 mg, 0.0989 mmol), (^{tBu}PCP)H (43.6 mg, 0.110 mmol), and benzene (5 mL). The reaction was stirred at room temperature for 3 days. The volatiles were removed under reduced pressure, resulting in a gray solid. The product was washed with cold pentane (3 x 4 mL) to remove excess ligand and dried under vacuum. Yield: 27.8 mg (54%).

$^{31}P\{^1H\}$ NMR (121 MHz, C_6D_6): 72.7 (d, J_{PC}= 10.6Hz). ^{1}H NMR (300 MHz, C_6D_6): 0.48 (dvt, 3H, $J \approx$ 4.8Hz, $J \approx$ 114Hz, Pd-$^{13}CH_3$), 1.23 (vt, 36H, $J \approx$ 6.4Hz, C(CH_3)$_3$), 3.31(vt, 4H, $J \approx$ 3.7Hz, CH_2-P), 6.97-7.09 (m, 3H, PCP aryl-*H*). $^{13}C\{^1H\}$ NMR (75.47 MHz, C_6D_6): -15.44 (t, J_{PC}= 10.5Hz).

2.6.4 Reactions of [(^{tBu}PNP)PdMe]Cl (1), (^{tBu}PCP)PdMe (6), and (^{iPr}PCP)PdMe (9) with O_2:

Representative Procedure of reaction of [(^{t}Bu PNP)PdMe]Cl (**1**), (^{t}Bu PCP)PdMe (**6**), or (^{i}Pr PCP)PdMe (**9**) with O_2

Thermal Reactions: A NMR tube fitted with a J. Young Teflon valve was charged with either **1**, **6**, or **9**, AIBN, hexamethylbenzene or hexamethyldisiloxane (internal standard), and C_6D_6 (0.4 mL). The NMR tube was degassed (by three freeze, pump, thaw cycles) and pressurized with 5 atm O_2. The NMR tube was heated to 65 °C in an aluminum sleeve submerged in the oil bath. At specified time intervals, the NMR tube was removed from the oil bath and examined by ^{1}H and ^{31}P NMR spectroscopy. After recording an NMR spectrum, the tube was placed back into the sleeve in the oil bath. This was repeated until the NMR spectra indicated the reaction was complete by full disappearance of starting material.

Photolysis Reactions: A borosilicate NMR tube fitted with a J. Young Teflon valve was charged with either **1**, **6**, or **9**, hexamethylbenzene or hexamethyldisiloxane (internal standard), and CD_3CN or C_6D_6 (0.4 mL). The NMR tube was degassed (by three freeze, pump, thaw cycles) and pressurized with 5 atm O_2. The NMR tube was placed in the path of UV light and covered with a dark cloth to exclude ambient light. At specified time intervals, the NMR tube was removed from the path of UV light and examined by ^{1}H and ^{31}P NMR spectroscopy. After recording an NMR spectrum, the tube was placed back into the path of UV light. This procedure was repeated until the NMR spectra indicated the reaction was complete by full disappearance of starting material.

Control Photolysis Reaction: A borosilicate NMR tube fitted with a J. Young Teflon valve was charged with either **1**, **6**, or **9**, hexamethylbenzene or hexamethyldisiloxane (internal standard), and CD_3CN or C_6D_6 (0.4 mL). The NMR tube was placed in the path of UV light and covered

with a dark cloth to exclude ambient light. At specified time intervals, the NMR tube was removed from the path of UV light and examined by ^{1}H and ^{31}P NMR spectroscopy. After recording an NMR spectrum, the tube was placed back into the path of UV light. This procedure was repeated until the NMR spectra indicated the reaction was complete by full disappearance of starting material.

2.6.5 ^{1}H and ^{31}P $\{^{1}H\}$ NMR spectra of reactions with [(^{tBu}PNP)PdMe]Cl (1) and (^{tBu}PNP)PdCl (4):*

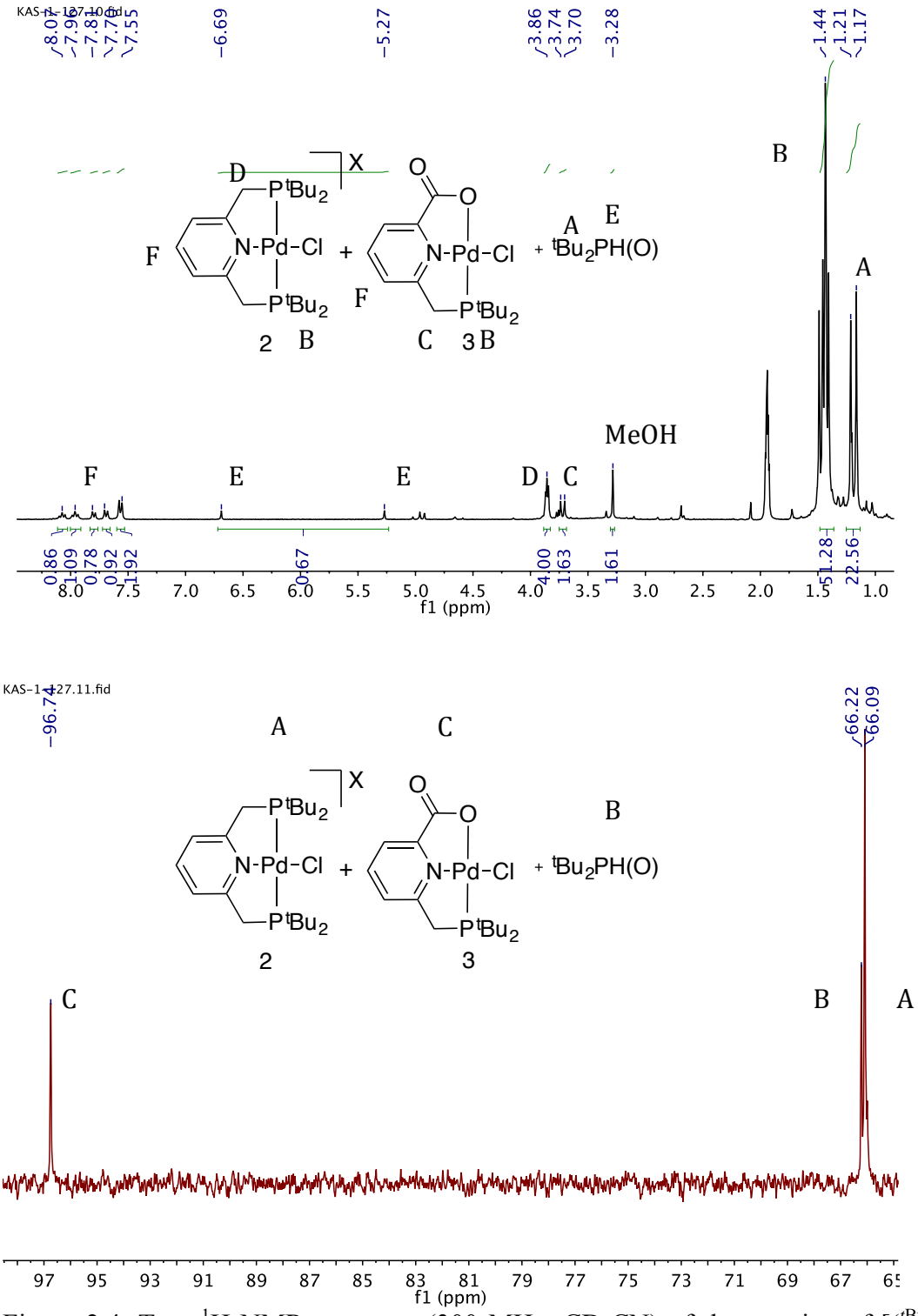

Figure 2.4. Top: ^{1}H NMR spectrum (300 MHz, CD_3CN) of the reaction of [(^{tBu}PNP)PdMe]Cl with O_2 and light after completion. Bottom: ^{31}P NMR spectrum (121 MHz, CD_3CN) of the corresponding reaction.

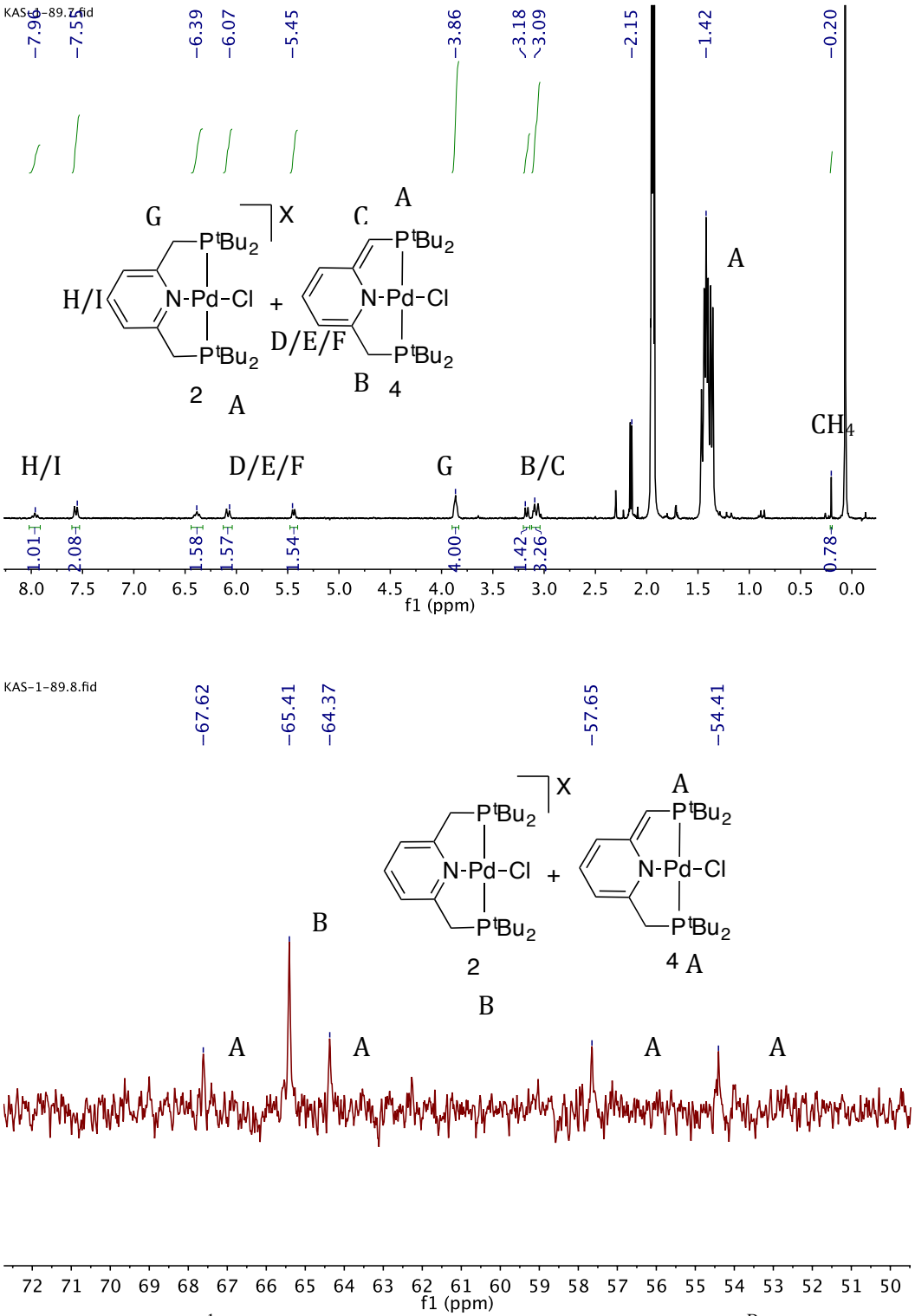

Figure 2.5. Top: ^{1}H NMR spectrum (300 MHz, CD3CN) of [($^{t\text{Bu}}$PNP)PdMe]Cl under an N_2 atmosphere in the path of UV light after completion. Bottom: ^{31}P NMR spectrum (121 MHz, CD_3CN) of the same reaction mixture. Internal standard: hexamethyldisiloxane.

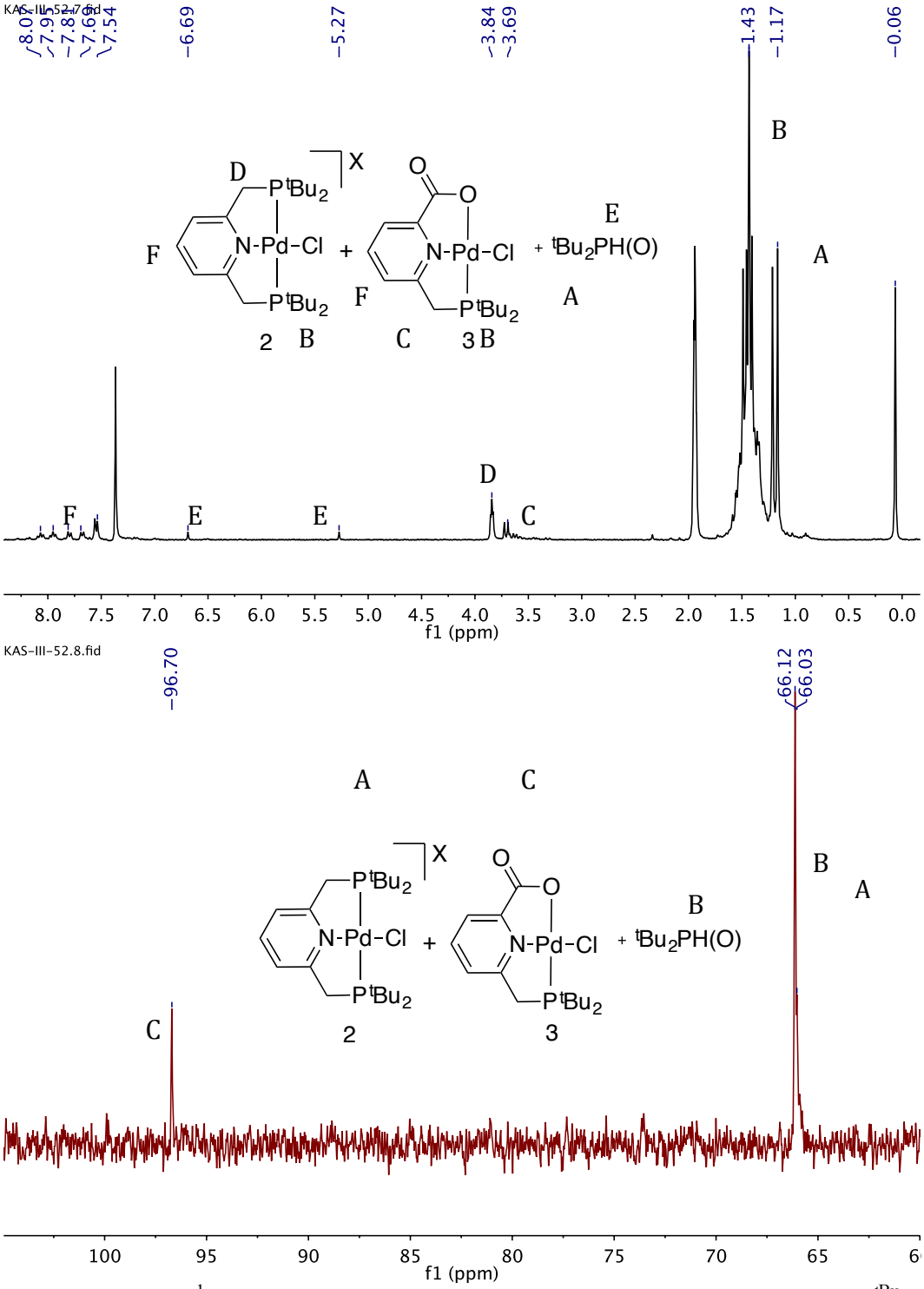

Figure 2.6. Top: ^{1}H NMR spectrum (300 MHz, CD_3CN) of the reaction of ($^{t\text{Bu}}$PNP*)PdCl with O_2 after reaction completion. Bottom: ^{31}P NMR spectrum (121 MHz, CD_3CN) of the same reaction mixture. Internal standard: Hexamethyldisiloxane.

2.6.6 ^{1}H, $^{31}P\ \{^{1}H\}$, and $^{13}C\ \{^{1}H\}$ NMR spectra of reactions with (^{tBu}PCP)PdMe (6) and (^{tBu}PCP)Pd($^{13}CH_3$) (6-^{13}C):

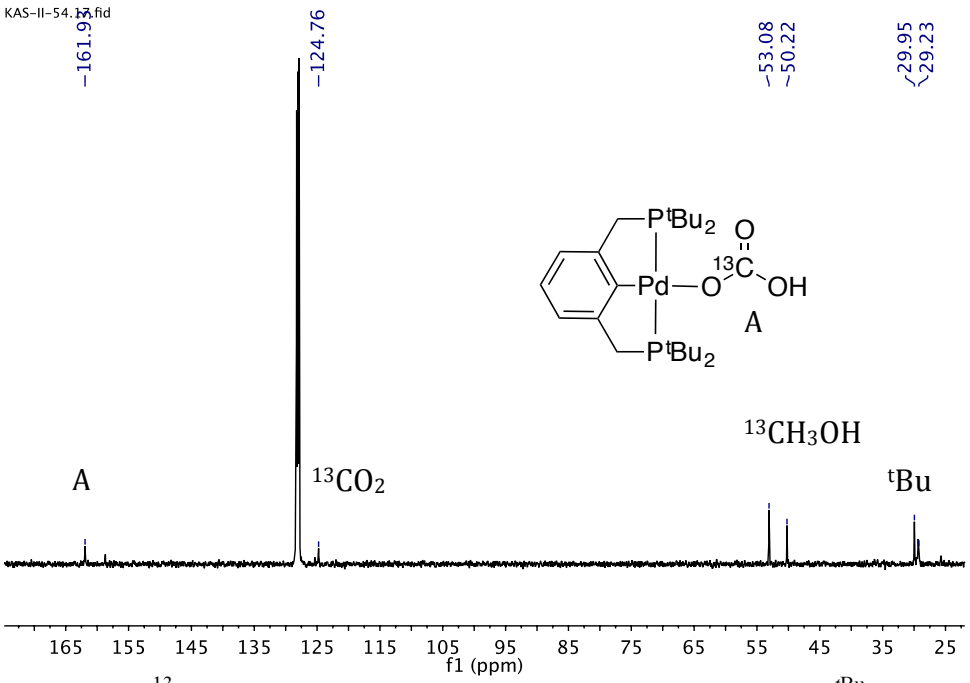

Figure 2.7. ^{13}C NMR spectrum (126 MHz, C_6D_6) of reaction of ($^{t\text{Bu}}$PCP)Pd($^{13}CH_3$) with O_2 under UV light after completion.

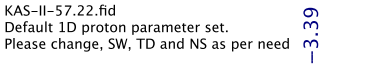

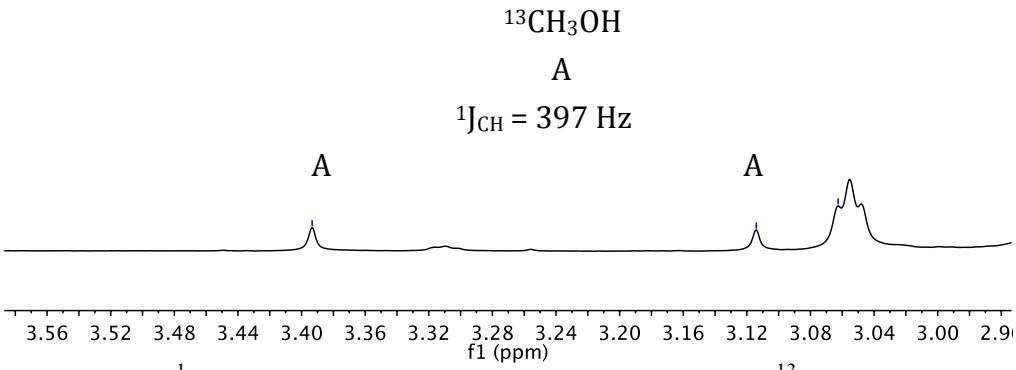

Figure 2.8. ^{1}H NMR spectrum (500 MHz, C_6D_6) of $^{13}CH_3OH$ region from reaction of ($^{t\text{Bu}}$PCP)Pd($^{13}CH_3$) with O_2 under UV light after completion.

2.6.7 GC-MS Traces and Analyses:

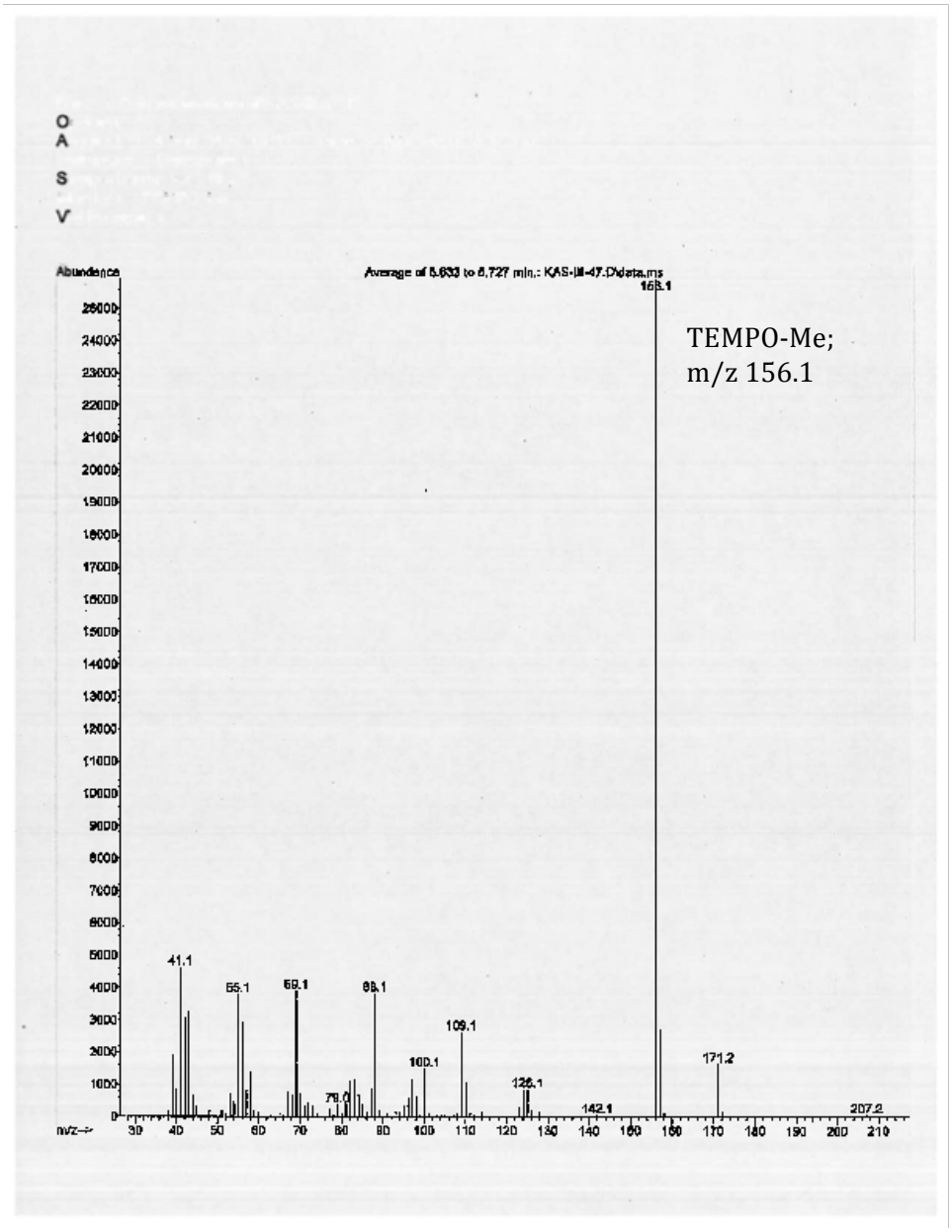

Figure 2.9. GC-MS analysis for detection of TEMPO-Me obtained from reaction of [($^{t\text{Bu}}$PNP)PdMe]Cl + TEMPO in UV light.

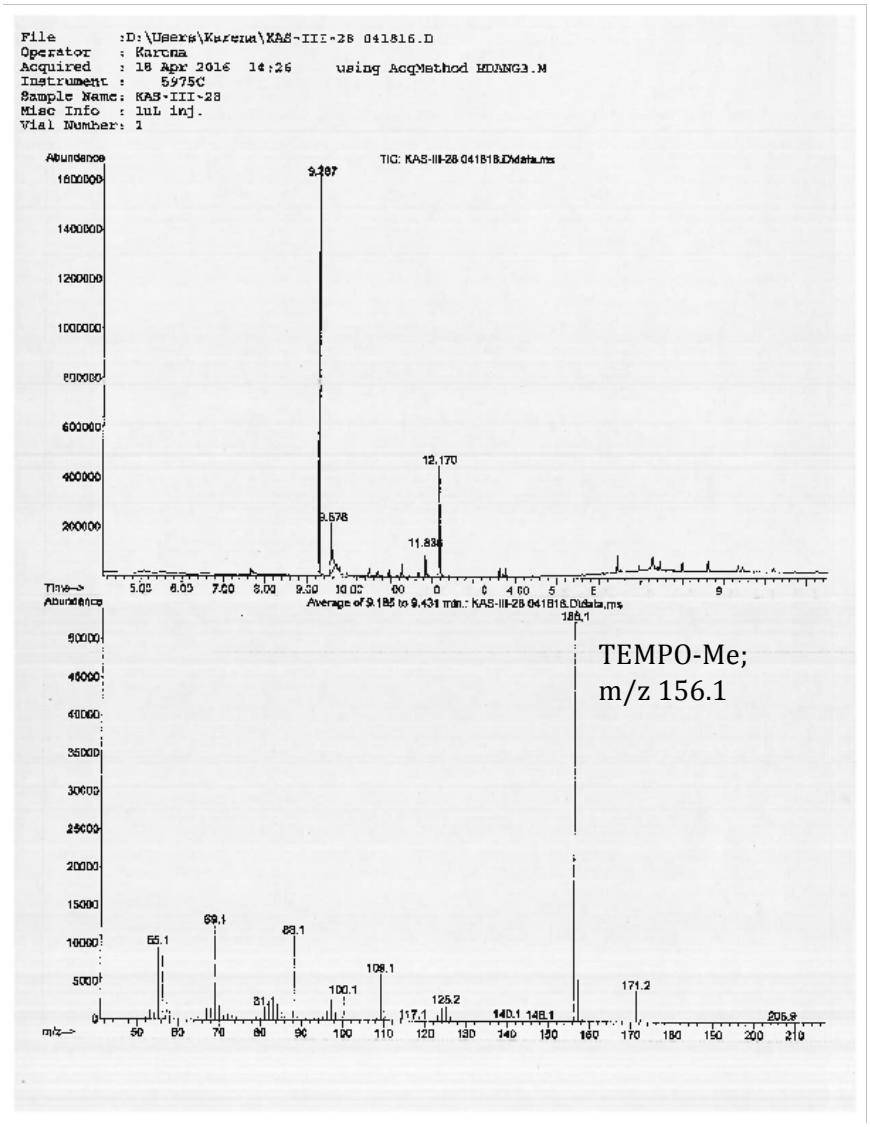

Figure 2.10. GC-MS analysis for detection of TEMPO-Me obtained from reaction of ($^{t\text{Bu}}$PCP)PdMe + TEMPO in UV light.

2.6.8 IR Spectra:

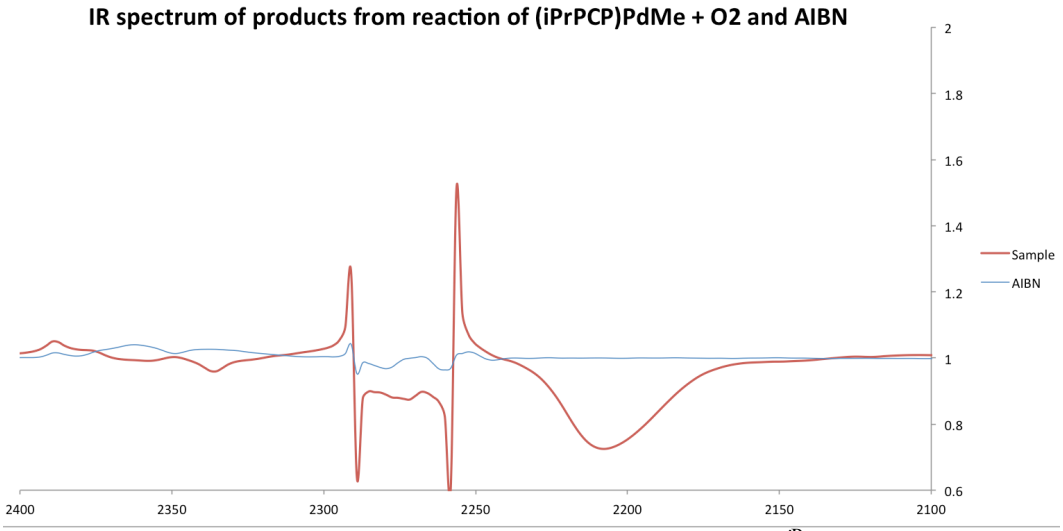

Figure 2.11. IR spectrum of product solution for reaction of (^{iPr}PCP)PdMe + O_2 with AIBN.

2.6.9 X-ray Crystallographic Methodology and Data Tables:

Occlusion free single crystals were mounted on a loop with oil. Data was collected at -173 °C and -180 °C on a Bruker APEX II single X-ray diffractometer, Mo-radiation. Crystal-to-detector distance was 40 mm and exposure times were 30 and 60 seconds per frame, depending on the crystal size (see Table 2.1). The scan width was 0.75° and 0.5°. The data was integrated and scaled using SAINT, SADABS within the APEX2 software package by Bruker.[47] Solution by direct methods (SHELXS, SIR97[48]) produced complete heavy atom phasing models consistent with the proposed structures. The structures were completed by difference Fourier synthesis with SHELXL97.[49,50] Scattering factors are from Waasmair and Kirfel.[51] Hydrogen atoms were placed in geometrically idealized positions and constrained to ride on their parent atoms with C---H distances in the range 0.95-1.00 Angstrom. Isotropic thermal parameters U_{eq} were fixed such that they were 1.2U_{eq} of their parent atom U_{eq} for CH' s and 1.5U_{eq} of their parent atom U_{eq} in case of methyl groups. All non-hydrogen atoms were refined anisotropically by full-matrix least squares. The data was slightly twinned for **3**, which was not completely resolvable. Thus some

residual electron density is still observed. Solvent analysis of **7** with SQUEEZE[52] discovered infinte channels along [1 0 1] filled with delocalized O_2.

Table 2.1. Crystallographic data for compounds **3** and **7**.

Complex	**3**	**7**
Empirical formula	$C_{15}H_{23}C_1NO_2PPd$	$C_{25}H_{44}O_3P_2Pd$
Formula weight	422.16	560.94
Temperature (K)	90(2)	105(2)
Wavelength (Å)	0.71073	0.71073
Crystal system	Monoclinic	Monoclinic
Space group	P 2_1/c	P 2_1/n
Unit cell axis a (Å)	10.1012(9)	12.2751(7)
Unit cell axis b (Å)	7.9912(7)	15.1747(10)
Unit cell axis c (Å)	21.0452(19)	16.0414(10)
Unit cell angle α (°)	90	90
Unit cell angle β (°)	92.170(5)	106.188(3)
Unit cell angle γ (°)	90	90
Volume ($Å^3$)	1697.6(3)	2869.6(3)
Z	4	4
Density (Mg/m^3), calculated	1.652	1.298
Absorption coefficient (mm^{-1})	1.348	0.780
F(000)	856	1176
Crystal size (mm^3)	0.30 x 0.08 x 0.01	0.03 x 0.02 x 0.01
Theta range for data collection	2.02 to 26.62°	2.29 to 26.43°
Index ranges	-12<=h<=12, -10<=k<=10, -26<=l<=26	-15<=h<=15, -18<=k<=18, -19<=l<=20
Reflections collected	48729	33962
Independent reflections, R(int)	3531, 0.0779	5881, 0.1102
Completeness to theta = 25.00 (%)	98.7	99.6
Max. and min. Transmission	0.9866 and 0.6879	0.9922 and 0.9770
Data / restraints / parameters	3531 / 0 / 167	5881 / 0 / 293
Goodness-of-fit on F^2	1.203	0.934
Final R indices [I>2sigma(I)]	R1 = 0.0964, wR2 = 0.2128	R1 = 0.0479, wR2 = 0.0839
R indices (all data)	R1 = 0.1071, wR2 = 0.2180	R1 = 0.0909, wR2 = 0.0952
Largest diff. peak and hole ($e.Å^{-3}$)	5.135 and -2.357	0.544 and -0.417

2.7 Notes and References to Chapter 2

1. a) Lersch, M.; Tilset, M. *Chem. Rev.* **2005**, *105*, 2471-2526. b) Neufeldt, S.R.; Sanford, M.S. *Acc. Chem. Res.* **2012**, *45*, 936-946.
2. Scheuermann, M.L.; Goldberg, K.I. *Chem.- Eur. J.* **2014**, *20*, 14556-14568.
3. Boisvert, L.; Goldberg, K.I. *Acc. Chem. Res.* **2012**, *45*, 899-910.
4. Boisvert, L.; Denney, M.C.; Hanson, S.K.; Goldberg, K.I. *J. Am. Chem. Soc.* **2009**, *131*, 15802-15814.
5. Grice, K.A.; Goldberg, K.I. *Organometallics* **2009**, *28*, 953-955.
6. Petersen, A.R.; Taylor, R.A.; Vicente-Hernandez, I.; Mallender, P.R.; Olley, H.; White, A.J.P.; Britovsek, G.J.P. *J. Am. Chem. Soc.* **2014**, *136*, 14089-14099.
7. Fernandez-Alvarez, V.M.; Ho, S.K.Y.; Britovsek, G.J.P.; Maseras, F. DOI: 10.1039/c8sc01161c.
8. Guan, Z.; Combes, J.R.; Menceloglu, Y.Z.; DeSimone, J.M. *Macromolecules* **1993**, *26*, 2663-2669.
9. Wenzel, T.T. *Stud. Surf. Sci. Catal.* **1991**, *66*, 545-554.
10. Feller, M.; Ben-Air, E.; Iron, M.A.; Diskin-Posner, Y.; Leitus, G.; Shimon, L.J.; Konstantinovski, L.; Milstein, D. *Inorg. Chem.* **2010**, *49*, 1615-1625.
11. The symmetrical ligand signals associated with **2** increased relative to an internal standard and shifted downfield by 0.03 ppm upon addition of [($^{t\text{Bu}}$PNP)PdCl]Cl. This slight shift is associated with a difference in counter ions. The identity of the counterion X is unknown, but it is hypothesized to be OH^- from adventitious water or t-Bu_2PO^-, depending on the experiment.
12. No other oxidation products were observed by ^{1}H NMR spectroscopy.
13. Photolytic homolytic cleavage of Pd-C bonds: a) Fafard, C.M.; Adhikari, D.; Foxman, B.M.; Midiola, D.J.; Ozerov, O.V. *J. Am. Chem. Soc.* **2007**, *129*, 10318-10319. b) Burns, C.T.; Shen, H.; Jordan, R.F. *J. Organomet. Chem.* **2003**, *683*, 240-248. c) Van Leeuwen, P.W.N.M.; Roobeek, C.F.; Huis, R. *J. Organomet. Chem.* **1977**, *142*, 233-241.
14. Khusnutdinova, J.R.; Rath, N.P.; Mirica, L.M. *J. Am. Chem. Soc.* **2010**, *132*, 7303-7305.
15. Hoey, G.R.; Kutschke, K.O. *Can. J. Chem.* **1955**, *33*, 496-506.
16. Hoare, D.E.; Walsh, A.D. *Trans. Faraday Soc.* **1957**, *53*, 1102-1110.
17. Hanst, P.L.; Calvert, J.G. *J. Phys. Chem.* **1959**, *63*, 71-77.
18. Bell, E.R.; Raley, J.H.; Rust, F.R.; Seubold, F.H.; Vaughan, W.E. *Discuss. Faraday Soc.* **1951**, *10*, 242-249.
19. a) Weiss, M.C.; Goedken, V.L. *J. Am. Chem. Soc.* **1976**, *98*, 3389-3392. b) Yokota, S.; Tachi, Y.; Itoh, S. *Inorg. Chem.* **2002**, *41*, 1342-1344. c) Scheuermann, M.L.; Luedtke, A.T.; Hanson, S.K.; Fekl, U.; Kaminsky, W.; Goldberg, K.I. *Organometallics* **2013**, *32*, 4752-4758.
20. Grau, M.; Kyriacou, A.; Cabedo Martinez, F.; de Wispelaere, I.M.; White, A.J.P.; Britovsek, G.J.P. *Dalton Trans.* **2014**, *43*, 17108-17119.
21. Denney, M.C.; Smythe, N.A.; Cetto, K.L.; Kemp, R.A.; Goldberg, K.I. *J. Am. Chem. Soc.* **2006**, *128*, 2508-2509.
22. A C_6D_6 solution of **6** with AIBN at 60 °C without O_2 results in thermal decomposition of AIBN but no change to **6**. Additionally, a C_6D_6 solution of AIBN and O_2 (1 atm) at 65 °C results only in decomposition of AIBN. Therefore, the products observed require the prescence of **6**, AIBN, and O_2 together.

23. The yield of ($^{t\text{Bu}}$PCP)PdOCO_2H varied depending on the light source used. When using the Hg/Xe arc lamp, more decomposition to Pd(0) occurred and a lower % yield of product was obtained. Using the TLC lamp (254 nm) resulted in less decomposition and higher % yield of product.
24. The reaction was done on the Bagley rooftop to maximize sunlight exposure.
25. Johansson, R.; Jarenmark, M.; Wendt, O.F. *Organometallics* **2005**, *24*, 4500-4502.
26. Fulmer, G.R.; Miller, A.J.M.; Sherden, N.H.; Gottlieb, H.E.; Nudelman, A.; Stoltz, B.M.; Bercaw, J.E.; Goldberg, K.I. *Organometallics* **2010**, *29*, 2176-2179.
27. One hypothesis is the formation of methyl formate where the expected $–CH_3$ signal would appear at 53 ppm in the ^{13}C NMR spectrum.
28. Pecul, M.; Helgaker, T. *Int. J. Mol. Sci.* **2003**, *4*, 143-157.
29. Kim, J.S.; Reibenspies, J.H.; Darensbourg, M.Y. *J. Am. Chem. Soc.* **1996**, *118*, 4115-4123.
30. Raley, J.H.; Porter, L.M.; Rust, F.F.; Vaughan, W.E. *J. Am. Chem. Soc.* **1951**, *73*, 15-17.
31. It is possible that adventitious water contributes to the formation of products such as **7** and methanol. Adding water to the reaction of **6** with O_2 in UV light yielded a comparable amount of **7** (47 % yield) and an increase in methanol (31 % yield). The addition of polyvinylpyridine (as a proton scavenger) to the reaction resulted in decreased yield of **7** (25 % yield) but a similar amount of methanol (12 % yield).
32. Goldberg, J.M.; Wong, G.W.; Brastow, K.E.; Kaminsky, W.; Goldberg, K.I.; Heinekey, D.M. *Organometallics* **2015**, *34*, 753-762.
33. A C_6D_6 solution of **9** at 60 °C results in slight decomposition (12 %) over 10 days. A C_6D_6 solution of **9** with AIBN at 60 °C without O_2 results in thermal decomposition to AIBN and slight decomposition of **9** but no new products grow in. Additionally, a C_6D_6 solution of **9** and O_2 at 60 °C results in decomposition of **9** over ca. 7 days but no distinct new products grow in.
34. Independent synthesis of **11** was not attempted due to the dangers of cyanide reagents.
35. Boro, B.J. Ph.D Dissertation. University of New Mexico, 2009.
36. Hannah Zeitler, *manuscript in preparation* (unpublished results)
37. Fulmer, G.R.; Herndon, A.N.; Kaminsky, W.; Kemp, R.A.; Goldberg, K.I. *J. Am. Chem. Soc.* **2011**, *133*, 17713-17726.
38. Johnson, M.T.; Johansson, R.; Kondrashov, M.V.; Steyl, G.; Ahlquist, M.S.G.; Roodt, A.; Wendt, O.F. *Organometallics* **2010**, *29*, 3521-3529.
39. Fulmer, G.R.; Muller, R.P.; Kemp, R.A.; Goldberg, K.I. *J. Am. Chem. Soc.* **2009**, *131*, 1346-1347.
40. Byers, P.K.; Canty, A.J.; Jin, H.; Kruis, D.; Markies, B.A.; Boersma, J.; Koten, G.V. *Inorg. Synth.* **1998**, *32*, 167-168.
41. Johansson, R.; Wendt, O.F. *Organometallics* **2007**, *26*, 2426-2430.
42. Campora, J.; Palma, P.; del Rio, D.; Alvarez, E. *Organometallics* **2004**, *23*, 1652-1655.
43. Frech, C.M.; Shimon, L.J.W.; Milstein, D. *Angew. Chem. Int. Ed.* **2005**, *44*, 1709-1711.
44. Kraatz, H-B.; Van der Boom, M.E.; Ben-David, Y.; Milstein, D. *Israel J. Chem.* **2001**, *41*, 163-171.
45. Lee, H.J.; Lee, S.H.; Kim, H.C.; Lee, Y.E.; Park, S. *J. Organo. Chem.* **2012**, *717*, 164-171.
46. Farrugia, L.J. *J. Appl. Cryst.* **2012**, *45*, 849-854.

47. Bruker (2007), APEX2 (version 2.1-4), SAINT (version 7-34A), SADABS (version 2007/4), Bruker AXS Inc, Madison, Wisconsin, USA.
48. a) Altomare, A.; Burla, C.; Camalli, M.; Cascarano, G.L.; Giacovazzo, C.; Guagliardi, A.; Moliterni, A.G.G.; Polidori, G.; Spagna, R. *J. Appl. Cryst.* **1999**, *32*, 115-119. b) Altomare, A.; Cascarano, G.L.; Giacovazzo, C.; Guagliard, A. *J. Appl. Cryst.* **1993**, *26*, 343-350.
49. Sheldrick, G.M. (1997) SHELXL-97, Program for the refinement of crystal structures. University of Gottingen, Germany.
50. MacKay,S.; Edwards, C.; Henderson, A.; Gilmore, C.; Stewart, N.; Shankland, K.; Donald, A. (1997) MaXus: a computer program for the solution and refinement of crystal structures from diffraction data. University of Glasgow, Scotland.
51. Waasmaier, D.; Kirfel, A. *Acta, Crystallographica A.* **1995**, *51*, 416-430.
52. a) Spek, A.L. *Appl. Cryst.* **2003**, *36*, 7-13. b) van der Sluis, P.; Spek, A.L. *Acta. Cryst.* **1990**, *A46*, 194-201.

Chapter 3

Synthesis and Characterization of a Series of 1,3-bis(arylimino)isoindoline ligands

3.1 Introduction

The reactivity of transition metal complexes is greatly influenced by the ligands bound to the metal center.[1] Pincer ligands, tridentate ligands that are typically bound in a meridional fashion, have been extensively explored in transition metal coordination chemistry and organometallic chemistry for a variety of transformations.[2] Pincer ligands are of particular interest because many of them are easily synthesized, are highly modular, and their electronic, steric, and physical properties can be readily modified without significantly affecting the coordination geometry.[2,3] One such pincer ligand family is based on the 1,3-bis(arylamino)isoindoline (^{R}BPI-H, R= varying substituents) motif. In addition to the attributed mentioned above, 1,3-bis(arylamino)isoindoline ligands are also O_2 and functional group tolerant, making them ideal for potential use in aerobic alkane dehydrogenation.[3,7-11]

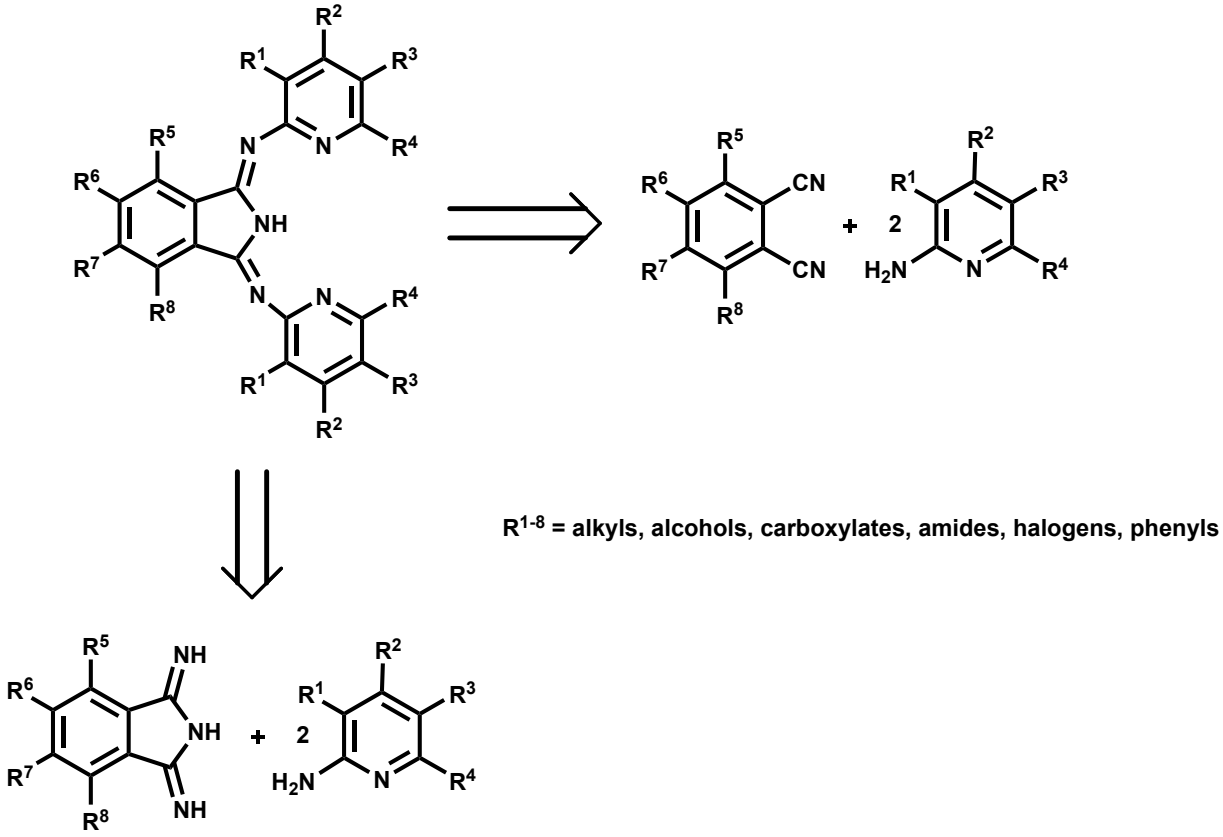

Scheme 3.1. General retrosynthesis of BPI-H variations previously synthesized

The parent 1,3-bis(2-pyridylimino)isoindoline was first synthesized in 1952 by Linstead and coworkers via a diimine intermediate.[4] A year later, Linstead and coworkers prepared the parent 1,3-bis(2-pyridylimino)isoindoline directly from phthalonitrile and 2-aminopyridine in a single step.[5] Siegl has since optimized the synthesis of the parent isoindoline and prepared a variety of other 1,3-bis(arylimino)isoindoline ligands with different substituents around the pyridine ring and the aryl backbone.[6] Scheme 3.1 shows the general synthesis of 1,3-bis(arylimino)isoindoline ligands and indicates the positions that can be modified to accomodate a variety of functional groups including alkyls, alcohols, carboxylates, and amides. Since their discovery, variations of the ^{R}BPI-H ligand framework have been used in both stoichiometric and catalytic organic transformations including hydroxylation, epoxidation, and hydrosilylation.[3,7-11]

The modifications made to the BPI-H framework can have a significant impact on the reactivity observed. For example, Szymczak and coworkers have synthesized a (^{OH}BPI)Ru complex for use in H_2 cleavage.[10a] They found that hydrogen bonding with the –OH group helped promote heterolytic H_2 cleavage across the metal center and ligand. Gade has synthesized BPI-H ligands with linker units that can be used to attach to surfaces and in this way, the researchers can combine the virtues of homogeneous and heterogeneous catalysis.[12] Herein, we report the synthesis and characterization of a variety of known and novel ^{R}BPI-H ligands for use in aerobic alkane dehydrogenation studies.

3.2 Synthesis and Characterization of ^{R}BPI-H ligands

3.2.1 General synthesis of ^{R}BPI-H ligand variations

The syntheses of all ^{R}BPI-H variations investigated are summarized in Scheme 3.2. Each ligand was prepared using the optimized reaction conditions previously reported by Siegl.[6] In the synthesis, phthalonitrile is treated with 2 equivalents of the corresponding aminopyridine to produce ligands **12**-**17**. There are certain characteristics required for good yields of these ligands. First, alcohols, such as 1-hexanol and 1-butanol, are the preferred solvents.[6] Secondly, alkaline earth salts, such as $CaCl_2$, are required in catalytic quantities. It is hypothesized that the metal ion of the Lewis acid interacts with the nitrile of phthalonitrile, resulting in a polarized C-N bond that is activated toward nucleophilic attack.[6] Finally, the choice of amine affects reactivity; electron-withdrawing amines and amino heterocycles are less reactive substrates, suggesting that more electron-donating and nucleophilic amines are more reactive.[6] The reported reactivity suggests that the mechanism is stepwise, where one equivalent of amine reacts with phthalonitrile in an intramolecular cyclization followed by addition of the second amine to form the parent 1,3-bis(arylimino)isoindoline. Ligands **12**, **13**, **15**, and **16** and an analog of **17** have

been previously published; however, the syntheses have been modified for some systems, as reported below. 1,3-bis[2-(6-methoxypyridyl)imino]isoindoline (^{OMe}BPI-H, **14**) is a new BPI-H derivative. Each ^{R}BPI-H ligand has been fully characterized by NMR spectroscopy (^{1}H, ^{13}C, HMQC, HMBC) and X-ray crystallography.

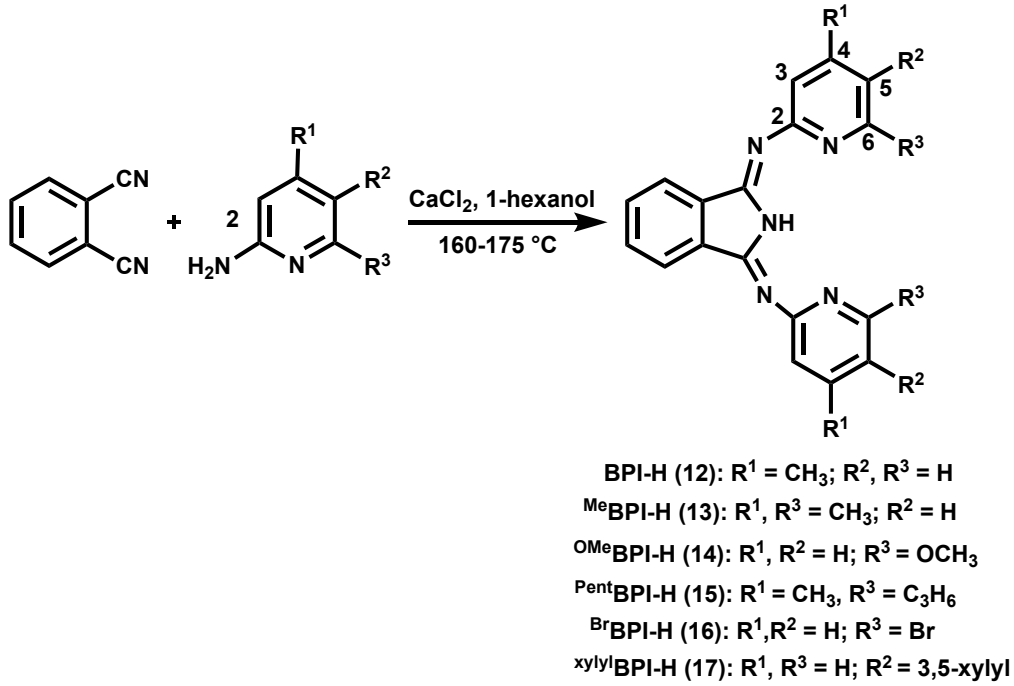

Scheme 3.2. General synthesis of ^{R}BPI-H ligands 12-17

*3.2.2 Synthesis and characterization of BPI-H (**12**)*

1,3-bis[2-(4-methylpyridyl)imino]isoindoline (BPI-H, **12**) was one of the first synthesized BPI variations.[3-6] Preparation of **12** involves heating phthalonitrile and 2-amino-4-methylpyridine to reflux in 1-hexanol for 48 hours. Complex **12** was then isolated as a green solid in 38% yield after workup. The ^{1}H NMR spectrum of **12** features a singlet at 2.40 ppm (C*H*$_3$, 6H) and 5 signals between 6.5-9.0 ppm (Ar-*H*, for full assignment see experimental below). The N-H proton appears as a broad singlet at 13.9 ppm. X-ray quality crystals were grown from vapor diffusion of pentane into a solution of **12** in CH_2Cl_2 at -20 °C. The solid-state

molecular structure is shown in Figure 3.1. The ligand backbone is planar, and both pyridine arms slightly bend out of the plane with torsion angles of 12.9 (3)° and 29.5 (3)°. The space-filling model shows that the ligand pocket is relatively unhindered (Table 3.4). The percent volume buried provides a more quantitative comparison of the steric environment around the ligand binding pocket.[13] This measure was developed for analyzing the binding catalytic pocket on any complex.[13] BPI-H has 59% volume buried.[14] The higher % volume buried, the more sterically hindered the binding pocket is and less likely to be able to accommodate a metal in the binding pocket (Chapter 4 discusses the metalation of ^{R}BPI-H ligands).

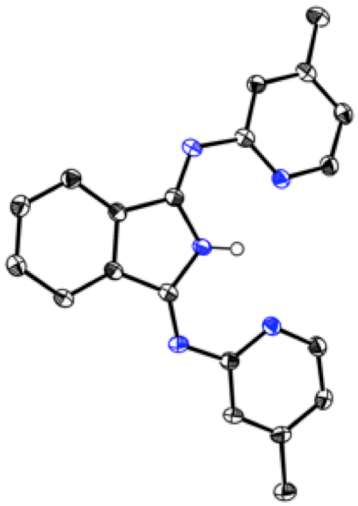

Figure 3.1. ORTEP[43] drawing of 12 with thermal ellipsoids at 50% probability. Hydrogen atoms excluded for clarity.

*3.2.3 Synthesis and characterization of ^{Me}BPI-H (**13**)*

1,3-bis[2-(4,6-dimethylpyridyl)imino]isoindoline (^{Me}BPI-H, **13**) has also been previously synthesized,[6] but never fully characterized by NMR spectroscopy and X-ray crystallography. The preparation of **13** involves heating phthalonitrile and 2-amino-4,6-dimethylpyridine to reflux in 1-hexanol for 48 hours. Complex **13** was then isolated as an orange solid in 50% yield after workup. The ^{1}H NMR spectrum of **13** features two singlets at 2.33 and 2.48 ppm for the two inequivalent methyl groups and four aryl signals between 6.5-8 ppm, respectively (for full assignment see experimental section below). The N-H proton appears as a broad singlet at 12.3 ppm. X-ray quality crystals were grown from vapor diffusion of pentane into a CH_2Cl_2 solution of **13** at -20 °C. The solid-state molecular structure is shown in Figure 3.2. The ligand backbone

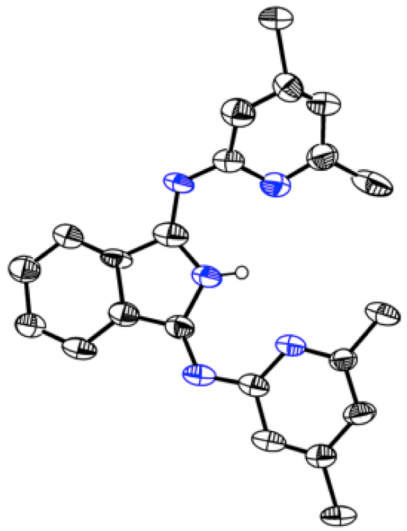

Figure 3.2. ORTEP[43] drawing of 13 with thermal ellipsoids at 50% probability. Hydrogen atoms excluded for clarity.

and one pyridine arm are coplanar, and the other pyridine arm is puckered out of the plane with a torsion angle of 14(3)°. This pucker is likely to prevent steric clashing of the methyl groups on the 6 positions of the pyridine rings. Unlike **12**, a space-filling model shows that the ligand pocket is relatively hindered (Table 3.4). Compound **13** has a % volume buried of 64.8, which suggests the binding pocket is more hindered then **12** and metalation of this ligand may be difficult.[13,14]

*3.2.4 Synthesis and characterization of ^{OMe}BPI-H (**14**)*

1,3-bis[2-(6-methoxypyridyl)imino]isoindoline (^{OMe}BPI-H, **14**) is a novel ^{R}BPI-H ligand derivative. The multi-step synthetic procedure is shown in Scheme 3.2. In the first step, 2-bromo-6-methoxy pyridine (**19**) is synthesized from 2,6-dibromopyridine (**18**) by nucleophilic displacement.[15] 2-bromo-6-methoxy pyridine (**19**) is converted to 6-methoxy-2-pyrdinamine (**20**) in the second step via amination.[16] This C-N coupling procedure is one of the few examples that uses a cheap copper (I) catalyst and aqueous ammonia as the nitrogen source. Elmkadden *et. al.* found that these reaction conditions were successful for a variety of aminopyridine derivatives with both electron withdrawing and donating groups under mild conditions.[16] In the final step, phthalonitrile and 2-bromo-6-methoxy pyridine (**20**) are refluxed for 48 hours. Complex **14** is then isolated as a dark green solid after workup (Scheme 3.2 and 3.3).

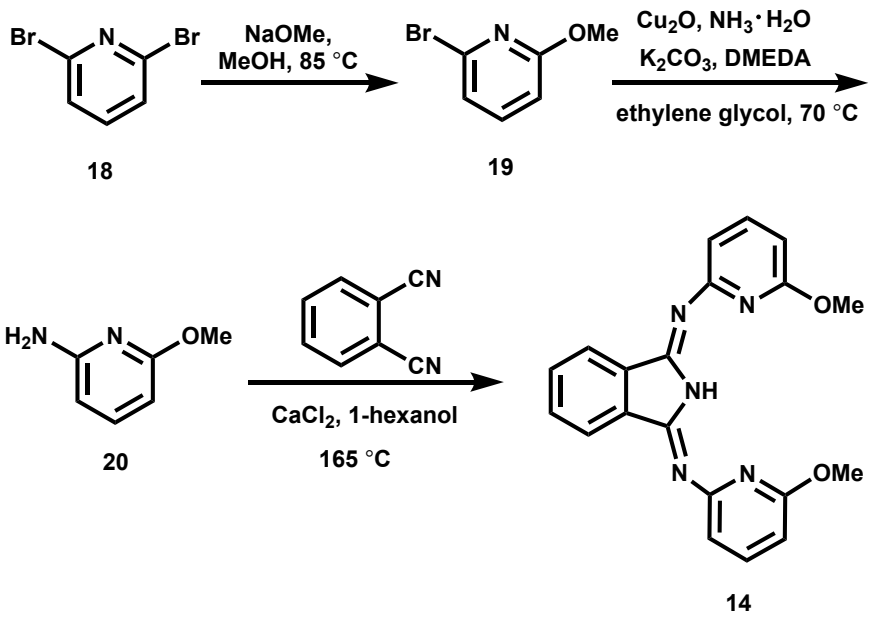

Scheme 3.3. Synthetic procedure devised for the synthesis of ^{OMe}BPI-H(14)

Novel ligand **14** was fully characterized by NMR spectroscopy and X-ray crystallography. The ^{1}H NMR spectrum of **14** features the diagnostic methoxy singlet at 3.65 ppm. The 5 aryl signals appear between 6.5-8.10 ppm (for full assignment see experimental section below). The N-H proton appears as a broad singlet at 11.6 ppm. X-ray quality crystals were grown from slow evaporation of CH_2Cl_2 at room temperature, and the solid-state molecular structure is shown in Figure 3.3. The ligand backbone is planar, and the pyridine arms are bent out the plane with torsion angles of 1.8 (2)° and 54.9 (2)°, respectively. One pyridine arm is significantly bent out of the plane to prevent steric clashing of the methoxy groups. A space-filling model shows that **14**, as

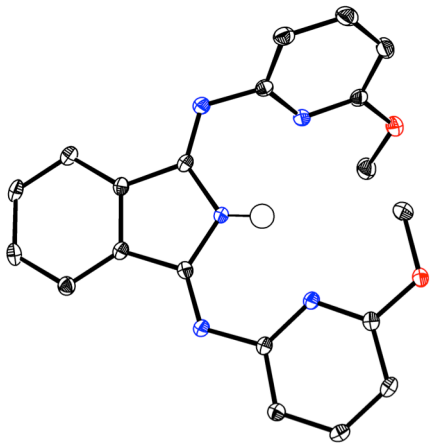

Figure 3.3. ORTEP[43] drawing of 14 with thermal ellipsoids at 50% probability. Hydrogen atoms excluded for clarity.

crystallized, has an even more hindered binding pocket, relative to **13** (Table 3.4). Compound **14** has a % volume buried of 71.9.[13,14] This suggests that this ligand is the most sterically hindered compared to **12** and **13**, and has even less available space to bind a metal.

*3.2.5 Synthesis and characterization of ^{Pent}BPI-H (**15**)*

1,3-bis[2-(4-methyl-5-cyclopentapyridyl)imino]isoindoline (^{Pent}BPI-H, **15**) was previously synthesized by Gade and coworkers via a 3-step procedure (Scheme 3.4).[9] In the first step, pyridone, **21**,[17] is converted to penttriflate, **22**, by reaction with triflic anhydride. This step is facile and **22** was isolated as a yellow oil in 81% yield. The second step involves displacement of the triflate via Buchwald-Hartwig amination. To do this, Gade and coworkers use benzophenone as the nitrogen source and a palladium acetate catalyst.[9] Unfortunately, reproducing the synthesis of pentamine, **23**, with this reported procedure was unsuccessful and resulted only in unreacted starting material. As a result, a slightly modified procedure was envisioned as shown in Scheme 3.4. In this synthetic strategy, the same key pentamine intermediate, **23**, was targeted, but the precursor to it includes any halogenated or pseudo-halogenated precursor accessible. Challenges were encountered in the preparation of **24** and **25**. However, from **26**, Buchwald-Hartwig amination conditions were optimized to reach **23**. Finally, BPI ligand **15** was accessed using the standard reaction with phthalonitrile in 1-hexanol.

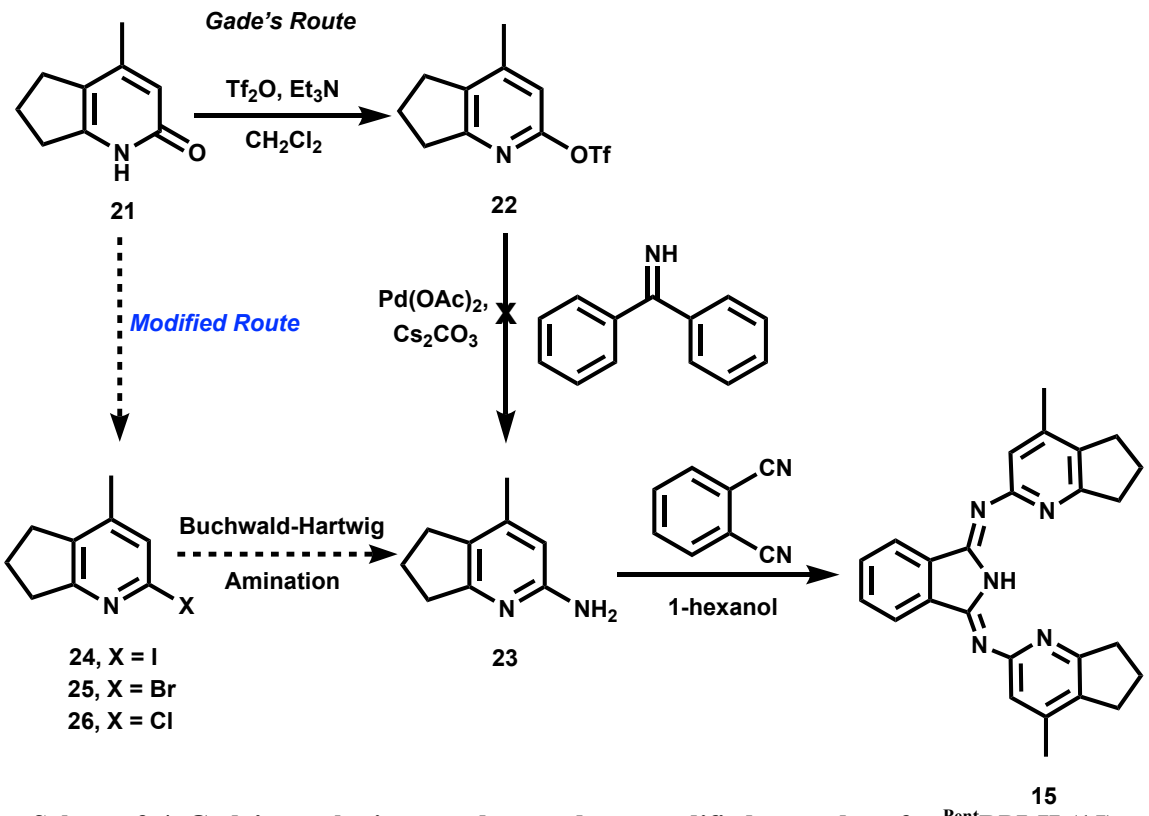

Scheme 3.4. Gade's synthetic procedure and our modified procedure for ^{Pent}BPI-H (15)

The synthesis of halogenated pyridines, **24**, **25**, and **26** was first explored (Step 1, Scheme 3.4). Preparation of iodopyridine, **24**, was first attempted because it is hypothesized to be the most reactive intermediate for the following amination step. Indeed, iodopyridines have been shown to participate in C-N Buchwald-Hartwig coupling reactions.[18] Although iodopyridines are important intermediates for a variety of organic reactions,[19] we were only able to find one report of a direct method for the iodination of hydroxypyridines.[20] In 2009, Maloney and coworkers reported a procedure for the one-pot iodination of hydroxypyridines tolerant to a variety of functional groups. In their one-pot protocol, hydroxypyridine is first activated by reaction with sulfonic anhydride followed by reaction with sodium iodide.[20] The reported conditions were applied to the synthesis of **24** (Scheme 3.5). Unfortunately, **24** was never isolated, but instead the

intermediate penttriflate **22** was recovered. It appears these conditions were not sufficient to activate **21** to **24**, likely a result of the electron-donating groups. Indeed, it was found that pyridines with electron-withdrawing groups were more labile toward activation and iodination. However, substrates without substituents or with electron-donating groups were found to react more slowly.[20]

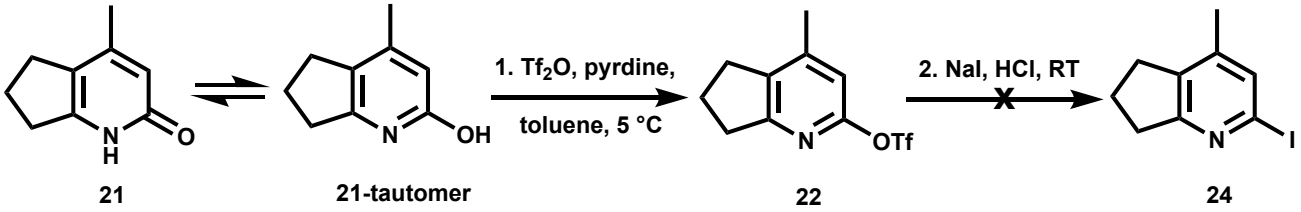

Scheme 3.5. Attempted synthesis of 24 via Maloney's synthetic procedure

We next turned our attention to bromopyridine **25** since we hypothesized it would be the second reactive precursor for the subsequent amination. Indeed, a comparison of aryl-bromide bond dissociation energy (BDE) vs. aryl-chloride BDE shows that aryl-bromide bonds are weaker (81 vs 96 kcal/mol, respectively).[21] Furthermore, unlike iodopyridine, there are many reports for the direct synthesis of bromopyridines from hydroxypyridines.[20,22-27] Based on these literature reports, a variety of conditions were explored for the formation of our desired bromopyridine and summarized in Table 3.1 (Scheme 3.6).[20,22,24-27]

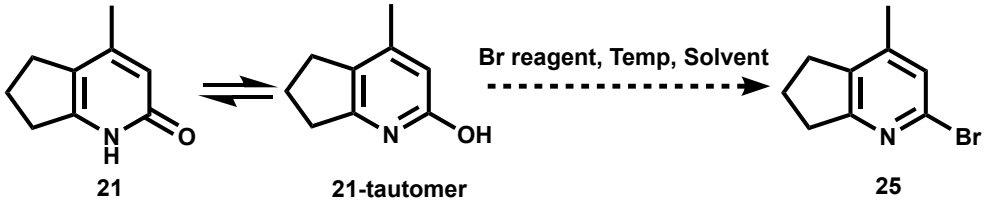

Scheme 3.6. Attempted synthesis of 25 from pyridone

Table 3.1. Reaction conditions and results for attempted synthesis of bromopyridine 25

Trial #	Bromine Reagent	Additives	Solvent	Temperature (°C)	Result	Ref.
1	PBr_3	-	Neat	175	Multiple Products	24
2	CBr_4	PPh_3	toluene	111	Majority starting material recovered	25
3	Bu_4NBr	P_2O_5	*o*-dichlorobenzene	180	Insoluble black oil	22
4	NBS	PPh_3, Et_3N	dioxane	101	Unknown product	26, 27
5[a]	LiBr	1. pyridine, Tf_2O 2. TfOH	toluene	1. 5 2. RT	Intermediate Penttriflate **22** isolated	20

a. Two step, one-pot procedure

Entry 1 was the only published procedure found for the formation of the desired bromopyridine **25**.[24] In this protocol, pyridone **21** was treated with new PBr_3 and heated to reflux overnight, resulting in a black sludge. The ^1H NMR showed multiple products, and attempts at isolating the desired product by column chromatography were unsuccessful. Entry 2 is based on a procedure by Chavasiri and coworkers.[25] In this report, various hydroxypyridines were refluxed with PPh_3/brominating agents to generate the desired bromopyridines. Unfortunately, these conditions resulted in no conversion of our substrate. In the proposed mechanism, PPh_3 reacts with the halogenating agent, for example CBr_4, to generate $[Br\text{-}PPh_3]Br_3C$. This intermediate then reacts with hydroxypyridine to form the corresponding aryloxyphosphium salt, which decomposes to form the desired bromopyridine and triphenylphosphine oxide. The lack of reactivity was surprising because we hypothesized based on this mechanism that electron-donating groups would make the pyridone more nucleophilic, favoring attack of the $[Br\text{-}PPh_3]Br_3C$ intermediate.

Similarly, entry 3 is based on a procedure by Kato and coworkers where P_2O_5 reacts with a halogen source to form a dihalogenophosphate ester, then the halide ion nucleophilicly displaces the phosphate ion.[22] It was found that substrates containing electron-withdrawing groups reacted more readily than electron-donating groups.[22] Therefore, the lack of reactivity in this case is likely due to the electron-donating groups on pyridone **21**. Entry 4 involves reaction of PPh_3 and N-bromosuccinimde (NBS) with **21**. Under these conditions, PPh_3 and NBS interact to form a phosphonium salt that subsequently reacts with hydroxypyridines.[26,27] The ^1H NMR spectrum showed that the desired bromopyridine was not present, but instead one unknown product was obtained.[28] The final attempt to synthesize bromopyridine (Entry 5) was based on the two-step, one-pot procedure reported by Maloney and coworkers.[20] Like the attempt to synthesize iodopyridine **24** using this method, penttriflate **22** was the only product isolated suggesting the lack of activation of **21** under these conditions.

As discussed above, none of these reaction conditions resulted in formation of the desired bromopyridine **25**. Therefore, final efforts focused on the formation of chloropyridine **26**, the least reactive intermediate for amination. Like bromopyridine, there are many reports on the direct synthesis of chloropyridines from hydroxypyridines.[20,25-27,29] In fact, our desired chloropyridine **26** has been previously synthesized by Wilson and coworkers using neat phenylphosphonic dichloride ($PhP(=O)Cl_2$) (Scheme 3.7).[29] Gratifyingly, this procedure resulted in formation of **26** as a white crystalline solid in 82% yield.

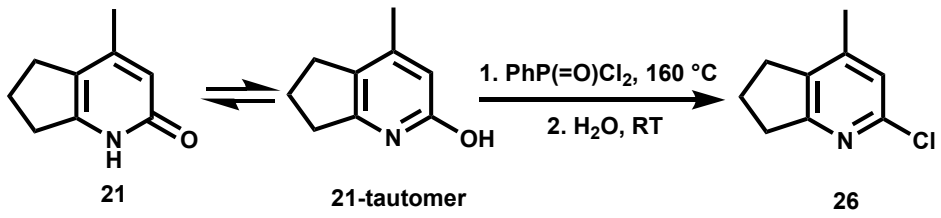

Scheme 3.7. Synthesis of chloropyridine 26

With chloropyridine **26** and penttriflate **22** in hand, we were ready to begin optimization of the C-N coupling reaction to from pentamine **23** (Step 2, Scheme 3.4). The Buchwald-Hartwig amination is a well-documented C-N coupling reaction with various conditions optimized for a variety of aryl halide and aryl pseudo-halide subtrates.[30-37] However, the particular transformation of interest is the conversion of aryl halides/pseudo halides to their corresponding *primary* amines, a useful but not well reported transformation.[33-36] Therefore, conditions needed to hydroaminate pseudo-halide penttriflate **22** were first explored, and the results are summarized in Table 3.2 (Scheme 3.8).

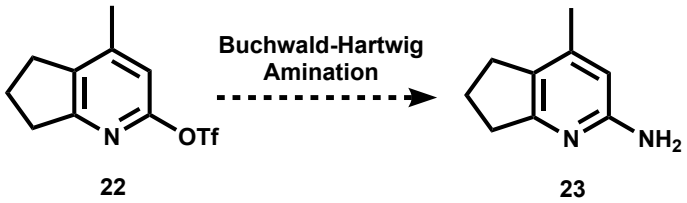

22 23

Scheme 3.8. Conversion of 22 to pentamine 23 via Buchwald-Hartwig amination

Table 3.2. Reaction conditions and results for the synthesis of pentamine from penttriflate

Trial #	Nitrogen Source	Catalyst/ Pre-catalyst	Additives	Solvent	Temperature (°C)	Result	Ref.
1[a]	$NH_3 \bullet H_2O$	Cu_2O	K_2CO_3, DMEDA	Ethylene glycol	60	No product isolated	17
2	Benzophenone imine	$Pd(OAc)_2$	Cs_2CO_3, BINAP	toluene	100	No reaction	9

a. ^{1}H NMR spectrum showed a majority of solvent with minor product peaks.

In addition to Gade's protocol that was attempted earlier (Entry 2, Table 3.2),[9] the conversion of penttriflate **22** to pentamine **23** was also attempted using a solution of aqueous ammonia as the nitrogen source (Entry 1).[17] Unfortunately, both attempts failed to result in the desired pentamine. Conditions for converting chloropyridine **26** to pentamine **23** were also

concurrently explored (Scheme 3.9, Table 3.3). Both Pd and Ni pre-catalysts and various nitrogen sources were tried.[32,34-36] Gratifyingly, several conditions resulted in formation of the desired pentamine (Entries 1-3), with the best result obtained using LiHMDS and $Pd(dba)_2$ (Entry 1). This coupling reaction produced the desired pentamine as a tan solid in 70% yield.

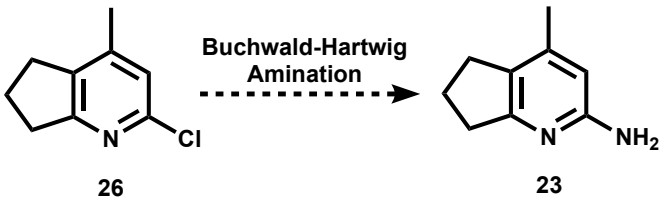

26 23

Scheme 3.9. Conversion of 26 to pentamine 23 via Buchwald-Hartwig amination

Table 3.3. Reaction conditions and results for the synthesis of pentamine from chloropyridine

Trial #	Nitrogen Source	Catalyst/ Pre-catalyst	Additives	Solvent	Temperature (°C)	Result	Ref.
1	LiHMDS	$Pd(dba)_2$	P^tBu_3	toluene	90	Desired product obtained	32
2[a]	LiHMDS	$Pd(dba)_2$	Ligand 1	THF	65	Two products obtained	34
3	Benzophenone Imine	$Ni(COD)_2$	DPPF, Na^tOBu	toluene	100	Desired product obtained	35
4	NH_3 (0.4 M in THF)	$Pd(dba)_2$	DPPF, Na^tOBu	toluene	100	No reaction	36

a. Ligand 1 = 2-(dicyclohexylphosphino)biphenyl; One product is the desired pentamine.

With pentamine **23** in hand, the last step of the modified procedure was accomplished by heating pentamine with phthalonitrile in 1-hexanol overnight, resulting in **15** as a yellow solid in 48% yield.[9] The ^1H NMR spectrum of **15** features the diagnostic cyclopentyl signals at 2.18 (q, 4H), 2.89 (t, 4H), and 3.08 (t, 4H) ppm, respectively. X-ray quality crystals were grown from

slow evaporation of CH_2Cl_2 at room temperature. The solid-state molecular structure is shown in Figure 3.4. The ligand backbone is planar, and the pyridine arms are slightly bent out of the plane with torsion angles of 4.5 (2)° and 2.1 (2)°, respectively. The small torsion angles suggest no significant steric clashing of the cyclopentyl rings. Compound **15** has a % volume buried of 62.9,[13,14] suggesting that this ligand is slightly more hindered than **12**, but less hindered than **13** and **14** (Table 3.4). This difference in the steric environment around the binding pocket could be explained by the fact that the cyclopentyl moiety is pulled back into a ring.

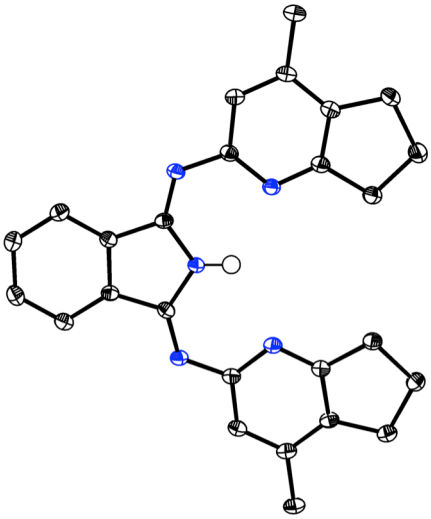

Figure 3.4. ORTEP[43] drawing of 15 with thermal ellipsoids at 50% probability. Hydrogen atoms excluded for clarity.

*3.2.6 Synthesis and characterization of ^{Br}BPI-H (**16**)*

1,3-bis[2-(6-bromopyridyl)imino]isoindoline (^{Br}BPI-H, **16**) has recently been synthesized by Szymczak and coworkers.[10a] Preparation of **16** involves heating phthalonitrile and 2-bromo-6-aminopyridine to reflux in 1-hexanol for 48 hours. Complex **16** was then isolated as a bright yellow solid in 58% yield after workup of the reaction. The ^{1}H NMR spectrum of **16** features all aryl protons between 7.0-8.10 ppm, which agrees with the literature.[10a] X-ray quality crystals were grown from slow evaporation of CH_2Cl_2 at room temperature. The solid-state molecular structure is shown in Figure 3.5. The ligand backbone is planar, and the pyridine arms

Figure 3.5. ORTEP[43] drawing of 16 with thermal ellipsoids at 50% probability. Hydrogen atoms excluded for clarity.

are bent out of the plane with torsion angles of 19.0 (3)° and 1.3 (3)°, respectively. Compound **16** has a % volume buried of 67.0,[13,14] suggesting that this ligand is more hindered than **12**, **13**, **15**, but less hindered the methoxy derivative **14** (Table 3.4). The binding pocket of **16** is quite hindered without the possibility of rotation about the Br bond, suggesting metalation may be difficult.

*3.2.7 Synthesis and characterization of ^{xylyl}BPI-H (**17**)*

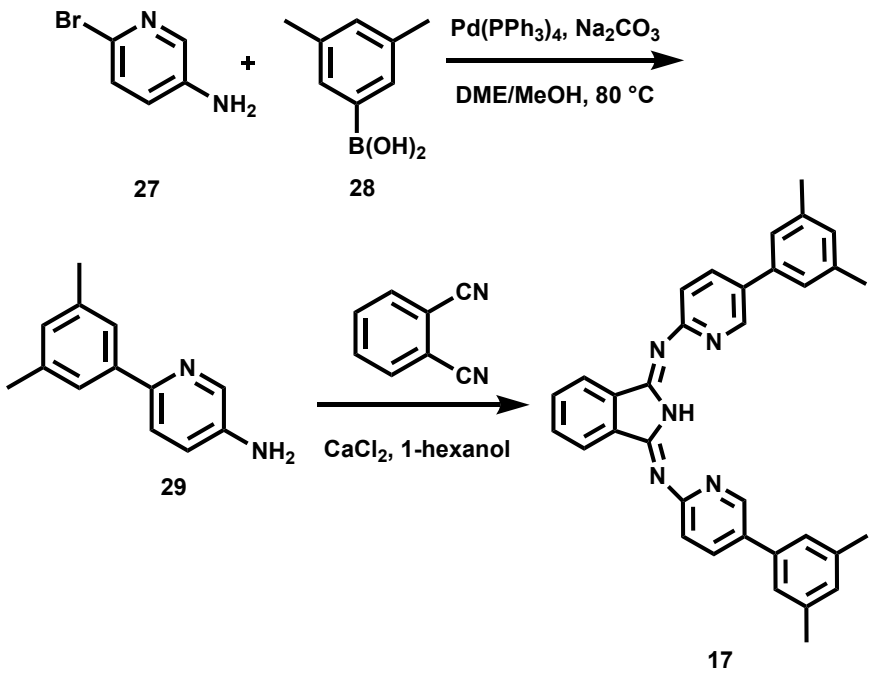

Scheme 3.10. Synthetic procedure of ^{xylyl}BPI-H (17)

An analog of 1,3-bis[2-(5-(3,5-xylyl)pyridyl)imino]isoindoline (^{xylyl}BPI-H, **17**) has been synthesized by Gade and coworkers in 2011.[8] The two-step synthetic procedure is shown in Scheme 3.10. Coupling of 2-amino-5-bromopyridine (**27**) and 3,5-xylylboronic acid (**28**) using a palladium catalyst generates 2-amino-(3,5-xylyl)pyridine (**29**) which was isolated as a pale yellow solid in 30% yield after reaction workup.[38] Compound **29** was subsequently heated with

phthalonitrile to reflux in 1-hexanol for 72 hours, furnishing **17** as a green solid in 65% yield after reaction workup. This particular analog has never been synthesized and therefore was fully characterized by NMR spectroscopy and X-ray crystallography. The ^{1}H NMR spectrum of **17** features a singlet for the methyl groups at 2.42 ppm (12 H) and the corresponding aryl signals between 7-9 ppm (for full assignment see experimental section below). The N-H proton appears at 14 ppm. X-ray quality crystals were grown from slow evaporation of CH_2Cl_2 at room temperature with the solid-state molecular structure shown in Figure 3.6. The ligand backbone is planar, and the pyridine arms are bent out of the plane with torsion angles of 13.0 (2)° and 24.0 (2)°, respectively. The xylyl moieties are also staggered to prevent steric clashing. A space-filling model of **17** shows that the binding pocket is relatively unhindered with 60.5% volume buried (Table 3.4).[13,14] The xylyl moieties in the 5 position of the pyridine rings make **17** only slightly more hindered than **12**, which is expected because **12** has no additional groups in the 5 or 6 position of the pyridine rings to create steric hindrance.

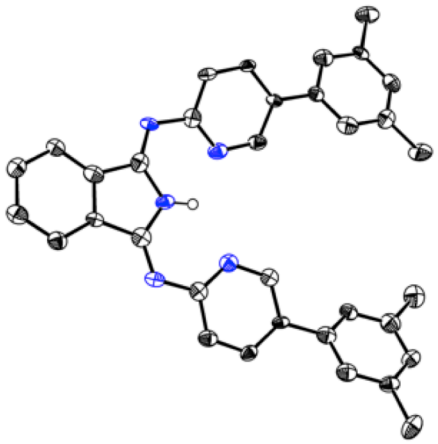

Figure 3.6. ORTEP[43] drawing of 17 with thermal ellipsoids at 50% probability. Hydrogen atoms excluded for clarity.

3.3 Summary

In summary, six ^{R}BPI-H ligands were synthesized and fully characterized. Ligands **12-13** and **15-17** (or similar variations) have been previously synthesized. The procedures published for **12**, **13**, **16**, **17** resulted in successful isolation of the corresponding ^{R}BPI-H derivatives. However, the published synthetic route for **15** was slightly modified to improve a problematic transformation, enabling facile and reliable access to **15**. The novel ligand ^{OMe}BPI-H (**14**) has also been synthesized and fully characterized. Each ligand was fully characterized by NMR

spectroscopy and X-ray crystallography. The steric environment of each ligand was examined and compared in relation to the geometry and binding pocket. The % volume buried was calculated and revealed subtle differences in sterics between each ligand. These comparisons are summarized in Table 3.4. The most sterically hindered ligand was **14** with the least sterically hindered being **12** (Scheme 3.11). Substituents in the 6-position of the pyridine ring appear to affect the % volume buried the most, whereas sterics in the 5 position, as evidenced by **17**, only slightly affect the sterics around the binding pocket. These finding provide valuable insight into the ease of metalation for each of these ligands as discussed in Chapter 4.

Table 3.4. Space-filling model and % volume buried of ^{R}BPI-H ligands 12-17

Compound #	Space-fill diagram (end on view)	Space-fill diagram (top view)	% Volume buried
12	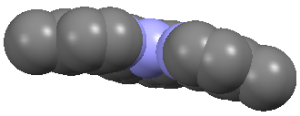	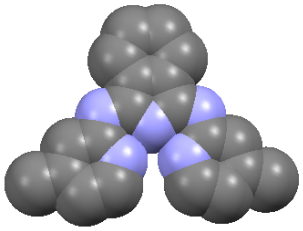	59.0
13	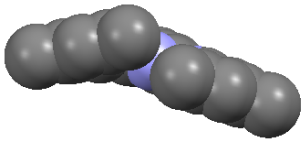	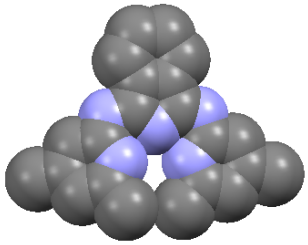	64.8
14	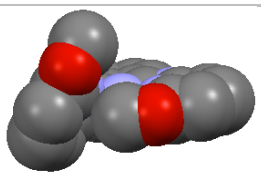	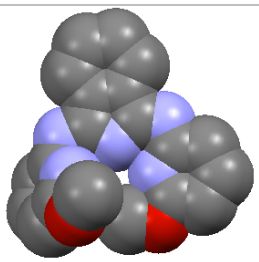	71.9

15	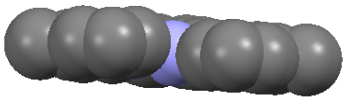	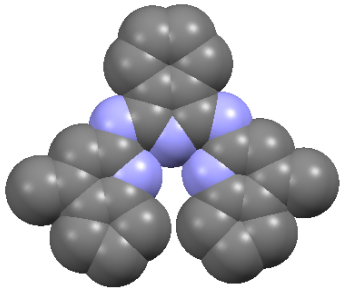	62.9
16	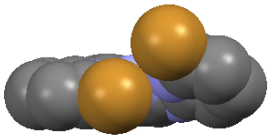	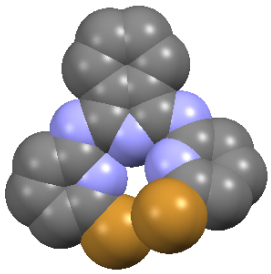	67.0
17	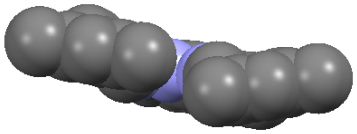	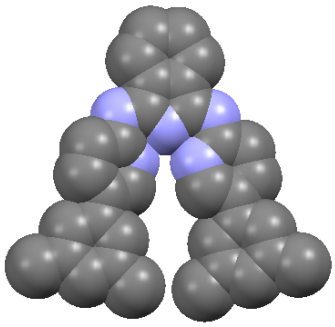	60.5

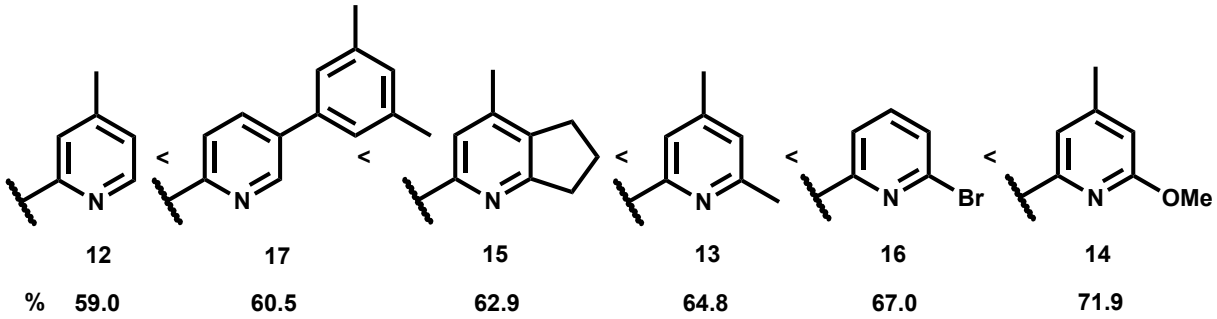

Scheme 3.11. Scale of the least hindered BPI-H ligand to the most hindered

3.4 Experimental

3.4.1 General Experimental:

Unless otherwise noted, all experiments and manipulations were done under inert atmosphere (Schlenk line/glovebox). Glassware was oven-dried or flame-dried prior to use. Dichloromethane, diethyl ether, toluene, and tetrahydrofuran were dried by passage through activated alumina and molecular sieves columns under a stream of argon. Methanol was dried by refluxing over magnesium turnings, distilled, and stored over 4 Å sieves. All other solvents were sparged with N_2 before use. Toluene-d_8 and THF-d_8 were dried over Na^0/benzophenone and vacuum-transferred prior to use or stored over molecular sieves. CD_2Cl_2 was dried over CaH_2 and vacuum-transferred prior to use or stored over molecular sieves. $CDCl_3$ was used as received. Pyridone[39] and $Pd(PPh_3)_4$[40] were synthesized according to literature procedures. All other reagents were used as received from commercial suppliers. NMR spectra were acquired on Bruker AV200, AV300, AV301, DRX499, AV500, and AV700 spectrometers using 5mm medium-walled NMR tubes and 5mm medium-walled NMR tubes fitted with a J. Young Teflon valve. ^1H, ^{13}C, HMBC, and HMQC NMR spectra were referenced to residual protonated solvent signals. X-ray data was collected at -173 °C on a Bruker APEX II single crystal X-ray diffractometer using Mo-radiation.

3.4.2 Synthesis and Characterization of Compounds:

BPI-H (12): BPI-H was synthesized according to a literature procedure.[5] A 200 mL Schlenk flask equipped with a stir bar and fitted with a reflux condenser was charged with phthalonitrile (3.00 g, 23.4 mmol), 2-amino-4-methylpyridine (5.08 g, 47.0 mmol), and $CaCl_2$ (0.531 g, 4.78 mmol) and placed under inert atmosphere on Schlenk line. N_2-sparged 1-hexanol (75 mL) was subsequently added via syringe resulting in an opaque colorless solution. The reaction mixture was then heated to reflux (150 °C) for 48 hours. During that time the reaction solution turned

bright fluorescent green and then black with green tint. After 48 hours, the reaction was cooled to room temperature and subsequently placed in an ice bath. De-ionized H_2O (80 mL) was added to reaction solution while still in the ice bath, resulting in precipitation of a forest green solid (solid was sometimes yellow/green in color). The precipitate was filtered on a glass filter frit and washed with de-ionized H_2O (3x) and hexanes (3x). The resulting green solid was dissolved in CH_2Cl_2 and re-filtered to separate out a purple contaminant. The solvent was removed under reduced pressure. The green product was further dried under vacuum. The NMR values are similar to a previous report.[6a,42] Yield: 2.90 g (38%).

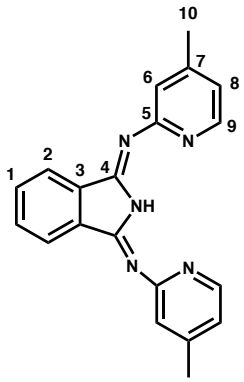

^{1}H NMR (700 MHz, CD_2Cl_2): 2.40 (s, 6H, H^{10}), 6.97 (d, 2H, $^3J_{HH}$ = 4.8 Hz, H^8), 7.27 (s, 2H, H^6), 7.65 (m, 2H, H^1), 8.03 (m, 2H, H^2), 8.46 (d, 2H, $^3J_{HH}$ = 5 Hz, H^9), 13.9 (s, 1H, N-*H*). $^{13}C\{^1H\}$ NMR (176 MHz, CD_2Cl_2): 21.1 (s, C^{10}), 121.8 (s, C^8), 122.7 (s, C^2), 124.0 (s, C^6), 131.9 (s, C^1), 136.4 (s, C^3), 147.9 (s, C^9), 149.9 (s, C^7), 153.8 (s, C^4), 160.8 (s, C^5).

^{Me}BPI-H (13): ^{Me}BPI-H was synthesized according to a literature procedure.[5] A 100 mL Schlenk flask equipped with a stir bar and fitted with a reflux condenser was charged with phthalonitrile (4.99 g, 38.9 mmol), 2-amino-4,6-dimethylpyridine (9.51 g, 77.9 mmol), and $CaCl_2$ (0.865 g, 7.79 mmol) and placed under inert atmosphere on a Schlenk line. N_2-sparged 1-hexanol (40 mL) was subsequently added via syringe, resulting in a white suspension. The reaction mixture was then heated to reflux (165 °C) for 48 hours. During that time the reaction turned to a black solution with blue tint. After 48 hours, the reaction was cooled to room temperature and subsequently placed in an ice bath. De-ionized H_2O was added to the reaction solution while still in the ice bath, resulting in precipitation of a dark green/blue solid. The precipitate was filtered on a glass filter frit and washed with de-ionized H_2O (3x) and hexanes (3x). The resulting solid

was dissolved in CH_2Cl_2 and re-filtered to separate out a purple/blue contaminant. The solvent was removed under reduced pressure, resulting in an orange solid. The product was further dried under vacuum. The ^{1}H NMR values are similar to the previous report of this complex.[6a] Yield: 6.89 g (50%).

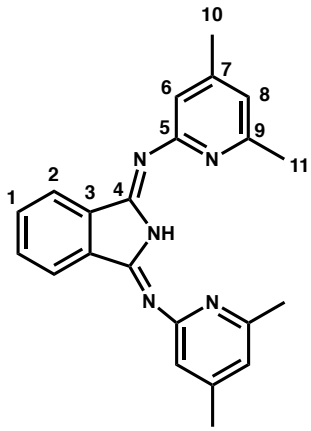

^{1}H NMR (700 MHz, CD_2Cl_2): 2.33 (s, 6H, H^{10}), 2.48 (s, 6H, H^{11}), 6.79 (s, 2H, H^8), 7.00 (s, 2H, H^6), 7.64 (m, 2H, H^1), 8.01 (m, 2H, H^2), 12.3 (bs, 1H, N-*H*). ^{13}C{^{1}H} NMR (176 MHz, CD_2Cl_2): 21.0 (s, C^{10}), 24.8 (s, C^{11}), 119.9 (s, C^6), 121.0 (s, C^8), 122.6 (s, C^2), 131.9 (s, C^1), 136.2 (s, C^3), 149.9 (s, C^7), 152.8 (s, C^4), 157.1 (s, C^9), 160.3 (s, C^5).

2-bromo-6-methoxypyridine (19): 2-bromo-6-methoxypyridine was synthesized via a literature procedure.[15,41] A 500 mL Schlenk flask equipped with stir bar and reflux condenser was charged with 2,6-dibromopyridine (11.4 g, 47.9 mmol), NaOMe (4.40 g, 81.5 mmol), and MeOH, resulting in a white suspension. The reaction was heated at reflux (85 °C) for 24 hours. After 24 hours, the reaction progress was checked via TLC, which showed no starting material present. The reaction was allowed to slightly cool and the solvent was removed under reduced pressure, resulting in a white solid. H_2O and ethyl acetate were added, and the product was extracted with ethyl acetate (3x). The combined organic layers were washed with brine, dried over $NaSO_4$, and filtered into a 500 mL round bottom. Solvent was removed under reduced pressure, resulting in a light yellow oil that matched previously reported characterization data.[15,41] Yield: 5.57 g (62 %).

^{1}H NMR (300 MHz, $CDCl_3$): 3.93 (s, 3H, C*H*$_3$), 6.69 (d, 1H, $^3J_{HH}$ = 8.2 Hz, aryl-*H*), 7.06 (d, 1H, $^3J_{HH}$ =7.5 Hz, aryl-*H*), 7.40 (t, 1H, $^3J_{HH}$ = 7.8 Hz, aryl-*H*).

6-methoxy-2-pyridinamine (20): 6-methoxy-2-pyrdinamine was synthesized via a literature

procedure.[16] A 100 mL Schlenk flask equipped with a stir bar was charged with 2-bromo-6-methoxypyridine (1 mL, 8 mmol), Cu_2O (59 mg, 0.41 mmol), N_2-sparged $NH_3 \bullet H_2O$ (11 mL, 163 mmol), K_2CO_3 (0.226 g, 1.64 mmol), DMEDA (92 μL, 0.81 mmol), and N_2-sparged ethylene glycol (20 mL). The reaction was stirred at 70 °C for 18 hours. The reaction was subsequently cooled to room temperature. The product was extracted with ethyl acetate. The organic layers were combined and the solvent was removed under reduced pressure, resulting in a brown oil. The crude product was purified via silica gel column chromatography with ethyl acetate as elutant. The first fraction was collected and solvent was removed under reduced pressure resulting in an orange oil that matched previously reported characterization data.[16] Yield: 2.03 g.

^{1}H NMR (300 MHz, $CDCl_3$): 3.83 (s, 3H, C*H*$_3$), 4.33 (bs, 2H, N*H*$_2$), 6.06 (t, 2H, $^3J_{HH}$ = 7.9 Hz, aryl-*H*), 7.33 (t, 1H, $^3J_{HH}$ = 7.8 Hz, aryl-*H*).

^{OMe}BPI-H (14): ^{OMe}BPI-H was synthesized based on a literature procedure.[5] A 50 mL Schlenk flask equipped with a stir bar and fitted with a reflux condenser was charged with phthalonitrile (0.514 g, 0.00401 mmol), 6-methoxy-2-pyrdinamine (1.01 g, 0.00814 mmol), and $CaCl_2$ (0.185 g, 0.00167 mmol) and placed under inert atmosphere on Schlenk line. N_2-sparged 1-hexanol (15 mL) was subsequently added via syringe. The reaction mixture was heated to reflux (165 °C) for 48 hours. During that time the reaction mixture turned from a yellow suspension to a yellow/orange, then changed to a red/brown color and ultimately turned to a black solution with a red tint. After 48 hours, the reaction was cooled to room temperature and subsequently placed in an ice bath. De-ionized H_2O was added to the reaction solution while still in the ice bath, resulting in precipitation of a dark green/black solid. The precipitate was isolated on a glass filter frit and washed with de-ionized H_2O (3x) and hexanes (3x). The resulting solid was dissolved in CH_2Cl_2 and re-filtered to separate out a black contaminant, resulting in a dark green solution.

The solvent was removed under reduced pressure, resulting in a green/yellow solid. The product was further purified by dissolving in a minimum amount of CH_2Cl_2, layering with hexanes, and placing in a freezer to recrystallize. The solution was decanted from the green solid that precipitated out and further dried under vacuum. Yield: 656 mg (45%).

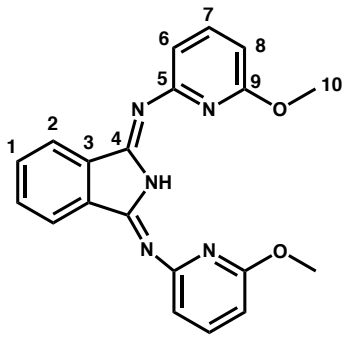

^{1}H NMR (700 MHz, $CDCl_3$): 3.65 (s, 6H, H^{10}), 6.54 (d, 2H, $^3J_{HH}$ = 8.0 Hz, H^6 or H^8), 6.93 (d, 2H, $^3J_{HH}$ = 7.4 Hz, H^6 or H^8), 7.64 (t, 2H, $^3J_{HH}$ = 7.7 Hz, H^7), 7.66 (m, 2H, H^1), 8.06 (m, 2H, H^2), 11.6 (s, 1H, N-*H*). ^{13}C{^{1}H} NMR (176 MHz, $CDCl_3$): 53.5 (s, C^{10}), 106.9 (s,C^6 or C^8), 113.8 (s, C^6 or C^8), 122.8 (s, C^2), 131.9 (s, C^1), 135.5 (s, C^4), 140.6 (s, C^7), 152.4 (s, C^3), 158.5 (s, C^5), 163.5 (s, C^9).

4-methyl-6,7-dihydro-5*H*-cyclopenta[*b*]pyridin-2-yl trifluoromethanesulfonate 22: Penttriflate **22** was synthesized via a literature procedure.[9] A 500 mL 3-neck round bottom flask equipped with a stir bar and an addition funnel was charged with pyridone (2.04 g, 13.7 mmol) and N_2-sparged CH_2Cl_2 (45 mL), resulting in a yellow suspension. The reaction was cooled to -45 °C in an acetonitrile/CO_2 bath and Et_3N (1.6 mL, 11.3 mmol) was subsequently added. Tf_2O (3.4 mL, 20.5 mmol) was added dropwise via the addition funnel over 10 minutes, during which time the reaction turned into an orange solution. The reaction was stirred at – 45 °C for 20 minutes. After 20 minutes, the reaction was slowly warmed to room temperature over 2 hours and subsequently stirred at room temperature for 1 hour. Ice (30 g) was added to the reaction mixture and stirred until melted, resulting in two distinct layers. The reaction was neutralized with 10% NaOH solution. The product was extracted with dichloromethane in a separatory funnel. The extract was washed with brine, dried over $NaSO_4$, and filtered into a 100 mL round bottom flask. The solvent was removed under reduced pressure, resulting in a brown oil. The

crude product was purified via silica gel column chromatography (9:1 hexanes:ether). The first fraction was collected and solvent was removed under reduced pressure, resulting in a yellow oil that matched previously reported characterization data.[9] Yield: 3.13 g (81%).

^{1}H NMR (200 MHz, $CDCl_3$): 2.17 (quintet, 2H, $^3J_{HH}$ = 7.5 Hz, $CH_2CH_2CH_2$), 2.31 (s, 3H, CH_3), 2.87 (t, 2H, $^3J_{HH}$ =7.8 Hz, $CH_2CH_2CH_2$), 3.00 (t, 2H, $^3J_{HH}$ =7.75 Hz, $CH_2CH_2CH_2$), 6.74 (s, 1H, aryl-*H*).

2-chloro-4-methyl-6,7-dihydro-5*H*-cyclopenta[*b*]pyridine 26: The synthesis of chloropyridine **26** is based on a literature procedure.[39] A 500 mL Schlenk flask equipped with a stir bar was charged with pyridone (2.02 g, 13.5 mmol) and phenylphosphonic dichloride (4.2 mL, 29 mmol), resulting in a yellow slurry. The reaction was heated at 165 °C for 19 hours. In the first few hours, gas emerged from solution as a white smoke and the solution turned orange/brown. After 19 hours, the reaction was allowed to cool to room temperature. The dark purple reaction solution was then diluted with H_2O (20 mL) slowly to quench excess phenylphosphonic dichloride. An additional 200 mL H_2O was then added. The acidic reaction solution was neutralized by careful addition of K_2CO_3 (6-7 g) until pH = 9. The product was extracted with chloroform (3x). The combined organic extracts were washed with H_2O (2x). The organic extracts were then dried over $MgSO_4$ and filtered into a 500 mL round bottom. The solvent was removed under reduced pressure, resulting in a white solid with purple mixed in. The crude product was purified by silica gel column chromatography using chloroform as the eluant. Solvent was removed under reduced pressure, resulting in a white crystalline solid that matched previously reported characterization data.[39] Yield: 1.86 g (82%).

^{1}H NMR (300 MHz, $CDCl_3$): 2.13 (quintet, 2H, $^3J_{HH}$ = 7.6 Hz, $CH_2CH_2CH_2$), 2.23 (s, 3H, CH_3),

2.82 (t, 2H, $^3J_{HH}$ =7.5 Hz, C*H*$_2$CH$_2$CH$_2$), 2.99 (t, 2H, $^3J_{HH}$ =7.8 Hz, CH$_2$CH$_2$C*H*$_2$), 6.91 (s, 1H, aryl-*H*).

4-methyl-6,7-dihydro-5*H*-cyclopenta[*b*]pyridin-2-amine 23: The synthesis of pentamine **23** from chloropyridine is based on a literature procedure.[34] A 100 mL Schlenk flask equipped with a stir bar and fitted with a reflux condenser was charged with chloropyridine (0.732 g, 0.00437 mmol), LiHMDS (0.804 g, 0.00480 mmol), Pd(dba)$_2$ trimer (0.125 g, 2.18x10^{-4} mmol), P^{t}Bu$_3$ (0.0447 g, 2.21x10^{-4} mmol), and toluene (36 mL). The reaction was heated at 105 °C for 45 hours, resulting in a dark red/brown suspension. After 45 hours, the reaction was allowed to cool to room temperature. The mixture was diluted with Et$_2$O (20 mL). The silylamide was deprotected by addition of 1M HCl (20 mL), creating two distinct layers. The aniline was then precipitated as a salt by further addition of 2M HCl in Et$_2$O (1:1). The precipitate was isolated by filtration, washed with Et$_2$O, and dissolved in CH$_2$Cl$_2$. The resulting solution was washed with 2M NaOH (2x). The organic layer was dried with MgSO$_4$, filtered, and transferred to a 100 mL round bottom flask. Solvent was removed under reduced pressure, resulting in an orange/red solid that matched previously reported characterization data.[34] Yield: 0.452 g (70%).

^{1}H NMR (300 MHz, CDCl$_3$): 2.07 (q, 2H, $^3J_{HH}$ = 7.4Hz, CH$_2$C*H*$_2$CH$_2$), 2.15 (s, 3H, C*H*$_3$), 2.74 (t, 2H, $^3J_{HH}$ = 7.2 Hz, C*H*$_2$CH$_2$CH$_2$), 2.85 (t, 2H, $^3J_{HH}$ = 7.5 Hz, CH$_2$CH$_2$C*H*$_2$), 4.20 (bs, 2H, N*H*$_2$), 6.13 (s, 1H, aryl-*H*).

^{Pent}BPI-H (15): ^{Pent}BPI-H was synthesized according to a literature procedure.[9] A 25 mL Schlenk flask equipped with a stir bar and fitted with a reflux condenser was charged with phthalonitrile (150 mg, 1.17 mmol), pentamine (364 mg, 2.46 mmol), CaCl$_2$ (66.5 mg, 0.599 mmol) and placed under inert atmosphere on a Schlenk line. N$_2$-sparged 1-hexanol (15 mL) was

subsequently added via syringe. The reaction mixture was heated to reflux (160 °C) for 22 hours. After 22 hours, the reaction was cooled to room temperature and subsequently transferred to a 50 mL round bottom flask. Solvent was removed under reduced pressure, resulting in a dark brown solid. The resulting solid was dissolved in CH_2Cl_2 and filtered through Celite to remove a blue/purple impurity. The solvent was removed under reduced pressure. The crude product was further purified by column chromatography (8:2 CH_2Cl_2:Et_2O). The second fraction was collected, and solvent was removed under reduced pressure, resulting in a bright yellow solid that matched previously reported characterization data.[9] Yield: 191 mg (40%).

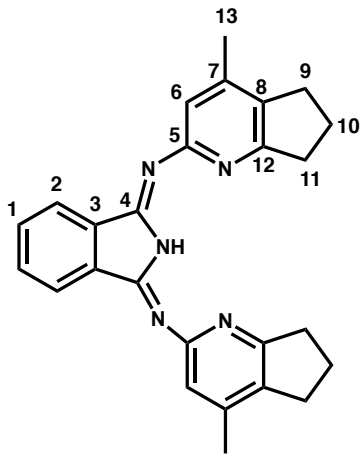

^{1}H NMR (700 MHz, $CDCl_3$): 2.18 (q, $^3J_{HH}$ = 7.6 Hz, 4H, H^{10}), 2.28 (s, 6H, H^{13}), 2.89 (t, 4H, $^3J_{HH}$ = 7.4 Hz, H^9), 3.08 (t, 4H, $^3J_{HH}$ = 7.6 Hz, H^{11}), 7.04 (s, 2H, H^6), 7.61 (m, 2H, H^1), 8.04 (m, 2H, H^2), 12.7 (s, 1H, N-*H*). ^{13}C{^{1}H} NMR (176 MHz, $CDCl_3$): 19.0 (s, C^{13}), 23.0 (s, C^{10}), 29.2 (s, C^9), 35.1 (s, C^{11}), 121.2 (s, C^6), 122.4 (s, C^2), 131.4 (s, C^1), 133.0 (s, C^7), 136.0 (s, C^4), 144.8 (s, C^8), 152.1 (s, C^3), 159.4 (s, C^5), 163.6 (s, C^{12}).

^{Br}BPI-H (16): ^{Br}BPI-H was synthesized according to a literature procedure.[10a] A 100 mL Schlenk flask equipped with a stir bar and fitted with a reflux condenser was charged with phthalonitrile (0.943 g, 7.36 mmol), 2-bromo-6-aminopyridine (2.67 g, 15.4 mmol), $CaCl_2$ (0.0806 g, 0.726 mmol) and placed under inert atmosphere on Schlenk line. N_2-sparged 1-hexanol (25 mL) was subsequently added via syringe. The reaction mixture was heated to reflux (173 °C) for 48 hours. During that time the reaction turned to a dark green solution. After 48 hours, the reaction was cooled to room temperature and subsequently placed in a freezer to induce precipitation of product overnight. The precipitate was filtered on a glass filter frit and

washed with D.I. H_2O (3x), diethyl ether (3x), ethyl acetate (3x), and hexanes (3x) to afford a yellow/green solid. The resulting solid was dissolved in $CHCl_3$ and re-filtered to separate out a purple contaminant. To further purify, the solution was concentrated, ethyl acetate was subsequently added, and the solution was placed in the freezer overnight, resulting in a bright yellow crystalline solid. The product was filtered and dried under vacuum. The NMR matched the previous report of this compound.[10a] Yield: 1.96 g (58 %).

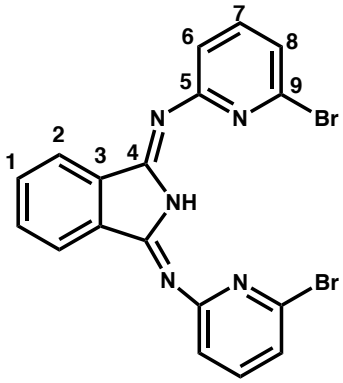

^{1}H NMR (700 MHz, $CDCl_3$): 7.27 (d, 2H, $^3J_{HH}$ = 12.8 Hz, H^6 or H^8), 7.29 (d, 2H, $^3J_{HH}$ = 12.9 Hz, H^6 or H^8), 7.60 (t, 2H, $^3J_{HH}$ = 7.8 Hz, H^7), 7.67 (m, 2H, H^1), 8.03 (m, 2H, H^2), 11.9 (s, 1H, N-*H*). $^{13}C\{^1H\}$ NMR (176 MHz, $CDCl_3$): 120.2 (s, C^6 or C^8), 122.9 (s, C^2), 124.4 (s, C^6 or C^8), 132.3 (s, C^1), 135.3 (s, C^4), 140.2 (s, C^5 or C^9), 140.3 (s, C^7), 153.5 (s, C^3), 160.6 (s, C^5 or C^9).

2-amino-(3,5-xylyl)pyridine (29): 2-amino-(3,5-xylyl)pyridine was synthesized according to a written procedure.[38] A 100 mL Schlenk flask equipped with a stir bar was charged with 2-amino-5-bromopyridine (2.10 g, 12.2 mmol), 3,5-xylyl boronic acid (2.19 g, 14.6 mmol), dimethoxyethane (40 mL), and MeOH (8 mL), resulting in a yellow suspension. The reaction suspension was degassed (freeze-pump-thaw 3x). N_2-sparged saturated aqueous Na_2CO_3 (10 mL) and $Pd(PPh_3)_4$ (1.4 g, 1.2 mmol) were subsequently added. The reaction mixture was heated at 80 °C for 48 hours. After 48 hours, solvent was removed under reduced vacuum. The residue was dissolved in CH_2Cl_2, dried over $MgSO_4$, and filtered into 250 mL round bottom flask, resulting in a red/brown solution. Solvent was removed under reduced pressure. The crude product was purified by column chromatography with diethyl ether and 1 % MeOH as elutant. Solvent was removed to afford a pale yellow solid that matched previous characterization data.[38]

Yield: 0.713 g (30%).

^{1}H NMR (500 MHz, CD_2Cl_2): 2.35 (s, 6H, C*H*$_3$), 4.54 (bs, 2H, N*H*$_2$), 6.56 (d, 1H, $^3J_{HH}$ = 8.4 Hz, aryl-*H*), 6.96 (s, 1H, aryl-*H*), 7.13 (s, 2H, aryl-*H*), 7.65 (dd, 1H, $^3J_{HH}$ = 8.5 Hz, $^4J_{HH}$ = 2.4 Hz, aryl-*H*), 8.28 (d, 1H, $^4J_{HH}$ = 2.1 Hz, aryl-*H*).

^{xylyl}BPI-H (17): ^{xylyl}BPI-H was synthesized according to a literature procedure.[8] A 50 mL Schlenk flask equipped with a stir bar and fitted with a reflux condenser was charged with phthalonitrile (0.621 g, 4.84 mmol), 2-amino-(3,5-xylyl)pyridine (1.96 g, 9.87 mmol), $CaCl_2$ (0.077 g, 0.69 mmol) and placed under inert atmosphere on Schlenk line. N_2-sparged 1-hexanol (3 mL) was subsequently added via syringe. The reaction mixture was heated to reflux (157 °C) for 72 hours. During that time the reaction turned to a black solution with green tint. After 72 hours, the reaction was cooled to room temperature and a dark green solid precipitated out. The precipitate was collected on a glass filter frit and washed with hexanes (3x). The resulting solid was dissolved in CH_2Cl_2 and filtered through Celite to separate out a blue contaminant. Solvent was removed under reduced pressure to afford a green solid. The product was further dried under vacuum. Yield: 1.59 g (65%).

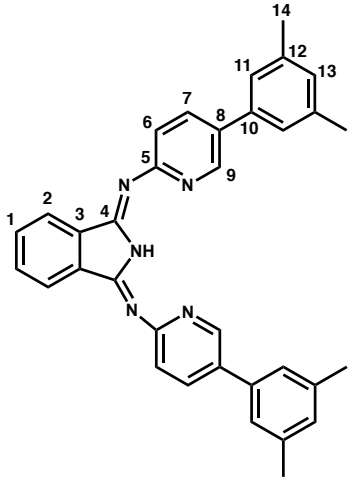

^{1}H NMR (700 MHz, $CDCl_3$): 2.42 (s, 12H, *H*^{14}), 7.06 (bs, 2H, *H*^{13}), 7.26 (s, 2H, *H*^{11}), 7.51 (d, 2H, $^3J_{HH}$ = 8.3 Hz, *H*^{6}), 7.66 (m, 2H, *H*^{1}), 7.94 (dd, 2H, $^3J_{HH}$ = 8.2 Hz, $^4J_{HH}$ = 2.5 Hz, *H*^{7}), 8.11 (m, 2H, *H*^{2}), 8.83 (d, 2H, $^4J_{HH}$ = 2.4 Hz, *H*^{9}), 14.0 (s, 1H, N-*H*). ^{13}C{^{1}H} NMR (176 MHz, $CDCl_3$): 21.5 (s, *C*^{14}), 122.7 (s, *C*^{2}), 123.2 (s, *C*^{6}), 125.1 (s, *C*^{11}), 129.7 (s, *C*^{13}), 131.7 (s, *C*^{1}), 133.6 (s, *C*^{8}), 135.9 (s, *C*^{3}), 136.6 (s, *C*^{7}), 137.9 (s, *C*^{10}), 138.8 (s, *C*^{12}), 146.4 (s, *C*^{9}), 153.6 (s, *C*^{4}), 159.9 (s, *C*^{5}).

3.4.3 X-ray Crystallographic Methodology and Data Tables:

Occlusion free single crystals were mounted on a loop with oil. Data was collected at -173 °C on a Bruker APEX II single X-ray diffractometer, Mo-radiation. Crystal-to-detector distance was 40 mm and exposure times were 5, 10, 15, 120, and 180 seconds per frame, depending on the crystal size (see Table 3.5 and Table 3.6). The scan width was 0.5°. The data was integrated and scaled using SAINT, SADABS within the APEX2 software package by Bruker.[44] Solution by direct methods (SHELXS, SIR97[45]) produced complete heavy atom phasing models consistent with the proposed structures. The structures were completed by difference Fourier synthesis with SHELXL97.[43,46] Scattering factors are from Waasmair and Kirfel.[47] Hydrogen atoms were placed in geometrically idealized positions and constrained to ride on their parent atoms with C---H distances in the range 0.95-1.00 Angstrom. Isotropic thermal parameters U_{eq} were fixed such that they were $1.2U_{eq}$ of their parent atom U_{eq} for CH’s and $1.5U_{eq}$ of their parent atom U_{eq} in case of methyl groups. All non-hydrogen atoms were refined anisotropically by full-matrix least squares. The structure of **13** exhibits tilted disorder for C16-C22, and N5. Two molecules of **17** appear to be related by a pseudo imperfect center of inversion, which is not part of the space group symmetry elements. The sample scattered badly, thus, restraints were required to all displacement parameters to keep them from diverging.

Table 3.5. Crystallographic data for compounds **12-15**.

Complex	**12**	**13**	**14**	**15**
Empirical formula	$C_{20}H_{19}N_5O$	$C_{22}H_{21}N_5$	$C_{20}H_{17}N_5O_2$	$C_{26}H_{25}N_5$
Formula weight	345.40	355.44	359.39	407.51
Temperature (K)	100(2)	100(2)	100(2)	100(2)
Wavelength (Å)	0.71073	0.71073	0.71073	0.71073
Crystal system	Monoclinic	Orthorhombic	Triclinic	Monoclinic
Space group	P 2_1	P 2_1cn	P -1	C 2/c
Unit cell axis a (Å)	12.943(3)	4.2770(18)	6.8808(7)	24.856(4)
Unit cell axis b (Å)	4.6627(11)	13.972(6)	11.0091(12)	8.0982(11)
Unit cell axis c (Å)	15.555(4)	30.321(13)	11.2937(12)	22.343(3)
Unit cell angle α (°)	90	90	79.950(6)	90
Unit cell angle β (°)	112.578(13)	90	86.299(6)	114.351(7)
Unit cell angle γ (°)	90	90	89.636(6)	90
Volume ($Å^3$)	866.8(4)	1811.9(13)	840.62(15)	4097.3(10)
Z	2	4	2	8
Density (Mg/m^3), calculated	1.323	1.303	1.420	1.321
Absorption coefficient (mm^{-1})	0.0086	0.080	0.096	0.081
F(000)	364	752	376	1728
Crystal size (mm^3)	0.63 x 0.15 x 0.14	0.440 x 0.170 x 0.120	0.45 x 0.22 x 0.11	0.34 x 0.18 x 0.12
Theta range for data collection	1.418 to 30.6657°	1.343 to 25.026°	1.84 to 28.33°	1.799 to 28.341°
Index ranges	-16<=h<=16, -32<=k<=32, -14<=l<=14	-5<=h<=5, -13<=k<=15, -36<=l<=36	-9<=h<=9, -14<=k<=14, -15<=l<=15	-33<=h<=33, -10<=k<=10, -29<=l<=29
Reflections collected	30657	8856	28576	104588
Independent reflections, R(int)	2954, 0.068	2704, 0.1977	4173, 0.0360	5095, 0.0957
Completeness to theta = 25.00 (%)	100.0	94.7	100.0	100.0
Max. and min. Transmission	0.6723 and 0.7461		0.9895 and 0.9581	0.587 and 0.754
Data / restraints / parameters	2954 / 1 / 249	2704 / 77 / 275	4173 / 0 / 251	5095 / 0 / 282
Goodness-of-fit on F^2	1.049	0.956	1.039	1.068
Final R indices [I>2sigma(I)]	R1 = 0.0237, wR2 = 0.0474	R1 = 0.0997, wR2 = 0.2170	R1 = 0.0399, wR2 = 0.0957	R1 = 0.0477, wR2 = 0.1127
R indices (all data)	R1 = 0.0352, wR2 = 0.0504	R1 = 0.2174, wR2 = 0.2752	R1 = 0.0535, wR2 = 0.1039	R1 = 0.0747, wR2 = 0.1273
Largest diff. peak and hole ($e.Å^{-3}$)	0.237 and -0.298	0.297 and -0.327	0.346 and -0.223	0.236 and -0.283

Table 3.6. Crystallographic data for compounds **16** and **17**.

Complex	**16**	**17**
Empirical formula	$C_{18}H_{11}Br_2N_5$	$C_{34}H_{29}N_5$
Formula weight	457.14	507.62
Temperature (K)	100(2)	100(2)
Wavelength (Å)	0.71073	0.71073
Crystal system	Monoclinic	Monoclinic
Space group	P 2_1/c	P 2_1/c
Unit cell axis a (Å)	12.509(2)	7.447(4)
Unit cell axis b (Å)	24.541(4)	23.222(13)
Unit cell axis c (Å)	11.059(2)	30.580(18)
Unit cell angle α (°)	90	90
Unit cell angle β (°)	105.110(9)	94.915(19)
Unit cell angle γ (°)	90	90
Volume ($Å^3$)	3277.5(10)	5269(5)
Z	8	8
Density (Mg/m^3), calculated	1.853	1.280
Absorption coefficient (mm^{-1})	4.958	0.077
F(000)	1792	2144
Crystal size (mm^3)	0.57 x 0.21 x 0.15	0.320 x 0.150 x 0.080
Theta range for data collection	1.660 to 28.413°	1.337 to 25.639°
Index ranges	-16<=h<=16, -32<=k<=32, -14<=l<=14	-9<=h<=9, -27<=k<=28, -37<=l<=37
Reflections collected	136420	19146
Independent reflections, R(int)	8150, 0.0593	9742, 0.6605
Completeness to theta = 25.00 (%) 98.7	100.0	99.9
Max. and min. Transmission	0.5531 and 0.7457	
Data / restraints / parameters	8150 / 0 / 451	9742 / 468 / 711
Goodness-of-fit on F^2	1.022	0.872
Final R indices [I>2sigma(I)]	R1 = 0.0237, wR2 = 0.0474	R1 = 0.1156, wR2 = 0.1866
R indices (all data)	R1 = 0.0352, wR2 = 0.0504	R1 = 0.4789, wR2 = 0.3227
Largest diff. peak and hole ($e.Å^{-3}$)	0.427 and -0.336	0.346 and -0.350

3.5 Notes and References to Chapter 3

1. Dupont,J.; Consort, C.S.; Spencer, J.; *Chem. Rev.* **2005**, *105*, 2527-2571.
2. a) Albrecht, M.; Van Koten, G. *Angew. Chem., Int. Ed.* **2001**, *40*, 3750-3781. b) van der Boom, M.E.E.; Milstein, D. *Chem. Rev.* **2003**, *103*, 1759-1792. c) Nishiyama, H. *Chem. Soc. Rev.* **2007**, *36*, 1133-1141. d) Choi, J.; MacArthur, A.H.R.; Brookhart, M.; Goldman, A.S. *Chem. Rev.* **2011**, *111*, 1761-1779.
3. Siegl, W.O. *J. Organometallic Chem.* **1976**, *107*, C27-C30.
4. Elvidge, J.A.; Linstead, R.P. *J. Am. Chem. Soc.* **1952**, 5000-5007.
5. Clark, P.F.; Elvidge, J.A.; Linstead, R.P. *J. Chem. Soc.* **1953**, 3593-3601.
6. a) Siegl, W.O. *J. Org. Chem.* **1977**, *42*, 1872-1878. b) Siegl, W.O. *J. Heterocylic Chem.* **1981**, *18*, 1613-1618. c) Siegl, W.O. *Inorg. Nucl. Chem. Lett.* **1974**, *10*, 825-829.
7. Saussine, L.; Brazi, E.; Robine, A.; Mimoun, H.; Fischer, J.; Weiss, R. *J. Am. Chem. Soc.* **1985**, *107*, 3534-3540.
8. Camerano, J.A.; Samann, C.; Wadepohl, H.; Gade, L.H. *Organometallics* **2011**, *30*, 379-382.
9. Sauer, D.C.; Wadepohl, H.; Gade, L.H. *Inorg. Chem.* **2012**, *51*, 12948-12958.
10. a) Geri, J.B.; Szymczak, N.K. *J. Am. Chem. Soc.* **2015**, *137*, 12808-12814. b) Tseng, K-N.T.; Kampf, J.W.; Szymczak, N.K. *ACS Catal.* **2015**, *5*, 5468-5485.
11. Muller, A.L.; Bleith, T.; Roth, T.; Wadepohl, H.; Gade, L.H. *Organometallics* **2015**, *34*, 2326-2342.
12. Meder, M.; Galka, C.H.; Gade, L.H. *Monatshefte fur Chemie* **2005**, *136*, 1693-1706.
13. Falivene, L.; Credendino, R.; Poater, A.; Petta, A.; Serra, L.; Oliva, R.; Scarano, V.; Cavallo, L. *Organometallics* **2016**, *35*, 2286-2293.
14. Calculated online at www.molnac.unisa.it/omtools/sambvca2.0/index.html
15. Tsukamoto, I.; Koshio, H.; Kuramochi, T.; Saitoh, C.; Yanai-Inamura, H.; Kitada-Nozawa, C.; Yamamoto, E.; Yatsu, T.; Shimada, Y.; Sakamoto, S.; Tsukamoto, S. *Bioorg. Med. Chem.* **2009**, *17*, 3130-3141.
16. Elmkaddem, M.K.; Fischmeister, C.; Thomas, C.M.; Renaud, J-L. *Chem. Commun.* **2010**, *46*, 925-927.
17. 21 is commercially available or can be synthesized easily via ref. 39.
18. a) Buchwald, S.L. *Top. Curr. Chem.* **2002**, *219*, 131-209. b) Jiang, L.; Buchwald, S.L. In metal-catalyzed cross-coupling reactions, 2nd ed.; De Meijere, A.; Diederich, F., Eds.; Wiley-VCH: New York, 2004; pp 699-760.
19. a) Knochel, P.; Dohle, W.; Gommerman, N.; Kneisel, F.; Kopp, F.; Korn, T.; Sapountzis, I.; Vu, V. *Angew. Chem., Int. Ed.* **2003**, *42*, 4302-4320. b) Miyaura, N.; Suzuki, A. *Chem. Rev.* **1995**, *95*, 2457-2483. c) Negishi, A. *Acc. Chem. Res.* **1982**, *15*, 340-348.
20. Maloney, K.M.; Nwakpuda, E.; Kuethe, J.T.; Yin, J. *J. Org. Chem.* **2009**, *74*, 5111-5114.
21. Cox, J.D.; Pilcher, D. Thermochemistry of organic and organometallic compounds, Academic press, London, 1970.
22. Kato, Y.; Okada, S.; Tomimoto, K.; Mase, T. *Tetrahedron Lett.* **2001**, *42*, 4849-4851.
23. Katritzky, A. *Org. Prep. Proced. Int.* **1994**, *26*, 436-444.
24. Lyle, M.P.A.; Draper, N.D.; Wilson, P.D. *Org. Biomol. Chem.* **2006**, *4*, 877-885.
25. Kijrungphaiboon, W.; Chantarasriwong, O.; Chavasiri, W. *Tetrahedron Lett.* **2012**, *53*, 674-677.
26. Sugimoto, O.; Mori, M.; Moriya, K.; Tanji, K. *Helvetica Chimica Acta* **2001**, *84*, 1112-1118.

27. Sugimoto, O.; Mori, M.; Tanji, K. *Tetrahedron Lett.* **1999**, *40*, 7477-7478.
28. Attempts at identifying this product was not undertaken because it was not the compound of interest.
29. Lyle, M.P.A.; Wilson, P.D. *Org. Lett.* **2004**, *6*, 855-857.
30. a) Wolfe, J.P.; Wagaw, S.; Marcoux, J-F.; Buchwald, S.L. *Acc. Chem. Res.* **1998**, *31*, 805-818. b) Hartwig, J.F. *Angew. Chem., Int. Ed.* **1998**, *37*, 2046-2067. c) Yang, B.H.; Buchwald, S.L. *J. Organomet. Chem.* **1999**, *576*, 125-146. d) Ruiz-Castillo, P.; Buchwald, S.L. *Chem. Rev.* **2016**, *116*, 12564-12649.
31. Ahman, J.; Buchwald, S.L. *Tetrahedron Lett.* **1997**, *38*, 6363-6366.
32. Wolfe, J.P.; Ahman, J.; Sadighi, J.P.; Singer, R.A.; Buchwald, S.L. *Tetrahedron Lett.* **1997**, *38*, 6367-6370.
33. Jaime-Figueroa, S.; Liu, Y.; Muchowski, J.M.; Putman, D.G. *Tetrahedron Lett.* **1998**, *39*, 1313-1316.
34. Lee, S.; Jorgensen, M.; Hartwig, J.F. *Org. Lett.* **2001**, *3*, 2729-2732.
35. Huang, X.; Buchwald, S.L. *Org. Lett.* **2001**, *3*, 3417-3419.
36. Vo, G.D.; Hartwig, J.F. *J. Am. Chem. Soc.* **2009**, *131*, 11049-11061.
37. Bhagwanth, S.; Adjabeng, G.M.; Hornberger, K.R. *Tetrahedron Lett.* **2009**, *50*, 1582-1585.
38. Christoph Samann Thesis, Univ. Heidelberg
39. Lyle, M.P.A.; Wilson, P.D. *Org. Lett.* **2004**, *6*, 855-857.
40. Coulson, D.R. *Inorg. Synth.* **1972**, *13*, 121-124.
41. Agarwal, P.K.; Saifuddin, M.; Kundu, B. *Tetrahedron* **2010**, *66*, 862-870.
42. Schilf, W. *J. Molec. Struct.* **2004**, *691*, 141-148.
43. Farrugia, L.J. *J. Appl. Cryst.* **2012**, *45*, 849-854.
44. 44.Bruker (**2007**) APEX2 (version 2.1-4), SAINT (version 7.34A), SADABS (version 2007/4), BrukerAXS Inc., Madison, Wisconsin, USA.
45. a) Altomare, A.; Burla, C.; Camalli, M.; Cascarano, G.L.; Giacovazzo, C.; Guagliardi, A.; Molitern, A.G.G.; Polidori, G.; Spagna, R. *J. Appl. Cryst.* **1999**, *32*, 115-119. b) Altomare, A.; Cascarano, G.L.; Giacovazzo, C.; Guagliardi, A. *J. Appl. Cryst.* **1993**, *26*, 343-350.
46. a) Sheldrick, G.M. (**1997**) SHELXL-97, Program for the refinement of crystal structures. University of Gottingen, Germany. b) Sheldrick, G.M. *Acta. Cryst.* **2015**, *C17*, 3-8.
47. Waasmaier, D.; Kirfel, A. *Acta. Cryst. A.* **1995**, *51*, 416-430.

Chapter 4

Synthesis and Reactivity of Late Transition Metal BPI Complexes: Applications toward Alkane Dehydrogenation

4.1 Introduction

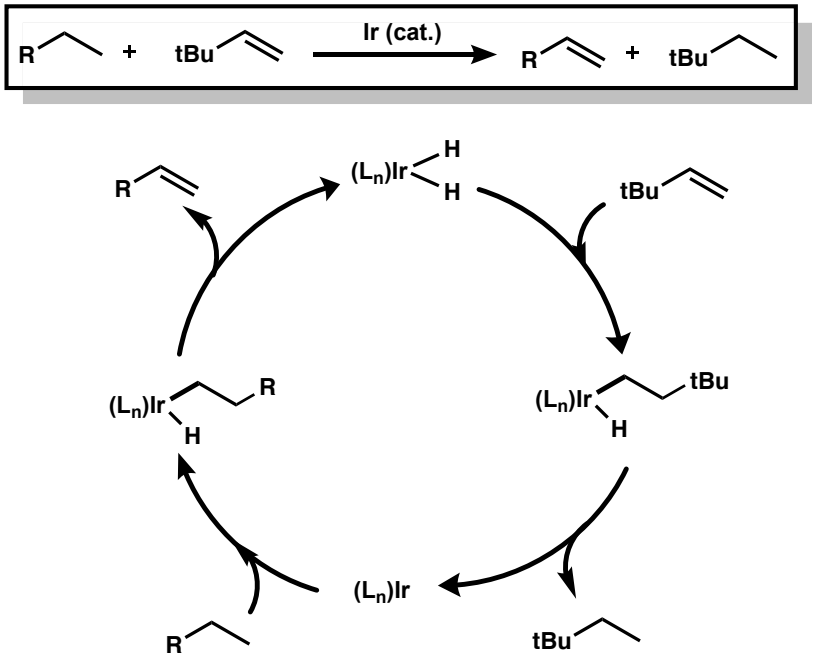

Scheme 4.1. Proposed cycle for transfer alkane dehydrogenation

As discussed in Chapter 1, the most successful homogeneous alkane dehydrogenation catalysts to date have been pincer-ligated Ir complexes.[1] In the proposed mechanism of alkane dehydrogenation with these complexes, the active catalyst is an Ir^{I} complex that oxidatively adds the alkane (Scheme 4.1).[2] This Ir^{I} complex is very reactive towards dinitrogen, water, oxygen, and the olefin product, all of which work to inhibit dehydrogenation.[3,4] This pathway would also not be amenable to using molecular oxygen as the hydrogen acceptor because of the highly reactive nature of Ir^{I}. To circumvent this problem, instead of oxidative addition, an alternative pathway to activate C-H bonds, concerted metalation-deprotonation (CMD), can be considered. In CMD, the metal oxidation state remains constant throughout. In the CMD mechanism, coordination of the alkane to the metal results in a C-H σ-complex and the M-R bond is formed when an internal base, such as a carboxylate, deprotonates the metal σ-bound alkane (Scheme 4.2).[5,6]

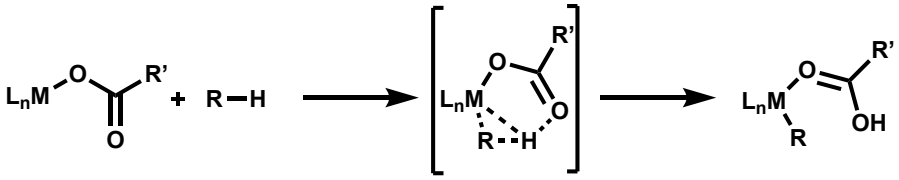

Scheme 4.2. Concerted metalation deprotonation mechanism

Nishiyama and coworkers reported that the Ir^{III} complex, (Phebox)$Ir(OAc)_2(H_2O)$ (Phebox = 2,6-bis(4,4-dimethyloxazolinyl)-3,5-dimethylphenyl) activates C-H bonds of arenes and alkanes at 80-160 °C to form the corresponding Ir^{III}-aryl/ Ir^{III}-alkyl complexes and acetic acid.[7] Later, Goldberg and coworkers found at higher temperatures (200 °C), (Phebox)$Ir(OAc)_2(H_2O)$ converted octane to octene via a stoichiometric dehydrogenation which

formed the novel Ir-H complex, (Phebox)Ir(OAc)(H). Notably, nitrogen, water, or the alkene product did not inhibit this dehydrogenation reaction.[8]

Furthermore, it was found that (Phebox)Ir$(OAc)_2(H_2O)$ could be regenerated from (Phebox)Ir(OAc)(H) using molecular oxygen and acetic acid at room temperature.[9] Together, alkane dehydrogenation of octane to octene followed by regeneration of the catalyst with oxygen represents a complete cycle of a potential catalytic reaction to accomplish aerobic octane dehydrogenation (Scheme 4.3). However, catalytic activity was not realized for this system and preliminary investigations suggested that the catalyst decomposed at 200 °C under an O_2 atmosphere.[10] There are a few strategies that can be employed to circumvent the problem of catalyst decomposition. The first is lowering the temperatures needed to achieve C-H activation (160 °C) and β-H elimination (200 °C). To that end, Goldman and coworkers have found that Lewis acids, such as $NaBAr^F{}_4$, lower the β-H elimination of (Phebox)Ir(OAc)(octyl), the product of C-H activation, to 55 °C, a drastic improvement from 200 °C that renders this step no longer rate-limiting.[11] $NaBAr^F{}_4$ was found to facilitate κ^1 coordination of the acetate ligand, therefore opening a coordination site for β-H elimination to occur. Even more recently, Jones and coworkers have shown that varying the carboxylate ligands can also affect the β-H elimination step. Kinetic studies on a series of (Phebox)Ir carboxylate complexes revealed that carboxylates with higher pK_a values (of the corresponding carboxylic acids) promote the rate of β-H elimination by facilitating κ^1 coordination.[12] In addition, the Goldberg lab continues to explore various pincer ligand systems to lower the energetic barrier to C-H activation.

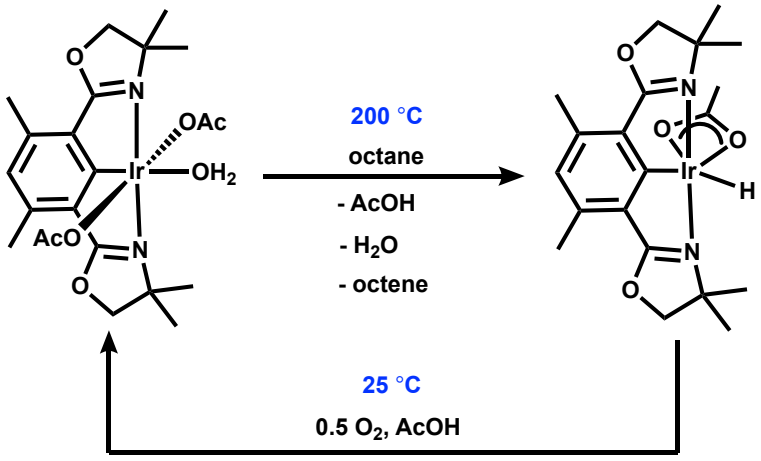

Scheme 4.3. Dehydrogenation of octane with Ir^{III}

Another approach is to identify a new ligand system and catalyst that is oxidatively stable at elevated temperatures, which is the strategy this work focuses on. To achieve this our ligands of choice, as discussed in Chapter 3, are the 1,3-bis(arylimino)isoindoline ligands. I have found that these ligands are stable up to 200 °C under aerobic conditions. The results reported below are efforts towards accessing new Ir^{III} complexes using each ligand variation synthesized (Chapter 3, Figure 4.1). The reactivity in relation to alkane dehydrogenation mediated by the successfully prepared complex (BPI)IrEt(OAc) (**35**) will also be discussed.

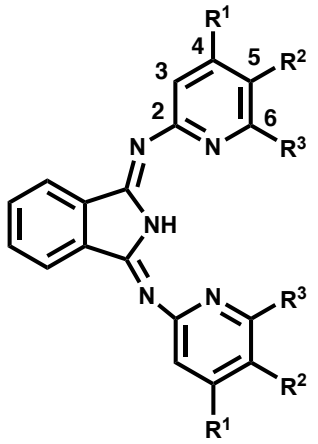

BPI-H (12): $R^1 = CH_3$; R^2, R^3 = H

^{Me}BPI-H (13): R^1, $R^3 = CH_3$; R^2 = H

^{OMe}BPI-H (14): R^1, R^2 = H; $R^3 = OCH_3$

^{Pent}BPI-H (15): $R^1 = CH_3$, $R^3 = C_3H_6$

^{Br}BPI-H (16): R^1,R^2 = H; R^3 = Br

^{xylyl}BPI-H (17): R^1, R^3 = H; R^2 = 3,5-xylyl

Figure 4.1. ^{R}BPI-H ligands synthesized and explored

4.2 Metalation and Attempted Metalation of ^{R}BPI-H Ligands

*4.2.1. Metalation of BPI-H (**12**)*

Efforts were initially focused on the metalation of 1,3-bis[2-(4-methylpyridyl)imino]isoindoline (BPI-H, **12**). This ligand has previously been metalated to many transition metals, including iridium, so it is feasible to synthesize a (BPI)Ir complex.[13,14] Our initial target molecule was the bis-acetate complex, (BPI)$Ir^{III}(OAc)_2$ (**30**), which would enable us to explore C-H activation and β-H elimination (Figure 4.2). To accomplish this, two approaches were taken. In the first route, **12** reacts with $[(COD)Ir(OMe)]_2$ resulting in (κ^2-BPI)Ir(COD) (**31**).[15] Oxidation of **31** with I_2 resulted in a clean reaction to form a deep red complex (Scheme 4.4).

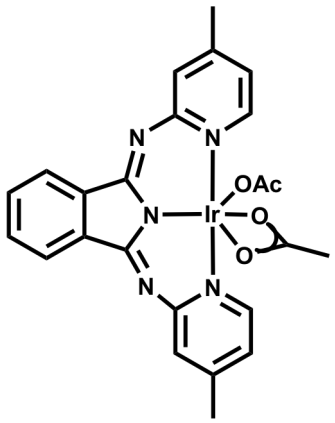

30

Figure 4.2. Initial target (BPI)Ir$(OAc)_2$

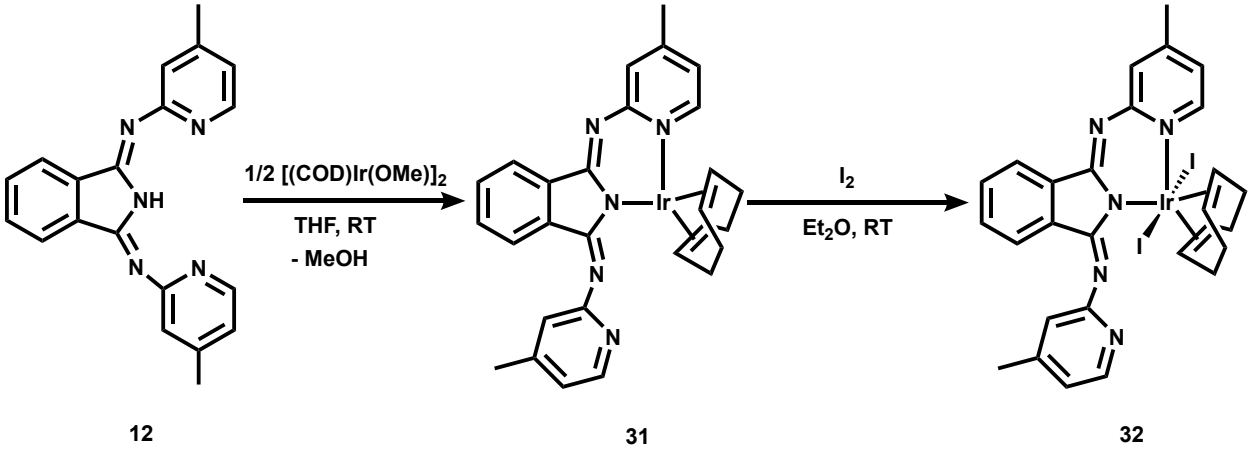

Scheme 4.4. Reaction of 12 with $[(COD)Ir(OMe)]_2$

The ^{1}H NMR spectrum of **32** had signals ranging from 6.18-8.26 ppm and singlets at 2.33 and 2.44 ppm corresponding to the BPI aryl and methyl protons, respectively. Additionally, broad signals associated with the protons of bound COD ligand were observed at 2.77, 3.20, 6.18, and 6.71 ppm. Analysis by X-ray crystallography identified the complex as (κ^2-BPI)Ir(COD)$(I)_2$ (**32**) (Figure 4.3). Complex **32** has a pseudo-octahedral geometry about the Ir center with the BPI ligand in a κ^2 coordination mode with one free (non-coordinated) pyridine arm. The iridium is also coordinated by two iodide ligands with Ir-I bond lengths of 2.72(4) and 2.74(4) Å. The Ir-I lengths are comparable to other Ir^{III}-I complexes.[16] Notably, the COD has not been displaced and remains bound to the Ir^{III} center. The Ir-C distances of the COD ligand are 2.24(5) (Ir-C21), 2.23(6) (Ir-C22), 2.24(6) (Ir-C25), and 2.23(5) (Ir-C26), respectively. These Ir-C bond lengths are longer

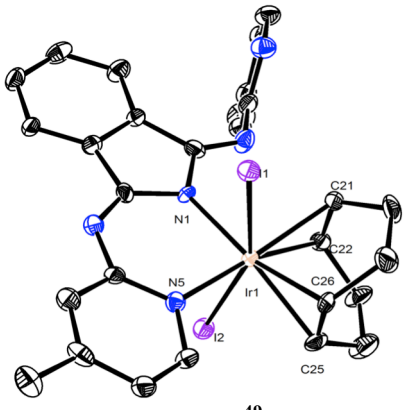

Figure 4.3: ORTEP[49] drawing of 32 with thermal ellipsoids at 50% probability. Hydrogen atoms excluded for clarity.

than those in **31**, which is expected with oxidation from Ir^{I} to Ir^{III}. Complex **32** is a rare example of an Ir^{III} with a bound COD.[17]

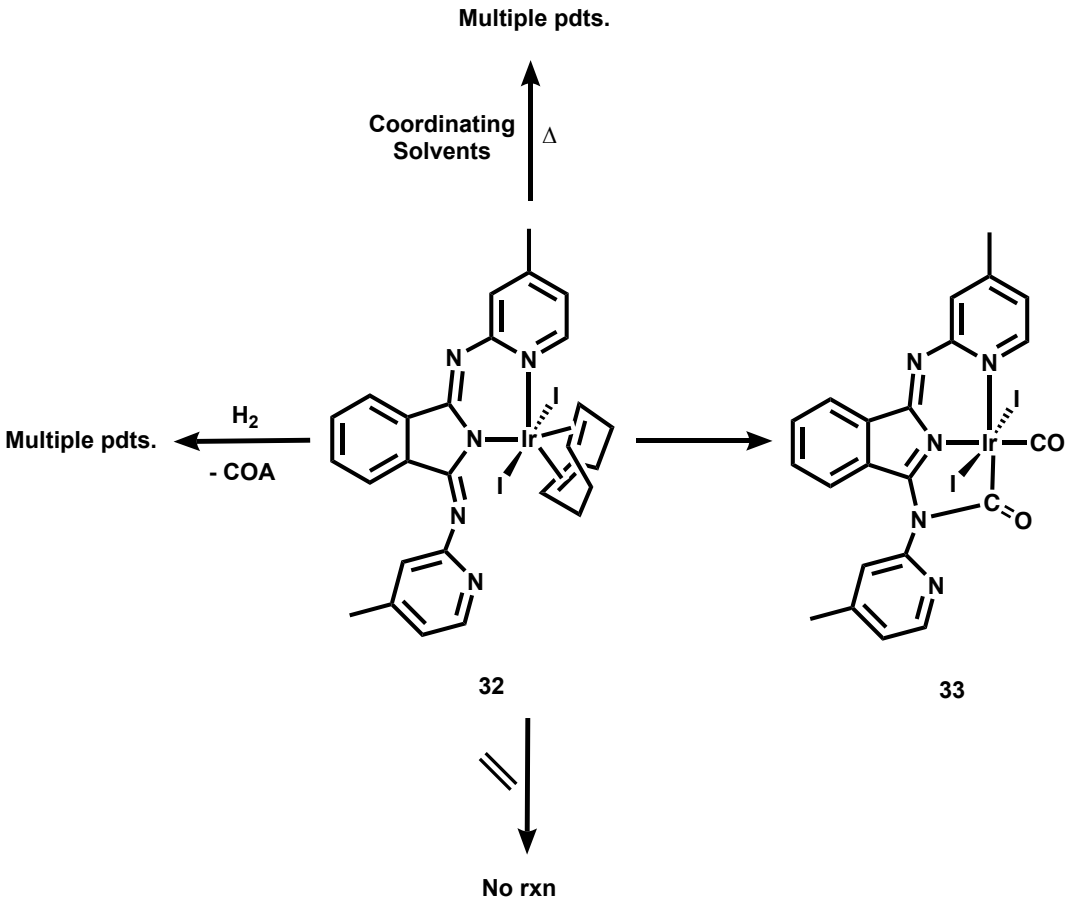

Scheme 4.5. Attempts to displace COD from 32

Attempts to displace COD from **32** and obtain κ^3 coordination of BPI were unsuccessful (Scheme 4.5).[18] Heating **32** in coordinating solvents (e.g. CD_3CN, THF-d_8) resulted in multiple products by ^1H NMR as well as insoluble precipitates, which may be indicative of oligomeric material. Another attempt to remove the COD was by hydrogenation. Treatment of **32** with 3 atm H_2 resulted in formation of cyclooctane (1.55 ppm, ^1H NMR), but also multiple metal containing products. Attempts to displace the COD with ethylene resulted in no observable reaction. In

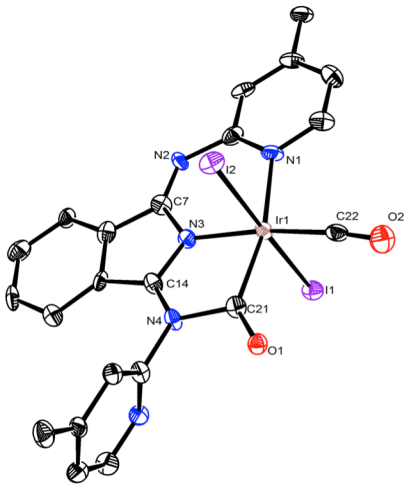

Figure 4.4: ORTEP[49] drawing of 33 with thermal ellipsoids at 50% probability. Hydrogen atoms excluded for clarity.

contrast, CO displaced the COD ligand to make one new product cleanly (Scheme 4.5). The ^{1}H NMR spectrum showed peaks associated with free COD (2.35 and 5.56 ppm) as well as new sets of aryl signals, ranging from 6.56-8.58 ppm, and methyl signals at 2.51 and 2.54 ppm. Analysis by X-ray crystallography revealed the product to be (κ^2-BPI)Ir(CO)$_2$(I)$_2$ (**33**) as shown in Figure 4.4. Interestingly, one of the CO ligands that replaced COD was attacked by the nitrogen on the BPI arm to form a new N-C bond. In addition, the N(3)-C(7) and N(3)-C(14) bond lengths are 1.40(1) and 1.332(9) Å, consistent with the latter being closer to a double bond. This result suggests that the nitrogen on the backbone is nucleophilic.

Due to the unsuccessful attempts at obtaining κ^3 coordination of BPI through the use of a COD ligated iridium starting material, another approach was taken. In this route, κ^3 coordination of BPI was achieved by treating deprotonated BPI ligand with Ir(C$_2$H$_4$)$_4$Cl generated *in situ*, resulting in (BPI)Ir(C$_2$H$_4$)$_2$ (**34**) as a dark violet solid (Scheme 4.6).[15] Complex **34** was fully characterized by NMR spectroscopy (^{1}H and ^{13}C) and X-ray crystallography. The ^{1}H NMR spectrum shows two triplets at 1.16 and 2.63 ppm corresponding to each bound ethylene, consistent with literature on a closely related complex.[15] Its solid-state molecular structure has Ir(1)-C(21), Ir(1)-C(22), Ir(1)-C(23),

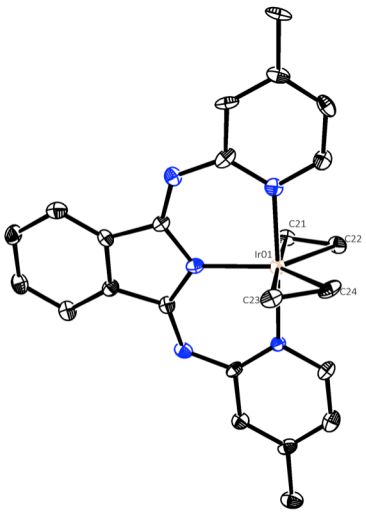

Figure 4.5: ORTEP[49] drawing of 34 with thermal ellipsoids at 50% probability. Hydrogen atoms excluded for clarity.

and Ir(1)-C(24) bond lengths of 2.131(9), 2.15(1), 2.142(8), and 2.141(7) Å, respectively (Figure 4.5). Additionally, the bond lengths of the bound ethylene carbons C(21)-C(22) and C(23)-C(24) are 1.41(1) and 1.43(2) Å, respectively. These values are comparable to the (Phebox)Ir(C_2H_4)$_2$ complex reported by Goldman and coworkers.[11]

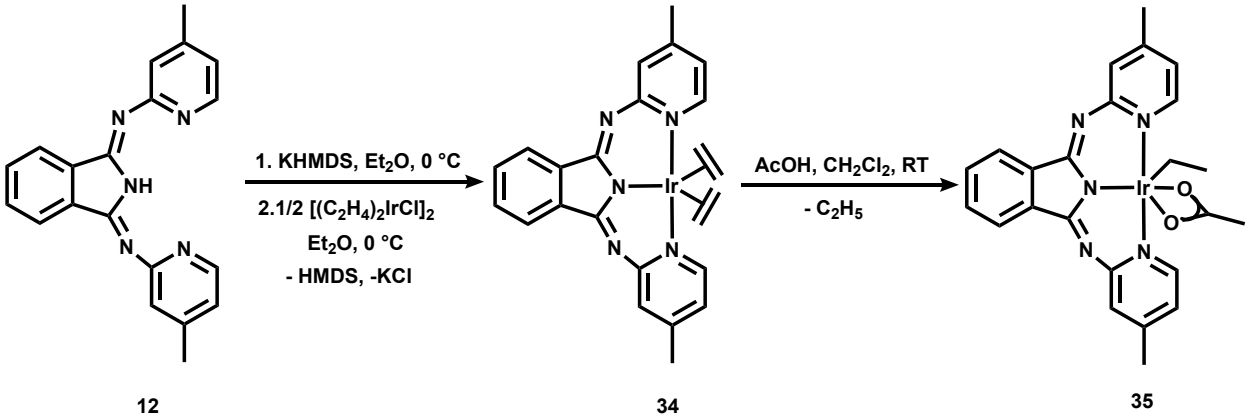

Scheme 4.6. Metalation of 12 with Ir to form a (BPI)Ir^{III} complex

Treatment of **34** with acetic acid (AcOH) at room temperature resulted in clean formation of novel Ir^{III} complex (BPI)IrEt(OAc) (**35**, Scheme 4.6). The ^{1}H NMR spectrum features triplet and quartet signals at 0.15 and 1.38 ppm consistent with an Ir-Et moiety. In addition, a singlet for the bound acetate is observed at 2.06 ppm. The solid-state molecular structure shows a distorted octahedral geometry with Ir(1)-O(1), Ir(1)-O(2), Ir(1)-C(23), C(23)-C(24), C(21)-O(1), and C(21)-O(2) bond lengths of 2.336(3), 2.124(3), 2.059(5), 1.530(6), 1.251(6), 1.308(6) Å, respectively (Figure 4.6). The Ir-OAc bond lengths are comparable to the previously published (Phebox)Ir(OAc)(hexyl) complex, suggesting κ^2 coordination.[7] To our knowledge, complex **35** is the first known example of an Ir^{III} complex with a meridonally bound BPI ligand. Gade and coworkers recently published (BPI)Ir^{III} complexes with the BPI ligand both κ^2 and κ^3 coordinated (Figure 4.7). In the κ^3 coordinated complex the BPI ligand is non planar.[19] Heating **35** to 200 °C

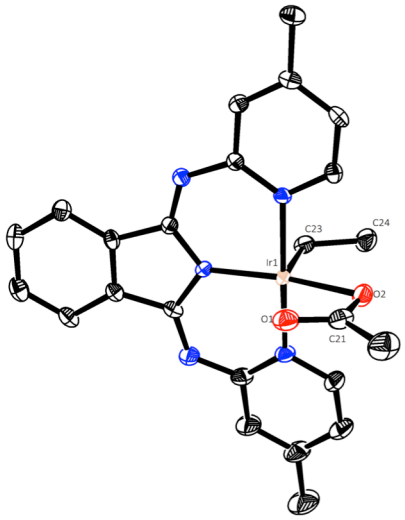

Figure 4.6: ORTEP[49] drawing of 35 with thermal ellipsoids at 50% probability. Hydrogen atoms excluded for clarity.

in the presence of excess AcOH did not result in a bis-acetate complex, suggesting that the bound ethyl is not labile. This is in contrast to the Phebox system where the (Phebox)Ir(octyl)(OAc) reacts with AcOH to form the bis-acetate (Phebox)Ir(OAc)$_2$.[7,8] The use of stronger acids, such as triflic acid (TfOH) results in multiple products with broad peaks downfield of 10 ppm often observed. These peaks likely correspond to an N-H bond because the imine backbone is susceptible to protonation.[20]

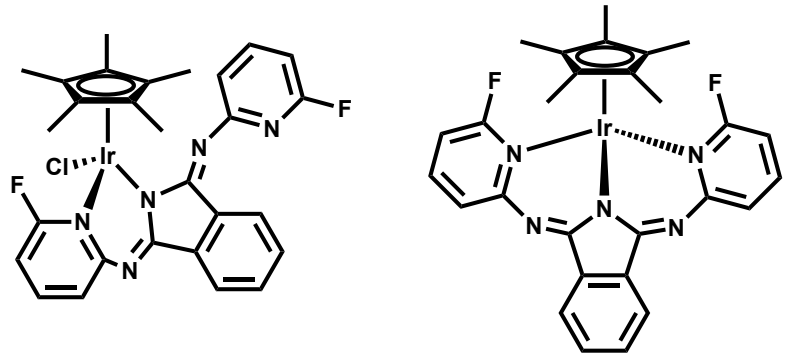

Figure 4.7. (BPI)Ir^{III} complexes published by Gade

*4.2.2. Metalation of ^{Me}BPI-H (**13**)*

Efforts to prepare the catalytically relevant intermediate (BPI)Ir(OAc)$_2$ (**30**) from (BPI)Ir(Et)(OAc) (**35**) have been unsuccessful (as alluded to above). Furthermore, as will be discussed below in detail, β-H elimination from **35** has also proved challenging. I hypothesized that placing bulky substituents on the 6-position of the ligand pyridine arms would add more steric hindrance around the metal center and promote κ^1 coordination of the acetate to facilitate

β-H elimination. In addition, this steric bulk may also work to weaken the Ir-Et, bond making it more susceptible to replacement. To this end, metalation of ^{Me}BPI-H (**13**) was explored. As discussed in Chapter 3, placing the methyl groups on the 6-position of the pyridine arms do make **13** more sterically bulky then **12** (Table 3.4). Unfortunately, all attempts at synthesizing either iridium and rhodium complexes with **13** were unsuccessful. The experimental conditions and results are summarized in Table 4.1 (Scheme 4.7). As shown, a variety of metal starting materials, bases, and reaction conditions were explored in an effort to metalate **13**.

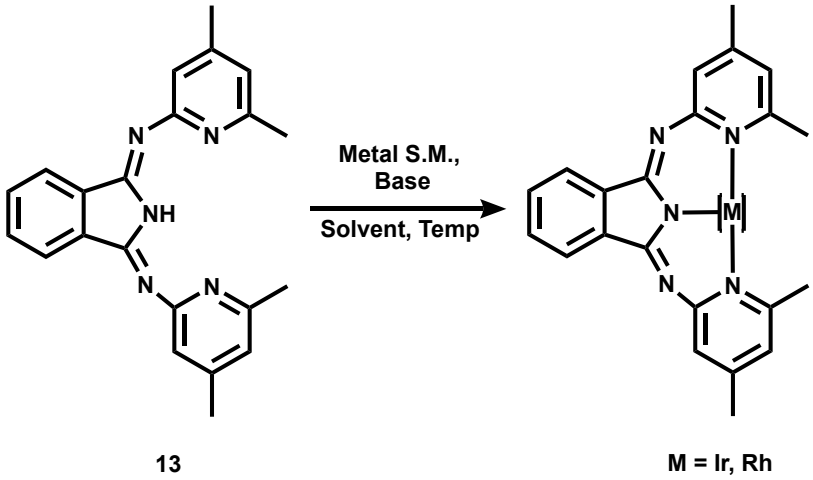

Scheme 4.7. Attempted metalation of 13

Table 4.1. Reaction conditions and results for the attempted metalation of 13

Trial #	Metal starting material	Base	Solvent	Temperature (°C)	Result
1[a]	$(C_2H_4)_4IrCl$ (in situ)	NaH	THF/Et_2O	0	Multiple species
2[b]	$IrCl_3•3H_2O$	NaOMe/ $NaHCO_3$	CD_3OD	RT or 60	No rxn
3	$Ir_3(OAc)_n$	-	CD_3OD	60	No rxn
4[c]	$[(COE)_2IrCl]_2$	-	tol-d_8	100	Free ligand and multiple species
5	$[(COD)Ir(OMe)]_2$	-	THF-d_8	RT	Majority free ligand
6[d]	$[(COD)IrCl]_2$	NaH	THF-d_8	RT or 100	Multiple species

7	$Ir(CO)_2Cl(pyridine)$	-	tol-d_8	100	No rxn
8	$RhCl_3•3H_2O$	NaOMe	MeOH	RT	No rxn
9	$[(COD)RhCl]_2$	NaH	THF-d_8	RT	Multiple species

a. Reaction performed under an ethylene atmosphere. Ligand was deprotonated in situ. b. This reaction was performed multiple times with both NaOMe and $NaHCO_3$ as base at RT and 60 °C. c. This reaction was done both under inert atmosphere and H_2 atmosphere. d. This reaction was performed multiple times with and without base at RT and 100 °C.

Notably, the same conditions used for the metalation of **12** to iridium to form **34** were unsuccessful with **13** and resulted in multiple species (Table 4.1, Entry 1). The ^{1}H NMR spectrum from the reaction was messy with many broad signals. Entries 2-5, 7, and 8 resulted in a majority of free ligand, suggesting no reaction occurred. The metal starting materials containing COD, entries 6 and 9, did result in a reaction, but the ^{1}H NMR spectrum from these reactions were quite messy, likely indicative that multiple products had formed. The challenges encountered in attaching **13** to the metal may be attributed to the binding pocket of **13** being too sterically hindered, therefore not allowing a metal to bind. As discussed in Chapter 3, the % volume buried of **13** is 64.8, higher than **12** (59%), suggesting that the binding pocket is in fact hindered.[21,22] Falivene *et. al.* reported that even "small structural differences" in the catalytic binding pocket could result in an energy difference of ca. 2 kcal/mol.[21] However, they did not specific what % volume buried change would correspond to a small structural difference.

*4.2.3. Metalation of ^{OMe}BPI-H (**14**)*

In addition to adding bulk around the metal center, it was simultaneously hypothesized that placing more electron-donating substituents, such as a methoxy group, on the pyridine ring should increase the electron donating ability of the BPI ligand, making the metal more electron-rich, and promoting κ^1 coordination of the carboxylate. κ^1 coordination of the carboxylate would then open a coordination site for β-H elimination to occur. The metalation of novel ^{OMe}BPI-H

(**14**) was attempted with a variety of both iridium and rhodium starting materials. The results of these attempts are summarized in Table 4.2 (Scheme 4.8).

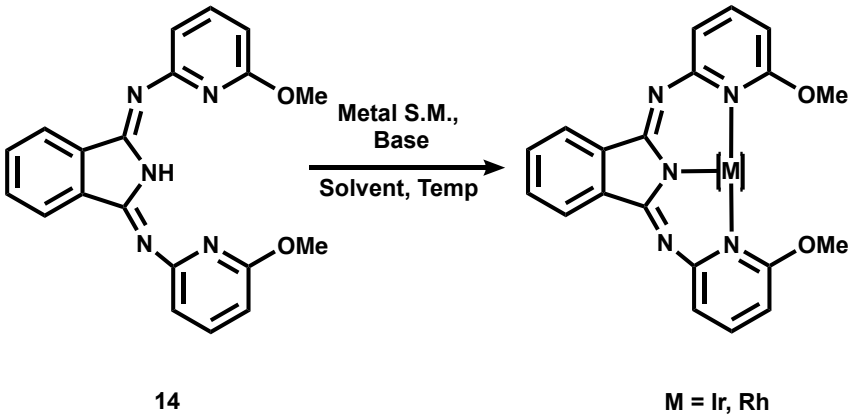

Scheme 4.8. Attempted metalation of 14

Table 4.2. Reaction conditions and results for the attempted metalation of 14

Trial #	Metal starting material	Base	Solvent	Temperature (°C)	Result
1[a]	$IrCl_3 \bullet 3H_2O$	NaOMe/ NaH/ $NaHCO_3$	CD_3OD/ CD_3CN/ THF-d_8	60 or 70	No rxn
2[b]	$(C_2H_4)_4IrCl$ (in situ)	NaH	THF/Et_2O	0	Broad indistinguishable NMR
3[c]	$[(COE)_2IrCl]_2$	-	tol-d_8	100	Multiple species
4	$[(COD)Ir(OMe)]_2$	-	THF	RT	Free ligand and multiple species
5[d]	$[(COD)IrCl]_2$	NaH	THF	RT or 100	Free ligand and Multiple species
6	$Ir(CO)_2Cl$(pyridine)	-	tol-d_8	100	No rxn
7	$RhCl_3 \bullet 3H_2O$	NaOMe	CD_3OD	60	Multiple species
8	$[(COD)RhCl]_2$	NaH	THF	RT	Broad indistinguishable NMR

a. This reaction was performed multiple times with both varying base and solvent at 60 and 70 °C. b. Reaction performed under an ethylene atmosphere. Ligand was deprotonated in situ. c. This reaction was done both under inert atmosphere and H_2 atmosphere. d. This reaction was performed multiple times with and without base at RT and 100 °C.

Similar to the reactions involving **13**, most metalation attempts with **14** resulted in no reaction or a majority of free ligand with minor species (Table 4.2, Entries 1, 4-6). All other reactions resulted in either multiple species or broad indistinguishable ^{1}H NMR spectra (Table 4.2, Entries 2-3, 7-8). When comparing the % volume buried of **14** to all other ligand variations, it has the highest calculated value (71.9),[21,22] suggesting that the binding pocket is the most hindered of the ligands investigated (Table 3.4).

*4.2.4. Metalation of ^{Pent}BPI-H (**15**)*

After the unsuccessful attempts at metalating both **13** and **14**, ^{Pent}BPI-H (**15**) was the next ligand of choice. I hypothesized that the inability of **13** and **14** to metalate was due to too much steric hindrance. Therefore, I reasoned that a cyclopentyl ring would still add some sterics near the metal center to potentially promote β-H elimination (en route to alkane dehydrogenation), but would be more open due to the pulled back ring system, thus allowing metalation to occur. This hypothesis is supported by the % volume buried calculation where **15** has a value of 62.9,[21,22] which is lower than both **13** and **14**, but still slightly more hindered than **12**. Table 4.3 shows the reaction conditions and results from the attempted metalations of **15** (Scheme 4.9).

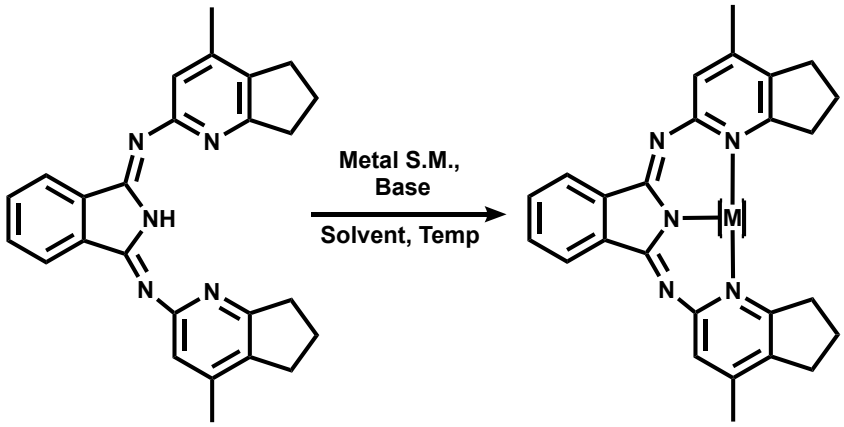

Scheme 4.9. Attempted metalation of 15

Table 4.3. Reaction conditions and results for the attempted metalation of 15

Trial #	Metal starting material	Base	Solvent	Temperature (°C)	Result
1[a]	$IrCl_3 \bullet 3H_2O$	NaOMe/ NaH/ $NaHCO_3$/ NaO^tBu	CD_3OD/ THF-d_8	60 or 80	No rxn or indistinguishable broad NMR
2[b]	$(C_2H_4)_4IrCl$ (in situ)	NaH	THF	0	No rxn
3[c]	$[(COE)_2IrCl]_2$	LDA	tol-d_8/ THF-d_8	100 or -78 to RT	Majority deprotonated ligand
4	$[(COD)Ir(OMe)]_2$	-	THF-d_8	RT	No rxn
5	$[(COD)Rh(OMe)]_2$	-	THF-d_8	RT	No rxn
6[d]	$[(C_2H_4)_2RhCl]_2$	LDA	THF-d_8	-78 to RT then 0	Deprotonated ligand
7	$RhCl_3 \bullet 3H_2O$	NaH	THF-d_8	80	Broad indistinguishable NMR
8	$[(COD)RhCl]_2$	LDA	THF-d_8	-78 to RT	One major species

a. This reaction was performed multiple times with both varying base and solvent at 60 and 80 °C. b. Reaction performed under an ethylene atmosphere. Ligand was deprotonated in situ. c. This reaction was done under inert atmosphere with and without base. d. This reaction was performed under ethylene atmosphere. Ligand was first deprotonated in situ then metal starting material was added.

With **15**, similar conditions for the attempted metalations with the other variations were explored, but did not produce any fruitful results. As such, I started exploring other bases with the hypothesis that the previous bases were not strong enough to completely deprotonate the ligand. The most successful base used was lithium diisopropylamide (LDA), which had been employed for the synthesis of (^{pent}BPI)Co complexes.[23] This base was in fact strong enough to deprotonate **15**, but there was still no reaction with the corresponding metal starting material (Table 4.3, Entry 3, 6). Interestingly, the reaction with $[(COD)RhCl]_2$ appeared to result in one major symmetric product. The ^{1}H NMR spectrum also had a signal at -3.46 ppm, which may suggest the formation of a Rh-H species. Identification and recrystallization of this product were attempted, but unsuccessful.

*4.2.5. Metalation of ^{Br}BPI-H (**16**)*

Metalation of ^{Br}BPI-H (**16**) was attempted concurrently with **15**. The experimental conditions and results of these attempted metalations are summarized in Table 4.4 (Scheme 4.10). LDA was kept as the base of choice for most of these metalations since it is strong enough to fully deprotonate the ligand. Most conditions resulted in either no reaction or formation of indistinguishable broad peaks in the ^{1}H NMR spectrum. Surprisingly, unlike with ligands **13**-**15**, reaction of **16** with $[(COD)Ir(OMe)]_2$, resulted in one unsymmetrical species (Table 4.4, Entry 4, Scheme 4.11). The ^{1}H NMR showed multiple broad peaks between 2.0–4.5 ppm, which correspond to bound COD. In addition, the number of aryl peaks (6.2-9 ppm) doubled, suggesting an asymmetrical species. The product of this reaction is hypothesized to be (κ^2-^{Br}BPI)Ir(COD) (**36**, Scheme 4.11).[24] Due to the previous unsuccessful attempts at displacing the COD from **31** and **32**, reactivity of this complex was not pursued.[25]

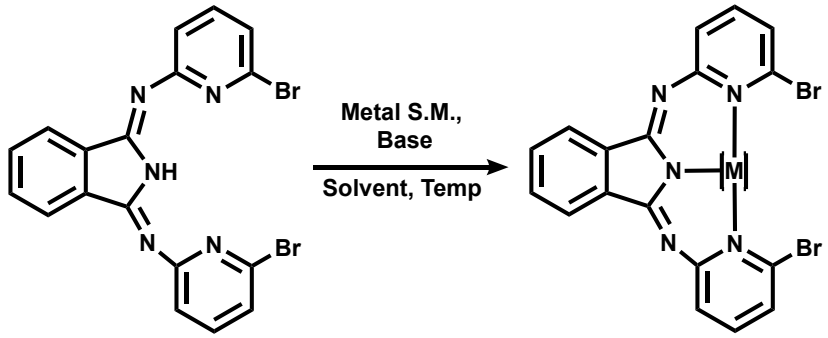

16 M = Ir, Rh

Scheme 4.10. Attempted metalation of 16

Table 4.4. Reaction conditions and results for the attempted metalation of 16

Trial #	Metal starting material	Base	Solvent	Temperature (°C)	Result
1	$IrCl_3 \bullet 3H_2O$	NaOMe	CD_3OD	60	No rxn
2[a]	$(C_2H_4)_4IrCl$ (in situ)	LDA	THF	-78 to RT then 0	Broad indistinguishable NMR
3[b]	$[(COE)_2IrCl]_2$	LDA	tol-d_8/ THF-d_8	100 or -78 to RT	Deprotonated ligand
4	$[(COD)Ir(OMe)]_2$	-	THF-d_8	RT	One unsymmetrical product
5	$[(COD)Rh(OMe)]_2$	-	THF-d_8	RT	No rxn
6[c]	$[(C_2H_4)_2RhCl]_2$	LDA	THF-d_8	-78 to RT then 0	Broad indistinguishable NMR
7	$RhCl_3 \bullet 3H_2O$	NaOMe	CD_3OD	60	No rxn

a. Reaction performed under an ethylene atmosphere. Ligand was deprotonated in situ. b. This reaction was performed multiple times with both varying base and solvent at 100 °C and -78 °C to RT. c. This reaction was performed under ethylene atmosphere. Ligand was first deprotonated in situ then metal starting material was added.

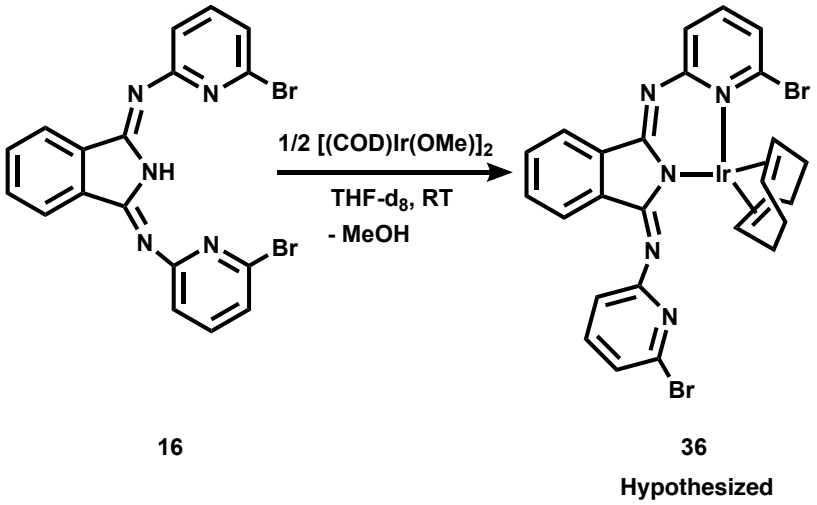

Scheme 4.11. Hypothesized product from reaction of 16 with [(COD)Ir(OMe)]$_2$

*4.2.6. Metalation of ^{xylyl}BPI-H (**17**)*

The final ligand used to metalate to iridum was ^{xylyl}BPI-H (**17**). After the numerous failed attempts at synthesizing a metal complex with ligands **13**-**16**, I revised my hypothesis and reasoned instead that the xylyl moietys in the 5-position of the pyridine rings would still offer some steric bulk around the metal center, but should significantly open up the binding pocket for metalation. This is supported by a % volume buried of 60.5,[21,22] which is only slightly more hindered than **12**, but less than the other ^{R}BPI-H variations investigated. A similar variation of **17** has also been successfully metalated to iridium by Gade and coworkers to form both κ^2 and κ^3 iridium complexes, suggesting that metalation is feasible.[15]

Metalation of **17** was achieved via a slightly modified Gade protocol by reacting deprotonated **17** with $Ir(C_2H_4)_4Cl$ *in situ*, resulting in (^{xylyl}BPI)$Ir(C_2H_4)_2$ (**37**) as a dark violet solid (Scheme 4.12).[15] Complex **37** is a novel iridium complex and was fully characterized by NMR spectroscopy (^{1}H and ^{13}C) and X-ray crystallography. The ^{1}H NMR spectrum of **37** shows two triplets at 1.29 and 2.82 ppm corresponding to each bound ethylene, consistent with literature on a closely related complex.[15] Its solid-state molecular structure has Ir(1)-C(35), Ir(1)-

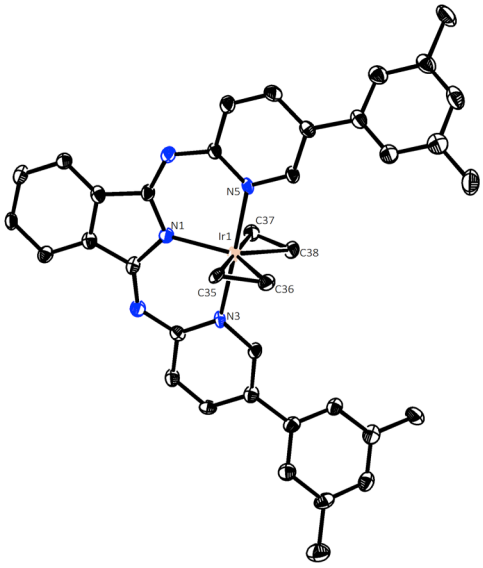

Figure 4.8: ORTEP[49] drawing of 37 with thermal ellipsoids at 50% probability. Hydrogen atoms excluded for clarity.

C(36), Ir(1)-C(37), and Ir(1)-C(38) bond lengths of 2.139(9), 2.140(9), 2.136(9), and 2.149(7) Å, respectively (Figure 4.8). Additionally, the bond lengths of the bound ethylene carbons C(35)-C(36) and C(37)-C(38) are 1.425(8) and 1.43(1) Å, respectively. These values are comparable to complex **34** and the (Phebox)Ir(C_2H_4)$_2$ complex reported by Goldman and coworkers.[11]

Subsequent treatment of **37** with AcOH at room temperature resulted in formation of novel Ir^{III} complex (^{xylyl}BPI)IrEt(OAc) (**38**, Scheme 4.12). The ^{1}H NMR spectrum of **38** features triplet and quartet signals at 0.19 and 1.53 ppm consistent with an Ir-Et moiety and comparable to **34**. A singlet for the bound acetate is observed at 2.15 ppm. The solid-state molecular structure shows a distorted octahedral geometry with Ir(1)-O(1), Ir(1)-O(2), and Ir(1)-C(35) bond lengths of 2.139(5), 2.379(4), 2.042(5) Å, respectively (Figure 4.9). The Ir-OAc bond lengths are comparable to **35** and the previously published (Phebox)Ir(OAc)(hexyl) complex, suggesting κ^2 coordination.[7] Interestingly, reaction of **38** in toluene-d_8 with excess AcOH at 100 °C resulted in the formation of ethane (0.81 ppm) and either two

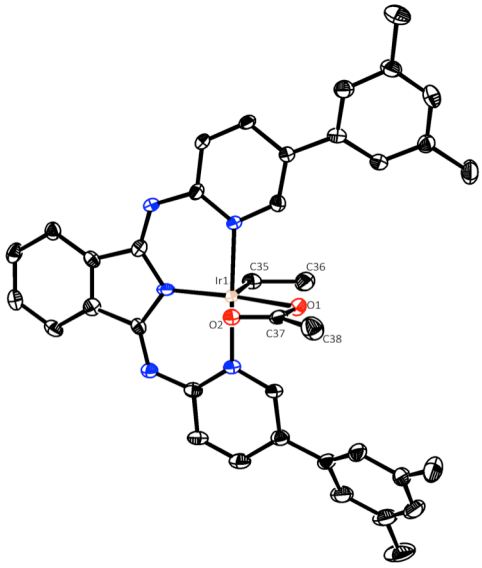

Figure 4.9: ORTEP[49] drawing of 38 with thermal ellipsoids at 50% probability. Hydrogen atoms excluded for clarity.

unknown products in similar concentration or one unknown unsymmetrical product according to the ^{1}H NMR spectrum. Spotting the product solution on a TLC plate revealed the presence of two distinguishable spots confirming the presence of at least two different products. Attempts at separating and recrystallizing these products are currently underway. The reactivity of **38** is in contrast to **35**, where the addition of excess AcOH resulted in no reaction. This result suggests that the bound ethyl in **38** may be more labile and susceptible to protonation, possibility due to the increased sterics of the ^{xylyl}BPI ligand.

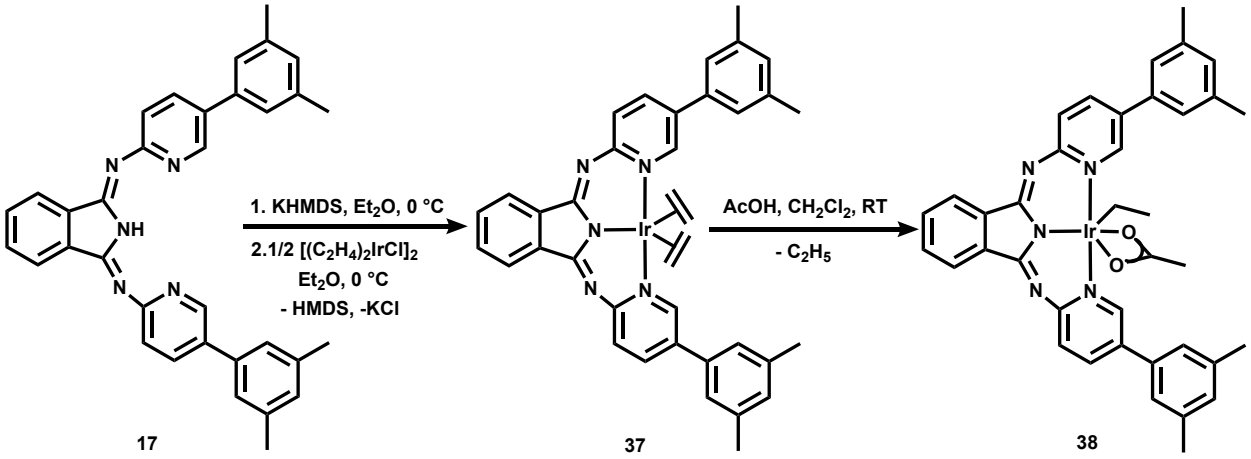

Scheme 4.12. Metalation of 17 with Ir to form a (^{xylyl}BPI)Ir^{III} complex

4.3 Reactivity of (BPI)IrEt(OAc) (35)

β-H elimination and C-H activation are proposed to be crucial steps in many catalytically relevant reactions including alkane dehydrogenation.[1,26] As discussed in the introduction, Allen *et. al.* found that (Phebox)Ir(OAc)$_2$(H$_2$O) dehydrogenated octane to octenes at 200 °C.[8,9] The reaction was proposed to proceed by C-H activation via a CMD-type mechanism to produce (Phebox)Ir(octyl)(OAc), followed by β-H elimination to form (Phebox)Ir(H)(OAc) (Scheme 4.3).[6,8,9] Later, Yang *et. al.* found that NaBAr$^{F}_{24}$ lowered the barrier to β-H elimination, allowing

the reaction to occur within minutes at 55 °C.[11] To probe the reactivity of (BPI)IrEt(OAc) (**35**), we first focused on the β-H elimination reactivity in the presence or absence of $NaBAr^F_{24}$.

Heating an octane solution of **35** to 200 °C for 4 days did not result in the formation of an Ir-H complex. The ^{1}H NMR spectrum of this reaction did not show any distinguishable peaks. However, a *p*-xylene-d_{10} solution of **35** was heated to 200 °C and resulted in disappearance of the Ir-ethyl signals and formation of ethylene (5.18 ppm, reference to *p*-xylene-d_{10}), but no Ir-H signal was observed. The ^{1}H NMR spectrum after reaction workup showed broad indistinguishable peaks. This is in stark contrast to the (Phebox)Ir(octyl)(OAc) complex that readily β-H eliminates at 200 °C to form the corresponding Ir-H complex.[8]

To determine if the identity of the carboxylate ligand affected the β-H elimination reactivity of **35**, as seen in a previous study for the Phebox system,[12] a variety of complexes with both electron-withdrawing and electron-donating carboxylate ligands (trifluoroacetate, benzoate, pivalate) were synthesized and used for β-H elimination studies. (BPI)IrEt(CO_2CF_3) (**39**), (BPI)IrEt(CO_2Ph) (**40**), and (BPI)IrEt($CO_2C(CH_3)_3$) (**41**) were each synthesized from the Ir-ethylene starting material **34** and the corresponding carboxylic acid (Scheme 4.13). *P*-xylene-d_{10} solutions of **39**, **40**, and **41** were each heated to 100 °C in the presence of $NaBAr^F_{24}$ (Scheme 4.13). For each of these reactions, the ^{1}H NMR spectra revealed the absence of the Ir-Et signals and formation of ethylene (5.20 ppm, referenced to *p*-xylene-d_{10}), but no Ir-H signal was observed, similar to **35**. Instead, each reaction generated different multiple products with indistinguishable peaks, which suggests that if β-H elimination is occurring the resulting Ir-H may not be stable and could instead decompose to many products. Overall, these reactions did not give useful information about the possibility of β-H elimination because of subsequent reactions taking place to give multiple indistinguishable species. To potentially gain useful

information, the reactions of **35** and **39-41** could be repeated at lower temperatures to determine the difference in the rate of reaction and potential halt any further reaction to unknown products. Based on Jones and coworkers recent publication it should be expected that **41** would react the fastest based on its pK_a.[12]

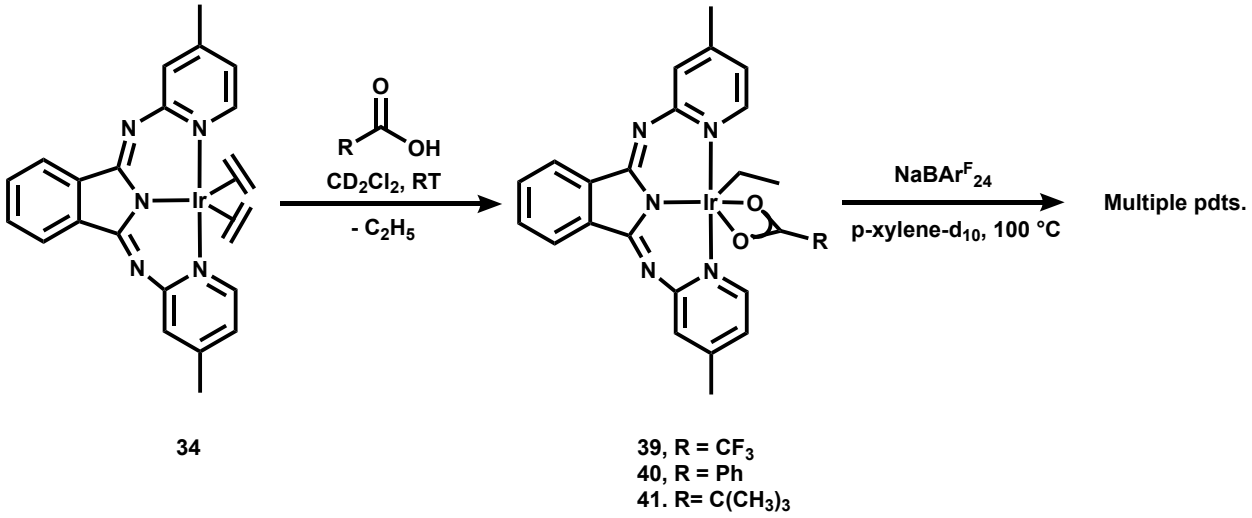

Scheme 4.13. Synthesis of 39-41 and their reactivity in the presence of $NaBAr^F_{24}$

However, the question still remains whether or not β-H elimination is actually occurring in our system and if we can probe this reactivity. Notably Goldman and coworkers demonstrated an equilibrium between the (Phebox)Ir-alkyl and (Phebox)Ir-H complexes.[11] Therefore, if β-H elimination is occurring with the BPI ligand system, there may be an equilibrium that exists between **35** and the corresponding (BPI)IrH(OAc) (**42-H**) with the Ir-Et being thermodynamically favored (Scheme 4.14).

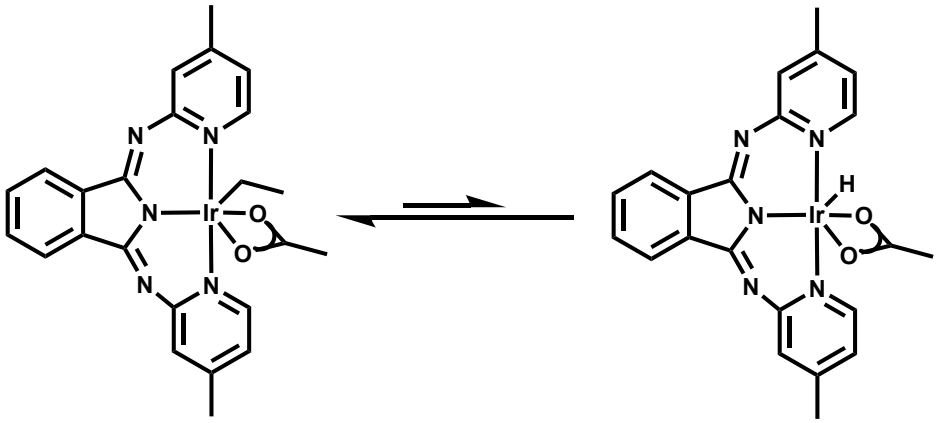

Scheme 4.14. Proposed equilibrium between 35 and 42-H

To probe this proposal, a *p*-xylene-d_{10} solution of **35** was placed under 1 atm of propylene and heated to 200 °C. It was hypothesized that if β-H elimination is occurring to form an Ir-H, insertion into propylene would be favored over insertion into ethylene, due to the abundance of propylene, allowing observation of an Ir-propyl complex. The ^{1}H NMR spectrum of this reaction showed the disappearance of complex signals associated with **35**, but resulted in the appearance of broad peaks that were not significantly distinguishable. On the other hand, heating a 1-octene solution of **35** in the presence of $NaBAr^F_{24}$ to 100 °C resulted in one major product according to the ^{1}H NMR spectrum. A new triplet at 0.77 ppm appeared, suggesting the possibility of the product being an Ir-octyl. Unfortunately, this result was not reproducible and therefore the products of this reaction were never fully characterized and identified.[27]

Finally, to definitively probe whether or not β-H elimination and re-insertion was occurring, a *p*-xylene-d_{10} solution of **35** was placed under 1 atm of deuterated ethylene (C_2D_4) and heated to 100 °C in the presence of $NaBAr^F_{24}$. If an equilibrium is operative as hypothesized, with re-insertion occurring, H-D exchange would be expected. Gratifyingly, monitoring this reaction by ^{1}H NMR revealed the disappearance of the Ir-CH_2CH_3 signals over time and the

appearance of a broad multiplet at 5.18 ppm corresponding to ethylene (reference to *p*-xylene-d_{10}).[28] The appearance of the ethylene signal and associated splitting pattern suggested that hydrogen was incorporated into C_2D_4.[29] This result validates our hypothesis that β-H elimination is occurring with an equilibrium present and represents an exciting advance in the project.

As discussed in the introduction, C-H activation remains one of the main challenges of alkane dehydrogenation with the (Phebox)Ir(OAc)$_2$(H_2O) system, with this step occurring at 100 °C for benzene and 160 °C for linear alkanes.[8] To this end, the C(sp^2)-H and C(sp^3)-H activation reactivity of **35** was explored both with and without $NaBAr^F_{24}$. Heating a C_6D_6 solution of **35** to 100 °C for 8 days results in the disappearance of the ^{1}H NMR signals associated with the Ir-Et and the appearance of a new set of aryl signals. Interestingly, the aryl signals of the starting material remained as the corresponding Ir-CH_2CH_3 signals disappeared over time. Signals for ethane (0.80 ppm) and ethylene (5.25 ppm) were also observed.[30] Continued heating of this reaction for ca. 10 days results in the disappearance of starting material aryl signals and sole formation of the new product **44** in 43% yield by ^{1}H NMR spectroscopy (Scheme 4.15).[31]

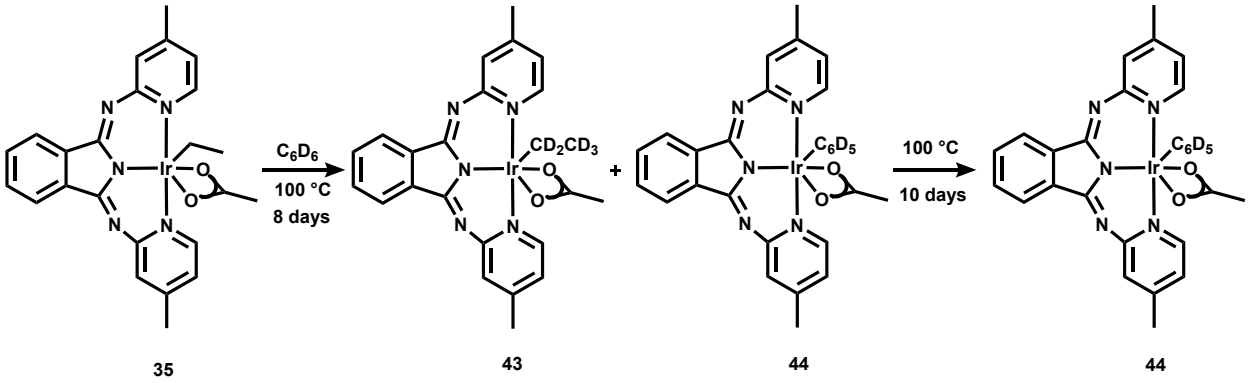

Scheme 4.15. Reaction of 35 in C_6D_6 at 100 °C in the absence of $NaBAr^F_{24}$

The thermolysis reaction of **35** in C_6D_6 at 100 °C is proposed to proceed as shown in Scheme 4.15, generating (BPI)Ir(CD_2CD_3)(OAc) (**43**) and (BPI)Ir(C_6D_5)(OAc) (**44**).[32] The formation of **43** is supported by the disappearance of the Ir-CH_2CH_3 signals over time with no change to the corresponding aryl signals, suggesting that H-D exchange with solvent is occurring and the ethyl moiety is becoming fully deuterated over time. Additionally, the signal associated with the ethylene protons was not a singlet, indicative of deuterium incorporation into the Ir-Et bond. After continued heating, **43** converts fully to **44**, the thermodynamic product of benzene C-H activation with accompanying ethane formation. A C_6H_6 solution of **35** with $NaBAr^F{}_{24}$ heated to 100 °C for 11 days resulted in a clean sample of (BPI)Ir(C_6H_5)(OAc) (**44-H**).[33] **44-H** has phenyl signals at 6.87 ppm (d, 2H), 6.72 ppm (t, 2H), and 6.64 (d, 1H) in the ^{1}H NMR spectrum.[34]

These results confirm that **35** is capable of activating benzene at 100 °C, making it comparable to (Phebox)Ir($OAc)_2(H_2O$). Heating a C_6D_6 solution of **35** at 70 °C for 19 days similarly results in the formation of **43** and **44**, respectively (Scheme 4.16). Ethane (0.80 ppm) and ethylene (5.25 ppm) were also formed. However, unlike at 100 °C, **43** did not fully convert to **44** at 70 °C after 19 days. This suggests that C-H activation and H-D exchange proceed at 70 °C, which is 30 °C lower than the (Phebox)Ir system, but sole formation to the thermodynamic product, **44**, is slower. Additionally, heating a C_6D_6 solution of **35** to 50 °C resulted in formation of **43** and **44**, but **35** was still present after 18 days.

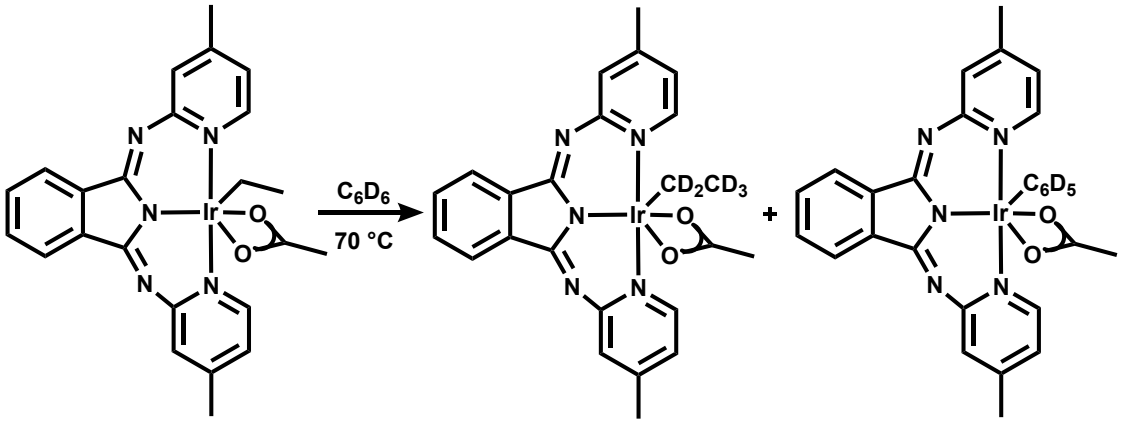

Scheme 4.16. Reaction of 35 in C_6D_6 at 70 °C in the absence of $NaBAr^F_{24}$

Goldman and coworkers found that $NaBAr^F_{24}$ also catalyzed C-H activation for the (Phebox)Ir system.[11] Therefore, C-H activation of benzene with **35** was attempted in the presence of $NaBAr^F_{24}$. A C_6D_6 solution of **35** and 0.3 equiv. $NaBAr^F_{24}$ was heated to 100 °C. Interestingly, after adding $NaBAr^F_{24}$ but before heating, all the complex signals shifted in the ^1H NMR spectrum. The Ir-CH_2CH_3 signals shifted from 0.59 ppm (t, 3H) and 1.84 ppm (q, 2H) to -1.28 (t, 3H) and 2.19 (q, 2H), respectively. After ca. 2 days of heating at 100 °C, the Ir-CH_2CH_3 signals disappeared and the aryl signals remained with no new signals growing. This suggests that the Ir-ethyl moiety is becoming fully deuterated over time. Repeating this reaction at 70 °C results in the same product after heating for 7-12 days. The formation of only one product facilitated identification and full characterization. The ^2H NMR spectrum of this reaction showed the presence of two signals at -1.36 and 2.21 ppm, suggesting a deuterated Ir-Et moiety in the product.

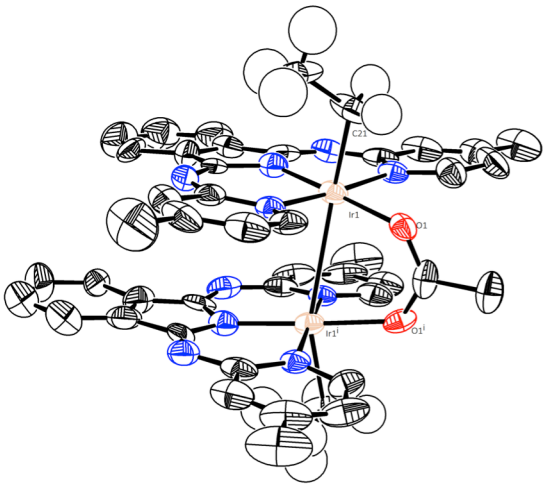

Figure 4.10: ORTEP[49] drawing of 45 with thermal ellipsoids at 50% probability. Hydrogen atoms and BAr^F_{24} counter-ion excluded for clarity.

X-ray analysis revealed the product of these reactions to be $[(BPI)Ir(CD_2CD_3)]_2(\mu\text{-}OAc)]BAr^F_{24}$ (**45**, Figure 4.10), a dinuclear complex with the Ir-Et moiety fully deuterated and a bridging acetate. The Ir(1)-C(21), Ir(1)-O(1), and Ir-Ir bond lengths are 2.09(2), 2.070(7), and 3.0146(9) Å, respectively. The Ir^{III}-Ir^{III} bond distance is similar to previously published Ir^{III}-Ir^{III} complexes.[35] **45** was also fully characterized by NMR spectroscopy (^1H and ^{13}C NMR), which supports this assignment in solution. The formation of a dinuclear complex was surprising and is hypothesized to form before C-H activation of the solvent occurs, as suggested by the initial shift in all peaks before heating the reaction. Indeed, independent preparation of the proteo-dinuclear species, $[(BPI)Ir(CH_2CH_3)]_2(\mu\text{-}OAc)]BAr^F_{24}$ (**45-H**), was achieved in 88% yield by mixing **35** with $NaBAr^F_{24}$ at room temperature. The ^1H NMR spectrum of **45-H** (in CD_2Cl_2) features the corresponding Ir-C*H*$_2$C*H*$_3$ signals at -1.22 ppm (t, 6H) and 2.27 ppm (q, 4H). The bridging acetate appears at 2.88 ppm (s, 3H) and the corresponding aryl and BAr^F_{24} counter-ion signals appear between 6.5-8.30 ppm. X-ray quality crystals of **45-H** were grown from vapor diffusion of CD_2Cl_2 and pentane at -30 °C. The solid-state molecular

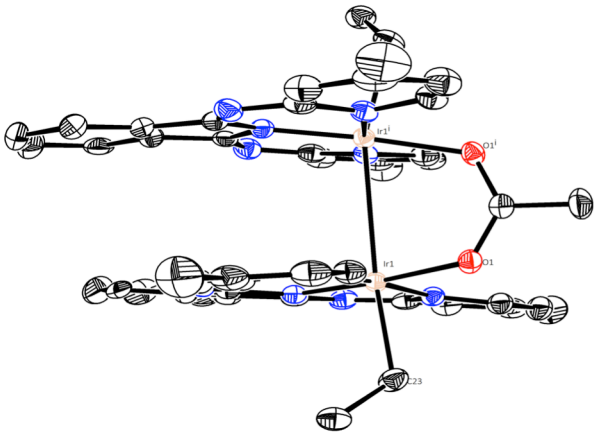

Figure 4.11: ORTEP[49] drawing of 45-H with thermal ellipsoids at 50% probability. Hydrogen atoms and BAr^F_{24} counter-ion excluded for clarity.

structure of independently prepared **45-H** is shown in Figure 4.11. The Ir(1)-C(23), Ir(1)-O(1), and Ir-Ir bond lengths are 2.087(6), 2.093 (3), and 3.0108 (9) Å, respectively. These values are similar to the deuterated version **45**. The reactivity observed with **35** and 0.3 equiv. $NaBAr^F_{24}$ at 100 °C and 70 °C is summarized in Scheme 4.17. Based on these results, it appears that C-H activation at the dinuclear complex is much faster than at the monomer, which required 19 days for full consumption of the Ir-CD_2CD_3 without $NaBAr^F_{24}$ present.

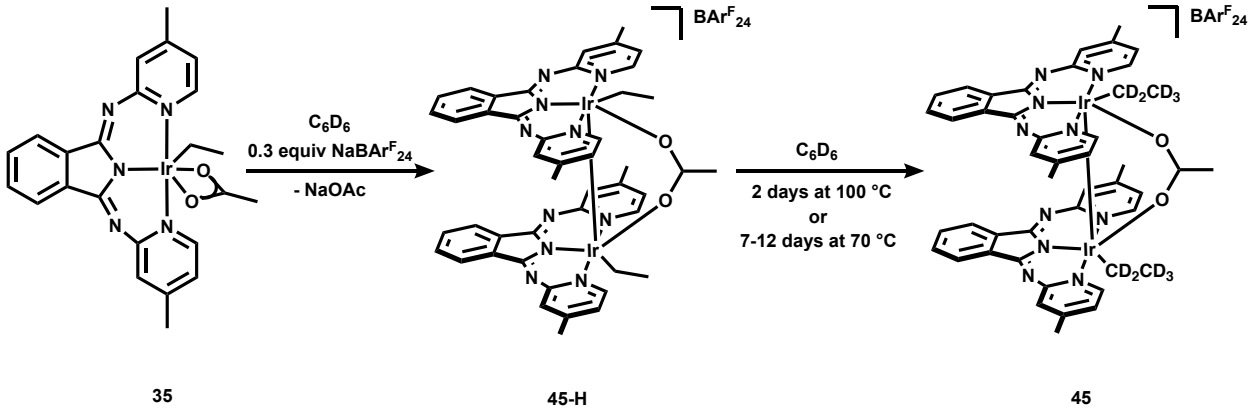

35 45-H 45

Scheme 4.17. Reaction of 35 and $NaBAr^F_{24}$ in C_6D_6 at 100 °C and 70 °C

Heating a C_6D_6 solution of **35** to 70 °C with either 0.5 or 1 equiv. $NaBAr^F_{24}$ also results in formation of **45**. In addition, heating a C_6D_6 solution of **35** and 0.3 equiv. $NaBAr^F_{24}$ to 50 °C for 16 days results in **45** and unreacted **45-H**, suggesting reaction at 50 °C is slow. Interestingly, the results obtained with $NaBAr^F_{24}$ differ from the previous reactions without $NaBAr^F_{24}$, where a dinuclear complex was not formed and the Ir-C_6D_5 complex **44** was formed (Scheme 4.15 and 4.16). Therefore, it appears that initial formation of dinuclear complex **45-H** allows C-H activation to still occur as evidenced by deuterium incorporation into the ethyl fragment, but prevents the formation of an Ir-C_6D_5 complex. To investigate this possibility, the independently prepared dinuclear complex **45-H** was heated to 100 °C and 70 °C in C_6D_6, and the only product

obtained was **45** in 38%[36] and 85% yields after 1 day and 6 days, respectively (Scheme 4.18). This result validates the hypothesis that once the dinuclear species is allowed to form in solution (from reaction of **35** with $NaBAr^F_{24}$) C-H activation and H-D exchange occurs but formation of an Ir-C_6D_5 complex is prevented, possibly due to steric hindrance.

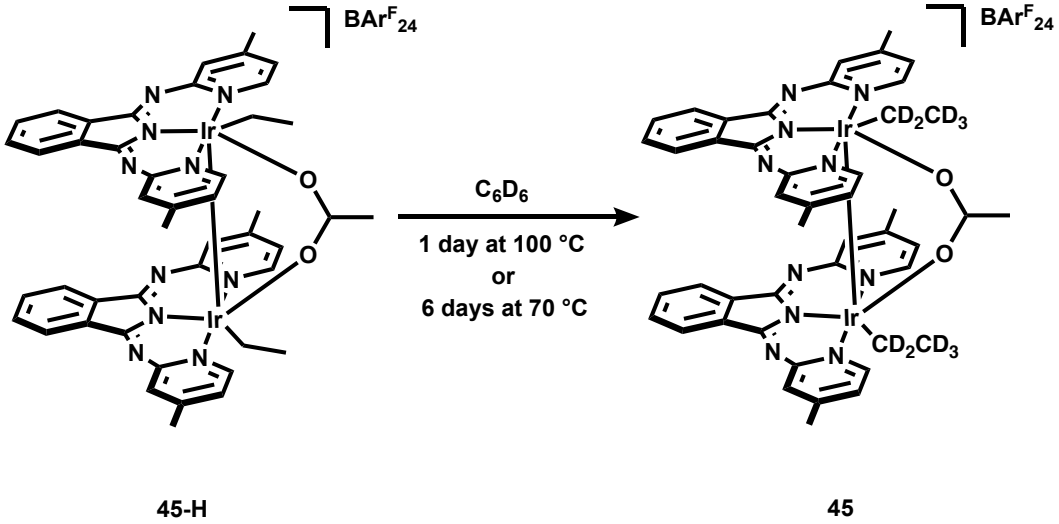

Scheme 4.18. Reaction of 45-H in C_6D_6 at 100 °C and 70 °C

There appear to be multiple mechanisms for C-H activation and the presence or absence of $NaBAr^F_{24}$ in solution is significant. In the absence of $NaBAr^F_{24}$, both **43** and **44** are produced. In this case, it is reasonable for the reaction to first proceed by β-H elimination to release ethylene and form (BPI)IrH(OAc) (**42-H**), followed by activation of C_6D_6 to eventually form (BPI)IrD(OAc) (**42**). As discussed above, re-insertion of ethylene can occur, resulting in D incorporation into the ethylene. Indeed, the ^{1}H NMR spectra of the reactions show the production of ethylene, and over time the signal turns into a broad multiplet. This process can occur multiple times to get full D incorporation into the ethylene, resulting in **43** (Scheme 4.19). Additionally, C-H activation of C_6D_6 can occur from any Ir-ethyl intermediate, to release ethane and produce

44 (Scheme 4.20). Ethane is also observed in the reaction and the ^{1}H NMR signal becomes a broad multiplet over time, suggesting this step can occur anywhere between the multiple elimination and insertions. This is evidenced by reaction of **35** at 100 °C (Scheme 4.15). Complex **43** with the fully deuterated ethyl was found to react with C_6D_6 over time to produce **44** as the only product. In addition, it is also possible that the Ir-C_6D_5 complex **44** could be formed from C-H activation at the Ir-H (**42-H**) or Ir-D (**42**) intermediates to release HD or D_2, although no evidence of HD formation was observed in the ^{1}H NMR spectra.

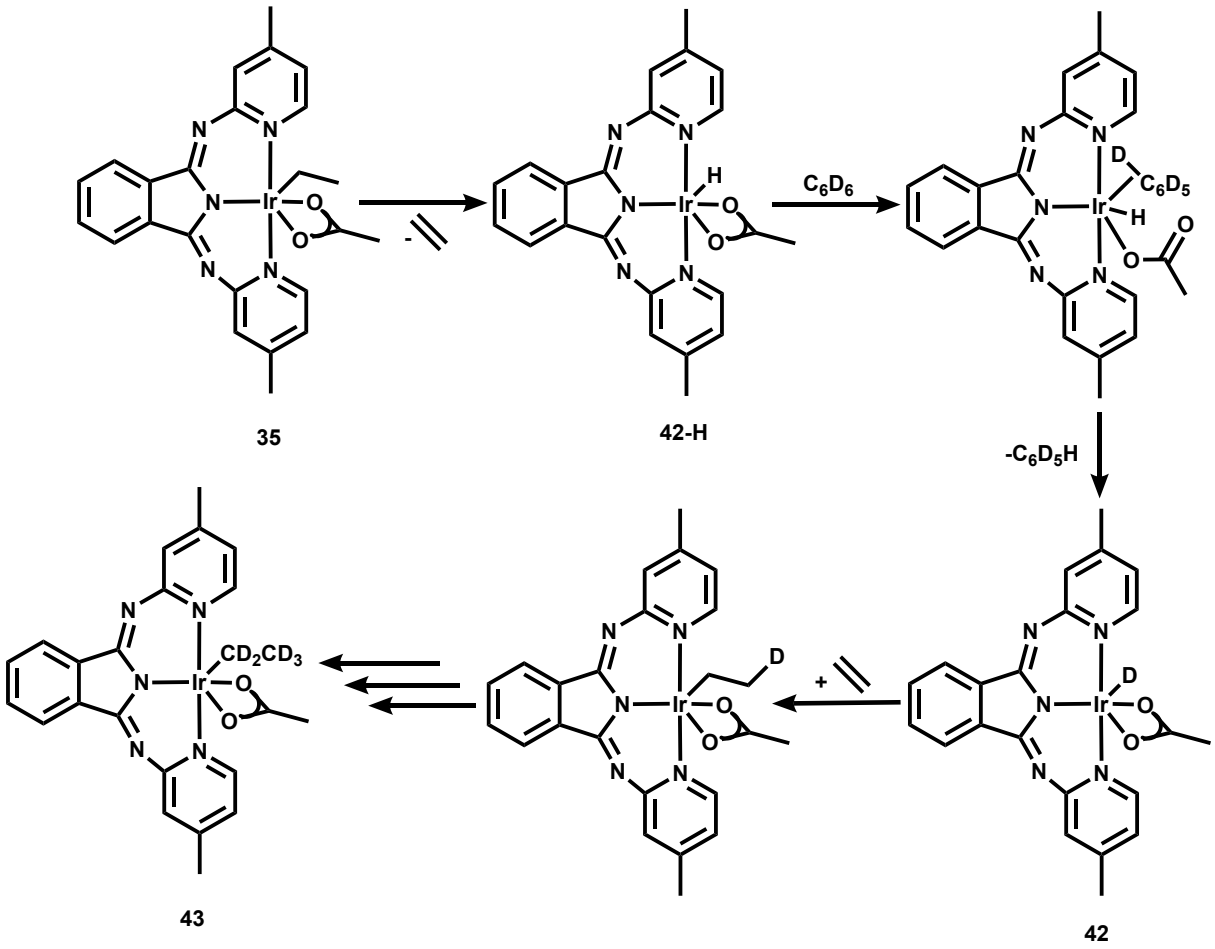

Scheme 4.19. Proposed mechanism for the formation of 43 from 35 in C_6D_6 in the absence of $NaBAr^F_{24}$

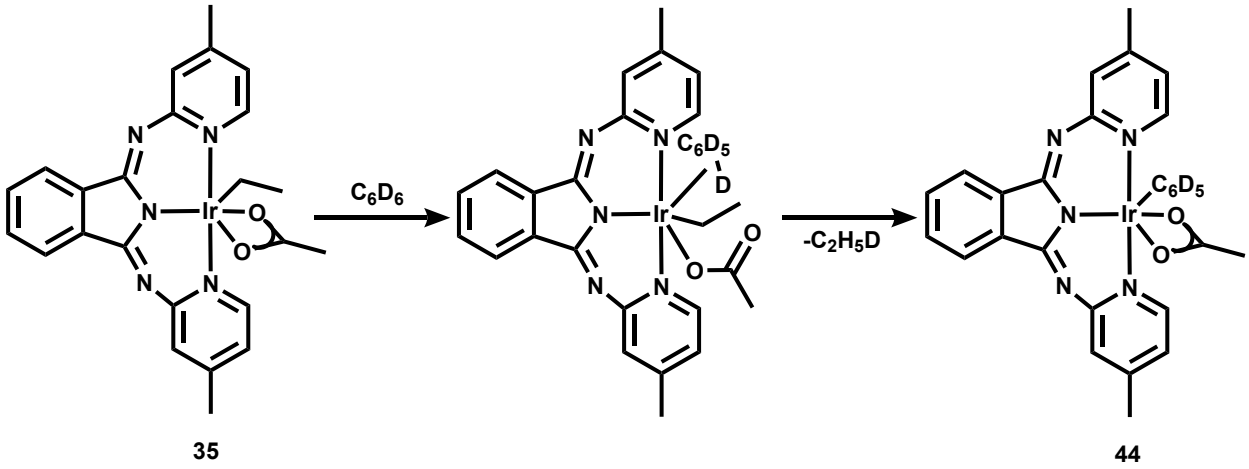

Scheme 4.20. Proposed mechanism for the formation of 44 from 35 in C_6D_6 in the absence of $NaBAr^F_{24}$

On the other hand, in the presence of $NaBAr^F_{24}$, **35** first reacts with $NaBAr^F_{24}$ to form the dinuclear species **45-H** and release sodium acetate (NaOAc) (Scheme 4.17).[37] Then, similar to reactivity without $NaBAr^F_{24}$, **45-H** can β-H eliminate to form an Ir-H dinuclear species that can perform C-H activation of C_6D_6. H-D exchange can occur with insertion of ethylene into the Ir-D moiety of the dinculear species to eventually form the fully deuterated product, **45**. However, an Ir-Ph complex is never observed in this reaction. The formation of the dinuclear arrangement could prevent displacement of the Ir-Et group to form an Ir-Ph complex, possibly due to steric hindrance or the rigidity of the dinuclear structure not allowing geometry distortion.

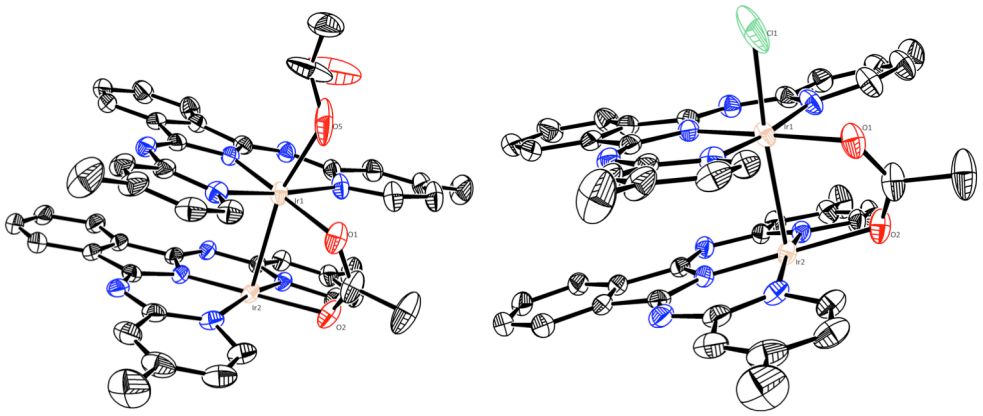

46 **47**

Figure 4.12: ORTEP[49] drawing of 46 and 47 with thermal ellipsoids at 50% probability. Hydrogen atoms excluded for clarity.

Encouraged by the ability of **35** to activate benzene at 70 °C, 30 °C lower than what was seen for the (Phebox)Ir system, we next pursued C(sp^3)-H activation studies. Unfortunately, heating an *n*-octane solution of **35** to 160 °C, an effective temperature for *n*-octane activation in the Phebox system,[8] did not appear to result in C-H activation. After 11 days at 160 °C, crystals precipitated from solution and X-ray analysis revealed the products to be a mixture of [(BPI)Ir(OAc)](μ-OAc)[(BPI)Ir] (**46**) and [(BPI)IrCl)(μ-OAc)[(BPI)Ir] (**47**) dinuclear species, with the ethyl groups no longer bound and a bridging acetate (Figure 4.12).[38] The Ir-Ir bond distance in both **46** and **47** is 2.6736(5) Å. This distance is comparable to other Ir-Ir bonds.[35] The ^{1}H NMR spectrum of the crystals showed broad indistinguishable features.[39] Likewise, heating an *n*-octane solution of **35** with 0.5 equiv.

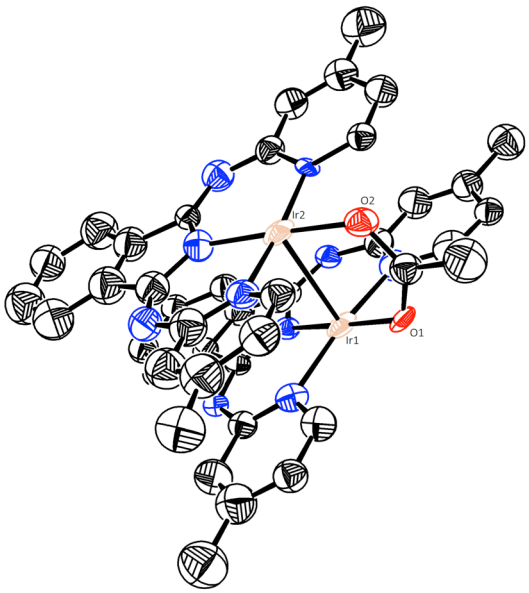

Figure 4.13: ORTEP[49] drawing of 48 with thermal ellipsoids at 50% probability. Hydrogen atoms and BAr^F_{24} counter-ion excluded for clarity.

$NaBAr^F_{24}$ to 160 °C results in crystals precipitating from solution, and X-ray analysis revealed the product to be $[(BPI)Ir]_2(\mu\text{-}OAc)]BAr^F_{24}$ (**48**) with infinite π-stacking interactions along the a-axis (Figure 4.13). The Ir(1)-Ir(2) bond distance in **48** is 2.717(1) Å, comparable to **46** and **47**. The ^{1}H NMR spectrum of the crystals also showed broad indistinguishable peaks.[39] It is unclear how the Ir-ethyl moiety reacts to form the respective dinuclear species, but so far this system does not appear to be effective for C-H activation of *n*-octane.

4.4 Reactivity of (^{xylyl}BPI)IrEt(OAc) (38)

The β-H elimination and C-H activation reactivity of (^{xylyl}BPI)IrEt(OAc) (**38**) was also explored, and preliminary results will be discussed below. We were interested to see how the different steric profile of **38** would affect the aforementioned reactivity compared to **35**. The xylyl moieties in the 5-position of the pyridine rings appear to facilitate protonation of the Ir-Et bond (as discussed above in section 4.2.6). In contrast, the reaction of **35** with acid did not result in protonation of the ethyl group but instead resulted in multiple products and protonation of the ligand backbone to form an imine. The increased sterics could also help stabilize formation of an Ir-H complex resulting from β-H elimination at **38**. Furthermore, the thermal reactivity of **35** (as discussed in section 4.3) suggested that **35** favors dinuclear formation, and we wondered if **38** also favors dinuclear formation. We hypothesized that the bulky xylyl moieties would prevent dinuclear formation, allowing both C_6D_6 and *n*-octane activation to occur.

The thermal reactivity of **38** was first explored. Heating a *p*-xylene-d_{10} solution of **38** to 100 °C in the presence of $NaBAr^F_{24}$ for 2 days results in the disappearance of the starting material and the growth of a new major product (Scheme 4.21). Formation of ethylene (5.20 ppm, referenced to *p*-xylene-d_{10}) was also seen in the ^{1}H NMR spectra. Gratifyingly, an Ir-H signal was observed at -25.6 ppm (referenced to *p*-xylene-d_{10}), suggesting that the major product

formed is (^{xylyl}BPI)IrH(OAc) (**49**). ^{1}H NMR in CD_2Cl_2 after reaction workup displayed that the Ir-H formed is stable in solution and under reduced pressure. This result is in stark contrast to the β-H elimination of **35**, which did not result in formation of a stable Ir-H but instead resulted in multiple indistinguishable products. Furthermore, this finding supports our hypothesis that increased sterics from the xylyl moieties could help facilitate β-H elimination and stabilize an Ir-H product. Attempts at identifying the product by X-ray crystallography were successful.

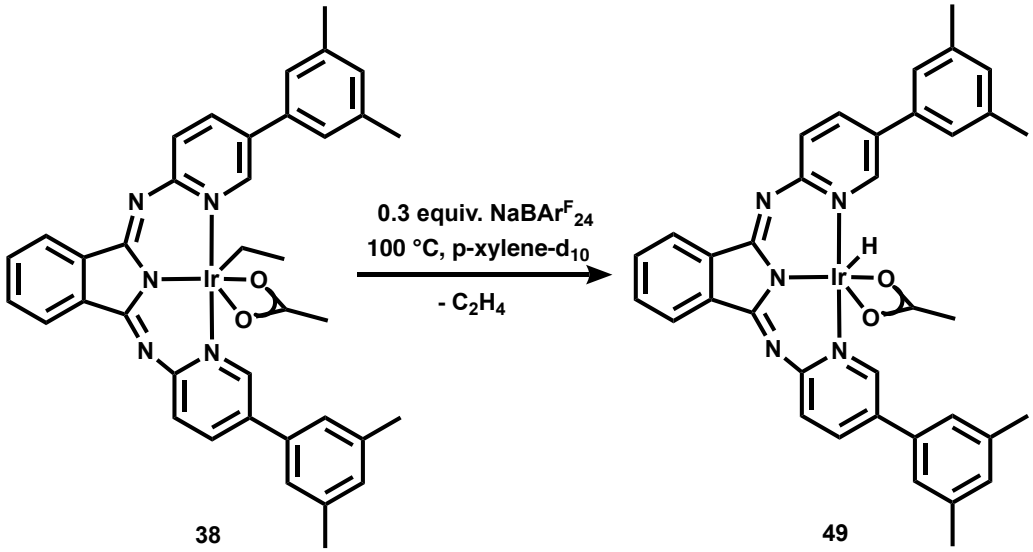

Scheme 4.21. β-H elimination reactivity of 38 in the presence of NaBAr$^F_{24}$

Encouraged by the β-H elimination reactivity of **38**, the thermal reactivity in C_6D_6 with and without NaBAr$^F_{24}$ was next explored. Heating a C_6D_6 solution of **38** at 70 °C for 18 days results in the disappearance of the ^{1}H NMR signals associated with the Ir-Et while the aryl signals remained unchanged throughout. A signal for ethylene (5.25 ppm) was also seen and broadened over time, consistent with deuterium incorporation. The product of this reaction is proposed to be (^{xylyl}BPI)Ir(CD_2CD_3)(OAc) (**50**) as shown in Scheme 4.22. This outcome would mirror the observed reactivity of **35**, wherein the Ir-Et signals became fully deuterated over time by C-H activation and H-D exchange. Interestingly, no new set of aryl signals appeared from

reaction with **38** as was seen with **35** (Scheme 4.16), suggesting that the increased steric profile of **38** still allows C-H activation and H-D exchange to occur but inhibits the formation of an Ir-C_6D_5 complex.

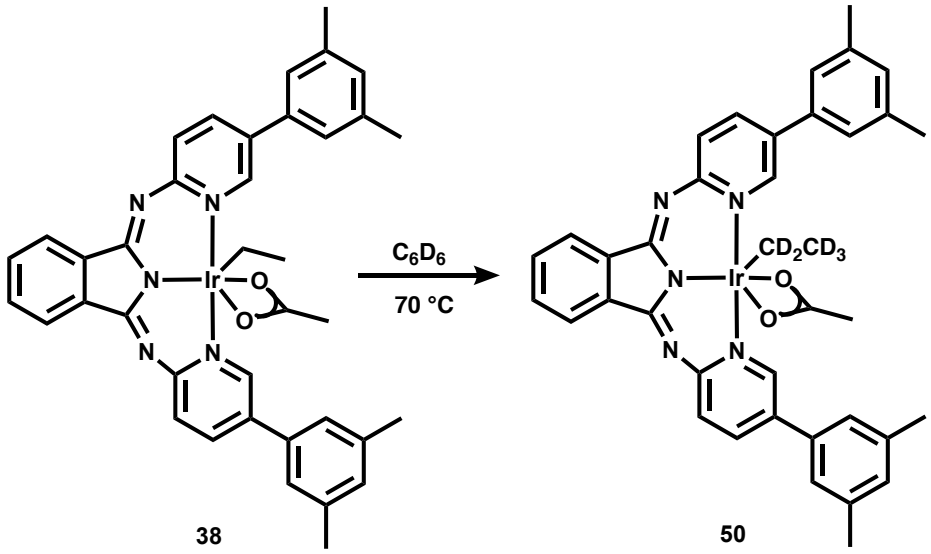

Scheme 4.22. Reaction of 38 in C_6D_6 at 70 °C in the absence of $NaBAr^F_{24}$

To determine if $NaBAr^F_{24}$ catalyzes the C-H activation with **38**, a C_6D_6 solution of **38** and 0.5 equiv. $NaBAr^F_{24}$ was heated to 70 °C. As observed with **35**, after adding $NaBAr^F_{24}$ but before heating, all the complex signals shifted in the ^{1}H NMR spectrum, suggesting formation of dinuclear species $[(^{xylyl}BPI)Ir(CH_2CH_3)]_2(\mu\text{-}OAc)]BAr^F_{24}$ (**51-H**). Complex **51-H** was fully characterized by NMR spectroscopy (^{1}H and ^{13}C), and the ^{1}H NMR spectrum (in CD_2Cl_2) features the corresponding Ir-C*H*$_2$C*H*$_3$ signals at -1.16 ppm (t, 6H) and 2.46 ppm (q, 4H). The bridging acetate signal appears at 2.93 ppm (s, 3H) and the corresponding aryl signals appear between 6.8-8.8 ppm. Subsequent heating of this dinuclear species in C_6D_6 at 70 °C up to 11 days resulted in the Ir-C*H*$_2$C*H*$_3$ signals decreasing by 75% while the acetate and aryl signals remained. Ethylene (5.12 ppm) was also observed, and the signal broadened over time. These

results are consistent with formation of the deuterated dinuclear species [(^{xylyl}BPI)Ir(CD_2CD_3)]$_2$(μ-OAc)]BAr^F_{24} (**51**) over time, similar to what was seen with **35** (Scheme 4.17). **51** was fully characterized by NMR spectroscopy (^{1}H and ^{13}C), which supports this assignment in solution. Additionally, the ^{2}H NMR spectrum of this reaction showed the presence of two signals at -1.51 and 2.26 ppm, consistent with a fully deuterated Ir-Et moiety in the product. The reactivity observed with **38** and 0.5 equiv. $NaBAr^F_{24}$ is summarized in Scheme 4.23. The increased steric profile does not appear to inhibit dinuclear formation as we originally hypothesized. The reactivity mimicked that of **35**, with formation of a dinuclear species first followed by C-H activation and H-D exchange. As with **35**, no Ir-C_6D_5 dinuclear species were observed in the thermal reaction of the C_6D_6 solution of **38** with $NaBAr^F_{24}$, likely due to the rigidity of the dinuclear structure not allowing distortion of the molecular geometry. Additionally, the rate of C-H activation and H-D exchange appears to be slower for **38** as compared to **35**; **38** takes 11 days to reach 75% completion and **35** takes 7-12 days to 100% completion. This difference is likely due to the increased sterics around the metal center of **38**.

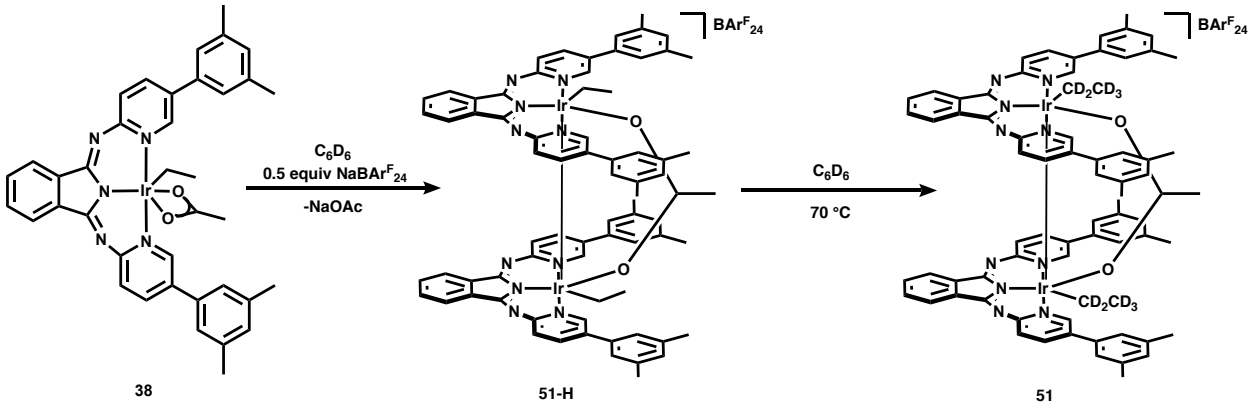

Scheme 4.23. Reaction of 38 and $NaBAr^F_{24}$ in C_6D_6 at 70 °C

Similar to **35**, there appear to be multiple mechanisms for C-H activation, and the presence or absence of $NaBAr^{F}_{24}$ in solution is significant. Scheme 4.19 summarizes the proposed mechanism of C-H activation and H-D exchange for **35** without $NaBAr^{F}_{24}$ present, which is also proposed to be the pathway for **38** to form **50**. In the presence of $NaBAr^{F}_{24}$, it is proposed that dinuclear species **51-H** is first formed, followed by the same series of C-H activation and H-D exchange steps to yield **51** as the sole product. The absence of an Ir-C_6D_5 product both in the absence and presence of $NaBAr^{F}_{24}$ is likely due to the increased steric profile of the ^{xylyl}BPI ligand (as discussed in Chapter 3).

4.5 Summary

In summary, these efforts have shed light on the varying metalation capabilities of the ^{R}BPI ligands and the reactivities of the resultant metal complexes in relation to alkane dehydrogenation. Specifically, the metalations of BPI-H (**12**) and ^{xylyl}BPI-H (**17**) were successful and resulted in novel Ir^{III} complexes, (BPI)IrEt(OAc) (**35**) and (^{xylyl}BPI)IrEt(OAc) (**38**). These complexes were fully characterized by NMR spectroscopy and X-ray crystallography. Unfortunately, metalations using the other ligand variations, ^{Me}BPI-H (**13**), ^{OMe}BPI-H (**14**), ^{Pent}BPI-H (**15**), and ^{Br}BPI-H (**16**) were unsuccessful. This lack of desired reactivity is hypothesized to be due to steric hindrance around the ligand binding pocket. Ligands **13**-**16** have relatively hindered binding pockets with percent volume buried numbers between 62-72% (as discussed in Chapter 3), higher than both **12** and **17** (59% and 60.5%, respectively).

The protonation, β-H elimination, and C-H activation reactivity of (BPI)IrEt(OAc) (**35**) was explored. It was found that β-H elimination of **35** was reversible, with the equilibrium favoring **35** at room temperature. Specifically, reaction of **35** with C_2D_4 demonstrated H-D exchange between the bound Ir-Et and fully deuterated C_2D_4. In addition, **35** was found to activate C_6D_6 at temperatures ranging from 50-100 °C. This was exciting because it

demonstrated that C(sp^2)-H activation could be promoted to occur at a reasonable rate at 70 °C, 30 °C lower than the previously studied (Phebox)Ir($OAc)_2(H_2O$) system. When $NaBAr^F_{24}$ was not present, C_6D_6 activation resulted in formation of (BPI)Ir(CD_2CD_3)(OAc) (**43**) and (BPI)Ir(C_6D_5)(OAc) (**44**). With a catalytic amount of $NaBAr^F_{24}$, formation of iridium dinuclear species [(BPI)IrEt]$_2$(μ-OAc)]BAr^F_{24} (**45-H**) preceded C-H activation, although D-incorporation to form [(BPI)Ir(CD_2CD_3)]$_2$(μ-OAc)]BAr^F_{24} (**45**) occurred later on. Failure to form an Ir-C_6D_5 species in the presence of $NaBAr^F_{24}$ is hypothesized to be due to steric hindrance and the rigidity of the dinuclear structure. This rigidity could possibly prevent the significant geometric distortion needed to accommodate an Ir-C_6D_5 moiety. The mechanisms of these reactions are hypothesized to proceed through β-H elimination followed by C-H activation and H-D exchange. C(sp^3)-H activation was also examined. Reaction of **35** with *n*-octane resulted in formation of a dinuclear species, but no apparent C-H activation was detected at 160 °C.

The β-H elimination and C-H activation reactivity of (^{xylyl}BPI)IrEt(OAc) (**38**) was also explored. β-H elimination of **38** was promoted at 100 °C in the presence of $NaBAr^F_{24}$ to produce (^{xylyl}BPI)Ir(H)(OAc) (**49**). This reactivity stood in contrast to **35**, which did not produce a stable Ir-H species and is attributed to the increased steric profile of the ^{xylyl}BPI ligand. The increased sterics could work toward stabilizing the resulting Ir-H. In addition, **38** was found to activate C_6D_6 at 70 °C, similar to **35** and 30 °C lower than the previously studied (Phebox)Ir($OAc)_2(H_2O$) system. When $NaBAr^F_{24}$ was not present, C_6D_6 activation resulted in formation of (^{xylyl}BPI)Ir(CD_2CD_3)(OAc) (**50**) as the sole product. This is in contrast to **35** where a mixture of (BPI)Ir(CD_2CD_3)(OAc) (**43**) and (BPI)Ir(C_6D_5)(OAc) (**44**) was formed at 70 °C. This difference is again attributed to the increased sterics from the xylyl moieties. With $NaBAr^F_{24}$, formation of iridium dinuclear species [(^{xylyl}BPI)IrEt]$_2$(μ-OAc)]BAr^F_{24} (**51-H**) preceded C-H activation,

although D-incorporation to form [(^{xylyl}BPI)Ir(CD_2CD_3)]$_2$(μ-OAc)]BAr^F_{24} (**51**) occurred later on. Failure to form an Ir-C_6D_5 species in the presence of $NaBAr^F_{24}$ is hypothesized to be due to steric hindrance and the rigidity of the dinuclear structure. This rigidity could possibly prevent the significant geometric distortion needed to accommodate an Ir-C_6D_5 moiety. The mechanisms of these reactions are hypothesized to proceed via the same pathway as **35**.

Both (BPI)IrEt(OAc) (**35**) and (^{xylyl}BPI)IrEt(OAc) (**38**) formed dinuclear species in the presence of $NaBAr^F_{24}$, suggesting that this may be a disadvantage of this system. It appears that once the dinuclear species are formed they are stable in solution due to the π-stacking interactions of the BPI ligand framework. Additionally, the acetate ligand appears to stabilize the dinuclear species by bridging between the Ir centers, an issue the Phebox system does not have. Therefore acetate may not be the best ligand of choice for BPI-supported metal centers. Future avenues for exploration could include adding steric bulk above and below the plane to inhibit dinuclear formation.

4.6 Experimental

4.6.1 General Experimental:

Unless otherwise noted, all experiments and manipulations were performed under air-free conditions (standard high vacuum or Schlenk techniques under argon or nitrogen atmosphere, or in a nitrogen-filled glovebox). All glassware was oven-dried or flame-dried prior to use. Borosilicate J. Young NMR tubes were used for NMR-scale reactions. 5mm medium-walled NMR tubes with a 14/20 joints were used for flame-sealed reactions. Reactions performed in J. Young NMR tubes were degassed with 3 freeze, pump, thaw cycles before H_2, propylene, or C_2D_4 pressurization. H_2 and propylene gas were introduced to reactions in J. Young NMR tubes on a high-pressure gas manifold.[40] C_2D_4 were introduced into reactions on a vacuum line. Toluene, dichloromethane, diethyl ether, tetrahydrofuran, and benzene were dried by passage through activated alumina and molecular sieves columns under a stream of argon. Methanol and methanol-d_4 were pre-dried over Na^0/benzophenone, vacuum-transferred, and stored over molecular sieves 4 Å. Mesitylene, *p*-xylene d_{10}, *n*-octane, and 1-octene were degassed with 3 freeze, pump, thaw cycles and stored over 4 Å molecular sieves. C_6D_6 was dried over Na^0/benzophenone or molecular sieves. Toluene-d_8 and THF-d_8 were dried over Na^0/benzophenone and vacuum-transferred prior to use or stored over 4 Å molecular sieves. CD_3CN and CD_2Cl_2 were dried over CaH_2 and vacuum-transferred prior to use or stored over 4 Å molecular sieves. $[(COD)IrCl]_2$,[41] $[(COD)Ir(OMe)]_2$,[42] $[(COE)_2IrCl]_2$,[43] $(C_2H_4)_5IrCl$ (*in situ*),[44] $Ir(CO)_2Cl(pyridine)$,[45] $[(COD)RhCl]_2$,[46] $[(COD)Rh(OMe)]_2$,[47] and $[(C_2H_4)_2RhCl]_2$[48] were all synthesized according to literature procedures. All other reagents were used as received from commercial suppliers. NMR spectra were acquired on Bruker AV200, AV300, AV301, DRX499, AV500, and AV700 spectrometers using 5mm medium-walled NMR tubes fitted with a J. Young Teflon valve or flame-sealed. ^1H and $^{13}C\{^1H\}$ NMR spectra were referenced to

residual protonated solvent signals. ^{19}F NMR shifts were referenced to trifluoroacetic acid external standard. X-ray data was collected at -173 °C on a Bruker APEX II single crystal X-ray diffractometer using Mo-radiation.

4.6.2 Safety note on the handling of pressurized NMR tubes:

Caution should be exercised when handling pressurized J. Young NMR tubes, and they should be transferred using secondary containment.

4.6.3 Synthesis and Characterization of Complexes:

(κ^2-BPI)Ir(COD) (31): A 20 mL vial equipped with a stir bar was charged with $[(COD)Ir(OMe)]_2$ (384 mg, 0.586 mmol), BPI-H (386 mg, 1.18 mmol), and tetrahydrofuran (10 mL) in a nitrogen-filled glove box. The reaction immediately changed from orange to a dark red solution. The reaction was stirred at room temperature for 2 hours. The volatiles were removed under reduced pressure, resulting in a bright orange/red solid. The crude product was purified by layering a saturated dichloromethane solution with pentane, resulting in an orange solid. The purified solid was dried under vacuum. Yield: 409 mg (56%)

^1H NMR (300 MHz, CD_2Cl_2): 1.65 (m, 4H, COD-*CH*$_2$), 2.24 (m, 4H, COD-*CH*$_2$), 2.33 (s, 6H, C*H*$_3$), 3.61 (bs, 2H, COD-C*H*), 5.56 (bs, 2H, COD-C*H*), 6.21 (d, 1H, $^3J_{HH}$ = 7.7 Hz, aryl-*H*), 6.68 (s, 1H, aryl-*H*), 6.74 (dd, 1H, $^3J_{HH}$ =6.4 Hz, $^4J_{HH}$ = 1.8 Hz, aryl-*H*), 6.90 (d, 1H, $^3J_{HH}$ = 5.0 Hz, aryl-*H*), 7.16 (t, 1H, $^3J_{HH}$ = 7.6 Hz, aryl-*H*), 7.33 (s, 1H, aryl-*H*), 7.43 (t, 1H, $^3J_{HH}$ = 7.5 Hz, aryl-*H*), 7.91 (d, 1H, $^3J_{HH}$= 7.6 Hz, aryl-*H*), 8.04 (d, 1H, $^3J_{HH}$ = 6.4 Hz, aryl-*H*), 8.25 (d, 1H, $^3J_{HH}$ =5.1 Hz, aryl-*H*).

(κ^2-BPI)Ir(COD)(I)$_2$ (32): A 20 mL vial equipped with a stir bar was charged with (κ^2-BPI)Ir(COD) (**31**) (113 mg, 0.180 mmol), I_2 (52.1 mg, 0.181 mmol), and diethyl ether (8 mL) in a nitrogen-filled glove box, resulting in a red solution. The reaction was stirred at room

temperature for 3 hours. The volatiles were removed under reduced pressure, resulting in a bright orange/red solid. The crude product was dissolved in dichloromethane and filtered. The volatiles were removed under reduced pressure, resulting in a red solid. Yield: 121 mg (76%)

^{1}H NMR (300 MHz, CD_2Cl_2): 2.33 (s, 3H, C*H*$_3$), 2.44 (s, 3H, C*H*$_3$), 2.77 (m, 4H, COD-C*H*$_2$), 3.20 (m, 4H, COD-C*H*$_2$), 5.73 (m, 2H, COD-C*H*), 6.18 (d, 1H, $^3J_{HH}$ = 7.6 Hz, aryl-*H*), 6.71 (m, 2H, COD-C*H*), 6.92 (d, 1H, $^3J_{HH}$ = 5.1 Hz, aryl-*H*), 7.11 (m, 2H, aryl-*H*), 7.25 (m, 2H, aryl-*H*), 7.38 (m, 2H, aryl-*H*), 7.93 (d, 1H, $^3J_{HH}$ = 7.6 Hz, aryl-*H*), 8.26 (d, 1H, $^3J_{HH}$= 5.2 Hz, aryl-*H*).

(κ^2-BPI)Ir(CO)$_2$(I)$_2$ (33): A J. Young NMR tube was charged with (κ^2-BPI)Ir(COD)(I)$_2$ (**32**) (7 mg, 0.008 mmol) and dichloromethane (0.4 mL) in a nitrogen-filled glove box, resulting in a red solution. The solution was degassed on the vacuum line (freeze, pump, thaw 3x) and subsequently pressurized with 3 atm CO. The reaction was stirred at room temperature for 2 hours. The solution was degassed on the vacuum line (freeze, pump, thaw 3x). The crude product was recrystallized by vapor diffusion of pentane into dichloromethane.

^{1}H NMR (300 MHz, CD_2Cl_2): 2.50 (s, 3H, C*H*$_3$), 2.54 (s, 3H, C*H*$_3$), 6.56 (dt, 1H, J_{HH} = 7.7 Hz, J_{HH} = 0.83 Hz, aryl-*H*), 7.08 (dd, 1H, J_{HH} = 5.7 Hz, J_{HH} = 0.6 Hz, aryl-*H*), 7.33 (m, 1H, aryl-*H*), 7.41 (m, 1H, aryl-*H*), 7.43 (td, 1H, J_{HH} = 7.7 Hz, J_{HH} = 1.1 Hz, aryl-*H*), 7.64 (td, 1H, J_{HH} = 7.6 Hz, J_{HH} = 0.9 Hz, aryl-*H*), 7.72 (d, 1H, J_{HH} = 1.4 Hz, aryl-*H*), 8.11 (dt, 1H, J_{HH} = 7.5 Hz, J_{HH} = 0.8 Hz, aryl-*H*), 8.57 (m, 2H, aryl-*H*).

(BPI)Ir(C_2H_4)$_2$ (34): (BPI)Ir(C_2H_4)$_2$ was synthesized via a modified literature procedure.[15] A 50 mL Schlenk flask equipped with a stir bar was charged with BPI-H (**12**) (202 mg, 0.617 mmol), KHMDS (124 mg, 0.622 mmol), and diethyl ether (10 mL), resulting in a bright green neon suspension. The reaction was stirred at room temperature under N_2 atmosphere for 3 hours.

Meanwhile, after 2.5 hours of stirring, a new 25 mL round bottom flask equipped with a stir bar was charged with $[(COE)_2IrCl]_2$ (276 mg, 0.308 mmol) and diethyl ether (8 mL), resulting in an orange suspension. The round bottom flask was subsequently cooled to 0 °C in an ice bath. Ethylene was bubbled through the suspension for 30 minutes, resulting in a clear slightly yellow solution of $(C_2H_4)_5IrCl$ monomer (*in situ*). After 3 hours, the deprotonation reaction of **12** was placed under ethylene atmosphere and cooled to 0 °C in an ice bath. The solution with *in situ*-formed $(C_2H_4)_5IrCl$ was subsequently cannula transferred into the 50 mL Schlenk flask with deprotonated ligand, resulting in a dark red solution. The reaction was stirred under an ethylene atmosphere at 0 °C for 8 hours. After 8 hours, fierce bubbling of ethylene through the solution evaporated the solvent, resulting in a dark violet solid. The crude product was dissolved in dichloromethane (3 mL), filtered into a tared 20 mL vial with pentane (3 mL), and placed in the freezer at -30 °C to facilitate crystallization. The solution was decanted and the remaining solid was dried under vacuum. Yield: 130 mg (37%).

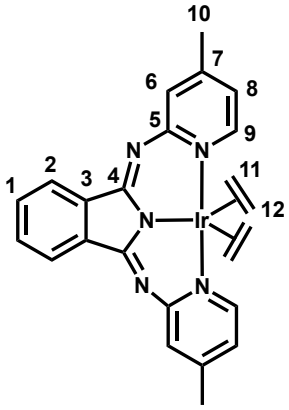

^{1}H NMR (500 MHz, CD_2Cl_2): 1.16 (t, 4H, J_{HH} = 9.6 Hz, H^{11} or H^{12}), 2.26 (s, 6H, H^{10}), 2.63 (t, 4H, J_{HH} = 9.8 Hz, H^{11} or H^{12}), 6.53 (d, 2H, $^3J_{HH}$ = 5.7 Hz, H^8), 7.26 (s, 2H, H^6), 7.64 (m, 2H, H^1 or H^2), 8.07 (m, 2H, H^1 or H^2), 8.15 (d, 2H, $^3J_{HH}$ = 5.9 Hz, H^9). $^{13}C\{^1H\}$ NMR (176 MHz, CD_2Cl_2): 20.7 (s, C^{10}), 30.4 (s, C^{11} or C^{12}), 35.2 (s, C^{11} or C^{12}), 121.2 (s, C^1 or C^2), 121.4 (s, C^8), 128.4 (s, C^6), 130.3 (s, C^1 or C^2), 140.3 (s, C^3), 147.6 (s, C^7), 152.9 (s, C^5), 154.7 (s, C^4), 155.1 (s, C^9).

(BPI)IrEt(OAc) (35): A 20 mL vial equipped with a stir bar was charged with $(BPI)Ir(C_2H_4)_2$ (**33**) (57.2 mg, 0.0994 mmol), AcOH (5.7 μL, 0.0997 mmol) and dichloromethane (3 mL) in a nitrogen-filled glovebox, resulting in a dark blue/black solution. The reaction was stirred at room

temperature for 3 hours. The volatiles were removed under reduced pressure, resulting in a dark blue/black solid. The product was fully dried under vacuum. Yield: 45.5 mg (75%).

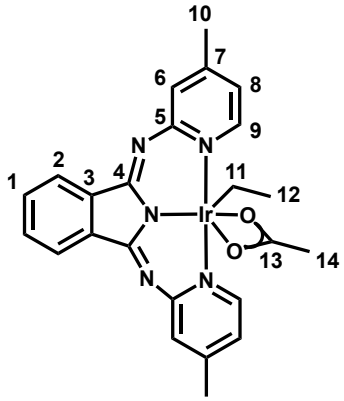

^{1}H NMR (700 MHz, CD_2Cl_2): 0.15 (t, 3H, $^{3}J_{HH}$ = 7.3 Hz, H^{12}), 1.38 (q, 2H, $^{3}J_{HH}$ = 7.3 Hz, H^{11}), 2.06 (s, 3H, H^{14}), 2.38 (s, 6H, H^{10}), 6.91 (d, 2H, $^{3}J_{HH}$ = 6.2 Hz, H^{8}), 7.52 (s, 2H, H^{6}), 7.60 (m, 2H, H^{1}), 8.08 (m, 2H, H^{2}), 9.15 (d, 2H, $^{3}J_{HH}$ = 6.2 Hz, H^{9}). ^{13}C{^{1}H} NMR (176 MHz, CD_2Cl_2): -16.0 (s, C^{11}), 15.7 (s, C^{12}), 21.0 (s, C^{10}), 25.0 (s, C^{14}), 121.2 (s, C^{2}), 121.6 (s, C^{8}), 128.9 (s, C^{6}), 130.4 (s, C^{1}), 139.5 (s, C^{3}), 147.2 (s, C^{7}), 149.0 (s, C^{9}), 149.9 (s, C^{4}), 151.0 (s, C^{5}), 187.9 (s, C^{13}).

(κ^2-^{Br}BPI)Ir(COD) (36): A 20 mL vial equipped with a stir bar was charged with ^{Br}BPI-H (**16**) (62.8 mg, 0.137 mmol), $[(COD)Ir(OMe)]_2$ (45 mg, 0.069 mmol), and THF in a nitrogen-filled glovebox, resulting in a dark red solution. The reaction was stirred at room temperature overnight. The volatiles were removed under reduced pressure. Layering a concentrated solution of dichloromethane with pentane purified the crude product. The solution was decanted off the brown solid that precipitated out and the product was dried under vacuum.

^{1}H NMR (300 MHz, THF-d_8): 1.48 (m, 2H, COD), 1.67 (m, 2H, COD), 1.99 (m, 1H, COD), 2.27 (m, 1H, COD), 2.71 (m, 2H, COD), 3.23 (m, 1H, COD), 4.06 (m, 1H, COD), 4.27 (m, 1H, COD), 4.47 (m, 1H, COD), 5.42 (m, 1H, aryl-*H*), 6.29 (m, 1H, aryl-*H*), 6.63 (d, 1H, J_{HH} = 7.8 Hz, aryl-*H*), 6.95 (m, 2H, aryl-*H*), 7.22 (d, 1H, J_{HH} = 7.6 Hz, aryl-*H*), 7.49 (m, 2H, aryl-*H*), 7.80 (t, 1H, J_{HH} = 7.7 Hz, aryl-*H*), 9.02 (d, 1H, J_{HH} = 7.8 Hz, aryl-*H*).*

*These assignments are made based on the proposed structure (Scheme 4.11).

(^{xylyl}BPI)Ir(C_2H_4)$_2$ (37): (^{xylyl}BPI)Ir(C_2H_4)$_2$ was synthesized via a modified literature procedure.[15] A 25 mL Schlenk flask equipped with a stir bar was charged with ^{xylyl}BPI-H (**17**) (126 mg, 0.248 mmol), KHMDS (50.1 mg, 0.251 mmol), and diethyl ether (8 mL), resulting in a green suspension. The reaction was stirred at room temperature under N_2 atmosphere overnight, resulting in an orange suspension. When the deprotonation reaction was complete, a 25 mL round bottom flask equipped with a stir bar was charged with $[(COE)_2IrCl]_2$ (112 mg, 0.125 mmol) and diethyl ether (8 mL), resulting in an orange suspension. The round bottom was subsequently cooled to 0 °C in an ice bath. Ethylene was bubbled through the suspension for 30 minutes, resulting in a clear slightly yellow solution of $(C_2H_4)_5IrCl$ monomer (*in situ*). After the metal precursor was made, the deprotonation reaction of **17** was placed under ethylene atmosphere and cooled to 0 °C in an ice bath. The solution with *in situ*-formed $(C_2H_4)_5IrCl$ was subsequently cannula transferred into the 25 mL Schlenk flask with deprotonated ligand, resulting in a dark red/brown solution. The reaction was stirred under an ethylene atmosphere at 0 °C for 12 hours. After 12 hours, fierce bubbling of ethylene through the solution evaporated the solvent, resulting in a dark brown/burgundy solid. The crude product was dissolved in dichloromethane (3 mL), filtered into a tared 20 mL vial with pentane (3 mL), and placed in the freezer at -30 °C to purify. The solution was decanted off the solid that precipitated and the solid was dried under vacuum. Yield: 78.4 mg (42%).

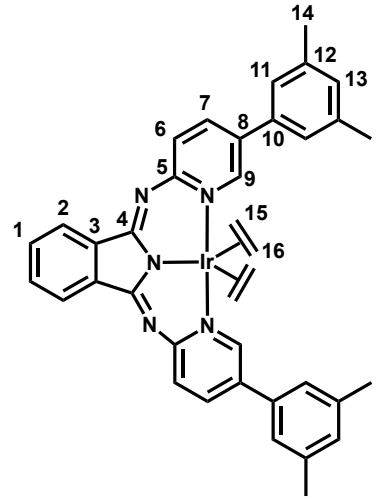

^{1}H NMR (500 MHz, CD_2Cl_2): 1.29 (t, 4H, J_{HH} = 9.7 Hz, H^{15} or H^{16}), 2.42 (s, 12H, H^{14}), 2.82 (t, 4H, J_{HH} = 9.7 Hz, H^{15} or H^{16}), 7.07 (s, 2H, H^{13}), 7.20 (s, 4H, H^{11}), 7.46 (d, 1H, $^3J_{HH}$ = 8.5 Hz, H^6), 7.68 (m, 2H, H^1), 7.89 (dd, 2H, $^3J_{HH}$ = 8.5 Hz, $^4J_{HH}$ = 2.1

Hz, H^7), 8.14 (m, 2H, H^2), 8.60 (d, 2H, $^4J_{HH}$ = 2.0 Hz, H^9). $^{13}C\{^1H\}$ NMR (125.7 MHz, CD_2Cl_2): 21.6 (s, C^{14}), 31.6 (s, C^{15} or C^{16}), 35.9 (s, C^{15} or C^{16}), 121.3 (s, C^2), 125.1 (s, C^{11}), 128.1 (s, C^6), 130.2 (s, C^{13}), 130.4 (s, C^1), 132.8 (s, C^8), 134.5 (s, C^7), 136.5 (s, C^5 or C^{10}), 139.2 (s, C^{12}), 140.2 (s, C^3), 152.0 (s, C^5 or C^{10}), 154.5 (s, C^4), 154.6 (s, C^9).

(^{xylyl}BPI)IrEt(OAc) (38): A 20 mL vial equipped with a stir bar was charged with (^{xylyl}BPI)Ir(C_2H_4)$_2$ (**37**) (44.1 mg, 0.0584 mmol), AcOH (5.1 μL, 0.0892 mmol) and dichloromethane (2 mL) in a nitrogen-filled glovebox, resulting in a dark green/black solution. The reaction was stirred at room temperature for 5 hours. The volatiles were removed under reduced pressure, resulting in a dark forest green solid. The product was fully dried under vacuum.

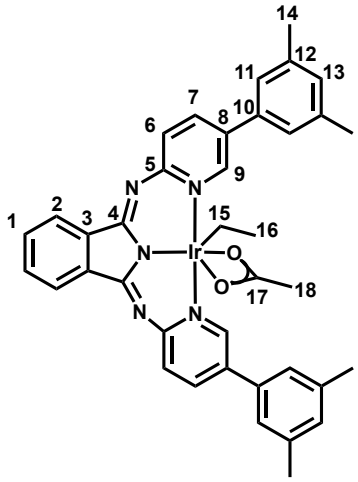

^1H NMR (300 MHz, CD_2Cl_2): 0.19 (t, 3H, $^3J_{HH}$ = 7.2 Hz, H^{16}), 1.53 (q, 2H, $^3J_{HH}$ = 7.4 Hz, H^{15}), 2.15 (s, 3H, H^{18}), 2.43 (s, 12H, H^{14}), 7.10 (s, 2H, H^{13}), 7.29 (s, 4H, H^{11}), 7.64 (m, 2H, H^1), 7.75 (d, 2H, $^3J_{HH}$ = 8.5 Hz, H^6), 8.15 (m, 4H, H^2 and H^7), 9.64 (s, 2H, H^9). $^{13}C\{^1H\}$ NMR (176 MHz, CD_2Cl_2): -15.1 (s, C^{15}), 16.1(s, C^{16}), 21.6 (s, C^{14}), 25.0 (s, C^{18}), 121.4 (s, C^2), 125.2 (s, C^{11}), 128.8 (s, C^6), 130.3 (s, C^{13}), 130.5 (s, C^1), 133.0 (s, C^8), 134.1 (s, C^7), 137 (s, C^{10}), 139.2 (s, C^{12}), 139.4 (s, C^3), 148.2 (s, C^9), 149.6 (s, C^4), 150.1 (s, C^5), 188.0 (s, C^{17}).

(BPI)IrEt(CO_2CF_3) (39): A J. Young NMR tube was charged with (BPI)Ir(C_2H_4)$_2$ (**34**) (5.4 mg, 0.0089 mmol), trifluoroacetic acid (1.8 μL, 0.0235 mmol) and dichloromethane-d_2 (0.4 mL) in a nitrogen-filled glovebox. The reaction was stirred at room temperature for 2 hours. The volatiles were removed under vacuum and the crude product was used without further purification.

^{1}H NMR (300 MHz, CD_2Cl_2): -0.30 (t, 3H, $^3J_{HH}$ = 7.5 Hz, CH_2CH_3), 2.14 (q, 2H, $^3J_{HH}$ = 7.3 Hz, CH_2CH_3), 2.24 (s, 6H, CH_3), 7.12 (d, 2H, $^3J_{HH}$ = 5.1 Hz, aryl-*H*), 7.51 (m, 4H, aryl-*H*), 8.00 (m, 2H, aryl-*H*), 9.07 (d, 2H, $^3J_{HH}$ = 5.3 Hz, aryl-*H*).

(BPI)IrEt(CO_2CPh) (40): A J. Young NMR tube was charged with (BPI)Ir(C_2H_4)$_2$ (**34**) (4.4 mg, 0.0072 mmol), benzoic acid (3.7 mg, 0.030 mmol) and dichloromethane-d_2 (0.4 mL) in a nitrogen-filled glovebox. The reaction was stirred at room temperature for 2 hours. The volatiles were removed under vacuum and the crude product was used without further purification.

^{1}H NMR (300 MHz, CD_2Cl_2): -0.07 (t, 3H, $^3J_{HH}$ = 7.4 Hz, CH_2CH_3), 1.76 (q, 2H, $^3J_{HH}$ = 7.5 Hz, CH_2CH_3), 2.34 (s, 6H, CH_3), 6.81 (dd, 2H, $^3J_{HH}$ = 6.6 Hz, $^4J_{HH}$ = 1.2 Hz, aryl-*H*), 7.54 (m, aryl-*H* for ligand and carboxylate + free benzoic acid), 8.10 (m, 2H, aryl-*H*), 8.17 (m, 2H, aryl-*H*), 9.16 (d, 2H, $^3J_{HH}$ = 6.4 Hz, aryl-*H*).*

* ^{1}H NMR taken with excess benzoic acid still present and signals from the acid overlapped with complex aryl signals.

(BPI)IrEt($CO_2C(CH_3)_3$) (41): A J. Young NMR tube was charged with (BPI)Ir(C_2H_4)$_2$ (**34**) (10.7 mg, 0.176 mmol), pivalic acid (8.7 mg, 0.085 mmol) and dichloromethane-d_2 (0.4 mL) in a nitrogen-filled glovebox. The reaction was stirred at room temperature for 2 hours. The volatiles were removed under vacuum and the crude product was used without further purification.

^{1}H NMR (300 MHz, CD_2Cl_2): 0.07 (t, 3H, $^3J_{HH}$ = 7.5 Hz, CH_2CH_3), 1.21 (s, 91H, $C(CH_3)_3$),* 1.49 (q, 2H, $^3J_{HH}$ = 7.5 Hz, CH_2CH_3), 2.38 (s, 6H, CH_3), 6.87 (dd, 2H, $^3J_{HH}$ = 6.4 Hz, $^4J_{HH}$ = 1.4 Hz, aryl-*H*), 7.53 (s, 2H, aryl-*H*), 7.61 (m, 2H, aryl-*H*), 8.10 (m, 2H, aryl-*H*), 9.06 (d, 2H, $^3J_{HH}$ = 6.4 Hz, aryl-*H*).

* Excess pivalic acid NMR signals overlapped with bound pivalate

[(BPI)Ir(CH$_2$CH$_3$)]$_2$(μ-OAc)]BAr$^F_{24}$ (45-H): A 20 mL vial equipped with a stir bar was charged with (BPI)IrEt(OAc) (**34**) (23.7 mg, 0.0391 mmol) and NaBAr$^F_{24}$ (12 mg, 0.0135 mmol) and C_6D_6 (2 mL) in a nitrogen-filled glovebox, resulting in a dark blue suspension. The reaction progress was monitored by ^{1}H NMR spectroscopy and if needed more NaBAr$^F_{24}$ was added. The reaction was stirred at room temperature for 2 days until ^{1}H NMR showed that the reaction was complete. The volatiles were subsequently removed under reduced pressure, resulting in a dark brown solid. Yield: 34.7 mg (88% based on Ir).

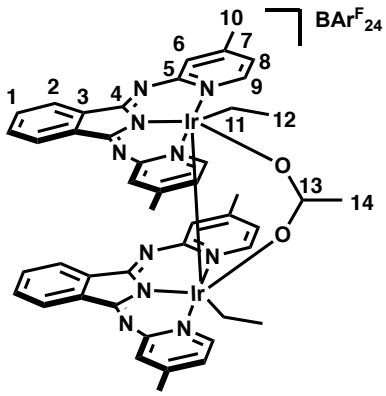

^{1}H NMR (300 MHz, CD_2Cl_2): -1.22 (t, 6H, $^3J_{HH}$ = 7.3 Hz, H^{12}), 2.27 (q, 4H, $^3J_{HH}$ = 7.4 Hz, H^{11}), 2.39 (s, 12H, H^{10}), 2.88 (s, 3H, H^{14}), 6.65 (dd, 4H, $^3J_{HH}$ = 6.6 Hz, $^4J_{HH}$ = 2.1 Hz, H^8), 7.35 (bs, 4H, H^6), 7.50 (m, 4H, H^2), 7.57 (m, 8H, H^1 and BAr$^F_{24}$), 7.74 (m, 8H, BAr$^F_{24}$), 8.30 (d, 4H, $^3J_{HH}$ = 6.6 Hz, H^9). ^{13}C{^{1}H} NMR (126 MHz, CD_2Cl_2): 9.87 (s, C^{11}), 19.4 (s, C^{12}), 20.9 (s, C^{10}), 26.4 (s, C^{14}), 117.9 (bs, BAr$^F_{24}$), 121.9 (s, C^1), 122.5 (s, C^8), 125.1 (q, $^1J_{CF}$ = 272 Hz, BAr$^F_{24}$), 129.4 (q, $^2J_{CF}$ = 32 Hz, BAr$^F_{24}$), 130.2 (s, C^6), 131.5 (s, C^2), 135.2 (s, BAr$^F_{24}$), 138.2 (s, C^3), 147.0 (s, C^9), 148.9 (s, C^7), 150.5 (s, C^4), 150.6 (s, C^5), 162 (q, J_{BC} = 50 Hz, BAr$^F_{24}$), 189.2 (s, C^{13}). ^{19}F NMR (470 MHz, CD_2Cl_2): 64 (s, BAr$^F_{24}$).

[(^{xylyl}**BPI)Ir(CH$_2$CH$_3$)]$_2$(μ-OAc)]BAr$^F_{24}$ (51-H):** A J. Young NMR tube was charged with (^{xylyl}BPI)IrEt(OAc) (**38**) (0.4 mL, from [**38**] = 0.021 M stock solution, 0.008 mmol) and NaBAr$^F_{24}$ (0.2 mL from [NaBAr$^F_{24}$] = 0.021 M stock solution, 0.004 mmol) in a nitrogen-filled glovebox. The solution was left to sit at room temperature and the volatiles were subsequently

removed under reduced pressure resulting in the product as a dark brown solid. Yield: quantitative.

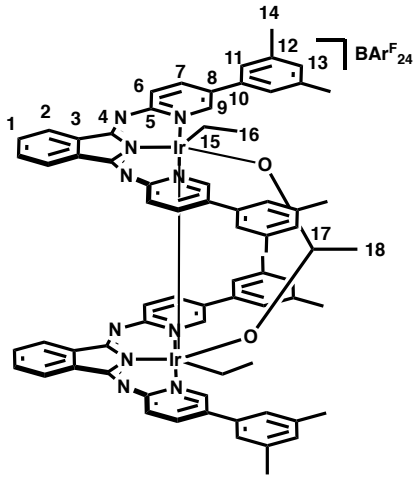

^{1}H NMR (700 MHz, CD_2Cl_2): -1.16 (t, 6H, $^3J_{HH}$ = 7.2 Hz, H^{16}), 2.24 (s, 24H, H^{14}), 2.47 (q, 4H, $^3J_{HH}$ = 7.3 Hz, H^{15}), 2.93 (s, 3H, H^{18}), 6.80 (s, 8H, H^{11}), 6.96 (s, 4H, H^{13}), 7.52 (m, 4H, H^1 or H^2), 7.56 (bs, BAr$^F_{24}$), 7.64 (d, 4H, $^3J_{HH}$ = 8.3 Hz, H^6), 7.66 (m, 4H, H^1 or H^2), 7.72 (m, BAr$^F_{24}$), 7.98 (dd, 4H, $^3J_{HH}$ = 8.5 Hz, $^4J_{HH}$ = 2.2 Hz, H^7), 8.81 (d, 4H, $^4J_{HH}$ = 2.2 Hz, H^9). ^{13}C{^{1}H} NMR (176 MHz, CD_2Cl_2): 12.6 (s, C^{15}), 19.7 (s, C^{16}), 21.4 (s, C^{14}), 25.74 (s, C^{18}), 117.9 (bs, BAr$^F_{24}$), 122.0 (s, C^1 or C^2), 125.1 (q, $^1J_{CF}$ = 272 Hz, BAr$^F_{24}$), 124.3 (s, C^{11}), 129.2 (q, $^2J_{CF}$ = 33 Hz, BAr$^F_{24}$), 130.1 (s, C^6), 130.8 (s, C^{13}), 131.7 (s, C^1 or C^2), 134.1 (s, C^8), 135.0 (s, C^7), 135.1 (s, C^4 or C^5 or C^{10}), 135.2 (bs, BAr$^F_{24}$), 138.0 (s, C^3), 139.5 (s, C^{12}), 145.7 (s, C^9), 149.7 (s, C^4 or C^5 or C^{10}), 150.2 (s, C^4 or C^5 or C^{10}), 162.0 (q, J_{BC} = 50 Hz, BAr$^F_{24}$), 188.5 (s, C^{17}).

4.6.4 Reactions of (BPI)IrEt(OAc) (35) and (^{xylyl}BPI)IrEt(OAc) (38) with C_6D_6:

Representative Procedure of reaction of (BPI)IrEt(OAc) (**35**) with C_6D_6 at 100 °C

A 5mm medium-walled sealable NMR tube fitted with a 14/20 joint and attached to a 180° Kontes stopcock was charged with (BPI)IrEt(OAc) (0.4 mL from [Ir] = 0.021 M stock solution in dichloromethane, 0.0084 mmol) and $NaBAr^F_{24}$ (0.12 mL from [$NaBAr^F_{24}$] = 0.021 M stock solution in diethyl ether, 0.0025 mmol). The volatiles were removed under reduced pressure. The NMR tube was then charged with hexamethyldisiloxane (0.1 μL, 0.00047 mmol) and C_6D_6 (0.4 mL). The solution was degassed on vacuum line (freeze-pump-thaw 3x) and subsequently flame-sealed while under dynamic vacuum. The reaction was placed in an aluminum sleeve submerged in a 100 °C oil bath. The reaction progress was monitored by ^{1}H NMR spectroscopy at specific time intervals until completion.

Representative Procedure of reaction of (BPI)IrEt(OAc) (**35**) with C_6D_6 at 70 °C and 50 °C

A J. Young NMR tube was charged with (BPI)IrEt(OAc) (0.4 mL from [Ir] = 0.021 M stock solution in dichloromethane, 0.0084 mmol) and $NaBAr^F_{24}$ (0.12 mL from [$NaBAr^F_{24}$] = 0.021 M stock solution in diethyl ether, 0.0025 mmol). The volatiles were removed under reduced pressure. The NMR tube was then charged with hexamethyldisiloxane (0.1 μL, 0.00047 mmol) and C_6D_6 (0.4 mL). The reaction was placed in a 70 °C or 50 °C oil bath. The reaction progress was monitored by ^{1}H NMR spectroscopy at specific time intervals until completion.

Representative Procedure of reaction of (^{xylyl}BPI)IrEt(OAc) (**38**) with C_6D_6 at 70 °C

A J. Young NMR tube was charged with (^{xylyl}BPI)IrEt(OAc) (**38**) (0.4 mL, from [**38**] = 0.021 M stock solution in dichloromethane, 0.008 mmol) and $NaBAr^F_{24}$ (0.2 mL from

[$NaBAr^F_{24}$] = 0.021 M stock solution in diethyl ether, 0.004 mmol) in a nitrogen-filled glovebox. The volatiles were removed under reduced pressure. resulting in the product as a dark brown solid. Yield: quantitative. The NMR tube was then charged with hexamethyldisiloxane (0.1 μL, 0.00047 mmol) and C_6D_6 (0.4 mL). The reaction was placed in a 70 °C oil bath. The reaction progress was monitored by ^1H NMR spectroscopy at specific time intervals until completion.

4.6.5 Representative ^{1}H NMR spectrum of reaction with (BPI)IrEt(CO_2CF_3) (39):

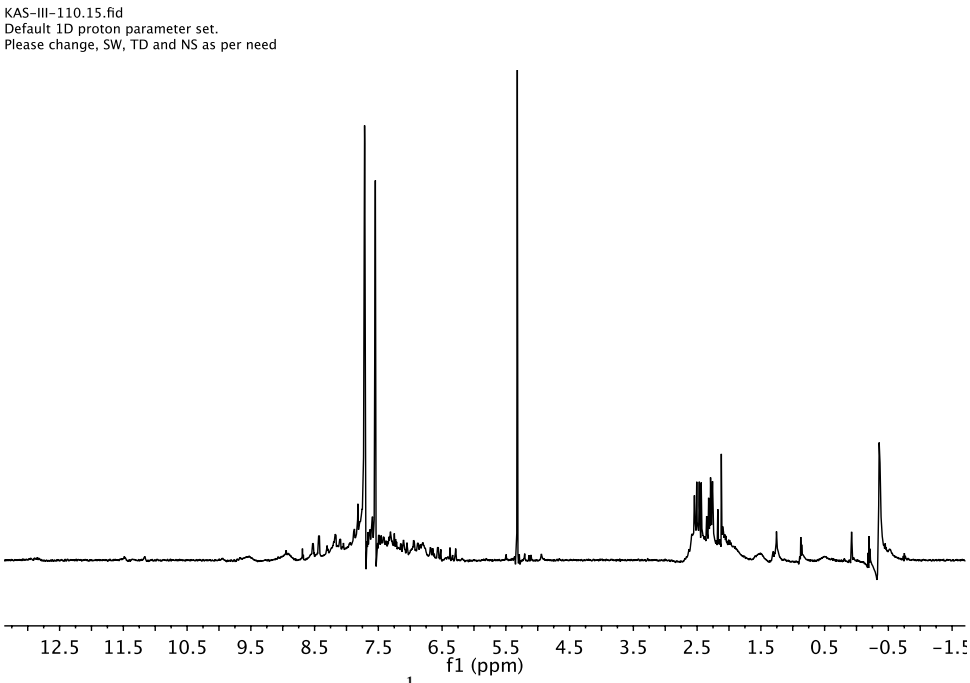

Figure 4.14. Representative ^{1}H NMR spectrum (500 MHz, CD_2Cl_2) of the reaction of (BPI)IrEt(CO_2CF_3) with $NaBAr^{F}_{24}$ in *p*-xylene-d_{10} at 100 °C after completion.

4.6.6 ^{1}H NMR spectra of reactions with (BPI)IrEt(OAc) (35):

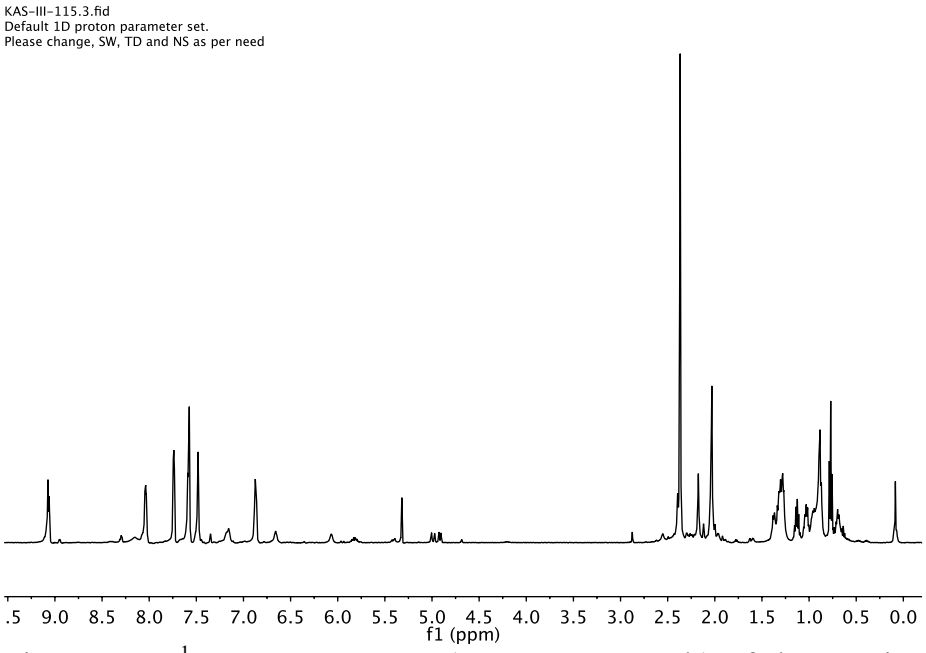

Figure 4.15. ^{1}H NMR spectrum (500 MHz, CD_2Cl_2) of the reaction of (BPI)IrEt(OAc) with $NaBAr^{F}_{24}$ in 1-octene at 100 °C after completion.*

* This reaction was not reproducible

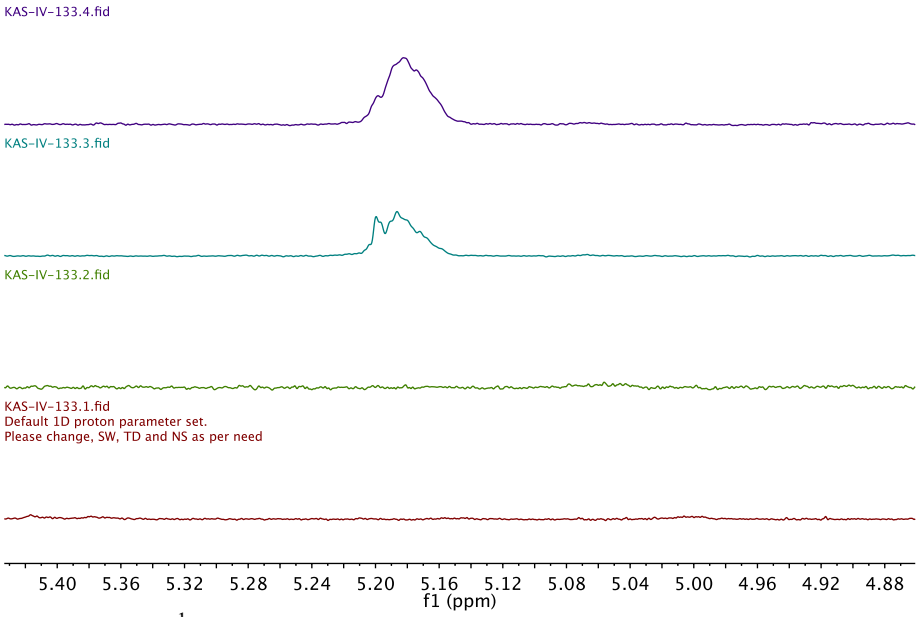

Figure 4.16. ^{1}H NMR spectrum (300 MHz, p-xylene d_{10}) of ethylene region from reaction of (BPI)IrEt(OAc) with C_2D_4 at 100 °C.

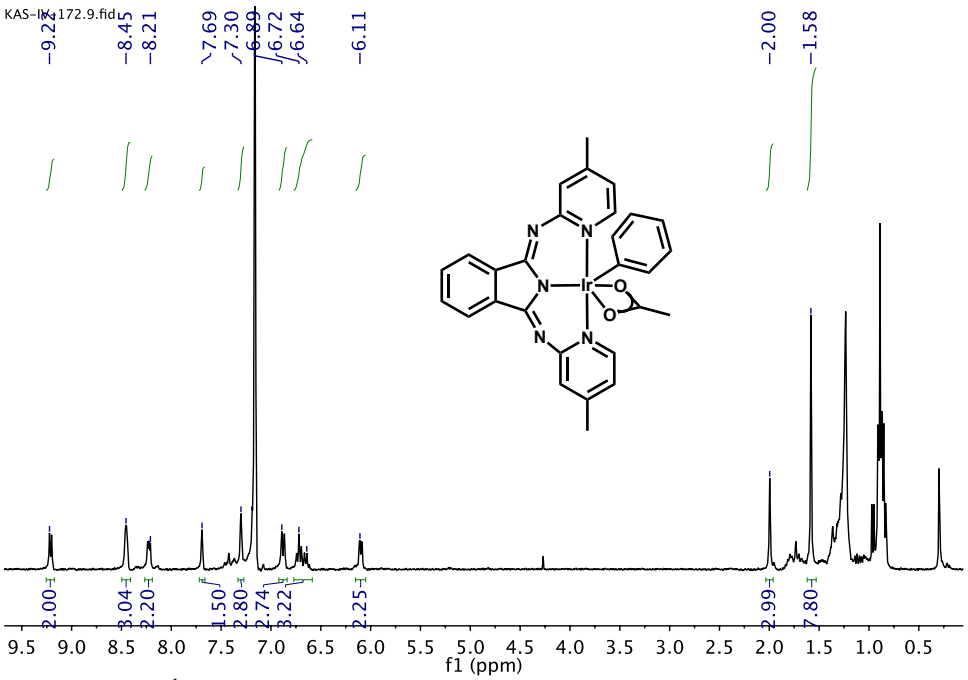

Figure 4.17. ^{1}H NMR spectrum (300 MHz, C_6D_6) from reaction of (BPI)IrEt(OAc) with C_6H_6 at 100 °C to form (BPI)Ir(C_6H_5)(OAc). Grease and pentane are impurities. $NaBAr^{F}_{24}$ also present.

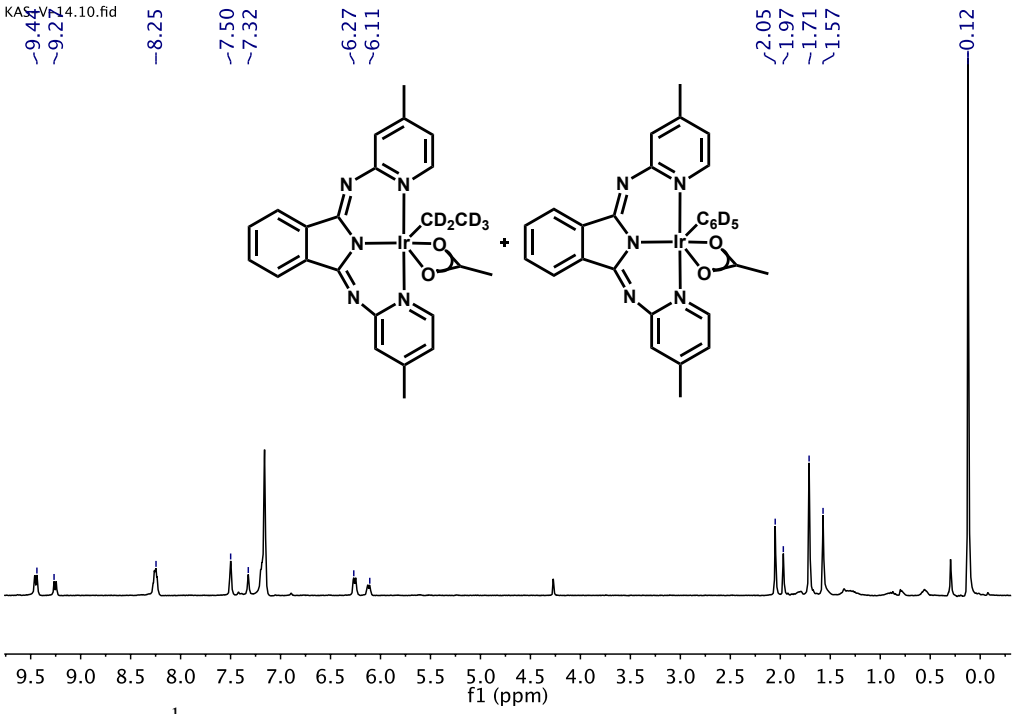

Figure 4.18. ^{1}H NMR spectrum (300 MHz, C_6D_6) from reaction of (BPI)IrEt(OAc) with C_6D_6 at 70 °C to form (BPI)Ir(CD_2CD_3)(OAc) and (BPI)Ir(C_6D_5)(OAc). Internal standard = hexamethyldisiloxane.

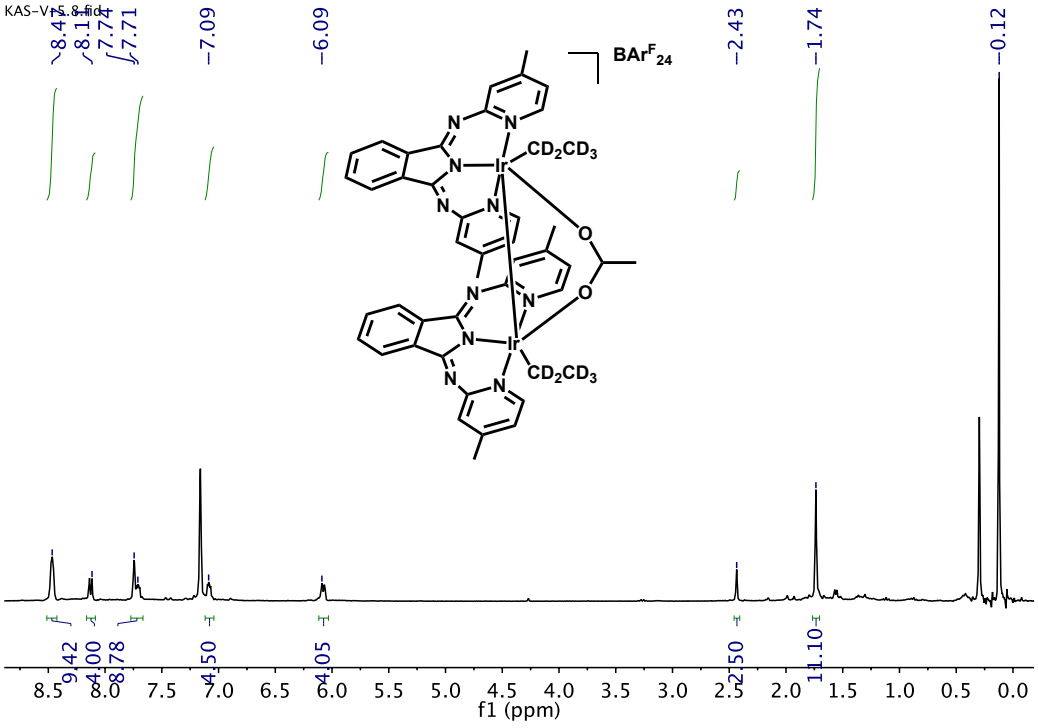

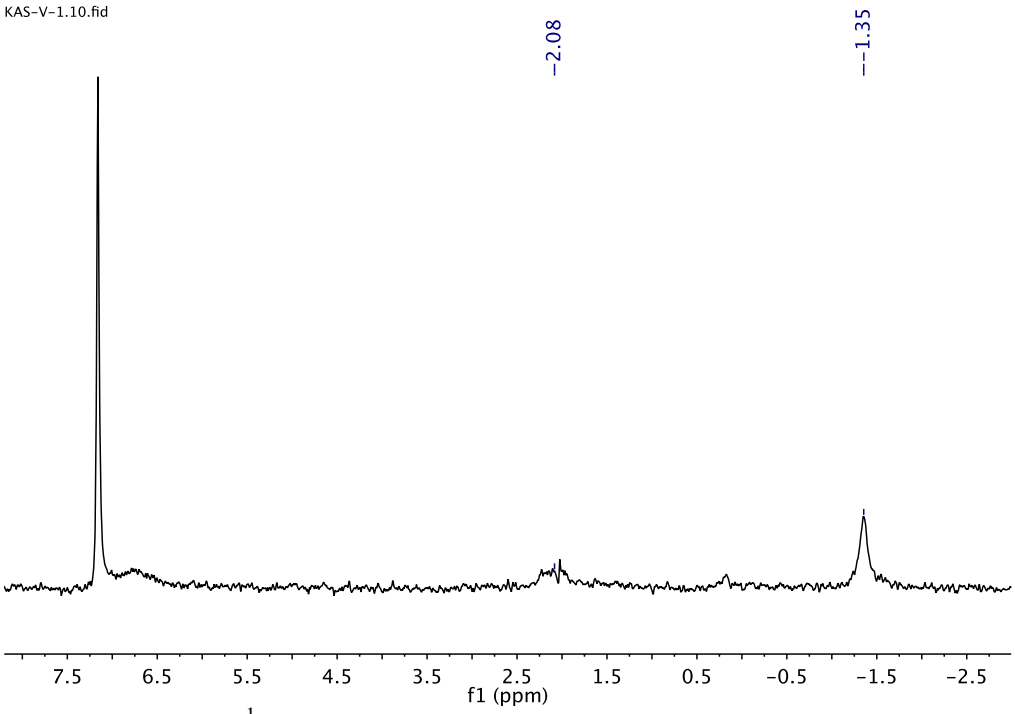

Figure 4.19. Top: ^{1}H NMR spectrum (300 MHz, C_6D_6) from reaction of (BPI)IrEt(OAc) + 0.3 equiv. $NaBAr^{F}{}_{24}$ with C_6D_6 at 70 °C to form $[(BPI)Ir(CD_2CD_3)]_2(\mu\text{-}OAc)]BAr^{F}{}_{24}$. Internal standard = hexamethyldisiloxane. Grease impurity present. Bottom: ^{2}H NMR spectrum (46.07 MHz, C_6H_6) of $[(BPI)Ir(CD_2CD_3)]_2(\mu\text{-}OAc)]BAr^{F}{}_{24}$.

4.6.7 ^{1}H NMR spectrum of reaction with [(BPI)Ir(CH$_2$CH$_3$)]$_2$(μ-OAc)]BAr$^F{}_{24}$ (45-H):

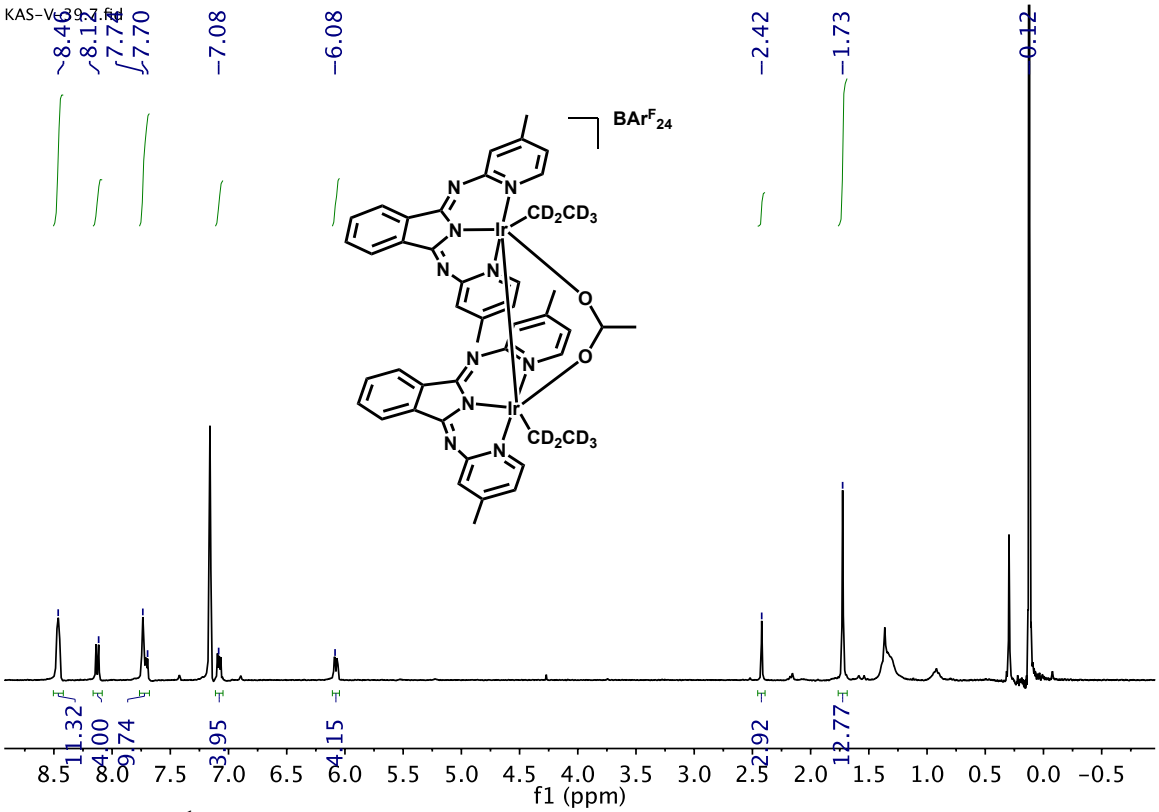

Figure 4.20. ^{1}H NMR spectrum (300 MHz, C_6D_6) from reaction of [(BPI)Ir(CH_2CH_3)]$_2$(μ-OAc)]BAr$^F{}_{24}$ with C_6D_6 at 70 °C to form [(BPI)Ir(CD_2CD_3)]$_2$(μ-OAc)]BAr$^F{}_{24}$. Internal standard = hexamethyldisiloxane. Grease impurity present.

4.6.8 ^{1}H NMR spectra of reactions with (^{xylyl}BPI)IrEt(OAc) (38):

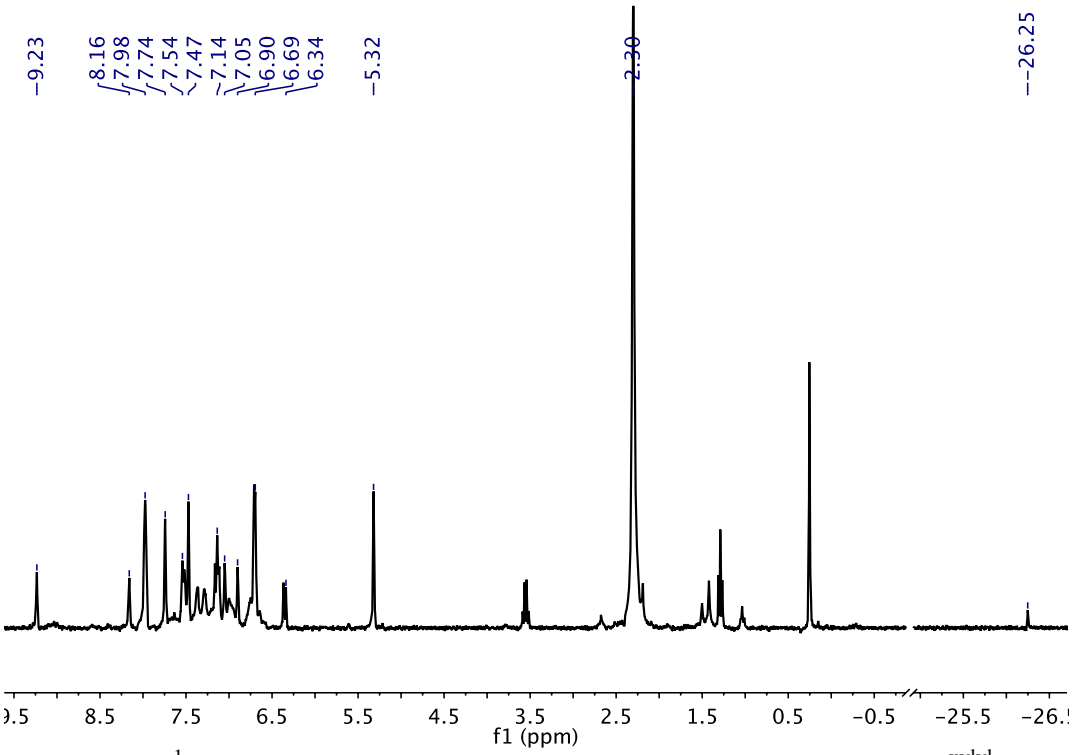

Figure 4.21. ^{1}H NMR spectrum (300 MHz, CD_2Cl_2) of the reaction of (^{xylyl}BPI)IrEt(OAc) with $NaBAr^{F}_{24}$ in *p*-xylene-d_{10} at 100 °C after completion. Diethyl ether and grease impurities are present.

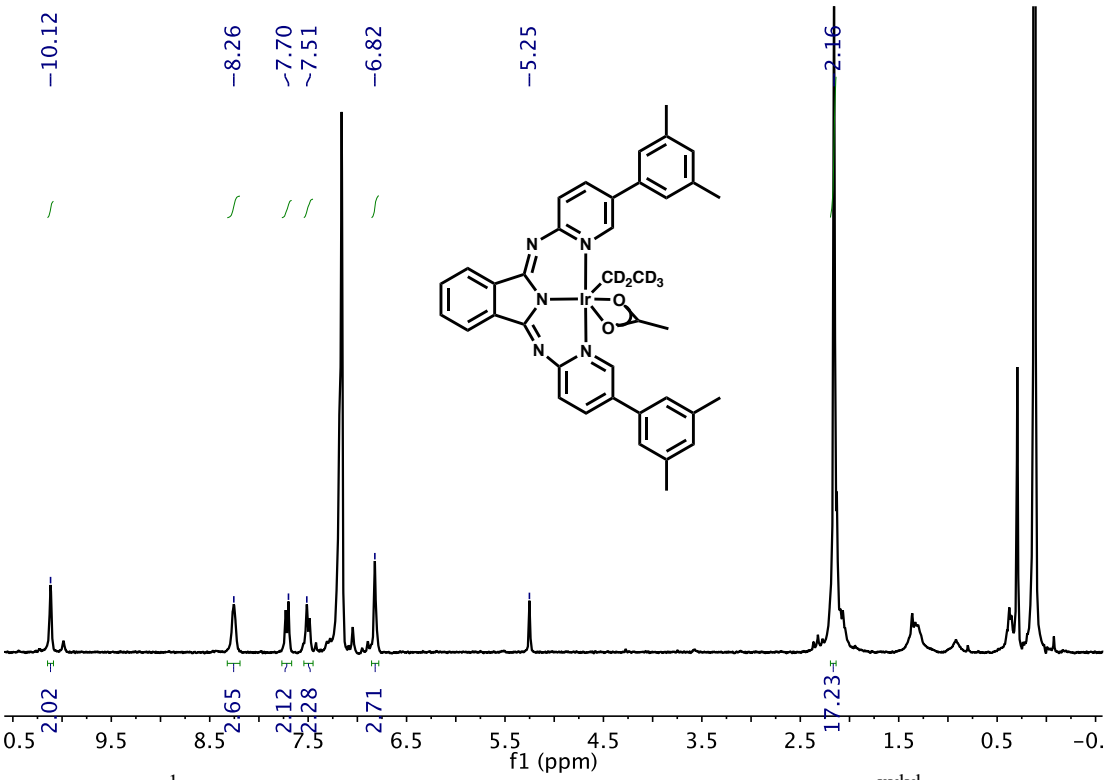

Figure 4.22. ^{1}H NMR spectrum (300 MHz, C_6D_6) from reaction of (^{xylyl}BPI)IrEt(OAc) with C_6D_6 at 70 °C to form (^{xylyl}BPI)Ir(CD_2CD_3)(OAc). Internal standard = hexamethyldisiloxane.*

*A complex peak overlaps with solvent signal.

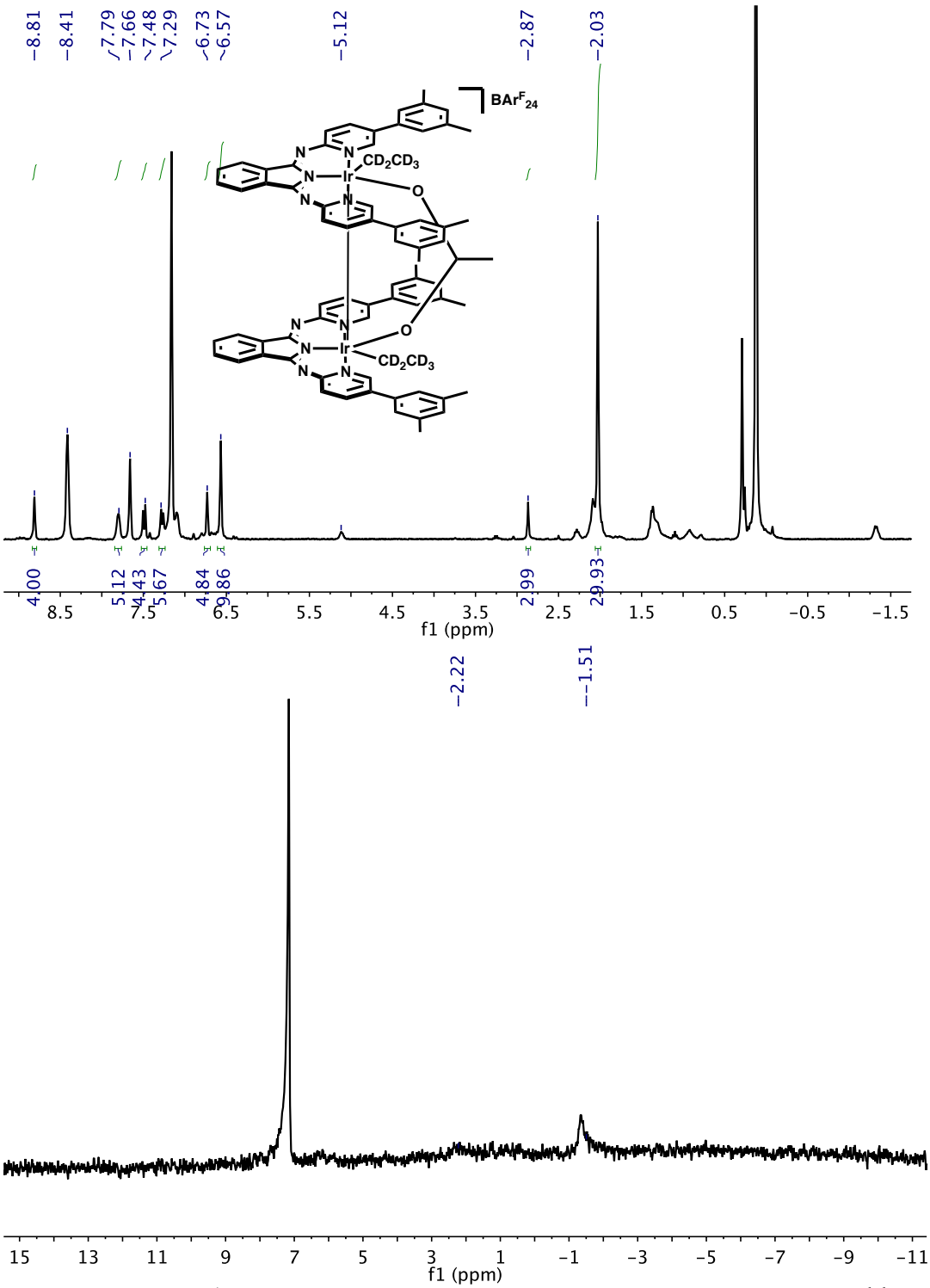

Figure 4.23. Top: ^{1}H NMR spectrum (300 MHz, C_6D_6) from reaction of (^{xylyl}BPI)IrEt(OAc) + 0.5 equiv. NaBAr$^{F}_{24}$ with C_6D_6 at 70 °C to form [(^{xylyl}BPI)Ir(CD_2CD_3)]$_2$(μ-OAc)]BAr$^{F}_{24}$ at 75 % completion. Internal standard = hexamethyldisiloxane. Grease impurity present. Bottom: ^{2}H NMR spectrum (46.07 MHz, C_6H_6) of [(^{xylyl}BPI)Ir(CD_2CD_3)]$_2$(μ-OAc)]BAr$^{F}_{24}$.

4.6.9 X-ray Crystallographic Methodology and Data Tables:

Occlusion free single crystals were mounted on a loop with oil. Data was collected at -173 °C on a Bruker APEX II single X-ray diffractometer, Mo-radiation. Crystal-to-detector distance was 40 mm and exposure times were 5, 10, 30, 60, 120, and 240 seconds per frame, depending on the crystal size (see Table 4.5, Table 4.6, and Table 4.7). The scan width was 0.5° and 1°. The data was integrated and scaled using SAINT, SADABS within the APEX2 software package by Bruker.[50] Solution by direct methods (SHELXS, SIR97[51]) produced complete heavy atom phasing models consistent with the proposed structures. The structures were completed by difference Fourier synthesis with SHELXL97.[52,53] Scattering factors are from Waasmair and Kirfel.[54] Hydrogen atoms were placed in geometrically idealized positions and constrained to ride on their parent atoms with C---H distances in the range 0.95-1.00 Angstrom. Isotropic thermal parameters U_{eq} were fixed such that they were $1.2U_{eq}$ of their parent atom U_{eq} for CH's and $1.5U_{eq}$ of their parent atom U_{eq} in case of methyl groups. All non-hydrogen atoms were refined anisotropically by full-matrix least squares. The crystal sample of **32** contained three different types of crystals. The lattices and symmetries between the different types depended on solvent incorporation into the structure. The best suited crystals were used for this report, which contained one pentane molecule per complex. The data for **33** show two complexes accompanied by disordered pentane which fills up an infinit channel along [0 1 0]. The data for **34** appeared twinned (CELL_NOW[55]) and after multi-domain integration the data was merged utilizing twinabs.[56] Complex **35** shows minute ligand disorder of 4%. Data of **37** and **45** showed disordered solvent and the best result was obtained when all solvent was removed via SQUEEZE.[57] The data of **48** had infinite Ir dinuclear species along the a axis. Along the same direction, there are infinite channels of disordered anions and solvent. One BAr^{F}_{24} anion, with

disordered CF_3 ligands was identified. After emptying out the channels and applying SQUEEZE,[57] a usable structure was obtained. The total removed electron density of 4160 electrons is shy of accounting for 12 BAr^F_{24} molecules per unit cell, as SQUEEZE[57] usually underestimates the electron density. 12 dimers account for Foo = 6324 electrons in the unit cell, thus 2/3 of the electrons of the total electrons are inside the voids.

Table 4.5. Crystallographic data for compounds **32-35**.

Complex	**32**	**33**	**34**	**35**
Empirical formula	$C_{33}H_{40}I_2IrN_5$	$C_{190}H_{160}C_{l8}I_{16}$ Ir_8 $N_{40}O_{16}$	$C_{24}H_{24}Ir_1N_5$	$C_{24}H_{24}IrN_5O_2$
Formula weight	952.70	7111.18	574.68	606.68
Temperature (K)	100(2)	100(2)	100(2)	100(2)
Wavelength (Å)	0.71073	0.71073	0.71073	0.71073
Crystal system	Monoclinic	Monoclinic	Monoclinic	Monoclinic
Space group	P 2_1/c	C 2/c	P -1	P 2_1/c
Unit cell axis a (Å)	8.7879(6)	40.1494(18)	7.8985(13)	15.0595(15)
Unit cell axis b (Å)	13.8991(10)	10.6843(4)	12.396(2)	11.6006(12)
Unit cell axis c (Å)	27.757(2)	28.4104(15)	12.694(2)	14.1905(14)
Unit cell angle α (°)	90	90	117.476(4)	90
Unit cell angle β (°)	90.929(4)	113.484(4)	100.682(4)	113.858(5)
Unit cell angle γ (°)	90	90	98.837(4)	90
Volume ($Å^3$)	3389.8(4)	11177.7(9)	1042.0(3)	2267.2(4)
Z	4	2	2	4
Density (Mg/m^3), calculated	1.867	2.113	1.832	1.777
Absorption coefficient (mm^{-1})	5.789	7.112	6.428	5.920
F(000)	1824	6616	560	1184
Crystal size (mm^3)	0.17 x 0.07 x 0.05	0.15 x 0.09 x 0.09	0.32 x 0.13 x 0.10	0.330 x 0.140 x 0.140
Theta range for data collection	1.47 to 30.58°	1.98 to 26.40°	1.891 to 28.293°	1.479 to 28.363°
Index ranges	-12<=h<=12, -19<=k<=19, -39<=l<=38	-50<=h<=50, -13<=k<=13, -35<=l<=35	-10<=h<=10, -16<=k<=14, 0<=l<=16	-20<=h<=20, -15<=k<=15, -18<=l<=18
Reflections collected	142163	155715	24618	10996
Independent reflections, R(int)	10212, 0.0751	11404, 0.1272	5027, 0.0571	5644, 0.0258
Completeness to theta = 25.00 (%)	98.5	99.6	99.1	100.0
Max. and min. Transmission	0.7606 and 0.4394	0.5670 and 0.4151	0.5531 and 0.7457	
Data / restraints / parameters	10212 / 0 / 375	11404 / 20 / 644	5027 / 12 / 298	5644 / 16 / 316
Goodness-of-fit on F^2	1.039	1.037	1.020	1.063
Final R indices [I>2sigma(I)]	R1 = 0.0432, wR2 = 0.0913	R1 = 0.0454, wR2 = 0.1000	R1 = 0.0368, wR2 = 0.0934	R1 = 0.0264, wR2 = 0.0530
R indices (all data)	R1 = 0.0686, wR2 = 0.0993	R1 = 0.0775, wR2 = 0.1119	R1 = 0.0420, wR2 = 0.0967	R1 = 0.0362, wR2 = 0.0556
Largest diff. peak and hole ($e.Å^{-3}$)	2.209 and -1.599	1.805 and -1.484	2.274 and -2.031	1.090 and -0.919

Table 4.6. Crystallographic data for compounds **37**, **38**, **45**, and **45-H**.

Complex	**37**	**38**	**45**	**45-H**
Empirical formula	$C_{38}H_{36}IrN_5$	$C_{39}H_{38}Cl_2IrN_5O_2$	$C_{78}H_{47}BD_{10}F_{24}Ir_2N_{10}O_2$	$C_{83}H_{69}BF_{24}Ir_2N_{10}O_2$
Formula weight	754.92	871.84	2027.60	2089.69
Temperature (K)	100(2)	100(2)	100(2)	100(2)
Wavelength (Å)	0.71073	0.71073	0.71073	0.71073
Crystal system	Triclinic	Triclinic	Monoclinic	Monoclinic
Space group	P -1	P -1	C 2/c	C 2/c
Unit cell axis a (Å)	11.3532(9)	10.0122(17)	26.5395(18)	26.6085(18)
Unit cell axis b (Å)	12.0574(9)	12.104(2)	21.2878(17)	21.2272(18)
Unit cell axis c (Å)	15.4065(11)	15.529(3)	19.188(2)	19.1045(18)
Unit cell angle α (°)	85.213(4)	85.600(5)	90	90
Unit cell angle β (°)	72.281(4)	72.736(5)	131.602(2)	131.506(7)
Unit cell angle γ (°)	63.748(4)	80.339(6)	90	90
Volume ($Å^3$)	1798.5(2)	1770.9(5)	8106(13)	8081.0(13)
Z	2	2	4	4
Density (Mg/m^3), calculated	1.394	1.635	1.661	1.718
Absorption coefficient (mm^{-1})	3.743	3.963	3.387	3.401
F(000)	752	868	3944	4112
Crystal size (mm^3)	0.140 x 0.110 x 0.100	0.100 x 0.050 x 0.030	0.22 x 0.18 x 0.06	0.340 x 0.090 x 0.080
Theta range for data collection	1.887 to 26.426°	1.374 to 28.356°	1.400 to 26.687°	1.402 to 28.639°
Index ranges	-14<=h<=14, -15<=k<=15, -19<=l<=19	-13<=h<=13, -16<=k<=16, -20<=l<=20	-31<=h<=33, -26<=k<=26, -23<=l<=23	-35<=h<=35, -28<=k<=28, -25<=l<=25
Reflections collected	18415	17267	27846	207468
Independent reflections, R(int)	7219, 0.0391	8803, 0.0635	8105, 0.0426	10168, 0.0638
Completeness to theta = 25.00 (%)	98.4	100.0	98.4	99.6
Max. and min. Transmission				
Data / restraints / parameters	7219 / 62 / 425	8803 / 0 / 448	8105 / 246 / 567	10168 / 52 / 593
Goodness-of-fit on F^2	1.052	1.004	1.046	1.119
Final R indices [I>2sigma(I)]	R1 = 0.0420, wR2 = 0.0904	R1 = 0.0482, wR2 = 0.0916	R1 = 0.0575, wR2 = 0.1358	R1 = 0.0302, wR2 = 0.0607
R indices (all data)	R1 = 0.0627, wR2 = 0.1030	R1 = 0.0767, wR2 = 0.1018	R1 = 0.929, wR2 = 0.1619	R1 = 0.0538, wR2 = 0.0724
Largest diff. peak and hole ($e.Å^{-3}$)	4.200 and -1.952	4.768 and -1.713	3.322 and -1.996	2.776 and -1.441

Table 4.7. Crystallographic data for compounds **46-48**

Complex	**46** and **47**	**48**
Empirical formula	$C_{43}H_{36}Cl_0Ir_2N_{10}O_3$ $C_{32}H_{98}Cl_{34}Ir_2N_{10}O_{32}$	$C_{42}H_{35}Ir_2N_{10}O_2$
Formula weight	1147.24	1096.20
Temperature (K)	100(2)	100(2)
Wavelength (Å)	0.71073	0.71073
Crystal system	Monoclinic	Monoclinic
Space group	P 2_1/n	P 2_1/n
Unit cell axis a (Å)	14.5814(14)	17.9305(11)
Unit cell axis b (Å)	16.9229(15)	39.258(4)
Unit cell axis c (Å)	15.8899(15)	26.208(2)
Unit cell angle α (°)	90	90
Unit cell angle β (°)	91.741(5)	96.948(4)
Unit cell angle γ (°)	90	90
Volume ($Å^3$)	3919.2(6)	18313(3)
Z	4	12
Density (Mg/m^3), calculated	1.944	1.193
Absorption coefficient (mm^{-1})	6.864	4.388
F(000)	2213	6324
Crystal size (mm^3)	0.180 x 0.120 x 0.040	0.200 x 0.090 x 0.040
Theta range for data collection	1.758 to 28.428°	1.552 to 25.349°
Index ranges	-19<=h<=19, -22<=k<=22, -21<=l<=21	-21<=h<=21, -47<=k<=47, -31<=l<=31
Reflections collected	227802	65643
Independent reflections, R(int)	9836, 0.0538	33395, 0.1966
Completeness to theta = 25.00 (%)	99.9	99.6
Max. and min. Transmission		
Data / restraints / parameters	9836 / 25 / 570	33395 / 1908 / 1528
Goodness-of-fit on F^2	1.092	1.018
Final R indices [I>2sigma(I)]	R1 = 0.0236, wR2 = 0.0518	R1 = 0.1030, wR2 = 0.2289
R indices (all data)	R1 = 0.0334, wR2 = 0.0564	R1 = 0.2420, wR2 = 0.2913
Largest diff. peak and hole ($e.Å^{-3}$)	1.666 and -0.767	2.756 and -4.359

4.7 Notes and References to Chapter 4

1. Choi, J.; MacArthur, A.H.R.; Brookhart, M.; Goldman, A.S. *Chem. Rev.* **2011**, *111*, 1761-1779.
2. Renkema, K.B.; Kissin, Y.V.; Goldman, A.S. *J. Am. Chem. Soc.* **2003**, *125*, 7770-7771.
3. a) Gupta, M.; Hagen, C.; Flesher, R.J.; Kaska, W.C.; Jensen, C.M. *Chem. Commun.* **1996**, 2083-2084. b) Gupta, M.; Hagen, C.; Kaska, W.C.; Cramer, R.E.; Jensen, C.M. *J. Am. Chem. Soc.* **1997**, *119*, 840-841.
4. Lui, F.; Pak, E.B.; Singh, B.; Jensen, C.M.; Goldman, A.S. *J. Am. Chem. Soc.* **1999**, *121*, 4086-4087.
5. a) Lapointe, D.; Fagnou, K. *Chem. Lett.* **2010**, *39*, 1118-1126. b) Ackermann, L. *Chem. Rev.* **2011**, *111*, 1315-1345.
6. Pahls, D.R.; Allen, K.E.; Goldberg, K.I.; Cundari, T.R. *Organometallics* **2014**, *33*, 6413-6419.
7. Ito, J.; Kaneda, T.; Nishiyama,H. *Organometallics* **2012**, *31*, 4442-4449.
8. Allen, K.E.; Heinekey, D.M.; Goldman, A.S.; Goldberg, K.I. *Organometallics* **2013**, *32*, 1579-1582.
9. Allen, K.E.; Heinekey, D.M.; Goldman, A.S.; Goldberg, K.I. *Organometallics* **2014**, *33*, 1337-1340.
10. Recent experiments have suggested that octane also undergoes nonselective oxidation in the presence of O_2 at 200 °C without catalyst present.
11. Gao, Y.; Guan, C.; Zhou, M.; Kumar, A.; Emge, T.J.; Wright, A.M.; Goldberg, K.I.; Krogh-Jespersen, K.; Goldman, A.S. *J. Am. Chem. Soc.* **2017**, *139*, 6338-6350.
12. Yuan, H.; Brennessel, W.W.; Jones, W.D. *ACS Catal.* **2018**, *8*, 2326-2329.
13. Siegl, W.O. *J. Organometallic Chem.* **1976**, *107*, C27-C30.
14. Saussine, L.; Brazi, E.; Robine, A.; Mimoun, H.; Fischer, J.; Weiss, R. *J. Am. Chem. Soc.* **1985**, *107*, 3534-3540.
15. Camerano, J.A.; Samann, C.; Wadepohl, H.; Gade, L.H. *Organometallics* **2011**, *30*, 379-382.
16. a) Leonard, N.G.; Williard, P.G.; Bernskoetter, W.H. *Dalton Trans.* **2011**, *40*, 4300-4306. b) Raynal, M.; Pattacini, R.; Cazin, C.S.J.; Vallee, C.; Bourbigou, H.O.; Braunstein, P. *Organometallics* **2009**, *28*, 4028-4047.
17. Graeupner, J.; Brewster, T.P.; Blakemore, J.D.; Schley, N.D.; Thomsen, J.M.; Brudvig, G.W.; Hazari, N.; Crabtree, R.H. *Organometallics* **2012**, *31*, 7158-7164.
18. Attempts at displacing COD from **31** were also unsuccessful.
19. Muller, A.L.; Bleith, T.; Roth, T.; Wadepohl, H.; Gade, L.H. *Organometallics* **2015**, *34*, 2326-2342.
20. Imine protonation examples: a) Lopez-Garriga, J.J.; Hanton, S.; Babcock, G.T.; Harrison, J.F. *J. Am. Chem. Soc.* **1986**, *108*, 7251-7254. b) Corset, J.; Froment, F. *J. Phys. Chem.* **1990**, *94*, 6908-6911. c) Fleischmann, M.; Drettwan, D.; Sugiono, E.; Rueping, M.; Gschwind, R.M. *Angew. Chem. Int. Ed.* **2011**, *50*, 6364-6369.
21. Falivene, L.; Credendino, R.; Poater, A.; Petta, A.; Seria, L.; Oliva, R.; Scarano, V.; Cavallo, L. *Organometalllics* **2016**, *35*, 2286-2293.
22. Calculated online at www.molnac.unisa.it/omtools/sambvca2.0/index.html
23. Sauer, D.C.; Wadepohl, H.; Gade, L.H. *Inorg. Chem.* **2012**, *51*, 12948-12958.
24. Attempts at obtaining a crystal structure of this complex were unsuccessful.

25. Reacting **36** with I_2 to oxidize the iridium center, similar to **32**, appeared to result in complex decomposition.
26. a) Crabtree, R.H. *J. Organometallic Chem.* **2004**, *689*, 4083-4091. b) Goldman, A.S.; Roy, A.H.; Huang, Z.; Ahuja, R.; Schinski, W.; Brookhart, M. *Science* **2006**, *312*, 257-261. c) Scheuermann, M.L.; Grice, K.A.; Ruppel, M.J.; Rossello-Merino, M.; Kaminsky, W.; Goldberg, K.I. *Dalton Trans.* **2014**, *43*, 12018-12025. d) Grice, K.A.; Kaminsky, W.; Goldberg, K.I. *Inorg. Chim. Acta* **2011**, *369*, 76-81.
27. This reaction was repeated four times and the same result was never obtained.
28. ^{1}H NMR spectra referenced to p-xylene d_{10} at 6.84 ppm.
29. The ^{1}H NMR spectrum of C_2D_4 in p-xylene d_{10} did not have any signals.
30. These signals were broad signals suggesting D incorporation.
31. % yield calculated relative to an internal standard.
32. These assignments are based on the C-H studies with $NaBAr^F_{24}$ as discussed in detail below.
33. If solution sat before heating in oil bath with $NABar^F_{24}$ the dinuclear species would form and Ir-C_6D_5 would not form therefore the reaction must be heated immediately after adding $NaBAr^F_{24}$ so that dinuclear formation does not occur.
34. Full characterization of **44** has been unsuccessful due to the inability to isolate **44** from $NABAr^F_{24}$. Recrystallizations have also been unsuccessful.
35. a) Chen, T-R.; Lee, H-P.; Chen, J-D.; Chen, K.H-C. *Dalton Trans.* **2010**, *39*, 9458-9461. b) Fujita, K.I.; Nakaguma, H.; Hamada, T.; Yamaguchi, R. *J. Am. Chem. Soc.* **2003**, *125*, 12368- 12369. c) Heinekey, D.M.; Fine, D.A.; Barnhart, D. *Organometallics* **1997**, *16*, 2530-2538.
36. After 24 hours the product started crashing out of solution at 100 °C.
37. NaOAc was never observed in the ^{1}H NMR, but there is always solid in the NMR tube.
38. The chlorine from **47** is from residual dichloromethane, the solvent in which the stock solution of **35** is made.
39. This reaction was not tracked by NMR spectroscopy because the starting material is not soluble in octane at room temperature.
40. Fulmer, G.R.; Herndon, A.N.; Kaminsky, W.; Kemp, R.A.; Goldberg, K.I. *J. Am. Chem. Soc.* **2011**, *133*, 17713-17726.
41. Herde, J.L.; Lambert, J.C.; Senoff, C.V. *Inorg. Synth.* **1974**, *15*, 18.
42. Uson, R.; Oro, L.A.; Cabeza, J.A. *Inorg. Synth.* **1985**, *23*, 128-129.
43. Cramer, R. *Inorg. Synth.* **1974**, *15*, 19-20.
44. Heinekey, D.M.; Millar, J.M.; Koetzle, T.F.; Payne, N.G.; Zilm, K.W. *J. Am. Chem. Soc.* **1990**, *112*, 909-919.
45. Roberto, D.; Cariati, E.; Psaro, R.; Ugo, R. *Organometallics* **1994**, *13*, 4227-4231.
46. Giordano, G.; Crabtree, R.H. *Inorg. Synth.* **1979**, *19*, 218-219.
47. Uson, R.; Oro, L.A.; Cabeza, J.A. *Inorg. Synth.* **1985**, *23*, 127-128.
48. Cramer, R. *Inorg. Synth.* **1974**, *15*, 14-16.
49. Farrugia, L.J.; *J. Appl. Cryst.* **2012**, *45*, 849-854.
50. Bruker (2007) APEX2 (version 2.1-4), SAINT (version 7.34A), SADABS (version 2007/4), Bruker AXS, Inc., Madison, Wisconsin, USA.
51. a) Altomare, A.; Burla, C.; Camalli, M.; Cascarano, G.L.; Giacovazzo, C.; Guagliardi, A.; Moliterni, A.G.G.; Polidori, G.; Spagna, R. *J. Appl. Crystal.* **1999**, *32*, 115-119. b)

Altomare, A.; Cascarano, G.L.; Giacovazzo, C.; Guagliardi, A. *J. Appl. Crystal.* **1993**, *26*, 343-350.
52. a) Sheldrick, G.M. (1997) SHELXL-97, Program for the refinement of crystal structures. University of Goettingen, Germany. b) Sheldrick, G.M. *Acta. Cryst.* **2015**, *C71*, 3-8.
53. MacKay, S.; Edwards, C.; Henderson, A.; Gilmore, C.; Stewart, N.; Shankland, K.; Donald, A. (1997) MaXus: a computer program fro the solution and refinement of crystal structures from diffraction data. University of Glasgow, Scotland.
54. Waasmaier, D.; Kirfel, A. *Acta. Crystal. A.* **1995**, *51*, 416-430.
55. Sheldrick, G.M. (2005) CELL_NOW. University of Goettingen, Germany.
56. Sheldrick, G.M. (2007) TWINABS. University of Goettingen, Germany.
57. a) Spek, A.L.J *J. Appl. Cryst.* **2003**, *36*, 7-13. b) van der Sluis, P.; Spek, A.L. *Acta. Cryst.* **1990**, *A46*, 194-201. c) Spek, A.L. *Acta. Cryst.* **2009**, *D65*, 148-155.

Bibliography

Ackermann, L. *Chem. Rev.* **2011**, *111*, 1315-1345.

Agarwal, P.K.; Saifuddin, M.; Kundu, B. *Tetrahedron* **2010**, *66*, 862-870.

Ahman, J.; Buchwald, S.L. *Tetrahedron Lett.* **1997**, *38*, 6363-6366.

Albrecht, M.; Van Koten, G. *Angew. Chem., Int. Ed.* **2001**, *40*, 3750-3781.

Allen, K.E.; Heinekey, D.M.; Goldman, A.S.; Goldberg, K.I. *Organometallics* **2013**, *32*, 1579-1582.

Allen, K.E.; Heinekey, D.M.; Goldman, A.S.; Goldberg, K.I. *Organometallics* **2014**, *33*, 1337-1340.

Altomare, A.; Burla, C.; Camalli, M.; Cascarano, G.L.; Giacovazzo, C.; Guagliardi, A.; Moliterni, A.G.G.; Polidori, G.; Spagna, R. *J. Appl. Cryst.* **1999**, *32*, 115-119.

Altomare, A.; Cascarano, G.L.; Giacovazzo, C.; Guagliard, A. *J. Appl. Cryst.* **1993**, *26*, 343-350.
Aoki, T.; Crabtree, R.H. *Organometallics* **1993**, *12*, 294-298.
Arndtsen, B.A.; Bergman, R.G. ; Mobley, T.A.; Peterson, T.H. *Acc. Chem. Res.*, **1995**, *28*, 154-162.
Baudry, D.; Ephritikhine, M.; Felkin, H.; Holmes-Smith, R. *J. Chem. Soc., Chem. Commun.* **1983**, 788-789.

Behr, A. In *Ullmann's Encyclopedia of Industrial Chemistry,* 5th Ed.; Elvers, B.; Hawkins, S.; Russey, W.; Eds.; VCH Verlagsgellschaft: Weinheim, **1989**, *A13*, 240-251.

Bell, E.R.; Raley, J.H.; Rust, F.R.; Seubold, F.H.; Vaughan, W.E. *Discuss. Faraday Soc.* **1951**, *10*, 242-249.

Bhagwanth, S.; Adjabeng, G.M.; Hornberger, K.R. *Tetrahedron Lett.* **2009**, *50*, 1582-1585.

Boisvert, L.; Denney, M.C.; Hanson, S.K.; Goldberg, K.I. *J. Am. Chem. Soc.* **2009**, *131*, 15802-15814.

Boisvert, L.; Goldberg, K.I. *Acc. Chem. Res.* **2012**, *45*, 899-910.

Boro, B.J. Ph.D Dissertation. University of New Mexico, 2009.

Brown, W.H.; Foote, C.S.; Iverson, B.L.; Anslyn, E.V. Reactions of Alkenes. Organic Chemistry, 5e; Brooks/Cole Cengage learning: Belmont, CA, 2009; 204-255.

Bruker (2007), APEX2 (version 2.1-4), SAINT (version 7-34A), SADABS (version 2007/4), Bruker AXS Inc, Madison, Wisconsin, USA.

Buchwald, S.L. *Top. Curr. Chem.* **2002**, *219*, 131-209.

Burk, M.J.; Crabtree, R.H. *J. Am. Chem. Soc.* **1987**, *109*, 8025-8032.

Burk, M.J.; Crabtree, R.H.; McGrath, D.V. *J. Chem. Soc., Chem. Commun.* **1985**, 1829-1830.

Burk, M.J.; Crabtree, R.H.; Parnell, C.P.; Uriarte, R.J. *Organometallics* **1984**, *3,* 816-817.

Burns, C.T.; Shen, H.; Jordan, R.F. *J. Organomet. Chem.* **2003**, *683*, 240-248.

Byers, P.K.; Canty, A.J.; Jin, H.; Kruis, D.; Markies, B.A.; Boersma, J.; Koten, G.V. *Inorg. Synth.* **1998**, *32*, 167-168.

Caballero, A.; Perez, P.J. *Chem. Soc. Rev.* **2013**, *42*, 8809-8820.

Camerano, J.A.; Samann, C.; Wadepohl, H.; Gade, L.H. *Organometallics* **2011**, *30*, 379-382.

Campora, J.; Palma, P.; del Rio, D.; Alvarez, E. *Organometallics* **2004**, *23*, 1652-1655.

Chen, T-R.; Lee, H-P.; Chen, J-D.; Chen, K.H-C. *Dalton Trans.* **2010**, *39*, 9458-9461.

Choi, J.; MacArthur, A.H.R.; Brookhart, M.; Goldman, A.S. *Chem. Rev.* **2011**, *111*, 1761-1779.

Christoph Samann Thesis, Univ. Heidelberg

Clark, P.F.; Elvidge, J.A.; Linstead, R.P. *J. Chem. Soc.* **1953**, 3593-3601.

Corset, J.; Froment, F. *J. Phys. Chem.* **1990**, *94*, 6908-6911.

Cossee, P. *Journal of Catalysis* **1964**, *3*, 80-88.

Coulson, D.R. *Inorg. Synth.* **1972**, *13*, 121-124.

Cox, J.D.; Pilcher, D. Thermochemistry of organic and organometallic compounds, Academic press, London, 1970.

Crabtree, R.H. *J. Organometallic Chem.* **2004**, *689*, 4083-4091.

Crabtree, R.H.; Mihelcic, J.M.; Quirk, J.M. *J. Am. Chem. Soc.* **1979**, *101*, 7738- 7740.

Cramer, R. *Inorg. Synth.* **1974**, *15*, 14-16.

Cramer, R. *Inorg. Synth.* **1974**, *15*, 19-20.

Denney, M.C.; Smythe, N.A.; Cetto, K.L.; Kemp, R.A.; Goldberg, K.I. *J. Am. Chem. Soc.* **2006**, *128*, 2508-2509.

Dupont,J.; Consort, C.S.; Spencer, J.; *Chem. Rev.* **2005**, *105*, 2527-2571.

Elmkaddem, M.K.; Fischmeister, C.; Thomas, C.M.; Renaud, J-L. *Chem. Commun.* **2010**, *46*, 925-927.

Elvidge, J.A.; Linstead, R.P. *J. Am. Chem. Soc.* **1952**, 5000-5007.

Fafard, C.M.; Adhikari, D.; Foxman, B.M.; Midiola, D.J.; Ozerov, O.V. *J. Am. Chem. Soc.* **2007**, *129*, 10318-10319.

Falivene, L.; Credendino, R.; Poater, A.; Petta, A.; Serra, L.; Oliva, R.; Scarano, V.; Cavallo, L. *Organometallics* **2016**, *35*, 2286-2293.

Farrugia, L.J. *J. Appl. Cryst.* **2012**, *45*, 849-854.

Felkin, H.; Fillebeen-Khan, T.; Gault, Y.; Holmes-Smith, R.; Zakrzewski, J. *Tetrahedron Lett.* **1984**, *25*, 1279-1282.

Felkin, H.; Fillebeen-Khan, T.; Holmes-Smith, R.; Lin, Y. *Tetrahedron Lett.* **1985**, *26*, 1999-2000.

Feller, M.; Ben-Air, E.; Iron, M.A.; Diskin-Posner, Y.; Leitus, G.; Shimon, L.J.; Konstantinovski, L.; Milstein, D. *Inorg. Chem.* **2010**, *49*, 1615-1625.

Fernandez-Alvarez, V.M.; Ho, S.K.Y.; Britovsek, G.J.P.; Maseras, F. DOI: 10.1039/c8sc01161c.

Fleischmann, M.; Drettwan, D.; Sugiono, E.; Rueping, M.; Gschwind, R.M. *Angew. Chem. Int. Ed.* **2011**, *50*, 6364-6369.

Frech, C.M.; Shimon, L.J.W.; Milstein, D. *Angew. Chem. Int. Ed.* **2005**, *44*, 1709-1711.

Fujita, K.I.; Nakaguma, H.; Hamada, T.; Yamaguchi, R. *J. Am. Chem. Soc.* **2003**, *125*, 12368-12369.

Fulmer, G.R.; Herndon, A.N.; Kaminsky, W.; Kemp, R.A.; Goldberg, K.I. *J. Am. Chem. Soc.* **2011**, *133*, 17713-17726.

Fulmer, G.R.; Miller, A.J.M.; Sherden, N.H.; Gottlieb, H.E.; Nudelman, A.; Stoltz, B.M.; Bercaw, J.E.; Goldberg, K.I. *Organometallics* **2010**, *29*, 2176-2179.

Fulmer, G.R.; Muller, R.P.; Kemp, R.A.; Goldberg, K.I. *J. Am. Chem. Soc.* **2009**, *131*, 1346-1347.

Gao, Y.; Guan, C.; Zhou, M.; Kumar, A.; Emge, T.J.; Wright, A.M.; Goldberg, K.I.; Krogh-Jespersen, K.; Goldman, A.S. *J. Am. Chem. Soc.* **2017**, *139*, 6338-6350.

Geri, J.B.; Szymczak, N.K. *J. Am. Chem. Soc.* **2015**, *137*, 12808-12814.

Giordano, G.; Crabtree, R.H. *Inorg. Synth.* **1979**, *19*, 218-219.

Goldberg, K.I.; Goldman, A.S. *Acc. Chem. Res.* **2017**, *50*, 620-626.

Goldberg, J.M.; Wong, G.W.; Brastow, K.E.; Kaminsky, W.; Goldberg, K.I.; Heinekey, D.M. *Organometallics* **2015**, *34*, 753-762.

Goldman, A.S.; Roy, A.H.; Huang, Z.; Ahuja, R.; Schinski, W.; Brookhart, M. *Science* **2006**, *312*, 257-261.

Gol'dshleger, N.F.; Es'Kova, V.V.; Shilov, A.E.; Shteinman, A.A. *Zh. Fiz. Khim.* **1972**, *46*, 1353.

Gol'dshleger, N.F.; Shteinman, A.A.; Shilov, A.E.; Es'Kova, V.V. *Russ. J. Phys. Chem.* **1972**, *46*, 785.

Gottker-Schnetmann, I.; White, P.; Brookhart, M. *J. Am. Chem. Soc.* **2004**, *126*, 1804-1811.

Graeupner, J.; Brewster, T.P.; Blakemore, J.D.; Schley, N.D.; Thomsen, J.M.; Brudvig, G.W.; Hazari, N.; Crabtree, R.H. *Organometallics* **2012**, *31*, 7158-7164.

Grau, M.; Kyriacou, A.; Cabedo Martinez, F.; de Wispelaere, I.M.; White, A.J.P.; Britovsek, G.J.P. *Dalton Trans.* **2014**, *43*, 17108-17119.

Grice, K.A.; Goldberg, K.I. *Organometallics* **2009**, *28*, 953-955.

Grice, K.A.; Kaminsky, W.; Goldberg, K.I. *Inorg. Chim. Acta* **2011**, *369*, 76-81.

Guan, Z.; Combes, J.R.; Menceloglu, Y.Z.; DeSimone, J.M. *Macromolecules* **1993**, *26*, 2663-2669.

Gupta, M.; Hagen, C.; Flesher, R.J.; Kaska, W.C.; Jensen, C.M. *Chem. Commun.* **1996**, *0*, 2083-2084.

Gupta, M.; Hagen, C.; Kaska, W.C.; Cramer, R.E.; Jensen, C.M. *J. Am. Chem. Soc.* **1997**, *119*, 840-841.

Hannah Zeitler, *manuscript in preparation* (unpublished results)

Hanst, P.L.; Calvert, J.G. *J. Phys. Chem.* **1959**, *63*, 71-77.

Hartwig, J.F. *Angew. Chem., Int. Ed.* **1998**, *37*, 2046-2067.
Heinekey, D.M.; Fine, D.A.; Barnhart, D. *Organometallics* **1997**, *16*, 2530-2538.

Heinekey, D.M.; Millar, J.M.; Koetzle, T.F.; Payne, N.G.; Zilm, K.W. *J. Am. Chem. Soc.* **1990**, *112*, 909-919.

Herde, J.L.; Lambert, J.C.; Senoff, C.V. *Inorg. Synth.* **1974**, *15*, 18.

Hoare, D.E.; Walsh, A.D. *Trans. Faraday Soc.* **1957**, *53*, 1102-1110.

Hoey, G.R.; Kutschke, K.O. *Can. J. Chem.* **1955**, *33*, 496-506.

Huang, X.; Buchwald, S.L. *Org. Lett.* **2001**, *3*, 3417-3419.
Ito, J.; Kaneda, T.; Nishiyama,H. *Organometallics* **2012**, *31*, 4442-4449.

Jaime-Figueroa, S.; Liu, Y.; Muchowski, J.M.; Putman, D.G. *Tetrahedron Lett.* **1998**, *39*, 1313-1316.

Jiang, L.; Buchwald, S.L. In metal-catalyzed cross-coupling reactions, 2nd ed.; De Meijere, A.; Diederich, F., Eds.; Wiley-VCH: New York, 2004; pp 699-760.

Johansson, R.; Jarenmark, M.; Wendt, O.F. *Organometallics* **2005**, *24*, 4500-4502.

Johansson, R.; Wendt, O.F. *Organometallics* **2007**, *26*, 2426-2430.

Johnson, M.T.; Johansson, R.; Kondrashov, M.V.; Steyl, G.; Ahlquist, M.S.G.; Roodt, A.; Wendt, O.F. *Organometallics* **2010**, *29*, 3521-3529.

Kato, Y.; Okada, S.; Tomimoto, K.; Mase, T. *Tetrahedron Lett.* **2001**, *42*, 4849-4851.

Katritzky, A. *Org. Prep. Proced. Int.* **1994**, *26*, 436-444.

Khusnutdinova, J.R.; Rath, N.P.; Mirica, L.M. *J. Am. Chem. Soc.* **2010**, *132*, 7303-7305.

Kijrungphaiboon, W.; Chantarasriwong, O.; Chavasiri, W. *Tetrahedron Lett.* **2012**, *53*, 674-677.

Kim, J.S.; Reibenspies, J.H.; Darensbourg, M.Y. *J. Am. Chem. Soc.* **1996**, *118*, 4115-4123.

Knochel, P.; Dohle, W.; Gommerman, N.; Kneisel, F.; Kopp, F.; Korn, T.; Sapountzis, I.; Vu, V. *Angew. Chem., Int. Ed.* **2003**, *42*, 4302-4320.

Kraatz, H-B.; Van der Boom, M.E.; Ben-David, Y.; Milstein, D. *Israel J. Chem.* **2001**, *41*, 163-171.

Labinger, J.A.; Bercaw, J.E. *Nature* **2002**, *417*, 507-514.

Lapointe, D.; Fagnou, K. *Chem. Lett.* **2010**, *39*, 1118-1126.

Lee, H.J.; Lee, S.H.; Kim, H.C.; Lee, Y.E.; Park, S. *J. Organo. Chem.* **2012**, *717*, 164-171.

Lee, S.; Jorgensen, M.; Hartwig, J.F. *Org. Lett.* **2001**, *3*, 2729-2732.

Leonard, N.G.; Williard, P.G.; Bernskoetter, W.H. *Dalton Trans.* **2011**, *40*, 4300-4306.

Lersch, M.; Tilset, M. *Chem. Rev.* **2005**, *105*, 2471-2526.

Liu, F.; Goldman, A.S. *Chem. Commun.* **1999**, 655-656.

Liu, F.; Pak, E.B.; Singh, B.; Jensen, C.M.; Goldman, A.S. *J. Am. Chem. Soc.* **1999**, *121*, 4086-4087.

Lopez-Garriga, J.J.; Hanton, S.; Babcock, G.T.; Harrison, J.F. *J. Am. Chem. Soc.* **1986**, *108*, 7251-7254.

Lyle, M.P.A.; Draper, N.D.; Wilson, P.D. *Org. Biomol. Chem.* **2006**, *4*, 877-885.

Lyle, M.P.A.; Wilson, P.D. *Org. Lett.* **2004**, *6*, 855-857.

MacKay,S.; Edwards, C.; Henderson, A.; Gilmore, C.; Stewart, N.; Shankland, K.; Donald, A. (1997) MaXus: a computer program for the solution and refinement of crystal structures from diffraction data. University of Glasgow, Scotland.

Maloney, K.M.; Nwakpuda, E.; Kuethe, J.T.; Yin, J. *J. Org. Chem.* **2009**, *74*, 5111-5114.

Meder, M.; Galka, C.H.; Gade, L.H. *Monatshefte fur Chemie* **2005**, *136*, 1693-1706.

Miyaura, N.; Suzuki, A. *Chem. Rev.* **1995**, *95*, 2457-2483.

Muehlhofer, M.; Strassner, T.; Herrmann, W.A. *Angew. Chem. Int. Ed.* **2002**, *41*, 1745-1747.

Muller, A.L.; Bleith, T.; Roth, T.; Wadepohl, H.; Gade, L.H. *Organometallics* **2015**, *34*, 2326-2342.

Negishi, A. *Acc. Chem. Res.* **1982**, *15*, 340-348.

Neufeldt, S.R.; Sanford, M.S. *Acc. Chem. Res.* **2012**, *45*, 936-946.

Nishiyama, H. *Chem. Soc. Rev.* **2007**, *36*, 1133-1141.

Pahls, D.R.; Allen, K.E.; Goldberg, K.I.; Cundari, T.R. *Organometallics* **2014**, *33*, 6413-6419.

Pecul, M.; Helgaker, T. *Int. J. Mol. Sci.* **2003**, *4*, 143-157.

Periana, R.A.; Taube, D.J.; Gamble, S.; Taube, H.; Saton, T.; Fujii, H. *Science* **1998**, *280*, 560-564.

Petersen, A.R.; Taylor, R.A.; Vicente-Hernandez, I.; Mallender, P.R.; Olley, H.; White, A.J.P.; Britovsek, G.J.P. *J. Am. Chem. Soc.* **2014**, *136*, 14089-14099.

Raley, J.H.; Porter, L.M.; Rust, F.F.; Vaughan, W.E. *J. Am. Chem. Soc.* **1951**, *73*, 15-17.

Raynal, M.; Pattacini, R.; Cazin, C.S.J.; Vallee, C.; Bourbigou, H.O.; Braunstein, P. *Organometallics* **2009**, *28*, 4028-4047.

Renkema, K.B.; Kissin, Y.V.; Goldman, A.S. *J. Am. Chem. Soc.* **2003**, *125*, 7770-7771.

Roberto, D.; Cariati, E.; Psaro, R.; Ugo, R. *Organometallics* **1994**, *13*, 4227-4231.

Ruiz-Castillo, P.; Buchwald, S.L. *Chem. Rev.* **2016**, *116*, 12564-12649.

Sauer, D.C.; Wadepohl, H.; Gade, L.H. *Inorg. Chem.* **2012**, *51*, 12948-12958.

Saussine, L.; Brazi, E.; Robine, A.; Mimoun, H.; Fischer, J.; Weiss, R. *J. Am. Chem. Soc.* **1985**, *107*, 3534-3540.

Scheuermann, M.L.; Goldberg, K.I. *Chem.- Eur. J.* **2014**, *20*, 14556-14568.

Scheuermann, M.L.; Grice, K.A.; Ruppel, M.J.; Rossello-Merino, M.; Kaminsky, W.; Goldberg, K.I. *Dalton Trans.* **2014**, *43*, 12018-12025.

Scheuermann, M.L.; Luedtke, A.T.; Hanson, S.K.; Fekl, U.; Kaminsky, W.; Goldberg, K.I. *Organometallics* **2013**, *32*, 4752-4758.

Schilf, W. *J. Molec. Struct.* **2004**, *691*, 141-148.

Sheldrick, G.M. (**1997**) SHELXL-97, Program for the refinement of crystal structures. University of Gottingen, Germany.

Sheldrick, G.M. (**2005**) CELL_NOW. University of Goettingen, Germany.

Sheldrick, G.M. (**2007**) TWINABS. University of Goettingen, Germany.

Sheldrick, G.M. *Acta. Cryst.* **2015**, *C17*, 3-8.

Siegl, W.O. *Inorg. Nucl. Chem. Lett.* **1974**, *10*, 825-829.

Siegl, W.O. *J. Organometallic Chem.* **1976**, *107*, C27-C30.

Siegl, W.O. *J. Org. Chem.* **1977**, *42*, 1872-1878.

Siegl, W.O. *J. Heterocylic Chem.* **1981**, *18*, 1613-1618.

Smoll, K.A.; Kaminsky, W.; Goldberg, K.I. *Organometallics* **2017**, *36*, 1213-1216.
Spek, A.L. *Appl. Cryst.* **2003**, *36*, 7-13.
Spek, A.L. *Acta. Cryst.* **2009**, *D65*, 148-155.

Sugimoto, O.; Mori, M.; Moriya, K.; Tanji, K. *Helvetica Chimica Acta* **2001**, *84*, 1112-1118.

Sugimoto, O.; Mori, M.; Tanji, K. *Tetrahedron Lett.* **1999**, *40*, 7477-7478.

Tseng, K-N.T.; Kampf, J.W.; Szymczak, N.K. *ACS Catal.* **2015**, *5*, 5468-5485.

Tsukamoto, I.; Koshio, H.; Kuramochi, T.; Saitoh, C.; Yanai-Inamura, H.; Kitada-Nozawa, C.; Yamamoto, E.; Yatsu, T.; Shimada, Y.; Sakamoto, S.; Tsukamoto, S. *Bioorg. Med. Chem.* **2009**, *17*, 3130-3141.

Uson, R.; Oro, L.A.; Cabeza, J.A. *Inorg. Synth.* **1985**, *23*, 127-128.

Uson, R.; Oro, L.A.; Cabeza, J.A. *Inorg. Synth.* **1985**, *23*, 128-129.

van der Boom, M.E.E.; Milstein, D. *Chem. Rev.* **2003**, *103*, 1759-1792.

van der Sluis, P.; Spek, A.L. *Acta. Cryst.* **1990**, *A46*, 194-201.

Van Leeuwen, P.W.N.M.; Roobeek, C.F.; Huis, R. *J. Organomet. Chem.* **1977**, *142*, 233-241.

Vo, G.D.; Hartwig, J.F. *J. Am. Chem. Soc.* **2009**, *131*, 11049-11061.

Waasmaier, D.; Kirfel, A. *Acta, Cryst. A.* **1995**, *51*, 416-430.

Weiss, M.C.; Goedken, V.L. *J. Am. Chem. Soc.* **1976**, *98*, 3389-3392.

Weissermel, K.; Arpe, H. *Industrial Organic Chemistry, 4th ed.*; Wiley-VCH: Weinheim, 2003.

Wenzel, T.T. *Stud. Surf. Sci. Catal.* **1991**, *66*, 545-554.

Wolfe, J.P.; Ahman, J.; Sadighi, J.P.; Singer, R.A.; Buchwald, S.L. *Tetrahedron Lett.* **1997**, *38*, 6367-6370.

Wolfe, J.P.; Wagaw, S.; Marcoux, J-F.; Buchwald, S.L. *Acc. Chem. Res.* **1998**, *31*, 805-818.

Xu, W.; Rosini, G.P.; Gupta, M.; Jensen, C.M.; Kaska, W.C.; Krogh-Jespersen, K.; Goldman, A.S. *Chem. Commun.* **1997**, 2273-2274.

Yang, B.H.; Buchwald, S.L. *J. Organomet. Chem.* **1999**, *576*, 125-146.

Yokota, S.; Tachi, Y.; Itoh, S. *Inorg. Chem.* **2002**, *41*, 1342-1344.

Yuan, H.; Brennessel, W.W.; Jones, W.D. *ACS Catal.* **2018**, *8*, 2326-2329.

Vita

Karena A. Smoll was born in 1991 to parents Catheryn Smoll and Eric Smoll. She grew up in Fontana, CA where she graduated high school at Fontana High School in 2009. She then attended the University of California, Irvine (UCI) in Irvine, CA where she graduated *Summa cum laude* with a Bachelor of Science degree in chemistry in 2013. While at UCI, Karena worked with Dean Kenneth Janda on the gas flow rate and temperature dependence on the kinetics of difluoromethane clathrate hydrate formation. Karena then attended graduate school at the University of Washington in Seattle, WA. There, she worked with Prof. Karen I. Goldberg on the synthesis and reactivity of late transition metal complexes for alkane functionalization. Karena obtained a Doctor of Philosophy degree in chemistry in 2018.